ProQuest Number: 10290258

ProQuest 10290258

EVALUATION OF STRESS INDUCED DAMAGE IN COMPOSITE MATERIAL

ANN-MARIE PRISTON

A thesis submitted in partial fulfilment of the requirements of The Nottingham Trent University for the degree of Doctor of Philosophy

December 1997

1   Abstract

The aim of this work was to investigate the growth of damage within a composite material. The work involved the use of acoustic emission to monitor the growth and evolution of damage within a composite material. A second part of the work considered the reduction in composite material elastic modulus to reflect the evolution of this damage in these composite materials.

The many failure mechanisms in the composite material produced different acoustic emission waveforms. The waveform parameters amplitude, ringdown count and risetime, were used to cluster the acoustic emission events into groups that characterised the evolution of damage in unidirectional glass fibre polyester composite material. The occurrence of high energy Cluster 1 events was confined to experimental periods where fibre debonding or failures were expected. Throughout the experiment small amplitude acoustic emission events were related to the deformation of the matrix.

A mesoscopic continuum damage model was developed to model the development of matrix cracking and fibre debonding damage in a composite material. The two increasing damage parameters (d, d') reflected the accumulation of damage by the reduction in the transverse and shear moduli. The fibre debonding from the matrix was controlled by the transverse stresses relative to the fibre pulling the fibre away from the matrix. The matrix crack was modelled as a combination of shear and transverse stresses.

Finite element analysis was combined with the model to provide examples of the damage growth pattern for a range of composite material with changing fibre angles. The results from three angle orientations showed that damage was initiated at a lower stress for weaker material with larger fibre angles. The growth patterns for the different angles were not similar, reflecting the differing development of shear and transverse induced damage. The influence of the element dimension in the mesh was tested with two different sizes and found to produce similar results.

Nomenclature

σ_{11} Longitudinal ply stress

σ_{22} Transverse ply stress

σ_{12} Shear ply stress

E_1^0 Longitudinal modulus

E_2^0 Transverse modulus

G_{12}^0 Shear modulus

d Damage parameter for changing shear modulus

d' Damage parameter for changing the transverse modulus

ν_{11} Poisson's ratio

σ_L^* Specimen longitudinal stress

ε_y^* Specimen transverse strain

ε_x^* Specimen longitudinal strain

$\mathbf{Y_d}$ Shear damage development

$\mathbf{Y_{d'}}$ Transverse damage development

$\underline{\mathbf{Y}}$ Quantity of matrix cracking damage

$\underline{\mathbf{Y'}}$ Quantity of fibre debonding damage

Y_s' Fibre debonding damage limit

Y_o Initial shear damage equation constant

Y_c Rate of change of shear damage constant

Y_o' Initial transverse damage equation constant

Y_c' Rate of change of transverse damage constant

b Factor for increased transverse damage over shear damage development

<u>2</u>   <u>**Contents**</u>

3   Introduction

The traditional materials used in the fabrication of components are no longer restricted to steels and natural products. Today, designers and engineers have a range of composite materials that combine two or more components to produce a composite that has improved or desired properties. More importantly, composite material properties are ideal for the new innovative designs being created. Composite materials are already well established in certain fields such as civil engineering (pre-stressed concrete), ship design (fibreglass hulls) and aerospace design (military jet fighters, ceramic heat shields). Composite materials are often a lighter weight option with comparable strength and loading properties to steel or wood.

This project investigated the deformation of composite material. This work was sponsored by British Gas Plc. The results went towards the programme of work undertaken by British Gas Plc. to develop new materials to store gas in tanks. Weight saving in the fabrication of the tank would allow for a greater weight of fuel to be stored for the tank weight limits.

The material of particular interest was glass fibre/polyester resin composite. There are many advantages in using this material. For example, it is practical and relatively cheap to fabricate the materials, they produce a good weight to strength ratio and allow complex shaped components to be fabricated. Much expertise in the use of these materials now exists, both in industrial fabrication companies and in universities.

Detailed evidence of the types of damage which occur in a composite material is available in the form of scanning electron microscope (SEM) pictures of the cracks and delamination observed [Hull (1993)]. To observe deformation in the material, the composite material has to be tested and then sectioned for the microscope. This destroys the specimen. A technique, which could monitor damage accumulation without the need to stop the test and cut up the sample at different loads, obviously has advantages. This could be achieved by monitoring the acoustic emission

emanating from the matrix and fibres cracking. Using transducers attached to the surface of a stressed sample the acoustic emission activity in the sample could be followed without interruption to the experiment or destroying the sample.

The acoustic emission associated with the deformation of the composite material is highly complex, reflecting the complexity of damage mechanisms developing in the composite material. It is expected that the acoustic emission frequency and amplitude information for plastic matrix or brittle fibre cracking would be different, allowing for the differentiation of the source type. The occurrence of acoustic emission from sources that have a more significant effect on the material performance would highlight that the material was undergoing severe deformation.

Distinguishing the different source mechanisms from the acoustic emission waveform should be possible using pattern recognition. The characteristic parameters of the waveform can be measured for each acoustic emission event captured. These parameters include peak to peak amplitude, ringdown count and risetime. These waveform variables are typical of the possible input data for clustering algorithms used to separate the events into distinct clusters with similar characteristics and hence similar source mechanisms.

Experiments can be tailored to favour the development of certain damage mechanisms by changing the orientation of the fibres in the composite material. From experience [Rotem and Hashin (1975)], the fibre dominates the deformation history when it is aligned close to the loading direction at high stresses. Once the fibre is at an angle to the load, the matrix and the interface between the fibre and the matrix will become sites for important amounts of deformation. It is the source orientation effects which should be mirrored in the acoustic emission emanating from the composite sample under test.

It is proposed that the clusters of acoustic emission data for specimens with different fibre angles should be separated in to distinguishable groups. Correlation of the cluster data with damage mechanisms could then be attempted.

Previously developed models that mathematically follow the progression of damage through a composite material are complicated by the complexity of the structure of fibres within the matrix and the many different damage mechanisms possible. Here a simplified model, proposed by Ladeveze and Le Dantec (1992), homogenised the detailed properties of the fibre and matrix to form a combined material property for the orthotropic directions in the material and provided a possible solution to this difficulty. Damage accumulation manifested itself as a reduction in the moduli of the composite. The inability to sustain previously possible loads indicated that damage had occurred and was reducing the effectiveness of the material.

The representation of fibres debonding shows as a reduction in the transverse modulus relative to the fibre direction. Positive transverse stresses pull the fibre away from the matrix along the interface region. Matrix cracking is represented as the combination of transverse and shear moduli reduction. Dilating transverse stress opens the crack, allowing the crack tip to migrate. The shear stress component moves the crack through the matrix. It is these defects that acoustic emission might reasonably be expected to distinguish between.

The summation of all these effects for a realistic volume of material comparable with the size of a composite material specimen requires a large amount of computation. The use of finite element analysis provides a framework for the model to separate the material and damage into manageable, representative volumes. The size of each volume, or element, is part way between the physical size of the microscopic failure source and the macroscopic component size. Therefore, the amount of time taken to calculate the damage effects at all the node positions is not excessive.

An important part of any validation of a model incorporating finite element analysis is to eliminate the model's dependency to react to the mesh element size. If the damage development is significantly different for the different element sizes then the model is not robust enough to accurately model any damage occurring. Therefore, meshes with different sized elements should be investigated.

The thesis consists of the following chapters. Following this general introduction, a review of the existing literature on damage mechanisms and resulting acoustic emission in a composite material is developed in Chapter 4. Existing knowledge regarding the use of the acoustic emission technique to monitor damage occurring in a composite material is identified. Chapter 4 also reports the different methods for theoretically modelling damage accumulation in a composite material. The chapter identifies the many limitations in the mathematical representation of damage accumulation due to the complex mixture of materials and the interactions with each other and the accumulating damage.

Chapter 5 describes the fabrication of the glass fibre-polyester composite material with details of the type of glass and resin systems used. The mechanical tensile tests are also described.

Chapter 6 describes the experimental methods used for the acoustic emission monitoring of stressed samples. This includes details of the equipment used to sense, digitise and store the acoustic emission waveforms.

Chapter 7 develops the necessary stages for post processing the acoustic emission waveforms for clustering into groups using VIEWDAC programs and CLUSTAN clustering algorithms. There are details on the automatic processing of the thousands of events to measure the characteristic parameters of the waveforms.

Results from the practical acoustic emission experiments are discussed in Chapter 8, highlighting the changing relationships between different material fibre orientations.

The theoretical development of a damage model to match the accumulation of damage in a composite material is developed in Chapter 9. The modifications to the equation constants from the work by Ladeveze and Le Dantec are discussed to account for the use of a different composite material type.

The practical implementations of the model in a series of computer programs are described in Chapter 10. The calculation of the damage state of every element in a model was controlled by an iterative program. The stress results from the finite element analysis of the damage model are used to calculate the progressing damage.

The results from finite element meshes with different element sizes and experiments with various material orientations are described in Chapter 11.

Conclusions from the work are summarised in Chapter 12. Remarks on the success of developing a damage monitoring system and the theoretical modelling of damage accumulation in composite materials are made with ideas for future complementary work.

4   Literature Survey of Damage in Composite Materials

4.1   Introduction

This chapter reviews the literature related to the damage that occurs in composite materials and its detection. It will describe the different mechanisms observed and the resulting effects on the material properties. Detailed descriptions of the location and the interactions between the many different mechanisms will be discussed that relate to glass fibre polyester composites. This is the material used in the experiments discussed in later chapters and is by far the most abundantly used in the manufacture of products made from polymeric composite materials. The damage mechanisms observed in the experiments will be correlated with the mechanisms reported for composite materials.

The monitoring of damage in a composite material is not easily achieved by the established methods of non-destructive testing. Electro-magnetic techniques are not generally usable on non-conducting polymer material. The widely used ultrasonic NDT technique of reflection ultrasonics was developed for testing isotropic metal material. Although the anisotropic nature of the laminate structure of composites adds complexity to the use of ultrasound scanning, ultrasound still remains one of the most frequently used NDT techniques for penetrating the laminate layers and highlighting anomalies. Ultrasound uses a surface source of energy that is directed into the material and is reflected back by internal changes to the material density. Alternatively the acoustic emission monitors the radiated ultrasonic energy liberated from defects within the material. Cracks that develop in the matrix and fibres, redistribute the stored stresses in the material, some of which converts into acoustic emission. The ability to remotely sense the acoustic emission at the surface allows for complicated component geometries with tight curves to be monitored.

It is important to improve the methods for monitoring the deformation of composite materials since the uses of advanced materials are increasingly more complex and varied. Areas sensitive to damage may not be accessible during service for inspection. Acoustic emission provides remote sensing of developing microcracks

and is able to operate effectively on components with complex geometry and provide monitoring of the full volume of material under test.

4.2   Review of the Damage Mechanisms and Failure in Composite Materials

An important aspect of materials testing is the identification of defects that occur in the material as it deforms and fractures. Cross sections from cut and polished experimental test specimens have provided evidence for different modes of failure appropriate to the stress regime undergone. Repeated experiments have established accepted trends in the accumulation of damage in a composite material. Cantwell and Morton (1991) have reviewed the reported evidence of the primary damage and defects in composite material (matrix cracks, debonding and broken fibres). They have also reported the testing techniques, destructive and non-destructive, that have been used to detect and monitor the location and progression of damage.

The types of damage mechanisms observed in a composite material are known to include matrix cracking, fibre debonding and fibre breaking. Each damage mechanism which is generated depends on both the type of applied stress and the material structure. Experimental work aims to reproduce the stresses likely to occur in the use of the composite material and hence study the resulting damage.

Cui *et al* (1992) reported the observed damage for three and four point testing of long fibre composite laminates. The damage zone was associated with the loading roller producing different tensional and compressional stresses through the material thickness. The surface under the roller displayed compressional damage, whilst the lower side was dominated by tensional stress damage. Intermediate levels of the composite had significant shear damage between the plies. The complex mixture of stresses produces a variety of damage mechanisms.

Damage in a composite made from two dissimilar materials such as glass and resin, is reflected in the location of the contrasting damage mechanisms. The interface has material properties unlike those of the fibre or the matrix. Therefore the composite material can be segmented into three zones with associated damage

mechanisms for the matrix, the fibres and the interface region between the two materials.

4.2.1 Matrix Cracking

The matrix is potentially the weakest component of the composite material with a low strength modulus, but it does provide the bridge for stress transfer between fibres. The matrix maintains the orientation of the load bearing fibres and minimises the out of plane movement of the fibres that are not bonded to the matrix. The ability of the matrix to plastically deform suppresses the rapid propagation of cracks.

The initial stages of degradation of the material at low stresses are dominated by significant amounts of matrix cracking throughout the specimen [Allen *et al* (1988), Laws *et al* (1983)]. Crazing, the dispersed occurrence of cracks, is reliant on both the local matrix strength and defects to control the size and any propagation direction of cracks.

Damage growth is influenced by the presence of manufacturing defects. Cracking can accumulate about inclusions such as dust, grease or air bubbles [Thomason (1995), part 1]. The care taken to maintain the quality of the manufacturing can reduce the number of defects added to the material at this early stage. An industrial application of process monitoring reported by Petrovskii and Shalygin (1991), used acoustic emission. The changing structure of the polymer during manufacturing heat treatment emitted acoustic emission. Careful control of the process reduced the chance of over heating the material.

Damage initiation points are also added in the post production stage through rough handling or environmental attack. Most composite material structures are finished with a coloured resin skin for mainly aesthetic reasons rather than for added strength purposes. However this outer layer may obscure the whitening of the resin due to impact damage. Impact has formed an important part of the experimental testing of composite material because of the difficulty of detecting the presence of this kind of damage as well as the subsequent repair required. The nature of the

progressive deformation of a composite material is unlike the traditional propagation encountered using metals.

In general, the resins used for the matrix material show less environmental degradation than other materials such as metals and wood. In contrast, the glass fibres and the adhesion of the fibres to the matrix can be dramatically damaged by the presence of water. Experiments have shown that water solutions can be drawn along the fibre interface and cause a reduction in the shear strength of the material. A combination of water, light and biological attack has been shown by Wagner *et al* (1996) to decrease the strength of the resin. The effect of heat and water together is discussed by Mori *et al* (1994). The results show a shift in the dominant damage sites from the accumulation in the matrix to the debonding of the fibre or fibre bundle from the resin. The changing mechanism was also detected by a changing acoustic emission amplitude spectrum. Strained specimens left in a bacterial solution failed earlier than strained specimens left in pure water. The micrographs showed nucleated damage in the resin that caused the damage to accumulate. Bouadi and Sun (1989) report results that show temperature can be the driving force behind composite material degradation. In moist environments at about 25°C (room temperature) the material moduli are little affected. However with increasing temperature, as experienced in tropical conditions, the strength is reduced.

The result of temporarily exceeding design limits for a composite material produces damage that may continue to accumulate when under desired loading conditions again. Microscopic optical pictures of over stressed matrix zones are dominated by cracking and plastic deformation [Steiner *et al* (1995)]. The resin, due to its elastic properties, shows large deformation strains compared to the inelastic glass fibres. However, due to the matrix's low strength it tends to accumulate much cracking.

In-service failures of pressure vessels made of composite material has led to the development of acoustic emission based testing methods, with acoustic emission evaluated during a predefined series of loading and unloading cycles [CARP, Fowler

(1992)]. This proof testing allows the reduction of the internal pressures in a controlled manner rather than risk a sudden burst or explosion.

As the population of cracks increases the cracks are in closer proximity to each other. The cracks merge to form significant cracks that have a greater effect on the material properties, particularly if they meet fibres or the material edge [Manders *et al* (1983)]. Matrix cracks that meet fibres continue to propagate around the fibre in the matrix, debonding the fibre from the matrix, or cause the fibre to fail. Cracks reaching the edges may cause the plys to delaminate and allow easier water penetration.

4.2.2   Fibre Debonding

Matrix cracking leads on to the debonding of the fibre from the matrix. The interface between the glass and resin materials acts as an important zone for the transfer of stress from load bearing fibres through the matrix to neighbouring fibres. The interface region between the fibre and the matrix has characteristic damage mechanisms. These mechanisms are termed debonding. Debonding is closely associated with the physical and chemical bonds between the elastically miss-matched fibre and matrix. To facilitate a good bond the fibres are coated in a film of size. This produces a chemical bond between the glass and resin phases. Kimpara *et al* (1989) showed the material properties of the interface between different carbon fibres had effects on the damage mechanisms that degraded the composite. Brittle failure rather than an accumulative degradation was associated with material with higher interfacial strength.

Glass has no great ability to adhere to the polyester resin, so the interface is inherently weak. The coupling agents coat applied to the fibres or added to the resin [Thomason (1995), part 1] improve chemical adhesion between the fibre and the matrix. Fibre manufactures have developed coatings, or sizes, for the glass fibres which protect the glass from frictional damage during manufacture and produce a chemical link to bridge the differences between the fibre and the resin chemistry. Different coatings have been developed to match the glass to the resin and account for the environment the component may be used in. Resin manufacturers have likewise

tailored the resin to be compatible with the size coating on the fibres, as well as the final use of the component made of composite material. The result of a well matched coating and resin is good wet out of the resin surrounding the fibres and a strong bond for stress transfer under load.

When a crack impinges on the interface zone it can cause the fibre to debond from the matrix. The route that the crack moves along is complicated by the chemistry of the bond. For composites with poor fibre attachment to the matrix, the crack takes the easier route of moving along the fibre face or very close to it. This is damage occurring at the interface of the fibre. The fracture plane observed using scanning electron microscopy (SEM) has fibres with clean surfaces. A weak or even non existent bond produces a material that is initially strong but when over stressed the material deforms by the fibres debonding and pulling out of the matrix. The void will allow water to penetrate and degrade the interface further [Thomason (1995), parts 1,2 and 3].

The route of a crack meeting a well bonded interface is for the crack path to be deflected into the interphase zone. The subtle difference between the location of the interface and the interphase is controlled by the chemistry of this zone. The matrix chemistry close to the fibre is different to the bulk matrix, due to the addition of the sizing chemicals to the fibre [Okoroafor and Hill (1995)]. SEM pictures show this failure mechanism has characteristic matrix material stuck to the fibre surfaces. A stiff well bonded fibre produces material that has a high initial modulus but reduces rapidly when damage proliferates in the stiffened, brittle interface zone. The stresses are transferred directly to the fibres with possible failure.

Frictional forces can supplement the chemical bonds linking the coated fibre to the matrix. These can be produced by the shrinking of the matrix around the fibre during fabrication. The closing stresses restrict the movement of the crack tip along the boundary. The residual compressive stresses have to be overcome before the crack can open and propagate. When the transverse stresses about the fibre became tensional the fibre debonds. The ability to redistribute the loading stresses between the fibres is reduced as the bonds between matrix and fibre are broken. The build up of

14

localised stress concentrations result in the fibres being over loaded and breaking. There are also frictional forces developed by the interlocking of the two surfaces, increasing the residual stresses [Thomason (1995), part 3].

Measurement of the adhesion of the composite material interface requires the testing of individual fibres in the resin. These techniques, which include fibre pull out tests from droplets of resin, fibre indentation testing and bundle tests, are fraught with experimental and interpretation problems, but are the only methods at present that provide any data for the adhesion between fibre and matrix [Herrera-Franco and Drzal (1992), Young (1993), Galiotis *et al* (1993)]. Okoroafor and Hill (1995) have proposed an alternative method based on the transverse failure of fibre bundle composites, which has the advantage of using the complete fibre bundle rather than a single fibre.

4.2.3 Fibre Breakage

The catastrophic effects of fibre deformation dominate damage mechanisms reported for higher stress levels. The fibres are the load bearing component of a composite material because they are significantly stronger than the surrounding resin.

Different types of fibre: glass, carbon or aramid, have different internal material structures so deform, buckle or break in different modes [Hull (1993)]. The diameters of fibres, 7-12μm, compared to the longitudinal dimensions requires the orientation of fibres parallel to the main load. The isotropic nature of glass means that it has the same bulk properties in the longitudinal and transverse directions. The fracture surface is characteristically clean cut. Carbon fibres have a more fibrous rough fracture due to the longitudinally aligned carbon ring structure having irregularities producing voids and ridges of carbon material. The organic aramid fibres, which include Kevlar, have a helical structure of aromatic carbon molecules. The stacked planar layers produce regular column structures. This accounts for the observation of fibrous fibre ends or the length ways splitting of damaged Kevlar fibres.

The orientation of the fibres with respect to the loads also has an effect on the observed failure modes. Rotem and Hashin (1975) showed the changes in deformation as the fibre angle was changed from parallel to the loading direction (0°), through 45° to more transverse orientations.

When the material is bent rather than compressed or pulled the damage mechanism is quite different again. Flexural failure mechanisms of composite material are dominated by the buckling of the fibres [Chen *et al* (1994), Agarwal *et al* (1989)]. The shear modulus and the shear strength of the material dictate the amount of buckling accommodated by the fibres within the matrix [Chen *et al* (1994)]. Glass and carbon fibres due to their structures are brittle in nature and show very little buckling. The aramid fibres accommodate the bending forces by compressional rippling on the inner surface of the fibre [Hull (1993)].

4.3 Modelling Damage in Composite Material

Modelling the reactions to loading in an anisotropic composite material poses many problems because of the complex interaction and orientation of failure modes [Hashin (1990)]. Mathematical models have approached the solution from two distinct mathematical concepts. The first type of model- the micromechanical model, sets stress requirements for individual fracture mechanisms to occur. The model restricts the location and number of defects in a particular volume. This reduces the complexity of the model to dealing with one or two mechanisms at one time. The second concept, which is adopted in this work, is continuum mechanics. From the thermodynamic energy equations for the whole system, damage is calculated from the changing energy state of a representative volume of composite material [Allen *et al* (1990), Murakami (1990)]. The internal damage is represented as variables that relate damage to the changes in the material properties. The type of damage present is determined from parallel experimental work. The summation of the unit volume predicts the response for a specimen sized model.

4.3.1 Micromechanical Models

The micromechanical approach develops predictions for the material conditions that make it possible for fracture mechanisms to occur. Matrix cracking,

16

fibre breaking, debonding and delaminations - the main damage mechanisms in a composite material, have different initiation stress field requirements and accumulate at different rates. The observed effects on the material's performance are different for the different damage types. To combine damage mechanisms becomes complex and mathematically verbose when individual damage sites are to be summed to achieve a model of any real component size.

Matrix cracking forms the main damage mechanism at low stresses. The accumulated effect of the development of cracks modifies and weakens the macroscopic material properties. The additional degradation due to temperature increases over time also adds to the amount of damage reported in the model proposed by Ponsot *et al* (1989). It may also produce zones that are the sites for more significant fibre associated damage mechanisms. Pyrz (1992) drew attention to the need for the models developed for matrix cracking be at a scale to reflect the microscopic scale of the fracture but still have the capabilities to represent the material as a continuous-homogenous medium for practical macroscopic analysis. He concludes that matrix cracking models are better suited to the continuum models, which are discussed in a later section.

Pyrz (1992) has also modelled the cracking pattern developed by different ply orientations. The model describes the development of planes of cracks in similar orientations. Experimental evidence was more difficult to produce to confirm the crack accumulations.

Models predicting the initial damage history or 'first ply failure' concentrate on the location and the migration of crack tips through the matrix [Gregory and Herakovitch (1986)]. The complex combinations of shear and tensile stresses about the crack tip are influenced by the dissimilar materials used in the composite material, as well as the laminate loading [Wang and Choi (1983)]. The propagation direction through the matrix towards the fibre interface can have a major impact on the correct predictions of orthotropic lamina failure [Gregory and Herakovich (1986)]. Where these cracks intercept the ply boundary it is possible to delaminate along the

boundary. Delaminations have been studied, especially at the free edge of the specimen, using energy release rate equations.

Laminates have characteristic mixed mode delaminations associated with failure [Allen *et al* (1988)]. Delamination failure requires further information about the shearing stresses involved at the interface region of the ply [Allix *et al* (1989)]. Measurement of these shearing stresses has been attempted by performing more complex experiments using end notched flexure specimens [Carlsson *et al* (1986), Kim and Hong (1986)] and short beam, 3 or 4-point bending tests [Rosensaft and Marom (1985), Whitney (1985), Kortschot and Beaumont (1990)]. The model results have been compared favourably with experimental damage growth and the post fatigue strength remaining using end-notched samples [Spearing and Beaumont (1992)].

4.3.2   Statistical Fibre Failure Methods

Other fracture mechanics models have concentrated on the fracturing of the load bearing fibres. The probability of a fibre breaking is statistically well defined using a Weibull function [Hahn and Kim (1975), Harlow and Phoenix (1979), Okoroafor and Hill (1995), Okoroafor et al (1995)]. The possibility of failure has been related to the static residual lifetime for a previously fatigued tested specimen. The idea of 'weakest link' failure, where the load is subsequently carried by the fibres not broken, works well for tension tests. This cannot be applied to compression tests where matrix shear stresses combine with the tensile fibre stresses to redistribute the load [Budiansky and Fleck (1993)].

As fibres fail the load once carried by the failed fibre is distributed to other fibres. By calculating the stress concentrations around the fracture sites this can lead to predictions of sample failure [Pyrz (1994)]. Effects from thermal residual stresses and Poisson effects can also be taken into account. Models that redistribute the stress evenly over the complete cross section have predicted higher failure stresses than in experimental work [Rosen (1964)]. Calculating the stress concentrations for such a situation is complex and time consuming. Therefore only small models of fibre/matrix bundles [Harlow and Phoenix (1981)] have been studied. Large scale structures are

not possible with this type of mathematical model. Redistribution of stresses to the nearest neighbour is less complicated if geometry is reduced to square or hexagonal cross sections rather than random [Kwon (1992), Gent and Wang (1992)]. Using the situation of multiple breaks to signify material failure, results have predicted lower strengths than in experimental work [Zweben and Rosen (1970), Wisnom and Green (1995)]. By calculating the stress redistribution to the nearest fibres only the theoretical values fall within the experimental range, lower than those of uniform stress redistribution and higher than values from multiple break predictions [Zhu *et al* (1989), Watson and Smith (1989)].

4.3.3   **Pseudo-Micromechanical Damage Models**

One of the deficiencies of the micromechanical models described above are the difficulties of scaling the models up to real size structures. The summation of individual defects is computationally difficult to perform and still produce a realistic material response for the material at a real component size. The orientation of the fibres within the resin matrix increases the complexity of the model. The models that are being developed for the representation of 3-D woven or embroidered glass reinforcement cloth involve a complex mathematical variation of the material properties in all orthogonal directions. Dumont *et al* (1987) and Murthy and Chamis (1988) for example, are unable to assume the material is transversely isotropic i.e. having fibres aligned in each ply, or that the material is quasi-homogeneous with random fibre orientations because of the stitching height and the crossing of fibre tows. Therefore the 3-D mathematics describes all variations in every direction. The reinforcement weave does repeat so the volume, or basic cell, is analysed and used to build a more extensive model.

The basic cell idea can also be used for less complicated fibre orientations, which leads to homogenisation of the composite's regularly occurring structure [Devries *et al* (1989)]. The basic cell is then loaded and the stress concentrations calculated are related back to the response of the whole structure.

Pseudo-micromechanical models enable micromechanical damage mechanisms to be combined with structural changes in the material properties [Budiansky and

Fleck (1993), Alix and Ladevese (1992)]. Damage accumulation in a lamina can be a useful start for a model of a real size laminate structure [Fukunaga *et al* (1984), Reddy and Pandey (1987), Poursartip (1990)]. However where the matrix and reinforcement fibre combination produces a highly anisotropic layer, the use of the rule of mixtures model gives poor predictions of the stress conditions.

Combinations of the different types of fibres (glass, carbon and aramid) have been used to fabricate hybrid filament wound pipe sections [Ikegami and Yoshida (1990)]. The results from the experimental work compared well with the predictions from laminate plate theory. The failure stress was determined by the laminate sequence and the position of the weakest material.

4.3.4 Finite Element Analysis of Composite Materials

The division of the composite material into basic cells lends itself to the mathematical analysis of composite material structure using finite element analysis. Finite element analysis is the mathematical representation of material changes at discreet positions, or nodes in a model. Stresses and restraints occurring about a component are represented as node displacements. Segmentation of the finite element model into the elements surrounded by nodes, can be at the same scale as the basic cell used in pseudo-micromechanical models that describes the repeating nature of the material.

The analysis of damage progression through a composite can be facilitated by the use of finite element (FE) analysis. FE analysis allows for more complex material geometries to be studied with the relative speed of the computer processor calculating the stress regimes for the segmented model mesh. Hybrid composite material with alternating plies of glass and carbon fibres have been investigated by Li,Y.L. *et al* (1992), for stacking sequence effects on the failure point. Using different material properties for the plies, the FE results confirmed the observed experimental results that the carbon ply with low elongation to failure deformed first.

The results from a mathematical approximation are limited by the accuracy of the constants entered at the start and the mathematical assumptions required for

20

boundary conditions. Work reported by Gillespie *et al* (1986), details the application of FE to investigating delamination in a specimen with an end notch, tested under three point loading. The crack tip of the mid plane split was modelled in detail so as to calculate the energy release rates as the damage progressed. The mesh element density was changed to investigate sensitivity to mesh geometry. In a similar fashion Tan (1991) reports the results from three different mesh densities about a central hole. Both investigations had predictions similar to the experimental results, and showed that increasing mesh density increases computational time without significantly improving the accuracy of the result. Gillespie *et al* (1986) went further and compared the detailed experimental results with the finite element analysis. They showed the need to take into account other interfering stresses such as friction as the crack opens. The mathematical assumptions implicit in the FE mathematics to calculate the shear stresses and energy release rates were modified to improve correlation with the experimental results. This highlights the on going improvements to classical, simple damage models.

Finite element results show the need for damage models to be refined further than the basic simple model. The propagation direction and predicted damage severity are related to observed damage in composite material. The time taken to calculate a particular damage growth pattern is closely related to the number of elements in the mesh and the modification of material parameters by damage parameters [Kwon and Byun (1990), Fan and Hsu (1992), Chang and Chang (1987)]. Finite element analysis has provided a useful tool for modelling the stress concentration field and structural responses of both micromechanical and macromechanical test examples. Kim and Hong (1992) matched the progressive failure about a hole in a composite material with the deformation and failure as modelled by a finite element mesh.

4.3.5 Continuum Damage Models

The continuum damage models avoid some of the errors incurred by separating the individual damage mechanisms into type and location (micromechanical models). Instead the continuum damage models concentrate on the summation of damage and the consequences of changing the material properties for the complete composite material. The stress regimes reported in experimental work that promotes

certain damage mechanisms are used to develop the changing model states and values of variables used to monitor the extent of the damage occurring.

The thermodynamic equations summarise the state of the material in all directions for all stresses acting on the material. With the addition of internal damage variables that change to reflect the degree of damage, the equations can be solved for the progression of damage development. The variables are associated with specific material moduli, so the models can describe the characteristic material stiffness changes associated with different mechanisms.

Talreja (1990) presented the example of the interlaminar cracking predicted by the continuum kinetic equations of damage accumulation and the experimental results from testing glass fibre epoxy laminates. The agreement between longitudinal Young's modulus changes of a $[0,90]_s$ laminate as measured and calculated, was better than for reported micromechanical predictions. Further work done by Li, S. *et al* (1992), using the ideas of the changing energy state of the whole material to reflect the damage accumulation, has produced another version of a continuum model that agrees well with experimental laminate tests. The relative ease with which continuum models can be adapted to reflect material changes such as fibre orientation or laminate ply lay-up, has been shown by other work by Allen *et al* (1990). In earlier work by Allen *et al* (1987) their report comprehensively describes the changing moduli as the result of distribute matrix cracking in composites.

The laminate structure of composite materials is susceptible to delamination failure. Continuum models predict the degree of delamination by the interacting shear stresses predicted between the different plies. Allix and Ladeveze (1992) modelled delaminations in carbon fibre laminate with central holes. Good agreement was achieved when the fibres were at 0°, but poor with fibres at 90°. The model was not extended to include the extensive transverse cracking damage most frequently found in 90° laminate, which may account for the shortcomings of the model. The significant degradation due to delaminations is modelled using finite element analysis following the initiation and growth patterns [Kondo and Aoki (1987), Herrmann and Ferber (1992)].

Applying the concepts of continuum damage to describe the global changes to the material has been used in work involving finite element analysis of crack interactions and localised stress concentrations about, for example, holes in laminates. Murakami (1990) describes the details for calculating the effective stresses that cause damage and the results of simulations to map the progression of cracks through a plate. The cracks are assumed to be within the matrix and parallel to the fibre orientation. These assumptions are consistent with experimental results. Work by Herrmann and Ferber (1992) describes the finite element results of predicting the damage development of a large scale model of fibres within the matrix. The Araldite fibre-modified epoxy matrix model displayed the characteristic matrix cracking and interface degradation. The finite element model reflected the damage calculated by the continuum model for similar stresses.

Later stages of material deformation are characterised by mechanisms in the matrix surrounding the fibre but not necessarily the fibres breaking. These models would include matrix cracking as well as interfacial debonding and splitting [Ladeveze and Le Dantec (1992), Ladeveze 1992]. Kaw *et al* (1992) detail the results of comparing five different mathematical representations of the interfacial characteristics of a composite material. The results show how the predictions for the composite material properties can vary greatly between models. Interfacial shear strength variations will have an effect on the prediction of material properties [Zhou *et al* (1992), Tissington *et al* (1991), Janankhani and Galiotis (1989)].

4.3.6 Conclusion to Damage Model Choice

From the above review, it is evident that the choice of model to predict the damage development for the complex structure of a composite material is difficult. The desired result from a model describing the macro or micro damage development, will dictate the choice of model used [Reifsnider (1986)]. Detailed microstructure results would require the detail from a micromechanical damage model. Whereas the scaling up to specimen scales would require the use of pseudo-micromechanical or continuum mechanics models. The model chosen here reflected the scale of the experimental work using standard test specimens. The continuum model by Ladeveze

23

and Le Dantec (1992), follows the damage development by monitoring the changing material moduli, which then reflects critical matrix cracking and fibre debonding damage in the composite material.

4.4   Acoustic Emission from the Deformation of Composite Material

4.4.1   Introduction

Materials subject to mechanical loads store energy within the material. Once the load reaches a critical level the material is damaged and the energy released. These microfailure mechanisms release the energy in a variety of ways including sound and heat. Of particular interest here is the stress wave (acoustic emission) emitted by the defect. This acoustic emission radiates from the damage site and is detected at the surface of the material as a surface displacement [Scruby (1987)]. By monitoring the acoustic emission, the damage occurring in the composite can be studied *in situ* and correlated to observed damage mechanisms, thus developing a complete picture of the deformation within a composite material.

The non-destructive technique of acoustic emission does not require the component to be removed from the assembly so speeds up the monitoring of damage accumulation. This technique allows for monitoring whilst in service and potentially detect changes in the material properties that may have disastrous results if allowed to continue [Murthy *et al* (1985)]. Acoustic emission has gained acceptance as an important part of the proof testing of fibreglass tanks or vessels [CARP code]. The recommended practice document emphasises the usefulness of acoustic emission to test rapidly the integrity of the shell as well as the fittings.

4.4.2   Acoustic Emission from Damage Mechanisms

The resin matrix of a composite material is potentially the weakest part of the composite and has the potential for considerable amounts of damage. The acoustic emission from tests at the early stages of loading have signals dominated by small magnitude and short duration events. These small packets of acoustic energy correlate with the minor releases of strain energy associated with cracks opening in the matrix. In contrast, in the final stages of testing, where the fibre reinforcement is failing, the acoustic emission events have characteristically high amplitude.

The development of *in situ* loading in a scanning electron microscope (SEM) chamber and simultaneous acoustic emission monitoring has been developed by Siegmann and Kander (1992) and Faudree *et al* (1988), to monitor composite material deformation. By changing the span-depth ratios of three-point bending tests, Siegmann and Kander observed different damage mechanisms correlate with different amplitudes of acoustic emission events. Small amplitude (65 to 75 dB) events were associated with the dominating shear stress damage seen in the matrix for short span tests (4:1) and low stress levels of other longer span ratios. Longer span experiments (26:1) have predominantly tensile-compressional failure related to cracks propagating through the matrix or along the interface of the fibres. The SEM results related crack debonding to acoustic emission events with higher amplitudes (70-80dB). Tensile/compressional fibre breaks were present in the longer span ratios, and at higher load levels. The few fibre breaks were correlated to the few high (>90dB) events detected. In the work by Faudree *et al*, the testing of a pure resin specimen confirmed that cracking within the matrix gave low amplitude acoustic emission.

The rate of acoustic emission occurring can be influenced by the type of matrix used. A study by Ghorbel *et al* (1991), contrasted the acoustic emission from a more brittle polyester resin composite with that from a visco-elastic, vinylester based matrix composite. The results reported the higher acoustic emission rate for the polyester compared to the vinylester matrix. The contrast was matched by a more rapidly decreasing material modulus for the polyester indicating greater material deformation.

Cracks at the fibre-matrix interface, that debond the matrix from the fibre, emit characteristic acoustic emission events. Differences in the acoustic emission have been observed by Okoroafor *et al* (1995) and (1996), for fibres with different fibre matrix adhesions. Typically a fibre that is well bonded to the matrix requires greater energy to break the bonds, compared to the energy for propagating a crack through the matrix. The extra energy imparted produces an acoustic emission event with higher ringdown count or higher energy content. Single fibre composite samples have utilised acoustic emission to detect the onset of fibre segmentation [Kimpara *et al*

(1989)]. Acoustic emission is able to count the number of breaks occurring before the critical fibre length is reached when no more fibre fracture occurs.

Mielke *et al* (1990) have observed differences between acoustic emission events from matrix and fibre dominated failure mechanisms when the acoustic emission events are analysed in the frequency domain. The associated fibre failure or fibre pull-out acoustic emission events have been found to have higher frequency content than the matrix cracking events.

Fibre failure has a dramatic effect on the material properties. Experimental work by Chow *et al* (1993), has directly related the acoustic emission from a crack started at a central hole in a composite material. The visible crack tip in the unidirectional glass fibre reinforced composite was coincident with the event locations. The ultrasonic tomography measurements also taken, mapped the changing material properties caused by damage evident as changed sound attenuation values. The progressing damage zone extended further than the crack itself. Indicating damage to the matrix surrounding failed fibres after redistribution of the stress concentrations.

The amplitude of the acoustic emission event has a strong correlation to the source mechanism [Barre and Benzeggagh (1994), Pollock (1973)]. The sudden release of strain energy as the material splits asunder produces burst type events with more energy. These will produce a larger amplitude which with similar attenuation paths, will be recorded as a larger event. The relative variation in the range of amplitudes recorded has been related to the different source mechanisms [Valentin (1985), Short and Summerscales (1984), Kander (1991), Mittelman and Roman (1991)]. The detailed investigation of the damage mechanisms occurring in a glass fibre/epoxy matrix laminate with a central hole, used a mixture of acoustic emission, SEM pictures and strain gauge changes to develop a damage model [Laksimi *et al* (1994)].

In the majority of work reported using the amplitude of acoustic emission to distinguish different damage mechanisms, the higher amplitude events have been

26

correlated to the fibre failures. Likewise the work reported here. However a paper by Valentin *et al* (1983) argue that acoustic emission from fibre breaks will be relatively smaller in amplitude than those from matrix cracking debonding a fibre. The argument involves the area of the fracture mechanism. The fractured fibre diameter is small, approximately 12μm and only one of about 20000 fibres per bundle, so the total stored energy is shared amongst many fibres. The observed interface debond area is significantly larger, (a fraction of a millimetre) and therefore has the potential to release a larger amount of energy. The study was not able to indicate the time over which the energies were released. The fracture time will be an important variable for controlling the characteristics of the acoustic emission signal waveform, especially the amplitude. The fibre will fracture rapidly compared to the time for interface debonding. The fibre debond may act in a stick-slip manner, and the observed rupture will be the sum of many individual minor debonds. For a fibre break the energy of many frequencies will be released in a shorter time and so produce a greater amplitude.

The fabrication of components generally involves the lay-up of the fibres in layers with different fibre directions or woven fibres. Delamination between the layers has been studied by Dharan (1987) considering the improved resistance to delamination of woven reinforcement compared to unidirectional plies. Acoustic emission played an important role in monitoring the initiation of the first stages of delamination and hence the predictions of the material fracture toughness.

4.4.3   The Propagation and Detection of Acoustic Emission

The acoustic emission source waveform will be attenuated by its passage through the anisotropic composite material [Suzuki *et al* (1994), Waschkies and Holler (1984)]. The layers of fibres and matrix will internally reflect and refract the signal due to the different sound velocity values for the materials. Ultrasonic work has concentrated on resolving the input or source waveform from the source mechanism after travelling through the layers of a composite material. The work has mathematically deconvolved the output with the known effects caused by the known layered structure. Acoustic emission experiments on composites are not endowed with prior detailed knowledge of the path taken by the sound wave through material

27

since the energy source is a randomly located damaged point. The waveform detected at the surface can only be deconvolved with a limited, homogenised estimate of the attenuation path. Composite materials have many acoustic scattering centres in the form of ply boundaries and fibres, which allows for only partial recovery of information on the source mechanism. Work similar to the geophysical earthquake deconvolution of seismic traces, uses information about the speed and the attenuation of the wave through the material for the characterisation of the source and the surrounding material [Drobot (1993), Kline and Ali (1985), Wu and Gong (1993), Higo *et al* (1980), Graham and Alers (1975), Glennie *et al* (1985), Stijnman (1995)]. Plate wave analysis has separated the signals originating from real source mechanisms from the noise from the grips [Prosser *et al* (1995)].

Work by Prosser *et al*, (1995), and Lorenzo and Hahn, (1988) have shown the transducer location will lead to discrepancies in the characteristics of the signal detected and the possibility that similar sources will produce unique signals due to differences in location within the composite material. The different path taken by a signal from a similar damage mechanism source will have varying affects on the final detected waveform. The longer the distance the acoustic emission must travel the greater the Lamb wave frequency dispersion in the signal. Material lay up also affects the acoustic signals detected. Work by Lorenzo and Hahn (1988), using cross ply material observed differences in the size of the acoustic emission events depending on the orientation of the fibres in the outer ply under the transducer. If there was a 90° ply under the transducer, since this ply accumulates early cracking parallel with the fibre direction, this increases the attenuation of signals travelling towards the transducer. This reduces the amplitude of recorded acoustic emission. Distinguishing different source mechanisms and locations from amplitude analysis alone can not be done on severely damaged laminated material. Dai and Harris (1988) have shown that when using laminated, filament wound, glass reinforced pipes with severe impact damage the amplitude differences alone can not differentiate the damage mechanisms.

The act of detecting the acoustic emission will distort the information in the waveform. The transducer's presence on the material dampens the surface movement so further reduces the frequencies with low amplitudes. The means by which the

transducer converts the surface movement into typically a changing voltage also distorts the original waveform information. The acoustic emission wave can be sensed and transformed into an electrical signal compatible for data storage by a piezoelectric transducer. The transducer attempts to oscillate with the material surface, but is usually unable to reproduce the broad frequency range associated with the transient stress wave, and particularly so for the resonant transducers used in this work. As the piezoelectric is deformed by the fluctuating material surface, the electrical potential difference between the front and back face of the piezoelectric changes. The voltage derived from a resonant transducer is considered to be proportional to the velocity of the material surface. The frequency range contained with the acoustic emission stress wave extends from approximately 100Hz to 5MHz and beyond. This large detection range is beyond the capabilities of most transducers.

The most widely used ceramic piezoelectric transducers are more practical for composite material tests but are limited by restricted frequency ranges. Ceramic transducers are, however, robust and can withstand the relatively rough treatment of using spring clips to attach the transducer to the material. Wide band transducers typically cover a frequency range from 200kHz to 2MHz. Resonant transducers have a narrow band of sensitive frequencies. For example a transducer quoted as 375kHz has a band of ±100kHz for a -3dB drop in response. Beyond this range the sensitivity is greatly reduced and the frequencies poorly detected and recorded.

For a resonant transducer the waveform takes the form of a complex decaying oscillation due to the transient excitation from the acoustic stress wave, with the decay largely controlled by the ringing in the piezoelectric material. The count per event (ringdown) is related to the energy content of the event [Favre and Laizet (1989), Brindley *et al* (1973)]. The larger events also produce a larger number of ringdown counts as the transducers' movements take time to decay [Salleh *et al* (1995)]. The frequency content of the acoustic emission is reflected in the number of oscillations of a sensitive transducer [Schiavon *et al* (1988)].

Another acoustic emission detection technique involves the use of lasers to sense the surface movements [Wagner and Huber (1994)]. The interferometer detects path difference changes associated with the surface movement of the solid created by

the passing acoustic emission stress wave. Accelerometers, which utilise a mass loaded piezoelectric, provide an alternative measurement system most widely used in the geotechnical applications of acoustic emission, such as slope stability [Styles *et al*].

The oscillating transducer voltages can be digitised and stored for later analysis. The instruments that use dedicated analogue electronic measurement are fast and precise in measuring a predefined set of acoustic emission characteristics. The speed of measurement is close to the rate of acoustic emission from a composite material, which might typically generate thousands of events per second. The separate circuits dedicated to evaluating waveform functions, such as the amplitude measurement, can also be interfaced with a digitiser to record the value per event.

An alternative procedure for event capture is to digitise the complete electrical acoustic emission waveform and develop computer programs to post-process the waveform data. The computer based system enables many different analyses to be used on the raw event data. This method does restrict the number of events it is possible to capture per second because of the storage time and deadtime to reset the configuration of the A to D board before the capture of the next event.

For the broad spectrum of a wide band transducer the digitising board must sample sufficient points to reproduce the oscillating voltage. For the upper transducer limit of 2MHz this would require a sampling frequency of 10MHz or more. This is an expensive data acquisition system. Use of narrow band transducers allows the use of a lower maximum digitising frequency. The use of a resonant transducer centred on a sensitive frequency reduces the range of frequencies that are detected. The A to D board used for waveform digitising in this work has a 1MHz rate which is adequate when working below 400kHz. By restricting the frequency content of the sensed input, using a resonant transducer, the detailed information about the source mechanism is reduced.

4.4.4 Acoustic Emission Waveform Processing.

Having established that there are likely to be distinct damage mechanisms in a composite material originating from distinctly different rupture patterns (section 4.2), then it may be possible to characterise types of acoustic emission signal, using acoustic emission signal parameters. The acoustic emission may than be related to distinct source mechanisms operative in the composite material. One method to achieve this is by using cluster analysis, which aims to bring together acoustic emission events with similar features.

Multivariate analysis (cluster analysis) uses differences in the waveform parameters to separate the events into groups [Yamaguchi *et al* (1991)]. Relatively simple algorithms are available to cluster events by comparison of the similarity or difference to neighbouring event [Cherfaoui *et al* (1987), Kawamoto and Ono (1990), Ono and Huang (1994)]. Pattern recognition of acoustic emission has also developed further towards service applications as computer processing speed has increased and the price reduced [Murthy *et al* (1985)].

The displacement of material from micro-crack events and the energy released, impart characteristic signatures to the acoustic emission waveform. Assuming similar attenuation paths, similar damage mechanisms would produce comparable proportions of amplitude and frequency range values in the source acoustic waveform. By selecting the parameters that highlight the differences between the various acoustic emission waveforms, then algorithms can cluster similar events together. When the population of a cluster reaches a significant level then conclusions on the materials degradation can be proposed [Ono and Huang (1994)].

Work done by Bhat and Murthy (1993) and Bhat *et al* (1994), showed that clustered acoustic emission can be used to monitor the progression of failure from fatigue testing. It showed the three distinctive stages of degradation, firstly the matrix cracking, followed by matrix crack growth and some fibre interface debonding, and finally fibre failure.

It is not reliable to use a single acoustic emission waveform parameter such as peak amplitude alone, to discriminate the different source mechanisms because of the fluctuation in the received signal caused by the attenuation in the material [Mori and Obata (1988)]. The use of neural networks 'teach' a computer to recognise the patterns attributable to specific source mechanisms from a large set of input variables [Almeida and Hill (1995), Belchamber *et al* (1985)]. The similarities and differences between a teaching set of many parameters from known mechanisms are analysed by the computer. A new set of events is tested for matches with the teaching set. The data set can include waveform parameter characteristics from the frequency domain as well as the time domain [Ivanov and Mirgazov (1993)]. These frequency parameters are then the input values for the source type pattern recognition or individually can highlight distinct variations between events [Elsley and Graham (1987)].

Multivariate analysis has used the frequency content of experimental acoustic emission as input variables to separate events into types [Maslouhi *et al* (1990)]. Using analysis of acoustic emission in the frequency domain, interfering sources of noise may be more apparent [Crostack (1977)].

There are some studies that have compared the frequency content of true acoustic emission events with simulations of source mechanisms [Meissner and Ranachowski (1993), Ohutsu (1989), Hsu and Eitzen (1980)]. Due to the complex number of decisions required about the source configuration and the complex travel path through the composite material, it is the simple structures that have been tested and compared for similarity with the observed acoustic emission.

Experiments to separate different events in the time domain have predominantly used waveform parameters such as the event occurrence rate, amplitude variation and ringdown count [Priston *et al* (1995)]. Other parameters include risetime from the start of the event to the maximum voltage [Uenoya (1994)], duration and energy (the area under the waveform outline, equivalent to the integration of the waveform).

32

The cumulative number of events has been recorded in fatigue experiments with mixed results. For the glass fibre specimens rather than the carbon specimens, the acoustic emission event rate increased rapidly close to the failure point [Holt and Worthington (1981)]. The total number of events and the number of ringdown counts have also been quantitatively related to the types of source mechanism via the stress intensity factor equations. Much work has shown that the stress intensity factor (K) has a good correlation with the degree of damage in the composite material if the stresses can be measured. Relating stress to the acoustic emission emitted would allow for direct calculation of the stress intensity factor without the need for stress measurement [Rotem and Altus, (1979), Ni and Jinen (1993)].

The use of acoustic emission to calculate the stress intensity factor has predicted the residual strength of a composite after impact damage has occurred [Caprino and Teti (1995), Hamstad *et al* (1992)] or for centre hole laminates [Caprino and Teti (1994)]. The stressing of the material by heating has shown that damaged material produces acoustic emission from the frictional rubbing of induced cracks [Sato *et al* (1988)].

Proof testing of pressure tanks and cylinders has used acoustic emission successfully to set a criterion for composite material vessel certification [Hamstad (1972)]. The testing of pressure vessels has used Kaiser and Felicity acoustic emission effects to detect the point at which the material fails to match previously attained stress levels [Awerbuch *et al* (1985), CARP code]. The ability to recognise the source mechanism from the acoustic emission signal has allowed the prediction of the lifetime and failure point of the component [CARP]. Design differences have also been compared, such as saddle or longitudinal beam supports [Warrender *et al* (1987)] and winding pattern changes using differences in the acoustic emission.

4.5   Conclusions

Composites do not have simple isotropic models to represent the damage accumulation because the complicated material responses to damage are dependent on direction. The two parts of a composite material - the reinforcing fibre and the matrix, have different material properties which dictate that the damage mechanisms will vary.

This complex structure generates the potential for a variety of damage mechanisms, which thereby requires any damage model to be mathematically complex. For the micromechanical models the homogenised material properties allow the stresses to be averaged for a small representative volume. Assumptions about the damage mechanisms occurring have to be made for the mathematical solution to be calculated. Calculating all possible orientations of matrix cracking, for example, is not an efficient method for developing a useful model for material degradation. In contrast, the continuum damage models formulate a series of equations that account for the damage accumulation considering the resulting damage changes to the macro-stresses in the composite material. Relating the mathematical damage accumulation to experimental evidence of the damage correlates the predicted mathematical damaged state to observed damage. The distinction between different material directions is accommodated in the continuum equations. The equation controlled damage accumulation can be applied to different volumes of material. By segmenting the component structure using finite element analysis, it is possible to concentrate on positions sensitive to damage accumulation and monitor the propagation of damage within a composite material.

This work uses the continuum model due to work by Ladeveze and Le Dantec, which allows the damage to be represented as two damage parameters. These parameters arise as a result of material stress changes and hence control the modification of material properties. Material equation constants derived from experimental damage accumulation set the initial damage level threshold and the rate of damage accumulation. The representation of matrix cracking parallel to the fibres affects the material properties in the shear and transverse stress directions. The fibre debonding from the matrix is dependent on the interface characteristics. The stress limit for debonding is the pure transverse stress at which the fibre pulls away from the matrix. The analysis of a single ply can be extended to a laminate structure using classical laminate analysis. The use of finite element analysis extends the damage study to the growth pattern which can be correlated with the principal material axis. More details of the damage theory and the mesh used are given in Chapter 9.

Developing a damage detecting system allows for further development and better design of components. Various designs for the component can be tested to destruction providing valuable working data for the engineer. Some evaluation techniques require the dismantling of the components before testing. Other techniques are more destructive requiring the slicing of the material for micro-structural observation using a scanning electron microscope (SEM).

Acoustic emission allows continuous monitoring of damage growth throughout a volume of composite, with acoustic emission detection at the component surface and relatively far from the damage site. Petitpas and Valentin (1992) have optically observed the fibre damage occurring at the edge of a polished unidirectional material and matched the observations to the acoustic emission emitted by fibre breaks. Much interest has been shown in relating the acoustic emission signals detected at the surface of the material to the damage mechanism that occurred within the material. If acoustic emission can reveal the severity of the damage then guidelines for the safe level of working for the component are possible. Using the composite material above safe levels will shorten the working life of the component.

Composite material damage development as represented by monitored acoustic emission is described further in Chapters 6 and 7. The digitised acoustic waveforms provide sets of descriptive characteristic parameters which form the input data to allow cluster analysis of similar events. From the analysis of the stresses at the time the acoustic emission occurred, the groups of similar events are related to the permanent material damage. Clustering allows events to be differentiated and related to damage growth due to rising stress. The differences between events provides the means for placing the events into a spectrum that ranges from the frequent, small events associated with matrix cracks, to the detrimental, relatively few, fibre breaks.

5 Composite Material Fabrication and Testing

5.1 Introduction

The type of composite material tested affects the nature and characteristics of the damage occurring. From previously discussed work in Chapter 4 the multiple layers of a laminate cause the acoustic emission signal to be distorted by multiple reflections at the boundaries of the plies. The signal is distorted and attenuated by the more involved path through the material to the surface mounted transducer. Therefore single ply, unidirectional fibre composite material was chosen for the acoustic emission experiments. The specimens had a single fibre orientation at different angles to the load. This change in the fibre angle was intended to promote different damage mechanisms. As the fibre angle to the loading direction increases, the stresses carried by the load bearing fibres alone are redistributed to the surrounding matrix, with the consequence of more matrix failure.

The theoretical damage model required the experimental testing of symmetrical laminates to determine the constants used in calculating the damage parameters. The angle of each of the plies, as in the acoustic emission experiments, promoted differing amounts of matrix and fibre dominated damage mechanisms. The symmetry of the material maintained the plane stress conditions through the thickness of the specimen and inhibited bending or twisting of the specimens under load.

The composite material used in experimental work was glass fibre reinforced with a matrix of polyester resin. Two methods of fabrication were used. The hand lay-up technique was used to prepare composite material used for acoustic emission testing. Wet winding was used in the preparation of cross-ply laminate. Experiments on this material provided information for calculating the theoretical damage model constants. Glass fibres are available in different arrangements such as woven mat or continuous fibre tows. A fabric containing fibres in one direction is used in many manufacturing techniques, such as resin injection moulding (RIM). However the fibre tows are held in place by cross-stitching at 90° to the fibre direction. This small amount of stitching would produce a possible site for misleading failure and associated acoustic emission, not directly associated with the degradation of the main composite

material. Therefore, all glass material manufactured, used continuous tows of glass fibres wound from large bobbins.

5.2 Hand Lay-up

The method of hand lay-up used a continuous fibre bundle wound on to an open metal frame (figure 5.2). In figure 5.1(b), the winding machine is shown with a solid metal mandrel occupying the position where the open frame would be fitted. The frame area was 500mm x 500mm, with a rigid, rectangular, steel cross section 4mm x 10mm. The empty frame was fitted to the winding machine (Pultrex, Modwind 1S-SN). As the frame rotated, the fibre guiding arm was computer controlled into position to accurately position the dry bundle of fibres adjacent to the previous strands. Two passes of the width of the frame were made. This stepping motion across the frame was controlled carefully to match the spreading width of the bundle of fibre. Badly positioned bundles form gaps which can become resin rich areas, or overlaying passes cause a ridge of fibres to displace the resin to form areas of high fibre concentrations. Producing an even spread of fibre across the frame produced a uniform material.

Control of the accuracy in laying down fibre obviously has an important effect on the uniformity of the composite material that is finally produced. The back tension applied by the winding machine to the bobbin of glass fibre was set very low (1/4 bar = 25kN/m^2). This produced a frame of fibres that were loosely hung on the frame. The slack in the fibres allowed the fibres to be compressed into a thin plate without the fibre tension causing the fibres to break. Tension in the fibres at the manufacturing stage would also cause the final composite to have high residual stresses. This would distort any relationship between the loading of the material and the damage development.

The rigid mould was a simple arrangement of plate glass used to sandwich the wet fibres to form a uniform thickness (figure 5.2). The glass bottom sheet was bigger than the frame, so the metal frame rested on the glass. A layer of Melinex polyamide release film covered the glass for easier release after cure and gave a better surface finish to the composite material. To impregnate the fibres on the frame, the resin was poured on to the fibres and carefully worked into the fibres using the long side of
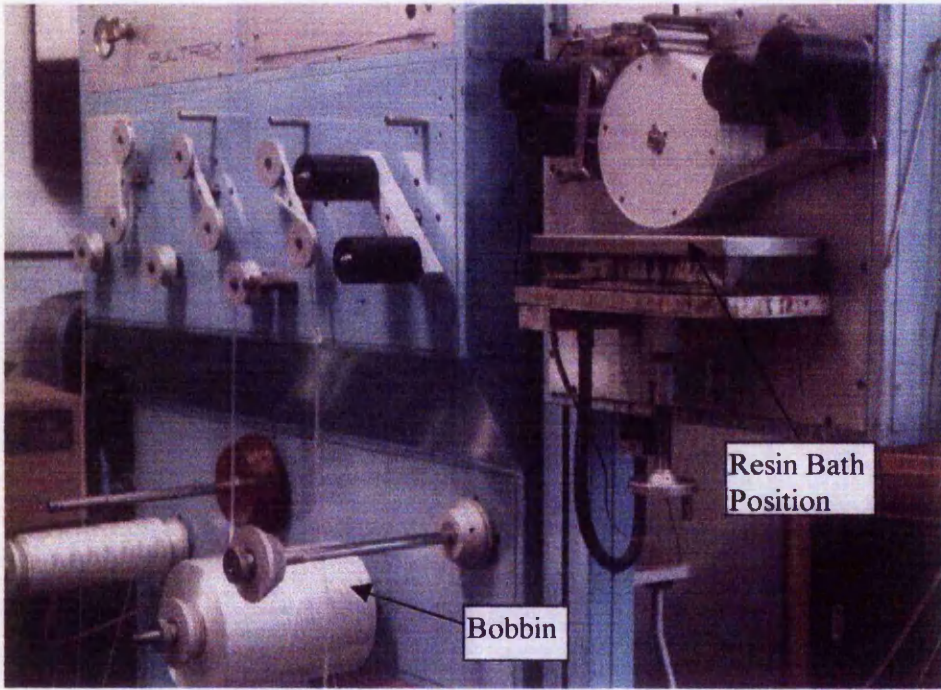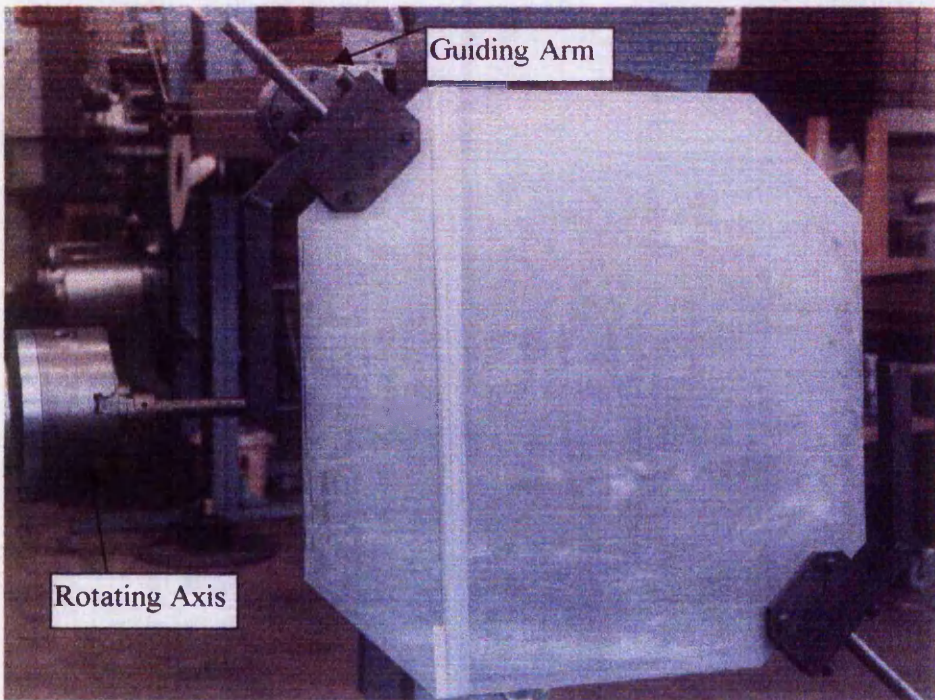
Figure 5.1 Winding machine layout (a) bobbins of glass and the series of rollers and (b) ±45° plate with a few dry glass fibre tows in place.
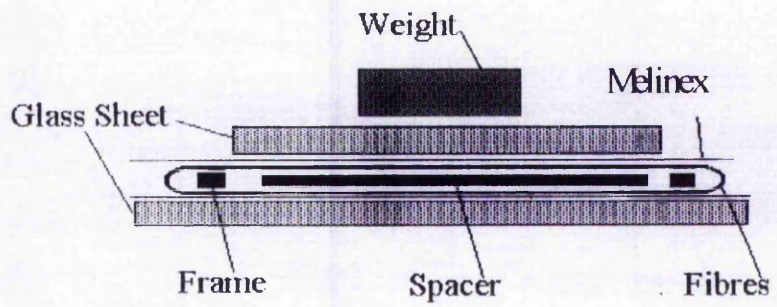
(a)
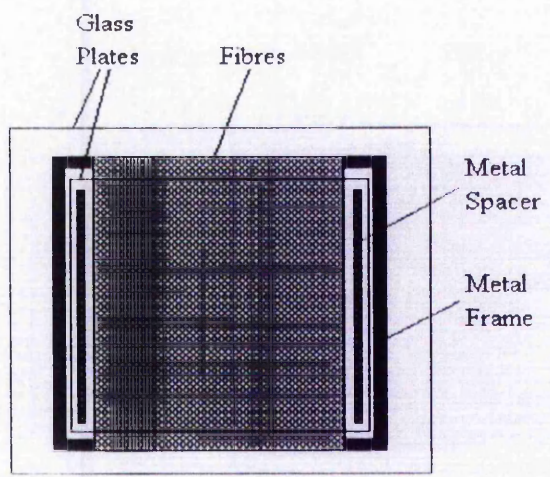
(b)

Figure 5.2 The rigid glass mould used to fabricate hand lay-up composite material.

a rectangular spatula. The spatula was dragged along the fibre direction, forcing the resin between the fibres. The action slightly separated the tows of fibres allowing better wet out where the bundle was twisted and the resin had difficulty penetrating. Since the resin and the fibres have similar refractive indexes, the final product had a uniform appearance. Poor wet out areas were easy to detect since they remained white. The action of rubbing the resin into the fibres did damage some fibres. However, the number of fibres rubbed out of alignment compared to the total was small. Any burs of fibres that formed were cut off. Another sheet of Melinex was smoothed on to the top of the wetted fibres and the top glass plate placed on top, as shown in figure 5.2. The top glass was cut to have dimensions small enough to fit inside the frame but long enough to overhang the edge of the fibres on one side. Two long strips of metal (4mm x 10mm x 30mm) were placed between the glass edges as thickness spacers. Approximately 35kg were placed on the top glass to compress the top glass plate on to the metal strips, so creating a uniform composite thickness equivalent to the metal strip thickness.

The complete mould was left in the wooden carrying tray to cure at room temperature for a day. The material was post cured in a large vented oven for a 12 hour period. The mould was released at room temperature, the Melinex helping to release the glass sheets from the composite.

The material was cut from the metal frame using a hand held jigsaw with a diamond coated blade. The test specimen positions were drawn onto the material using a marker pen and the main cuts made using a dry, flat bed saw with a diamond coated circular blade. The speed of the saw was preset to limit the amount of snagging and excessive heat production that could burn the resin. The final sample cutting was done on a semi-automated dry, parallel saw. Two blades set at a little more than 25mm apart cut two sides simultaneously. The winding gear of the machine controlled the movement of the sample past the blades. The return movement was manual, with the blades slowing. The final polishing and reduction of the sample width was done on a wet grinding machine. The long edges of the sample were ground by approximately 0.25mm producing a sample with parallel smooth sides. The total time for sample preparation, after mould release was 8 hours producing 15 to 20

samples. This preparation time could be reduced if the cut edges of the specimen proved of high enough quality to not need surface grinding and could have light sanding with wet and dry sanding paper (fine grade).

5.3   Wet Winding

The technique of wet winding produced material that was used to determine theoretical damage model constants (see Chapter 9). The basic principle of winding with a tow of glass is similar to the hand lay-up technique described previously, except the glass fibre was coated in resin before it was wound onto a solid flat plate mould instead of dry glass fibres wound on to an open square frame (figure 5.1).

The mandrel was a plate of rigid steel, cut to have parallel sides at the fibre orientations required (figure 5.3). For the two material orientations, $[\pm45^{\circ}]_{2s}$ and $[\pm67.5^{\circ}]_{2s}$ two different plates were needed. The angle of the leading edge of the metal plate was perpendicular to the fibre guiding arm of the winding machine, due to the orientation of the plate-extensions that fitted the plate to the revolving axis (figure 5.3). A groove cut into the plate edges and filled with plaster filler allowed a small cutter to slice the composite material from the plate after curing. The metal surfaces were coated in a resin release chemical (ChemTrend).

The glass was wound off the bobbin with a very low back pressure (1/4 bar = $25kN/m^2$) to hold the position of the glass on the plate. The glass fibres passed through a small trough of resin on the way to the plate. Details of the resin and glass fibre used are given in sections 5.4 and 5.5 respectively. The fibres in the bundle were completely covered in resin as the fibres separated on entering the resin bath. Excess resin was removed after passing over a rotating drum and scraper. The wet fibre tow was then guided along the fibre guiding arm towards the rotating metal plate, figure 5.1(b). The end of the bundle of glass was fixed to the metal plate using masking tape. The arm movements were synchronised with the revolving plate to control the final fibre position. The presenting edge of the revolving plate was at 90° to the moving arm which supported the wetted fibres. The height of the moving arm was also lowered and raised to meet the turning edge of the plate. This maintained the tension and the exact position of the fibres being laid down. At the end of each pass, when a
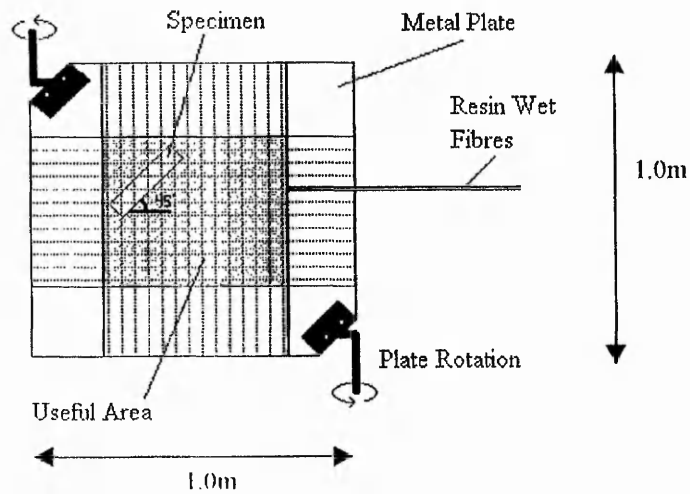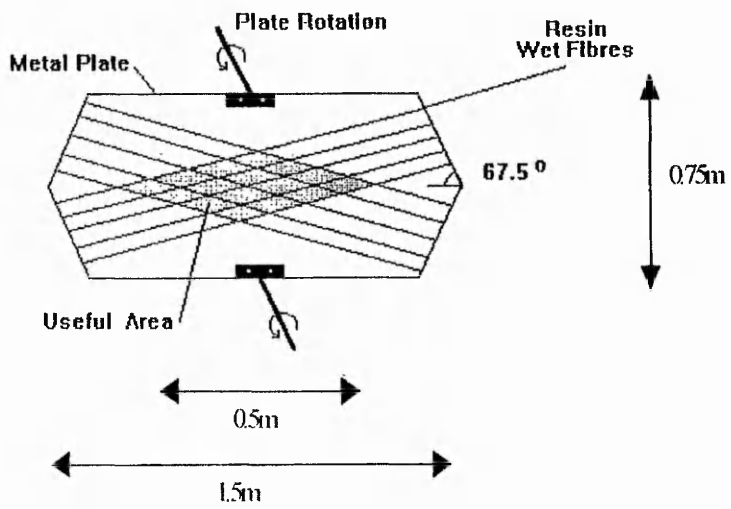
Figure 5.3 Wet winding plates to produce (a) ±67° and (b) ±45° material.

complete layer of fibre had been laid with one angular orientation, the fibre bundle was cut and secured to the plate edge using masking tape. The plate was detached from the winding machine and remounted in the matching angular position to allow fibre winding in the opposite direction.

The final wet plate was wrapped in a sheet of Melinex plastic and placed in a small metal press, between two large flat metal plates (surface area 500mm x 500mm). The metal plates were used instead of the glass plates used in the hand lay-up due to the possibility of smashing the glass in the press. The press was tightened to squeeze the metal plates against the composite for a flat surface finish. The complete sandwich was placed in a large oven to cure the resin.

The resin curing cycle in the oven was electronically controlled and logged for 18 hours. The ramp-up temperature rate of the oven was 1°C/minute. The initial temperature level was 80°C for 4 hours, then 100°C for 10 hours, then ramp down rate was 1°C/minute.

The composite material was cut at the groove positions along the edges of the plate. This produced two large composite plates, one from each side of the metal plate used during the winding process. The composite plates had a relatively small central useable area of fibres orientated in the two required directions. The test specimen positions were marked and cut in a similar manner to the hand lay-up specimens.

5.4   The Resin Systems

A different polyester resin system was used for the hand lay-up method compared to the wet winding method. This was to accommodate the different handling time required before the resin gelled and could not be manipulated further. The hand-lay up was a quicker process (30 minutes) for impregnating resin into the fibres, compared to the wet winding technique (50 minutes to 1 hour). It was also undesirable for resin to cure on the winding machine, so a heat activated catalyst was used to cure the resin in this case.

Both resins have the polyester dissolved in styrene. To solidify the polyester, the molecular chains have to be cross linked with other neighbouring polyester chains. The catalyst initiates the polymerisation of the resin, forming points along the long molecules that join similar active points on other chains. The final degree of cure is controlled by the proportion of catalyst used [Scott (1988)]. To speed up the curing time, higher curing temperatures were used and/or the presence of an accelerator to produce free radicals or linking points in the mixture ready to react with the catalyst. The accelerator lowers the energy requirements for polymerisation to occur at room temperature.

The polyester resin used in the hand lay-up fabrication cured at room temperature and the gel time controlled by the concentration of accelerator. The polyester resin was Synolac CVP6345.001, (Cray Valley Products Ltd, Grimsby). It was compatible with a liquid catalyst (MEKP) and accelerator (Cobalt Octoate). This resin combination cured at room temperature, with optional post cure at 80°C for 12 hours. The proportions of catalyst and accelerator are given in Table 5.1. The concentration of catalyst and accelerator was low, to allow for a long (30 minute) working time before gelation.

Hand Lay-up		Parts by Weight
Resin Type	CVP unsaturated polyester	100
Catalyst	MEKP	2
Accelerator	Cobalt	0.1
Wet-Winding		
Resin	Crystic 272 polyester	100
Catalyst	Powder B	2

Table 5.1. The resin, catalyst and accelerator proportions used

For the wet winding method, a resin that did not cure at room temperature was required. It was not desirable to have the resin harden on the winding machine or for it to gel before the long process (1 hour) of winding the glass onto the plate had finished. The resin used was Crystic 272 (Scot Bader) polyester resin with a solid catalyst, Catalyst Powder B (Scott Bader). This mixture required heat to cure. Hence the cure at 80°C for 4 hours and then at 100°C for 10 hours described in section 5.3. The proportions of resin and catalyst are given in Table 5.1.

5.5   Glass Specification

The fibre reinforcement chosen was glass rather than carbon or aramid fibres. It was chosen because of its application in many different components as well as its availability. The other fibre options, such as carbon and aramid fibres, are less frequently used in mass produced components made of composite materials and are more expensive than glass. The damage accumulations in carbon and aramid fibre composite materials are different to that in glass, as discussed in Chapter 4.2.

The same type of glass was used in the preparation of both the hand lay-up and the wet wound specimens. The E-glass rovings was from Silenka (Roving 084, 2400 TEX) with a Silane coating for reduced frictional damage and compatibility with polyester resin. This glass fibre type was compatible with both manufacturers' resins.

5.6   Mechanical Testing Methods

All composite material subjected to mechanical testing, was cut from the plaques manufactured as described above. The rectangular specimens cut from the plaques, had dimensions 25mm wide by approximately 200mm to 250mm long. The thickness of the specimens varied depending on the manufacturing technique used. The laminate specimens made by wet winding varied depending on the pressure applied to the press that compressed the mould. The use of metal spacing strips similar to the hand-lay up technique, would in future ensure the press was closed to the same thickness. The average wet wound thickness for the $[\pm67.5^{o}]_{2s}$ was 3.38mm $\pm$ 0.06mm, compared to the $[\pm45^{o}]_{2s}$ laminate with 4.64mm $\pm$ 0.05mm. The hand lay-up specimen thickness was 3.91mm $\pm$ 0.4mm. The fibre volume fraction for the different type of specimen were significantly different. For the $[\pm67.5^{o}]_{2s}$ it was

55.4%, for the $[\pm 45^{\circ}]_{2s}$ 40.4% and for the hand layup 24.0%. The laminates had higher fibre volume due to the low amount of resin used. The quantity of resin was limited by the amount that could adhere to, or wet, the fibres as they were dipped in the bath of resin as they travelled from bobbin, along the arm to the revolving plate. The hand layup specimens had more resin due to the excess quantities of resin poured on to the horizontal fibres so as to fill the mould completely.

End tabbing is part of the standard CRAG (Composite Research Advisory Group) testing method, but was not used for these experiments. One reason for end tabbing is to transfer the load from the testing machine grips to a wider area of the end zones of the specimens. The tab provides a non-slip surface onto which the loading machine's jaw-grips tighten. The assumption is that any damage caused by over tightening the grips produces defects in the tabs and not in the specimen under test. If however the jaws slip, this would add to the detected acoustic emission and alter stress to strain relationships. The bonding between the tab material and the specimen is prone to undesirable failure under loading. Finite element work by Sun and Chung (1993) has shown that the 90° angled end tabs produce high stress concentrations across the specimen end. They demonstrated that the tab should ideally have a sloping end that cuts across the end zone.

It was experimentally shown that the mechanical material characteristics differed for tabbed and non-tabbed laminate specimens. Experimental work using the $[\pm 67.5^{\circ}]_{2s}$ laminate material used for the theoretical model development, showed distinctively different responses for tabbed and non-tabbed [Lee and Priston 1995]. figure 5.4 shows the stress strain response curve for a $[\pm 67.5^{\circ}]_{2s}$ material with and without end tabs. Taking into account the delay for specimen 7 to register a load, the specimens show repeatable responses. The extensional zone between 0.008-0.01 strain for the specimens has significantly less extension for the un-tabbed samples. Extension for tabbed specimens is about 0.012 strain compared to 0.007 strain for un tabbed. The longer extension zone in figure 5.4, can be explained by the adhesive layer between the end tabs and specimen plastically deforming under load. There was no visible loss of adhesion, but differences in the material stress-strain characteristics

46
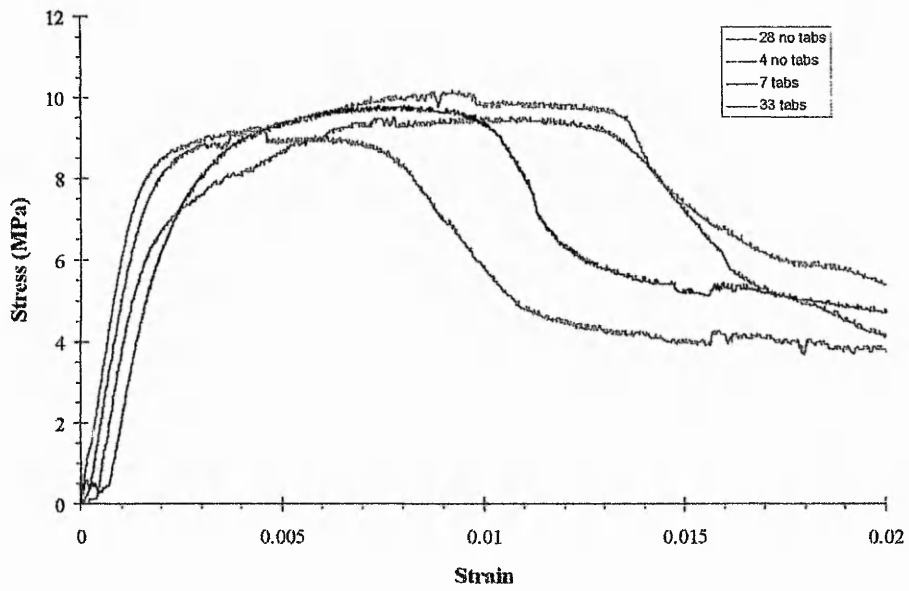
Figure 5.4 Test results from $[67.5^{o}]_{2s}$ composite material, with and without end tabs.

persisted. From these conclusions and the extra preparation time required to attach 4 end tabs on each specimen, it was felt that end tabbing was not advantageous.

The experiments reported here did not have end tabs and were gripped by parallel, clamping jaws, rated at 30kN (the maximum load of the load cell). The serrated jaws did bite into the surface of the specimen, but the slight damage to the surface was not significant, since it was not detected as acoustic emission deformation in the early loading stages. In figure 5.5, the photographs show failed unidirectional and laminate composite material. Figure 5.5(a) shows the distinct failure direction dictated by the angle of the fibres relative to the loading direction. The 0° sample shows the grip marks at the ends of the sample produced by stressing the sample to the machines' limit of 30kN. The laminate material (figure 5.5(b)) for $[45^o]_{2s}$ shows the colour change after testing. The major failure point has plys that have delaminated and skewed out of alignment. Likewise for the $[67.5^o]_{2s}$ laminate, the failure point is marked by massive ply delamination and slip.

The mechanical testing regimes showing constant extension of the composite material specimens was the same for the samples used to monitor acoustic emission and when acquiring data for the damage model constants. Mechanical testing was performed at room temperature (20^oC approximately), atmospheric barometric pressure and room humidity. Details of the specific loading rates for the acoustic emission and damage model experiments are described separately below, since two different machines were used at different loading rates for the two types of experiment.

5.6.1   Loading For Acoustic Emission Monitoring

The acoustic emission experiments monitored the acoustic emission whilst the specimens were loaded by a Lloyds R6000 tensile testing machine. The composite used was unidirectional, single ply, hand lay up material. The specimens had different fibre orientations relative to the loading axis. The testing machine measured the load and the crosshead extension and the information was saved in a computer data file. The crosshead was moved at a constant extension rate of 0.1%/minute strain per original specimen length. No extensiometers were used to measure transverse or
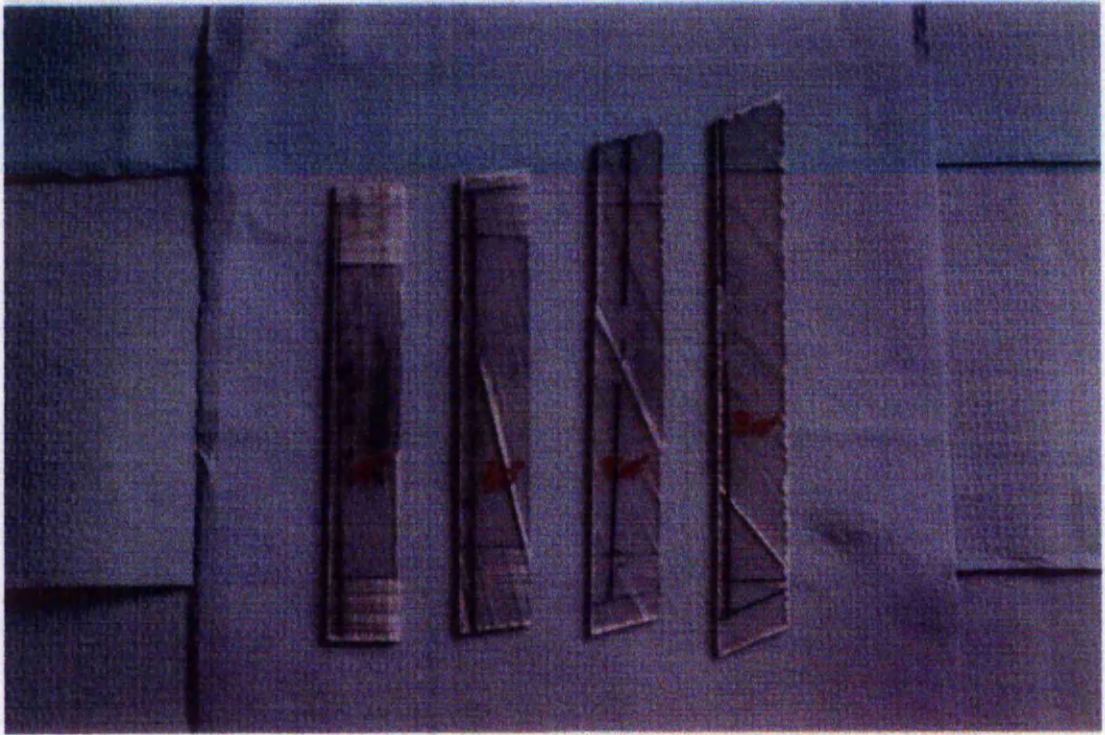
(a)
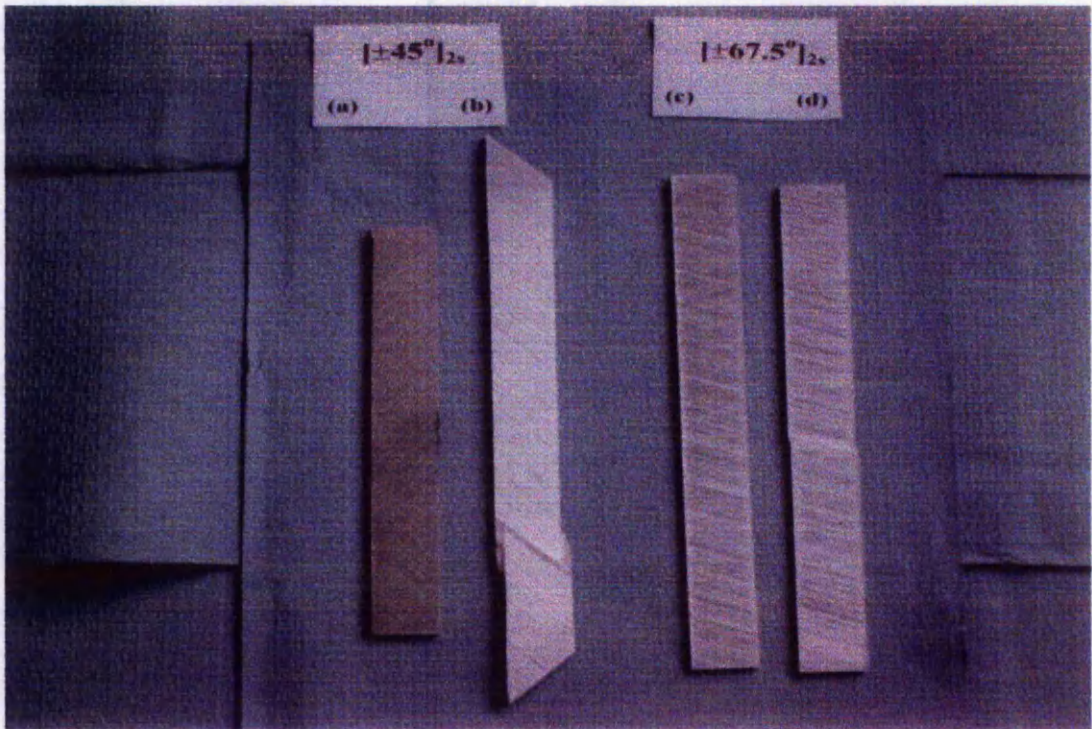
(b)

Figure 5.5 Failed (a) unidirectional and (b) laminate composite material samples.

longitudinal material strain. The longitudinal strain was inferred from the crosshead position relative to the initial specimen length. The Lloyds control program saved load/extension data, for post processing to stress (Pascal) and strain (no units) or time (minute) data files using the specimen dimensions.

5.6.2 Loading for Damage Model Data

The material used for the theoretical damage model was 8 ply laminate, produced by the wet winding technique. The specimens were tested using an Instron testing machine with longitudinal and transverse extensiometers used to measure strain. Using the material strain data it was possible to calculate transverse and shear stresses and strains required for the damage model calculations.

The need for detailed information about the changing strains at the start of loading required the straining rate to be decreased from that used for the acoustic emission tests. The Instron rate was reduced to 0.05%/minute, which allowed more data points to be collected, defining the initial stress and strain conditions of the material. The data was saved to disk for computer aided processing into stress/strain relationships used in the damage model calculations.

6. Acoustic Emission Experimental Measurement System

6.1 Acoustic Emission Equipment

The two main parts of the acoustic emission monitoring system are (1) the piezoelectric transducer used to detect the acoustic emission stress wave and the pre-amplification, and (2) the electronic system used for digitising and storage of the captured acoustic emission waveform on to computer hard disk. The arrangement of the experimental system is shown schematically in figure 6.1. The software used for post processing of the acoustic emission waveform is described in Chapter 7.

The transducers used to detect the acoustic emission were lead zirconate titanate (PZT) ceramic transducers (AECL). PZT ceramic piezoelectric devices produce a larger voltage per surface displacement compared to most other piezoelectric plastics or ceramics which might be used. Ceramics produce a more rugged transducer more suitable for repeated attachment to failing composite material specimens. The dimensions of the active ceramic disk in the transducer determines the preferred resonant frequencies. The backing materials behind the piezoelectric affect the response of the transducer by changing the damping characteristics- the ringing oscillations of the ceramic, after the initial electronic spike. There are two main transducer types - the resonant transducer and the wide band transducer. The resonant transducer used in the experiments described here had a piezoelectric ceramic disk producing resonances at peaks of 175 kHz or 365kHz. The response to frequencies a few thousand Hertz away from these specific values are dramatically reduced in sensitivity. A wide band transducer has a centre frequency but with a spread of many thousand Hertz and usually has reduced sensitivity.

The oscillating voltage from the transducer, caused by the fluctuating material surface displacement due to the acoustic emission, is amplified using a matched preamplifier (50dB). The amplifier matches the electrical impedance of the transducer's equivalent circuit. The amplifier also has integrated filters matched to the bandwidth of the transducer. For the 175 kHz transducer, for example, the filter had a bandpass of 55 kHz to 375 kHz. Power for the amplifier was tapped from the power

51
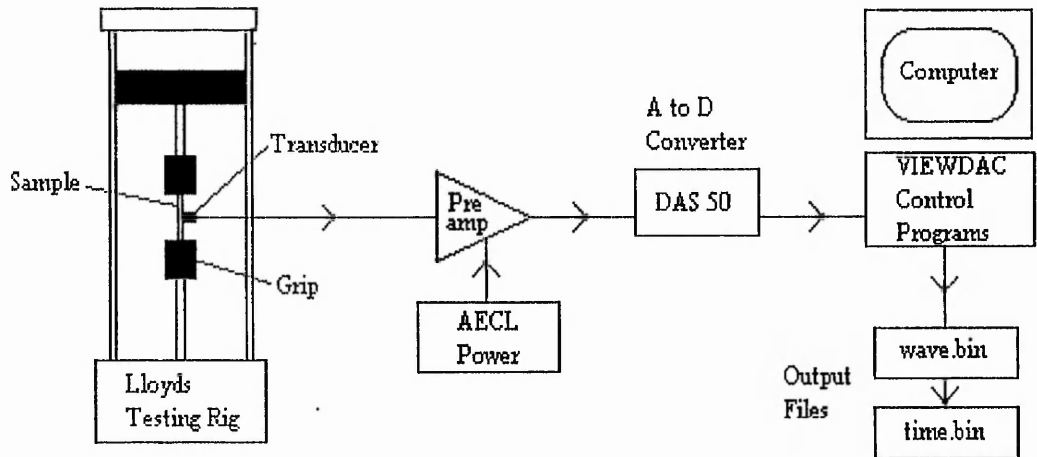
Figure 6.1 Schematic view of the acoustic emission acquisition system.

rail of the AECL 2111 AE system. An independent power supply was also possible using a TOPPS ±12V DC voltage supply unit and a three-way cable. The AECL unit was found to be more convenient to use. The choice of the lower 175kHz frequency transducer for some of the experiments was influenced by the digitising rate of the analogue to digital board. The lower transducer resonant frequency (175kHz) rather than 365kHz avoids any possible errors associated with violation of the Nyquist frequency and improves the accuracy of the acoustic emission parameters.

The amplified acoustic emission signals were digitised using a 1MHz analogue to digital converter board (A to D), DAS50 (Keithley). The board was resident in a Viglen 486DX-33MHz personal computer for ease of power supply and connection to the other electronic equipment. The connections to the A to D board were via a screened ribbon cable to a connection box containing BNC connectors for the signal input from the transducer.

Data management was controlled and directed by an operating system called VIEWDAC (Keithley). An acquisition program, described in full in the next section, was developed, which allowed capture and storage of the acoustic emission events to disk as rapidly as possible for further analysis at a later time. The digital data from the DAS50 was streamed to the cache memory of the computer for final storage on the hard disk.

With a single channel input to the DAS50 A to D board, the stream of changing voltage levels was sampled at a maximum rate of 1 MHz. The 175kHz transducer voltage signal had approximately 5 data points recorded per oscillation. This value of 5 points adequately meets the requirements of the Nyquist Theorem for digital representation of sampled analogue waves for the lower frequency transducer. The 365kHz transducer signal could be subject to errors by missing vital information at critical turning points in the oscillation waveform.

The subsequent signal analysis must bear in mind that the measured signal is a distorted representation of the original frequencies and amplitudes in the acoustic stress wave as it appears in the solid composite material. The transducer imposed a

dominant resonant frequency on the signals and reduced the presence of lower and higher frequencies. The A to D digitising rate is relatively slow using a 375kHz transducer which would alter the representation of higher frequencies. A less distorted representation of the acoustic emission waveform would be possible if the transducer used was wide band with a correspondingly more expensive, high digitisation rate, broadband A to D digitising system. The penalty for greater bandwidth is usually reduced sensitivity.

From experimental work on simple uniform material, it is possible to distinguish acoustic emission differences from elastic and brittle materials, such as pure resin and glass fibres [Okororafor *et al* (1996)]. Monitoring acoustic emission from composite material has the disadvantage that the material is highly attenuating, which distorts the signal content the longer the travel path is from defect to transducer. The multitude of interfaces between fibres and resin act as reflectors that scatter the signal further. Once the fracture energy reaches the surface of the composite material, the transformation of the vibrations into electrical energy by the transducer modifies still further the unique qualities of the acoustic emission signal. To be able to analyse the data further, the analogue signal must be digitised. This act of segmenting the signal if not done with careful consideration for the frequency content of the signal can result in serious distortion of the waveform. The results from waveform characteristics such as amplitude depend on the digitised acoustic emission waveform representing a fair approximation of the original energy packet released by the defect mechanism.

6.2   VIEWDAC Operating System.

VIEWDAC is a commercial package designed for the monitoring, acquisition and processing of data in analogue or digital format. The data can be in the form of real time, changing voltages accessed via the input channels, or previously stored data sets in many different data formats (e.g. ASCII, binary). The system can also be used to export data, control other processes and produce graphics.

VIEWDAC directed the capture sequence program, ACOUSTIC.BEQ, for the acoustic emission experiments. A full description of the program appears in

Chapter 6.2.1. The post processing of the acoustic emission data for representative waveform parameters is described in Chapter 7.

6.2.1 Acoustic Emission Capture Program

The program sequence responsible for the capture of emitted acoustic emission was called ACOUSTIC.BEQ. The three main features of the sequence were

(1) making ready the A to D board for fast sensing of acoustic emission events,

(2) the acquisition and digitising of the oscillating voltage and

(3) the efficient storage of data. A listing of the structure of ACOUSTIC.BEQ is given in figure 6.2.

Interfacing the DAS50 A to D board with the internal computer architecture was achieved using a block of commands (RESET BLOCK) at the start of the acquisition program (sequence). By directly writing to the DAS50 board, via the digital ports, it was possible to set the A to D board default to capture a stream of data including data points before the trigger time (pretrigger points). The trigger was set to activate on a rising voltage going through a set threshold value. A 255 unit scale between -10V and +10V set the resolution of the trigger level. The threshold trigger voltage value (129) was equivalent to +0.12V.

Having made ready the A to D board, the second feature of the sequence was to capture and digitise acoustic emission events. For most of the running time of ACOUSTIC.BEQ, the DAS50 was in a state of readiness to capture events, while waiting for the trigger to be activated. This burst capture arrangement meant that much less data was stored compared to ready streaming. The sampling of the input signal was controlled by an acquisition command, (A TO D). This command set the sampling rate (1MHz), the number of input channels to sweep across (one in this case) and the number of data points to capture and save. The number of digitised points per event was set at 200. Due to the sampling frequency, this produced a fixed window of 200μs, including a 10μs pretrigger before the trigger point. A separate command interrogated the computer clock to establish the trigger time in milliseconds.

ACOUSTIC.BEQ

RESET BLOCK

WRITE TO INPUT 1	Channel to sample
WRITE TO INPUT 2	Trigger on voltage level
WRITE TO INPUT 3	Trigger if voltage rising through voltage point
WRITE TO INPUT 4	Trigger voltage level
WRITE TO INPUT 5	Number of pre-trigger points
TIME	Clock time of the start of the experiment, in milliseconds.

A to D LOOP

A TO D	Number of channels to sweep
	Number of scans to take on each channel
	Frequency of sweeps over the selected channels
	Name of data array for digitised data
TIME OF TRIGGER	Clock time, in milliseconds, of the trigger point
TIME OF EVENT	Trigger time minus the start TIME of the experiment for the time of the event after the start of the experiment, in milliseconds.
BINARY WRITE WAVE	Appending the 200 waveform data points to a binary data file, WAVE.BIN.
BINARY WRITE TIME	Appending the double precision data point value for the trigger time of the event.
LINE GRAPH	Updating picture of the acoustic emission waveform. (Deleted for increased acquisition speed).

END

The procedure order for the program sections listed above:

RESET -	started by START BUTTON, run once, starts A TO D LOOP.
A TO D LOOP -	started by RESET BLOCK, loops indefinitely for every event trigger, stops for STOP BUTTON.

Figure 6.2 An outline of the sections of the VIEWDAC acquisition program, ACOUSTIC.BEQ, used to collect acoustic emission events automatically.

The third stage of the sequence was to store the digitised information in permanent memory. The wave data was saved to a binary file, WAVE.BIN and the time of the trigger to another binary file, TIME.BIN. Using direct memory access, binary data moved efficiently into the computer cache memory. The computer then directed the information to the hard disk memory at either moments when there was no sampling occurring, or the cache memory was full. At the high acoustic emission capture rates encountered for most of the experiment, the storage rate was dictated by the later situation.

No processing of the acoustic emission data was attempted at the data acquisition stage since it dramatically reduced the event sampling rate. Extra processing, such as graphical display of the waveform or parameter calculation, reduced the number of events it was possible to capture per second. The rate of computer capture of analogue acoustic emission was relatively low compared to a analogue electronic unit. Therefore only a representative sample of events was captured by the computer controlled VIEWDAC system. There will be some bias in the number of events captured at the later stages of experiments, when acoustic emission event rates were high. At this stage a smaller proportion of the total number of events occurring, were captured compared to the early stages, when all events were spaced sufficiently far a part to be captured effectively. The maximum rate of event capture was about 20 events per second. This was significantly lower than the reported capture rate for an analogue electronic processing system of 6000 events per second [AECL manual].

7   Acoustic Emission Waveform Processing

7.1   Introduction

From the review of previous research relating the acoustic emission waveform to the source mechanism in Chapter 4.4, there are certain waveform characteristics that correlate better to known damage mechanisms than others. A widely used parameter is the amplitude of the acoustic emission waveform. The acoustic emission amplitude is thought to be proportional to the surface velocity of the solid, which in turn is related to the amount of energy imparted to the acoustic emission wave by the failing material. However, these relationships are still only partially understood. Other characteristics of the waveform, such as ringdown count and the rise time to the maximum peak voltage, are also useful descriptors that might be used for differentiating the source mechanisms. These three parameters were used in this work to differentiate and characterise acoustic emission events and group them in an attempt to identify the likely mechanisms of fracture.

There are many more parameters that describe details of the waveform in the time and frequency domain, but these three parameters were felt to describe important waveform characteristics taking into account errors caused by the capture system limitations. The use of parameters such as the duration, energy and frequency domain information, have not been included at this stage since mathematical evaluation becomes more complex and will also be biased due to the measurement system. The limitations imposed by the equipment severely limits the effectiveness of the frequency analysis of the acoustic emission waveforms, particularly when using a resonant transducer and a relatively low sampling frequency A to D board.

An initial trial to separate events using these three parameters alone showed the potential for discriminating clusters of acoustic emission events that had similar waveform characteristics [Priston et al, 1995]. Principal component plots spread acoustic emission event data in the main according to the changing amplitude of the waveforms. The use of a clustering technique then produced a robust test of the event's correct position in a certain cluster.

The details of the program sequence to measure the waveform parameters are described in section 7.2. The details of the mathematics and program package used to cluster the acoustic emission are described in section 7.3.

7.2   VIEWDAC Parameter Calculations

Post processing the binary waveform data was achieved using the VIEWDAC program PARAMETER.BEQ. Each event was analysed separately for the parameters that would be used in the next stage of cluster analysis. Events not clearly captured were rejected at the first stage. The outline structure of this program, PARAMETER.BEQ, is shown in figure 7.1.

The 200 point digitised waveform was read from memory (WAVE.BIN) and checked by the software as being a true (good) event. Electronic spikes from other electrical equipment were captured and rejected at this stage of processing. In addition, events with distorted first data points need to be excluded. Some of these events were caused by the A to D board dwelling on the negative rail and the first point being recorded as -2.5V. Events caught after the beginning of the event were excluded and the next event processed. To ascertain the true start of an event, the initial few sampled points were checked. By counting the number of threshold crossing in the first 5µs, provided a check that the event had started inside the digitised window. The threshold was set to 0.1V, (relatively high for an acoustic event), so if there were threshold crossings then an event had already started prior to the data window opening. The background noise was below this threshold so should not trigger the system.

The event was analysed as a data array of 200 voltage points. The maximum and minimum voltage points were located in the array by a set command in the VIEWDAC functions. The magnitudes and positions were noted. The difference between maximum and minimum values was the waveform peak to peak amplitude (PA). The value per event was quickly and efficiently saved to a binary file (P_P.BIN). There was an upper limit to the maximum amplitude set by the A TO D board (±5V) when acquiring data. Any differences in amplitude of the more energetic

PARAMETER.BEO

WAVEFORM VALIDATION

READ BINARY WAVE DATA INTO 200 POINT ARRAY
READ BINARY TIME 1 POINT ARRAY

REJECT EVENT AND READ NEXT WAVEFORM DATA IF ONE POINT IN THE FIRST 10 BITS OF DATA IS

      1)   < -1 VOLT   *A to D board dwelling on the negative rail*
      2)   > 0.1 VOLT   *waveform of event already started*

RECALCULATE TRIGGER TIME TO THRESHOLD CROSSING IN FIRST 10 POINTS

PARAMETER CALCULATIONS

PEAK AMPLITUDE -   Maximum and minimum points in the wave array

PEAK TO PEAK AMPLITUDE = Voltage difference between max. and min. peaks

RISETIME = Array position difference between TRIGGER point and first max or min PEAK

RINGDOWN COUNT -   Array position that has a positive going voltage greater than the threshold voltage

ENERGY -   Integral of the whole WAVE array

DURATION -   Position differences between TRIGGER and last RINGDOWN position

CONVERSION OF ARRAY POSITION TO MILLISECONDS

DATA SAVING

BINARY WRITE to separate files =   EVENT NUMBER
                                      PEAK TO PEAK AMPLITUDE
                                      RISETIME
                                        RINGDOWN COUNT
                                        ENERGY
                                        DURATION

END

Figure 7.1 An outline of the VIEWDAC program, PARAMETER.BEQ, used to process the acoustic emission data automatically.

acoustic emission would not be recorded by this capture system. The majority of events were between ±1V, and so unaffected.

To measure the number of oscillations in the acoustic emission waveform (ringdown count), a threshold crossing command was swept through the data array to indicate the array positions where the values were above the set voltage level. The threshold value for this data analysis was set at 0.01V. The first crossing was taken as the modified start of the event. The trigger time (TIME.BIN) was corrected for any change. The subsequent crossings were taken as the number of ringdown counts (RD), or positive oscillations in the waveform. The number was rapidly stored to a binary file (RINGDOWN.BIN).

The risetime (RT) was the time between the first threshold crossing, the start of the event, and the maximum or minimum voltage peak which ever was the first to occur. Times were measured in milliseconds. The values were saved to a binary file (RISETIME.BIN).

For completeness, an extended processing program sequence calculated other waveform parameters. The parameter calculations investigated the flexibility and bias of the VIEWDAC system to extend the number of parameters possible with the current sets of acoustic emission data. For example, the energy content of the waveform was calculated from the integral function for the 200 data point array. There was no attempt to stop the calculation at the end of short events since the low amplitude signal tail should add very little to the total energy content. Further programme developments may be able to use another comparison command to stop the calculation after the threshold has not been exceeded for a set number of points. The energy calculation was dependent on the true representation of the event within the time window. Truncated or large amplitude waveforms seriously affected the true energy result. Another parameter, event duration was limited by the static window width of 200µs. The event duration measure saturated at 200µs for larger events which might take a longer time to decay below the threshold value and so end outside the 200µs window. The waveform parameters- energy and duration were severely

61

affected by the time of the sampling window and the measured end of the event. Therefore, these two parameters were not used for cluster analysis.

The VIEWDAC system was capable of developing the mathematical equations required to calculate any parameter desired. This includes transformations of data into the frequency domain. The limitation on the parameters calculated was due to the data quality. The range of acoustic emission parameters used reflected the limited time window per digitised event, the maximum voltage of the A to D board and the sampling frequency in relation to the transducer resonant frequency.

7.3   Cluster Analysis

The three parameters selected to be the input data for the clustering program were peak to peak amplitude (PA), ringdown count (RD) and risetime (RT). It was felt from the possible parameters available that these had the best possible range of values to discriminate different fracture source mechanisms within the composite material. The parameters were also calculated with a certain amount of completeness and accuracy from the digitised waveform.

Due to the different units of measurement, the range of values for the three parameters would bias the analysis to the larger values. Therefore the parameters were standardised or normalised [Everitt (1991)]. Standardisation converted the original variables into ratio values.

The standardisation of the parameters, z_{if}, is

$$z_{if} = \frac{x_{if} - m_f}{std_f} \qquad (7.1)$$

Where m_f is the mean for the parameter set f and std_f the standard deviation.

Standardisation of the data assumes equal weighting for all variables. No one parameter was any better at differentiating the different clusters of source mechanisms. Standardisation is a good approximate starting point when the exact relationship between parameters is not known. The standardised data is also the input data for principal component analysis discussed in section 7.4.

62

To measure the similarity or dissimilarity between events, the events were placed in a three-dimensional space corresponding to the three waveform parameters. A standardised data point was individually compared to all remaining standardised parameters to quantify the dissimilarity between each event. This was called the Euclidean distance. For the situation described, an event in a 3 dimensional space with the corresponding three descriptive parameters (M=3), has an Euclidean distance, $d(i,j)$, between two events (x_i and x_j), as follows,

$$d(i, j) = \frac{1}{M}\sqrt{(x_{i1} - x_{j1})^2 + (x_{i2} - x_{j2})^2 + (x_{i3} - x_{j3})^2} \qquad (7.2)$$

Partitioning the data into clusters required the calculation of the degree of best fit for the event into a particular cluster [Everitt (1993)]. Randomly placing the events into initial clusters does not predispose any event to a particular cluster. The mathematical test used to decide where an event is to be placed and retained in a cluster, was the sum of squares test. For the location of an event to be accepted it must either enhance the degree of cluster separation or be better than placing it in any of the other clusters available.

Each cluster was described by the position of the centroid point. This location is the average value in each of the directions of the M-dimensional space. The coordinate for the centroid using one of the variable dimensions, f, is:

$$E_p \quad \frac{1}{M}\sum_f (x_{if} - u_{pf})^2 \qquad (7.3)$$

Where E_p was the sum of squares for the cluster p, and u_{pf} the mean value for the variable f in cluster p. This is repeated for the other two parameters.

The degree with which the events were best placed in a certain cluster was assessed by the value of the error sum of squares (ESS). This was the comparison of

the sum of squares of Euclidean distance between the events in the two clusters p and q, relative to the position of the cluster centroids. To eliminate the effect of the event in the old cluster p the calculation is done without the presence of the event (x), thus producing the new centroid E_p. The new cluster (q) centroid position is found with the event included and the errors for the distances between event locations and the new centroids calculated E_q. If the location of the event in that cluster produces a centroid that is more central to the events in the cluster, then the spread of members is reduced which is desirable.

$$I_{pq} = E_{p+q} - E_p - E_q \qquad (7.4)$$

I_{pq} represents the extent to which there is scatter about the centre of the clusters. Therefore, it is desirable to have a lower value for I_{pq} for the new event cluster location to be accepted.

This requirement for position acceptance is summarised by the dissimilar coefficient for the event, calculated for its location in the two clusters:

$$d_{PX}^2 > d_{QX}^2 \qquad (7.5)$$

It is acceptable when the error sum of squares is lower in the new position than for the old cluster:

$$I_p - I_{p-x} > I_{q+x} - I_q \qquad (7.6)$$

This procedure promotes spherical clusters with a core number of representative results for each cluster.

7.4   Principal Component Analysis

To present the cluster analysis data clearly, the membership of an event to a cluster was plotted using principal component values. It is possible to present the data directly using the Euclidean distance data in a three dimensional plot of the three

64

waveform variables used. This would produce a complex and distorted view of the relationships between events depending on the viewing direction. The principal component analysis reduces the three separate variable values to a single representative value. This principal component value reflects the relationship of the events' variables to the complete variation in the data.

For the set of data, each point (event) is described by M or three variables. Principal component analysis projects the point in the three-dimensional space on to a new axis, (see figure 7.2). The distance from a point to the axis line is the Euclidean distance calculated for the three dimensions. The best fit of the axis position is calculated by minimising the squared distance (b^2) to the line, or this is equivalent to maximising the sum of the squared projections (c^2) on to the new axis.

The first principal component axis has the greatest variance between extreme new point positions on the axis. This spreads the population of events and describes the greatest difference in the three parameter values per acoustic emission event. The second principal component axis is orthogonal to the first, again with the maximum spread of the points along the axis.

7.5   CLUSTAN Program Requirements

Figure 7.3, lists the program commands used to cluster the acoustic emission data using the computer analysis package CLUSTAN [Clustan ltd, Wishart]. The method of clustering, described above in section 7.3, uses the minimisation of the error of the sum of squares of the Euclidean distance between the cluster centroid and the events in the cluster. The data file that contained the acoustic emission variables for the three dimensional space: peak to peak amplitude (PA), ringdown count (RD) and risetime (RT), also contained additional superfluous columns of data such as event number and other waveform parameters. Therefore, only parameters of interest were read into the program using the command:
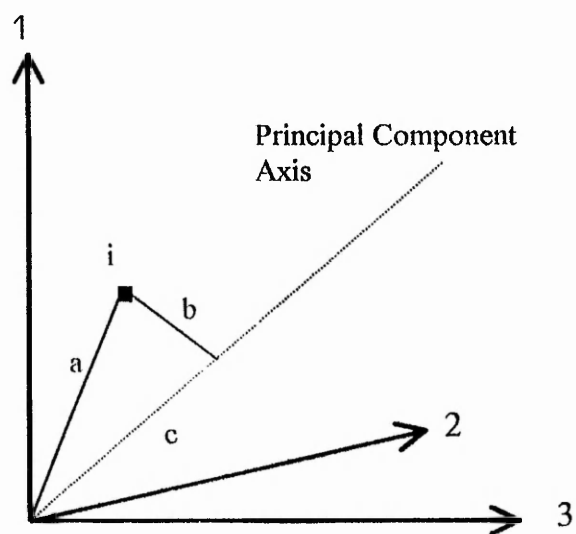
For each point i,

b=distance of i from new axis,

c=projection of vector i onto new axis,

a=distance of point from origin.

Figure 7.2 Projection of data on to new principal component axis
(Taken from Murtagh and Hech (1987), page 19).

CLUSTAN PROGRAM

assign file=data spec=f60_10d.dat   *reading in 998 rows of data from ASCI file*
read data variables continuous 1-7,cases 998 infile=data
standardisation
mask variables 1-2,6,7   *using only variables 3,4 and 5*
calc factor scores, factors=3   *Principal component analysis*
select graphics device

CLUSTER ANALYSIS

relocate coef 24, start random size=10
relocation remove maxit 20, fusion min 3

GRAPHICS OUTPUT
scatter Cplot axes outlines, class code 6,
Xaxis factor 1 label = 'glass/polyester 0 degrees factor 1',
Yaxis factor 2 label = 'factor 2   5 clusters (pa,rd,rt)',
dimension y = 7 x = 5.5
scatter Cplot axes outlines, class code 8,
Xaxis factor 1 label ='glass/polyester 0 degrees factor 1',
Yaxis factor 2 label = 'factor 2   3 clusters (pa,rd,rt)',
dimension y= 7 x= 5.5
scatter Cplot axes outlines codes, class code 6,
Xaxis factor 1 label = 'glass/polyester 0 degrees factor 1',
Yaxis factor 2 label = 'factor 2   5 clusters (pa,rd,rt)',
dimension y = 7 x = 5.5
scatter Cplot axes outlines codes, class code 8,
Xaxis factor 1 label = 'glass/polyester 0 degrees factor 1,
Yaxis factor 2 label = 'factor 2   3 clusters (pa,rd,rt)',
dimension y = 7 x = 5.5

DATA SAVED TO FILE
print results clas norm numb pca factor=3 statistics

stop

Figure 7.3 CLUSTAN program commands used to cluster the acoustic emission data, graphically display results and output results to a data file.

Assign file=data, spec=f60_10d.dat

Read data variables continuous 1-7, cases 998 infile=data

Mask 1-2,6-7

Standardisation

This selected the first 998, non binary cases or rows of data, in the data file called f60_10d.dat. The program then standardised the data of interest in columns 3 to 5 by masking or hiding unwanted data in columns 1, 2, 6 and 7. The standardised data had a zero mean value and unit standard deviation. For clear graphical representation of the clusters, the first two principal component scores were used as the axis coordinates. The command to calculate the first three principal components (PC1, PC2 and PC3) is as follows;

Calculate factor scores, factor=3

The command that actively clusters the data is **'Relocate'**. The relocation calculation for all events was performed by the following command,

Relocate, coefficient 24, fusion min 3, start random size 10, relocations remove maxit=20

The method used to calculate the positions for the events was the Euclidean sum of squares (**coef= 24** for continuous variables). The initial allocation of events was into 10 random clusters. After the cluster allocation, the program attempted to optimise the positions of the events in the 10 clusters. If the process did not converge to a natural optimum then the attempt was stopped at 20 iterations (**maxit=20**). The command **'remove'** ensured that the event was moved to the new cluster before the dissimilarity calculation for the two clusters was calculated. The reduction in the number of clusters from the initial 10 was done by fusing the two most similar clusters together. The location of every event in the new nine clusters was checked again for the best possible placement. Events were moved if a better solution was found. The result at each cluster level is placed in a temporary computer list CLASS$ as the next set of results.

The results were saved to an output file using the commands:

Print results, Classifications numbers, PCA statistics factors=3

A summary record of the clusters and a list of the principal component factor scores for the first three components were written to a results data file. The principal component statistics of eigenvalues and percentages, as well as the cumulative variance, were saved. The name of the results data file was entered at the initial program prompt to run the CLUSTAN package.

It was possible to graphically display results using the CLUSTAN commands below;

Select graphics device
Scatter, Xaxis factor 1, Yaxis factor 2,
Splot axes codes outlines, Classification code 5
Dimensions x=9, y=12

The graphics device was automatically set by the VAX operating system. The default black pen plotter was of poor quality so the plots are not reproduced here. The scatter plots were plotted after the clustering program had finished. The VAX command used was "$ CLUSPLOT". The data was displayed using the first two principal component values per event (**Factor 1 and 2**). The marker for each event was its cluster number. The outline could be drawn around the limit of each cluster. The number of clusters displayed was controlled by the '**classification code**'. The value '**5**' relates to the fifth data set calculated and placed in the $CLASS list. In this example, the fifth fusion level had six clusters. The classification code for the 3-cluster level would be code 8.

7.6   Conclusion

The success of clustering acoustic emission data to reveal damage mechanisms relies on the assumption that the source fracture mechanism in the composite material imparts to the wave signal certain characteristics that are useful for distinguishing the

different mechanisms. These characteristics must still be recognisable after travelling through the composite material and after being detected.

Acoustic emission events will be placed in clusters depending on calculations based on the initial data set containing the acoustic emission amplitude, ring down count and risetime values. With the best available data, clustering draws together data with similar features. The use of the Euclidean sum of squares criteria results in clusters approximating spheres of influence. The events nearest the centroid determine the mean parameters for that cluster. Events at the periphery and near other cluster domains are not as well matched to the ideal values for that cluster. Therefore the events near cluster boundaries are more prone to being misplaced and assigned the wrong source mechanism.

Clearly, these parameters contain information on basic microfracture mechanisms operating at points in the composite material. A tearing type of source might be expected to demonstrate long duration, while a short impulsive microfracture associated with a high stress might be expected to show peak amplitude and short risetime. As the discussion in section 4.4.3 indicated, Lamb wave dispersion and scattering of the stress wave will affect the detected acoustic emission when the source is some multiple of the sample thickness away from the transducer. These distortions to the waveform are relatively small compared to the distortions likely to be encountered when testing a composite material storage vessel, where the source to transducer distance will be many times the composite wall thickness. Clustering analysis attempts to deal with these distortions by looking at a large population of data and looking for similarities.

8   Results and Discussion of Acoustic Emission Tests

8.1   Introduction

The acoustic emission signals from various composite materials were collected and processed as discussed in Chapter 6. The material had different fibre orientations, 0°, 10°, 20°, 30° and 45°. The changing reinforcing fibre angle produced material with differing material strengths. It was anticipated that the different fibre positions relative to the loading direction would produce different amounts of damage as well as different damage mechanisms. The results from the experimental work with various fibre angles were analysed to distinguish clusters of similar events.

Experimental evidence was collected and processed from different batches of composite material made from glass fibre and polyester resin matrix. The specimens were cut from unidirectional single ply material. The unidirectional ply composite material was approximately 3.91 ±0.4mm thick and the dimensions of the rectangular test specimens approximately 25mm x 200mm. The difference between the specimens was the angle of the fibres with respect to the main material axis. The composite material was tested to failure or to the test machine load limit. The acoustic emission was monitored using a single central transducer. Details of the method of material preparation and the experimental method are given in Chapters 5 and 6 respectively. A selection of the data for different fibre angles is reproduced here.

The digitised acoustic emission waveforms were post processed to obtain the characteristic waveform parameters of peak to peak amplitude (PA), ringdown count (RD) and risetime (RT). Details of the techniques used to measure the characteristic waveform parameters are given in Chapter 7. The parameter file for each specimen was analysed by a clustering package using clustering techniques and principal component analysis to form groups of acoustic emission events.

Results from these experiments are discussed in the following section. The significance of certain acoustic emission clusters and the state of the material from the observed stresses being applied to the specimen will be discussed.

8.2 The Clustering of Acoustic Emission Events

The experimental data in the form of three variables per event was too cumbersome for similarities between events to be obvious in a 3-D plot. The use of principal component analysis helped to clarify the nature of the data. A 2-D graph displayed the three dimensional relationships for the three acoustic emission parameters. The events that have comparable waveforms and hence similar source mechanisms have similar principal component values and are placed in a similar part of the scatter graphs.

Extending the analysis further than the principal component analysis, the cluster analysis actively compared each event with the other events and brought together similar data. The experimental evidence for different source mechanisms producing waveform characteristics that are different relied on the cluster analysis resolving differences between acoustic emission waveforms.

Initially the cluster analysis resolved the data into the number of requested clusters. The CLUSTAN program segmented the data into 10 clusters. In figure 8.1, the separation of the data can be seen between the 10 and 3 cluster level for a specimen with fibres at 10° to the loading direction. At each cluster stage the most similar clusters were amalgamated, and then the repeated active testing of each acoustic emission event for its compatibility in the new clusters was re done. As displayed in figure 8.1, a high number of clusters separate the data into small areas with some overlap of the data.

The number of clusters was reduced to three to reflect the suggested mechanisms of matrix cracking, fibre debonding and fibre breakage. It was questionable whether there would be ten distinctly different mechanisms, producing ten separable waveforms, producing the ten clusters of events. The clustering was initiated at the 10-cluster level so as not to force the position of events located at the cluster boundaries into the wrong cluster. From the discussion in Chapter 4, concerning the damage in composite materials and its detection using acoustic emission, there were likely to be only three main damage mechanisms. These mechanisms were the cracking of the matrix material the debonding of fibres from the resin. The third mechanism of fibre breakage was likely to be limited to the higher stress levels towards the specimen failure point or due to sporadic failure at lower
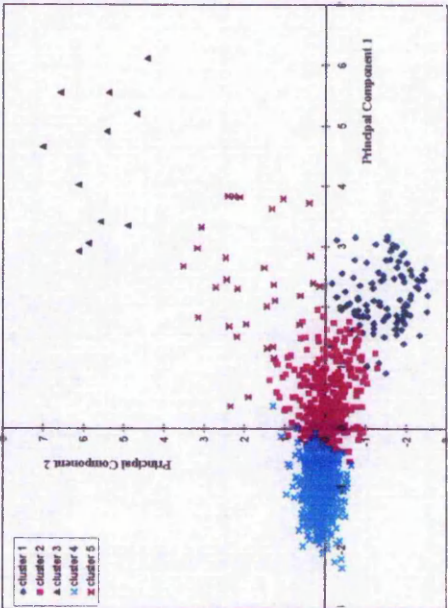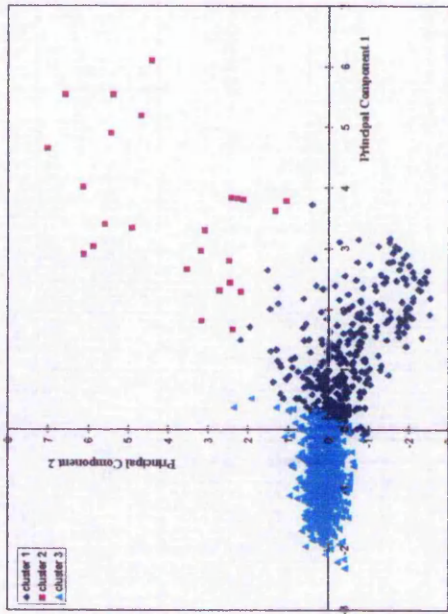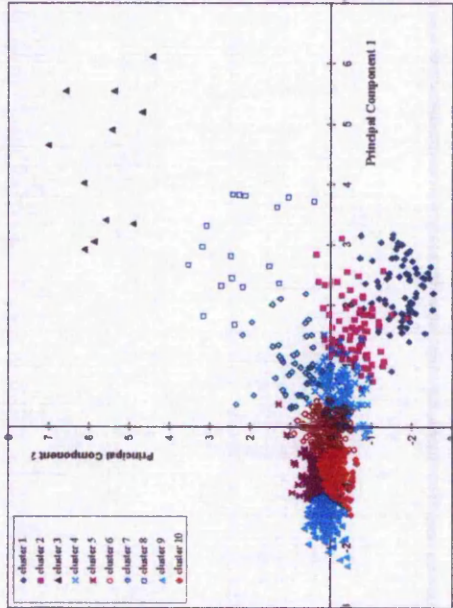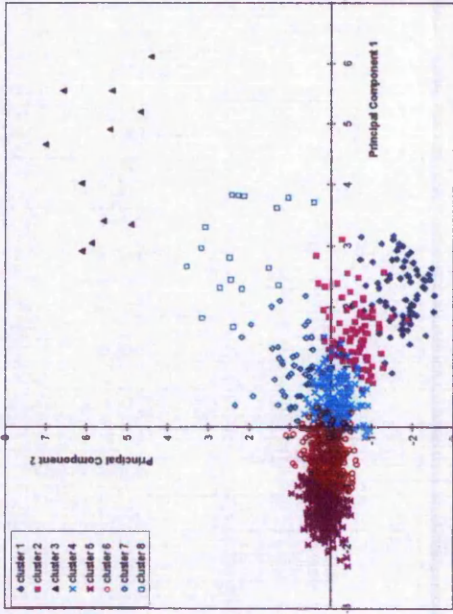
Figure 8.1 Cluster level reduction from a) 10 clusters, b) to 8 clusters, c) to 5 clusters d) to 3 clusters.

stress levels. The appearance of fibre debonding signals would also be expected to depend on the fibre orientation.

The relative positions of the clusters on the principal component graphs for different fibre angles show a consistent trend. Part (a) of figures 8.2 to 8.6 shows the clustering of acoustic emission events for the fibre angles of 0°, 10°, 20°, 30° and 45° respectively.

Cluster 3 events have more in common with the Cluster 2 events and are located far from Cluster 1 events. The figures show systematic separation of the events into clusters, with clusters showing some adjustment of position relative to the first two principal component axes with fibre orientation.

On closer examination of the waveform parameters per event in each cluster, the reason for the separation is most striking in the magnitude of the amplitude of the acoustic emission events. In Table 8.1 the average amplitude, ringdown count and risetime for the samples are recorded. A graphical representation is shown in figure 8.7. An overall trend can be seen for the clustered data from various fibre orientations. Cluster 1 (black, figure 8.7) has the largest peak amplitude, marginally larger ringdown count and longer risetimes. Cluster 3 (green) is at the other extreme with small peak amplitude, a small number of ringdown counts and quick risetimes. Cluster 2 (red) is between theses two extremes.

It is observed that there is a trend in the average values per cluster between the experiments using composite material with fibre orientations 0°, 20° and 30°. The average peak amplitude for a cluster decreases with increasing fibre angle. Likewise the average ringdown count decreases with increasing fibre angle and the risetime is observed to increased with increasing fibre angle. This may be due to changes in the material properties for different fibre angles affecting the attenuation path of the acoustic emission. This change to the acoustic emission signal was reported by Lorenzo and Hahn (1988). They reported that the amplitude of an acoustic emission event was dependent on the orientation of the fibre reinforcement under the transducers attached to opposing fibre orientations in a crossply composite material. The greater amount of damage in the 90° material within the matrix caused a reduction of the acoustic emission amplitude.
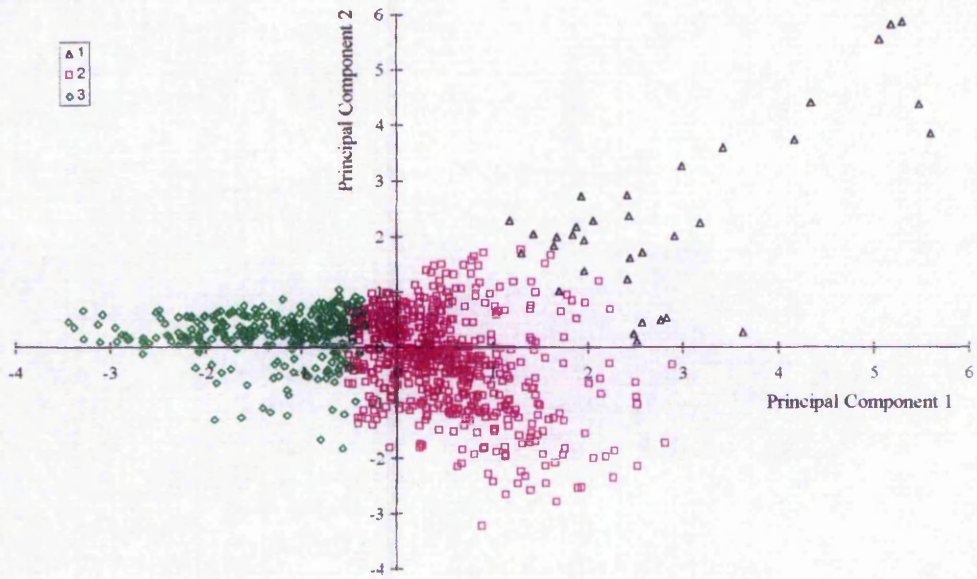
(a)
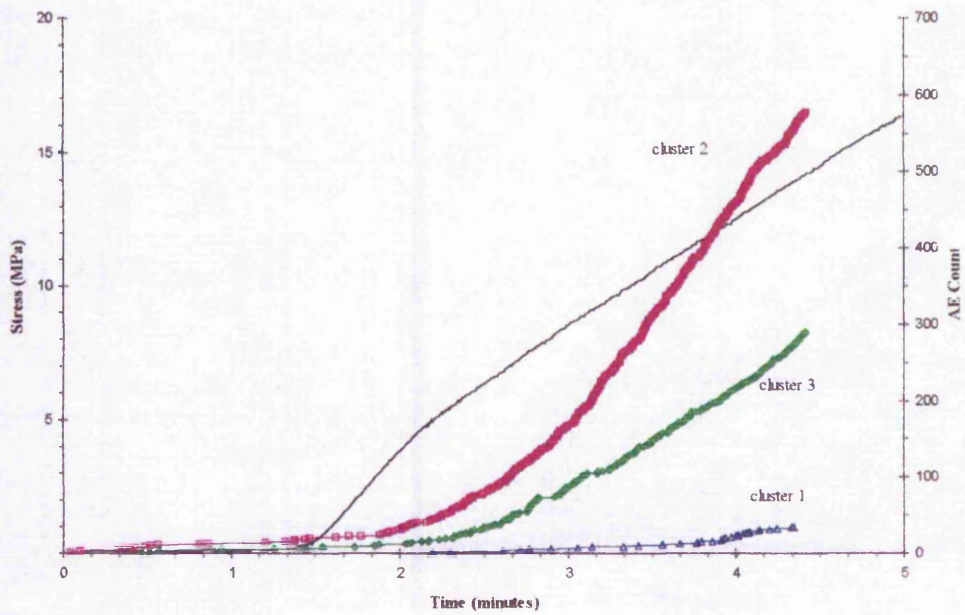
(b)

Figure 8.2 Acoustic emission results for 0° composite material, (a) principal component representation of cluster data, (b) stress and cluster arrival times. Transducer resonant frequency 375kHz.
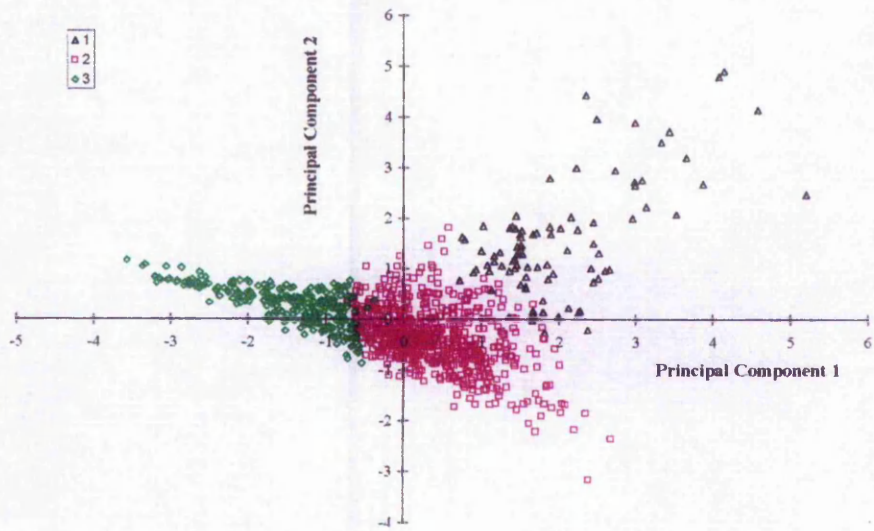
(a)
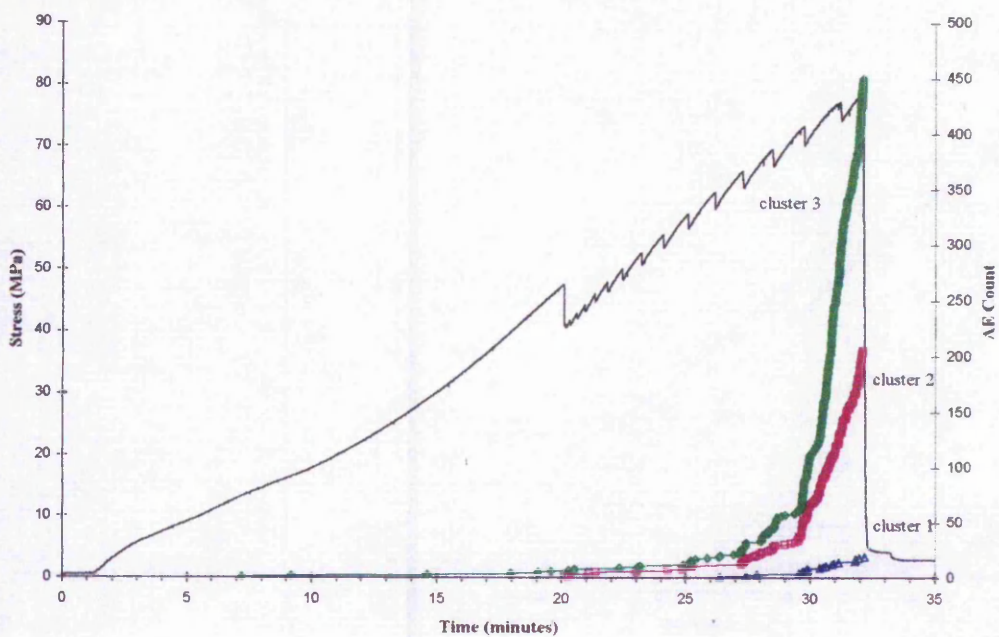
(b)

Figure 8.3 Acoustic emission results for 10° composite material, (a) principal component representation of cluster data, (b) stress and cluster arrival times. Transducer resonant frequency 175kHz.

(a)

(b)
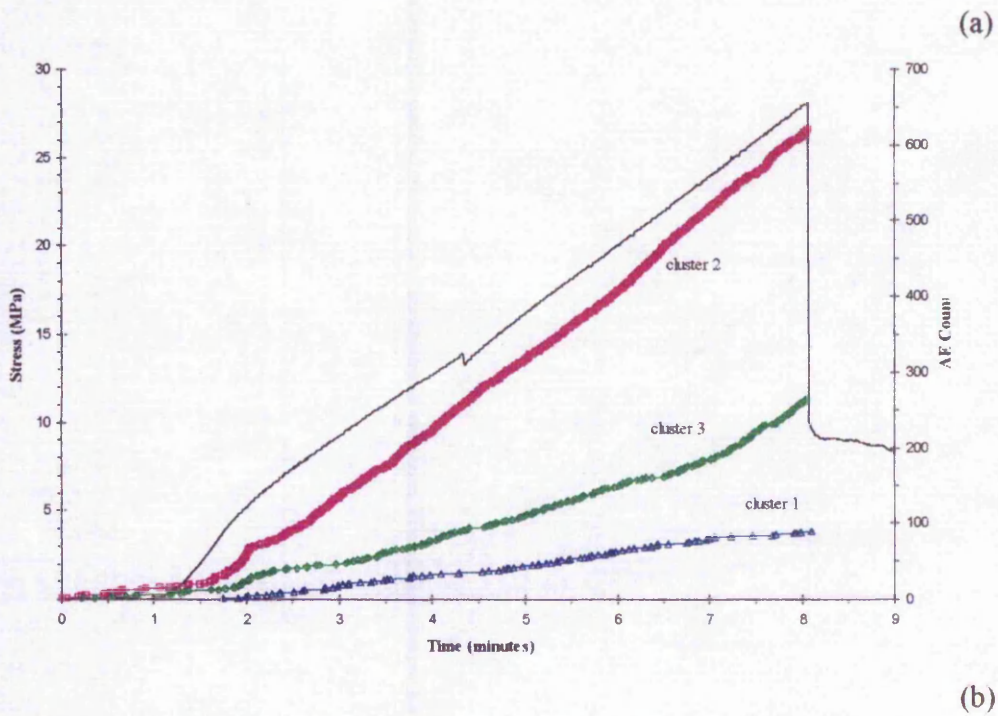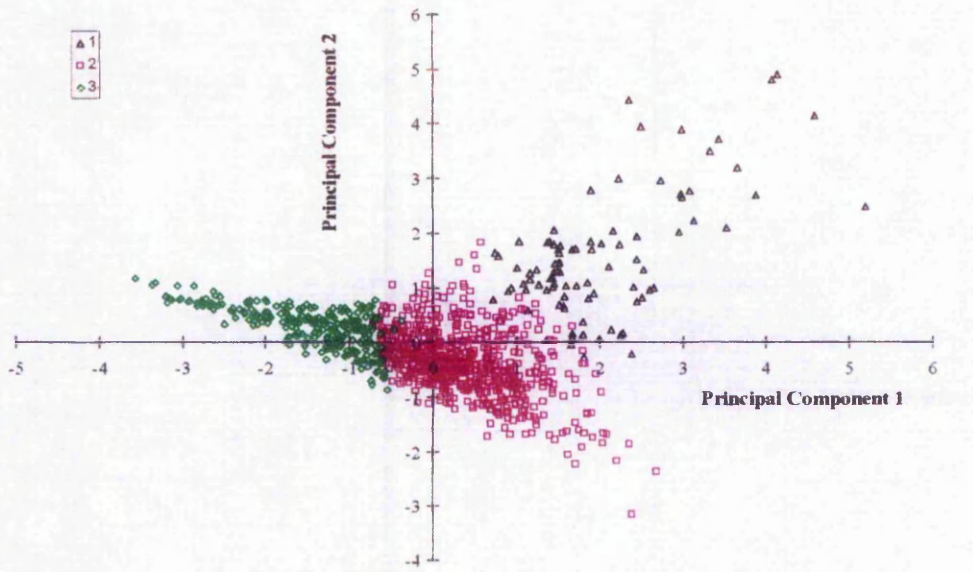
Figure 8.4 Acoustic emission results for 20° composite material, (a) principal component representation of cluster data, (b) stress and cluster arrival times. Transducer resonant frequency 375kHz.
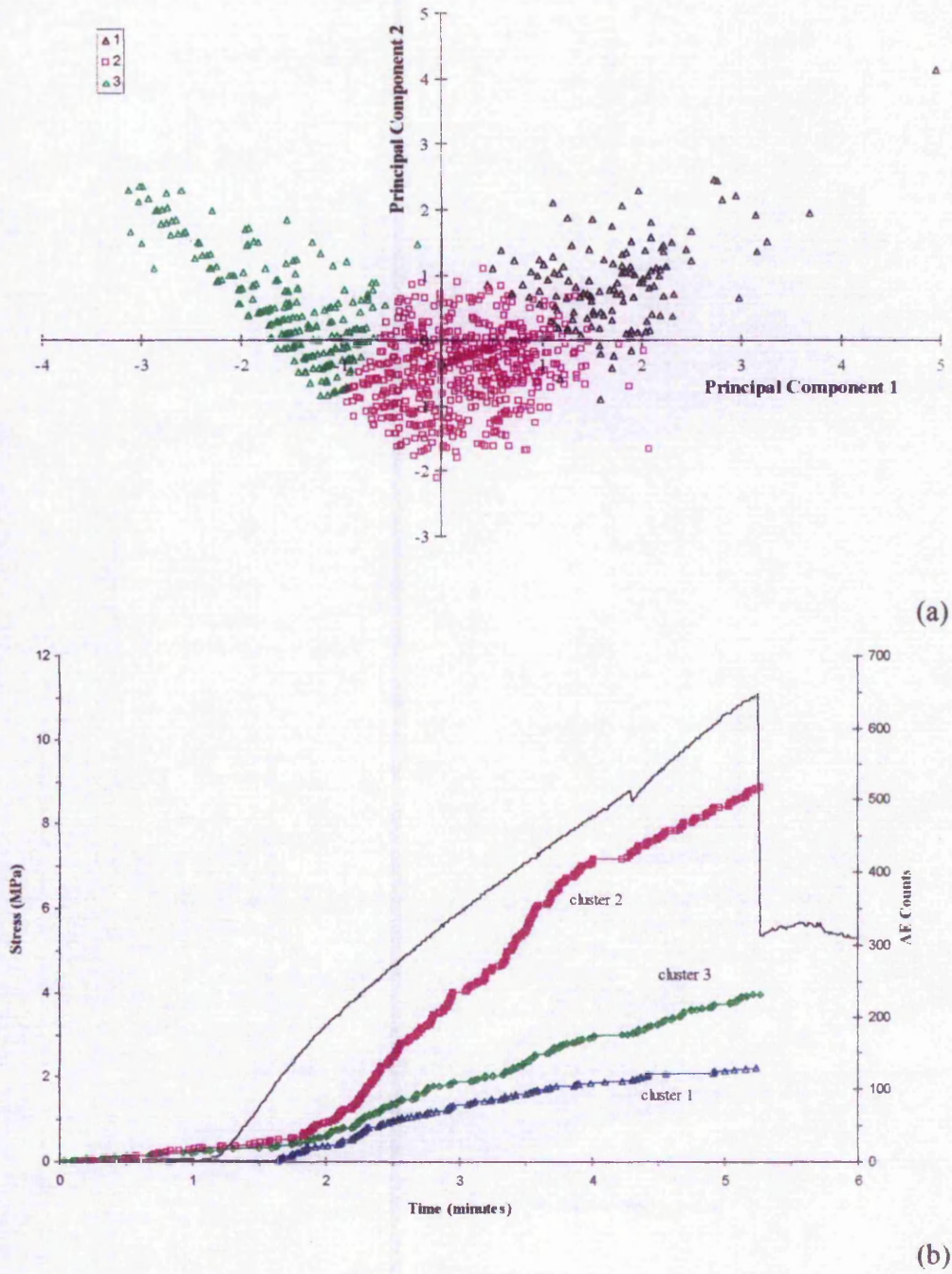
Figure 8.5 Acoustic emission results for 30° composite material, (a) principal component representation of cluster data, (b) stress and cluster arrival times. Transducer resonant frequency 375kHz.
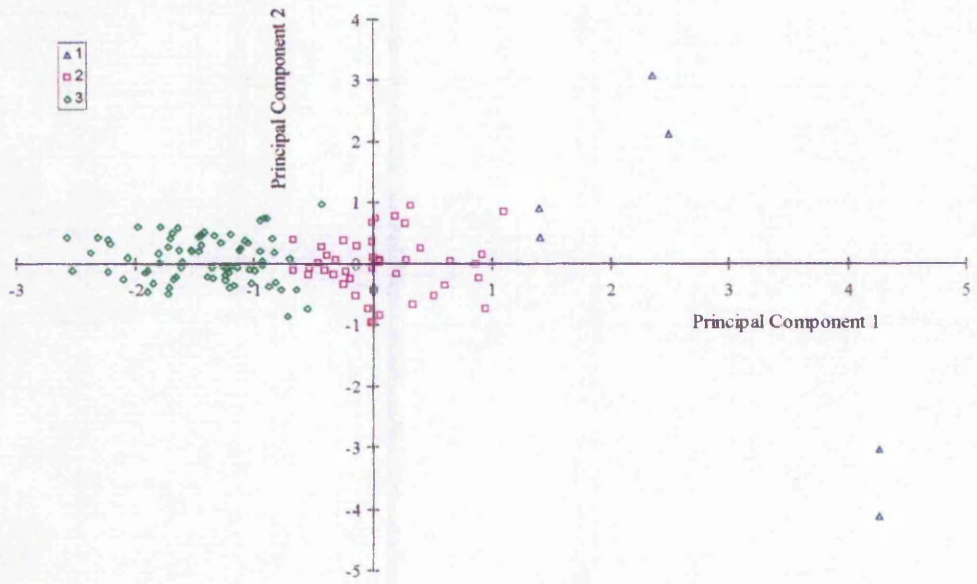
(a)
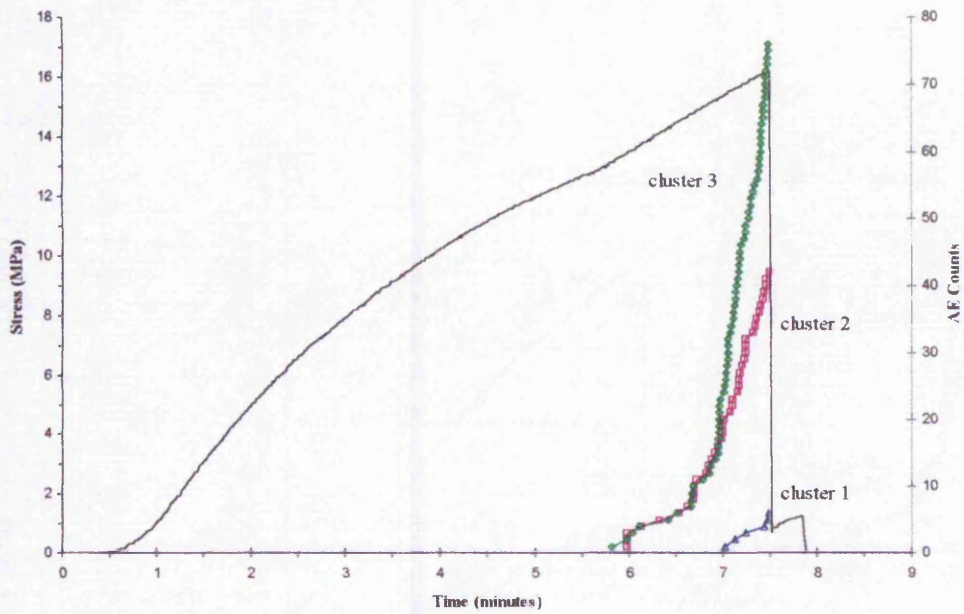
(b)

Figure 8.6 Acoustic emission results for 45° composite material, (a) principal component representation of cluster data, (b) stress and cluster arrival times. Transducer resonant frequency 175kHz.
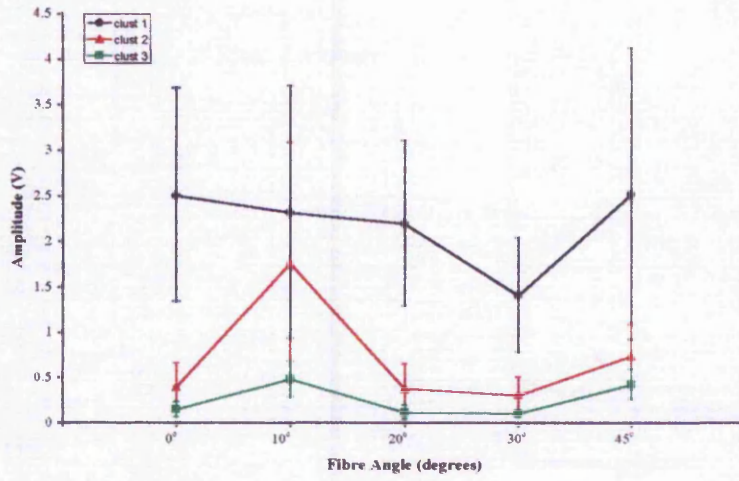
(a)
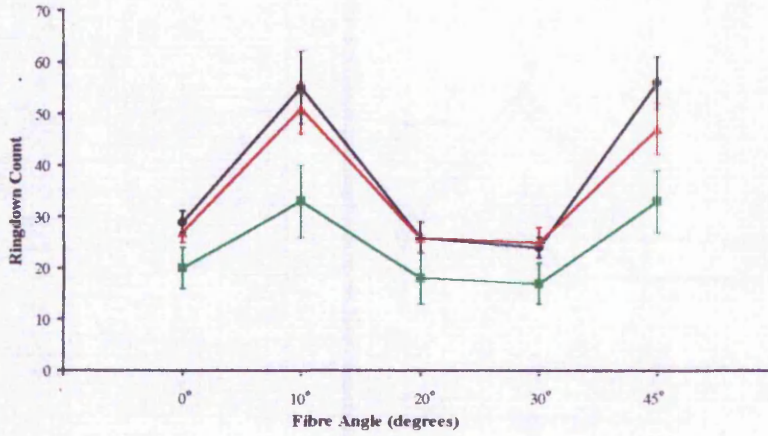
(b)
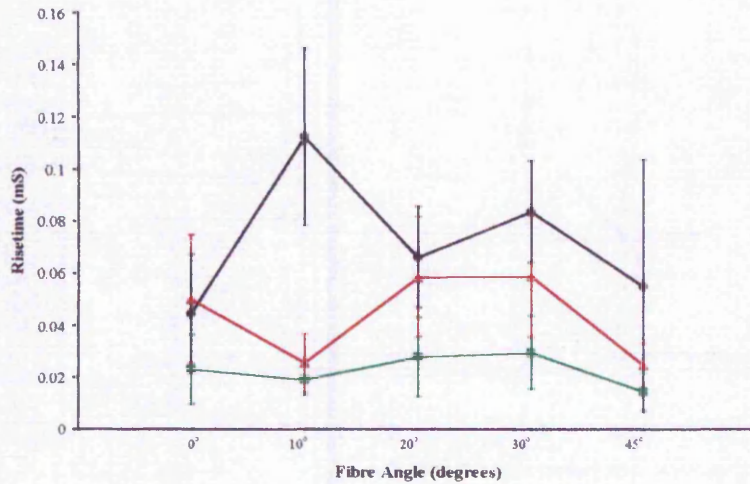
(c)

Figure 8.7 The average cluster values for (a) amplitude, (b) ringdown count and (c) risetime for the experiments with different fibre orientations.

The damage seen in these experiments for the larger 30° composite material may have caused a similar reduction in the acoustic emission wave amplitude.

Large magnitude, high ringdown count and long risetime dominate the events in Cluster 1. The events for the Cluster 3 events are comparatively much smaller in amplitude and number of ringdown counts. The dominance of the amplitude to separate the acoustic emission in to clusters has been reported by other workers when differentiating different source mechanisms. For example Bhat *et al* (1994) have seen that high amplitude events are linked with the occurrence of significant damage.

Further evidence of the dominance of the amplitude data in differentiating the clusters of events is the numerical Eigen value results of the principal component analysis. The Eigenvalues for the five different materials are summarised in Table 8.2. From the Eigen values per event, calculated by the principal component analysis, the dominance of the peak amplitude can be clearly seen, over 50% for all fibre angles. The ringdown count makes up a greater proportion of the Eigen value than the risetime values, 20%-30% compared to less than 22% respectively.

It should be noted that transducers with different resonant frequencies have been used for some of the experiments. There is a marked difference between the experiments carried out using the two transducer frequencies. The average values of particularly the ringdown count are higher in the 10° and 45° material experiments, (see figure 8.7 where 175kHz transducer has been used). The use of the 175kHz transducer has altered the representation of assumed comparable acoustic emission waveforms coming from similar damage mechanisms in the composite material.
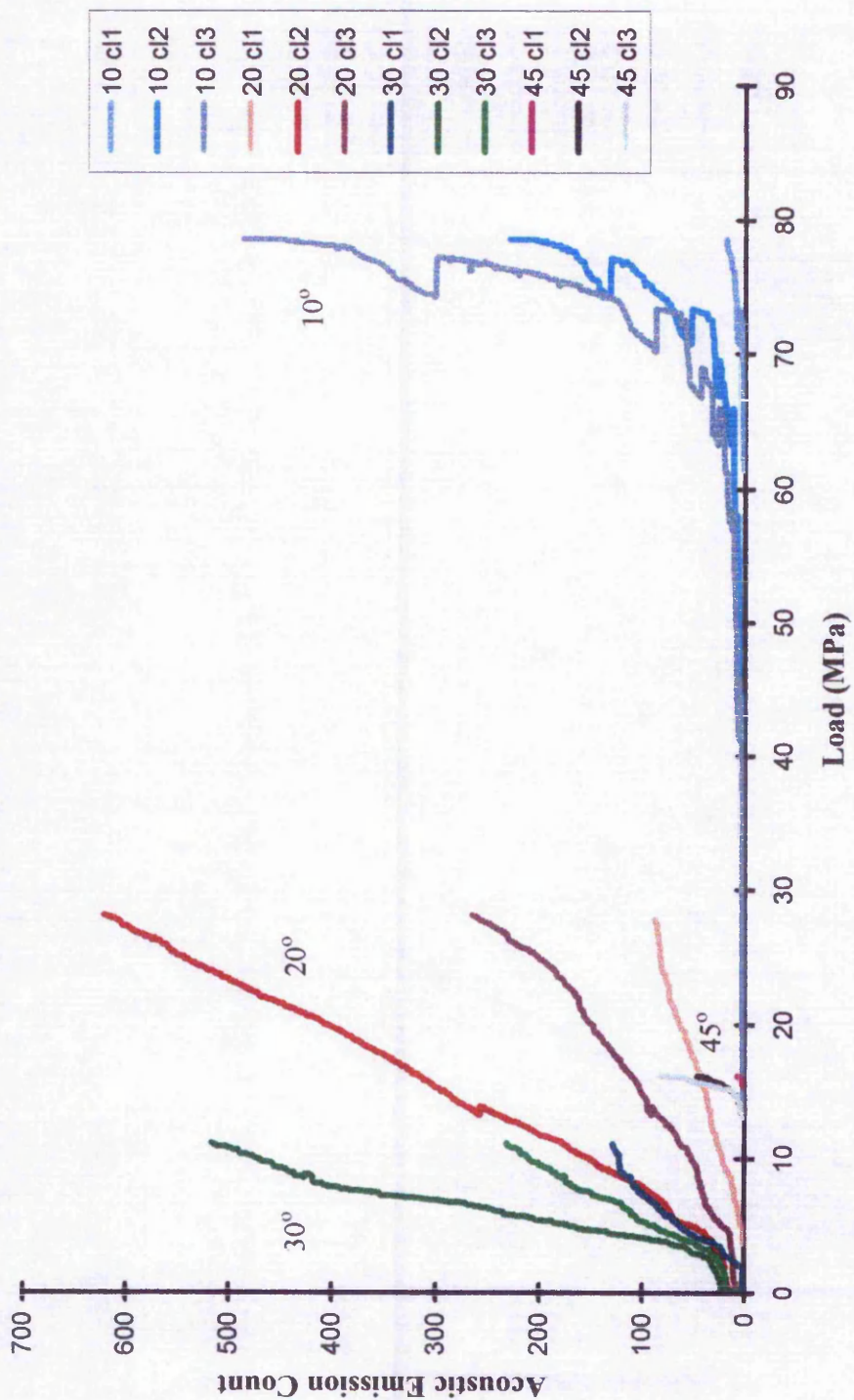
Figure 8.8 Summary of acoustic emission cumulative occurrence plotted against load.

Specimen	Amplitude (PA)			Ringdown Count (RD)			Risetime (RT)		
	Volts			Count			Ms		
Cluster	1	2	3	1	2	3	1	2	3
0° (375kHz)	2.508 (1.170)	0.398 (0.261)	0.146 (0.083)	29 (2)	27 (2)	20 (4)	0.0444 (0.0227)	0.0499 (0.0247)	0.0229 (0.0134)
10° (175kHz)	2.318 (1.385)	1.761 (1.318)	0.479 (0.198)	55 (7)	51 (5)	33 (7)	0.1124 (0.0340)	0.0254 (0.0113)	0.0189 (0.0060)
20° (375kHz)	2.195 (0.908)	0.376 (0.273)	0.117 (0.077)	26 (3)	26 (3)	18 (5)	0.0661 (0.0194)	0.0586 (0.0230)	0.0278 (0.0154)
30° (375kHz)	1.408 (0.629)	0.304 (0.196)	0.098 (0.039)	24 (2)	25 (3)	17 (4)	0.0835 (0.0196)	0.0588 (0.0236)	0.0294 (0.0141)
45° (175kHz)	2.517 (1.599)	0.739 (0.348)	0.424 (0.164)	56 (5)	47 (5)	33 (6)	0.0550 (0.0484)	0.0245 (0.0084)	0.0144 (0.0073)

Table 8.1 Average values for the waveform parameters per clusters, (standard deviations in brackets). Different transducer frequencies are shown in column 1.

Fibre angle	Eigenvalues (Proportion %)		
	Peak Amplitude (PA)	Ringdown Count (RD)	Risetime (RT)
0°	1.51 (50.24)	0.90 (30.03)	0.59 (19.73)
10°	1.55 (51.74)	0.93 (30.84)	0.52 (17.42)
20°	1.56 (52.14)	0.76 (25.34)	0.68 (22.52)
30°	2.03 (67.64)	0.80 (26.82)	0.17 (5.55)
45°	1.99 (66.39)	0.59 (19.58)	0.42 (14.02)

Table 8.2. Eigenvalues (proportional percentages in brackets), from the principal component analysis (PCA) of the acoustic emission waveforms.

8.3 Further Discussion of Acoustic Emission Results from Composite Material Testing

The cluster analysis has separated the acoustic emission events into groups containing strong similarities. The clusters plotted on principal component axes confirm the two analysis techniques can bring together acoustic emission events with similar waveform characteristics. Relating the clusters to deformation mechanisms has relied on the observation of the arrival time and material stress. From the stress/strain value at the time of the event it has been possible to relate the Cluster 1 events with the periods of significant damage and damage mechanisms associated with fibre debonding and breakage, causing visible changes to the material modulus. Cluster 2 and 3 events were noted to occur throughout the experiment, which would correspond to matrix deformation that occurs throughout the loading history. The distinction between Cluster 1 events and Cluster 2 and 3 events was due predominantly to the influence of event amplitude. The amplitude had a strong relationship with the energy released by the defect. So the occurrence of Cluster 1 events with high amplitude, was indicating the presence of more severe strength reducing defects.

The results for 0°, 10°, 20°, 30° and 45° material are shown in figures 8.2 to figure 8.6 respectively. Part (a) of the figures have the separation of clusters plotted on principal component axes, principal component 1 and principal component 2. This clarifies the relationships between clusters. Part (b) in each figure shows the arrival of cluster data with respect to the material loading and time into the experiment. The experiments had a constant strain rate of 0.1%/minute, so the horizontal axis is also proportional to strain within the sample.

Clustering has separated the acoustic emission data into three distinct but predefined groups. There is little over lap between clusters indicating the three parameters chosen have rigorously delimited changes in the acoustic emission waveform. However there are no areas devoid of data between clusters, indicating a gradation in the principal component values corresponding to a range of values accepted as representing each of the clusters. Some of the gradual change from one cluster to another will be due to the attenuation affects of the composite material modifying the acoustic emission waveform.

The results from the clustering of data for the 0° composite material, shown in figure 8.2(a), displays the clusters without significant overlap. In Cluster 1 the events have large amplitude, over 2.5V. This large magnitude produced a large ringdown count and long risetime values. The events in Cluster 2 have intermediate amplitudes, 0.40 ± 0.26V. The events also have large risetimes and ringdown counts. Cluster 3 has small events with low amplitudes, small risetimes and fewer ringdown counts.

There are fewer events in Cluster 1 compared to Clusters 2 and 3 for the 0° material tested. This would be consistent with the larger events associated with the few significant damage mechanisms occurring. In figure 8.2(a) for the 0° material, the multitude of events assigned to Clusters 2 and 3 can be correlated to observations of matrix cracking dominating the low stress levels. The stronger fibre axis being aligned with the loading direction would mean few fibre breaks expected until higher loads were reached.

The results of the acoustic emission from the 20° and 30° composite materials (figures 8.4 and 8.5) demonstrate the sensitivity of acoustic emission technique to monitoring the occurrence of damage even at low stress levels. In the initial stages of testing when very little stress was being applied acoustic emission was still emitted and detected. The source mechanisms may have been defects caused by rough handling and the manufacturing technique. As the specimen was loaded and elongated the initial defects opened impulsively and released small amounts of residual energy from the manufacturing processes. The clustering process placed these similar events in to clusters containing small magnitude acoustic emission. This type of minor damage did not critically alter the material properties up to a test time of about 2 minutes in the case of 0°, 20° and 30° material.

The pronounced change of the material modulus at different stress levels depended on the fibre orientation. The 20° and 30° materials in figures 8.4 and 8.5 have pronounced changes in the stress/strain curve after 2 minutes of testing. The larger angle 30°, as expected, has a slightly lower stress turning point, (3MPa), for the modulus change compared to the 10° material at 6MPa. The 0° material, figure 8.2, shows a modulus

change at a similar time and stress if the initial flat, low stress portion of the stress/strain graph, possibly caused by the specimen straightening, is taken in to account.

The changing modulus is the response to damage accumulation causing irreversible changes to the material's elastic properties. Up to the point of inflection, the material would recover most of the elastic extension. After the change in modulus, the material has suffered permanent plastic deformation. This point of important damage accumulation is coincident with the first occurrence of events in Cluster 1. Results from the 20° and 30° experiments show that before this point there are no Cluster 1 events in the low stress stages of the tests. Associated with the material modulus change there was also a sharp increase in the number of events occurring in Clusters 2 and 3 in the 20 seconds prior to the point when Cluster 1 events start to occur. These smaller amplitude events in Clusters 2 and 3 were possibly the precursor to the damage emitted by the large amplitude Cluster 1 acoustic emission. The initiation of Cluster 1 events at different stress levels highlights some of the problems of the complex mixing of damage mechanisms that mathematical models try to simulate.

Acoustic emission monitoring of damage from composite material is sensitive to changes in the deforming material and to any changes to the monitoring technique and equipment. Data monitored using different equipment, with different transducers and settings, can not be directly compared. The changes to the experimental method acts as a changing filter, selecting a different proportion of the acoustic emission events and changing the representation of the frequency and energy content of the acoustic emission.

The acoustic emission detecting system was different for the 10° and 45° specimens since a 175kHz transducer was used. The material was from a different batch of composite material made on a different day compared to the 0°, 20° and 30° material, but made with the same fibre and resin components. It is assumed that there was no difference in the material properties that would significantly change the behaviour between batches since the same manufacturing method was used for both days. Any change in the results was due to the acoustic emission equipment modifications.

The different transducer accounts for the differences seen in the amount and the arrival time of the acoustic emission detected. It appears that the lower frequency transducer used was not detecting the same amount of acoustic emission as the better matched 375kHz frequency transducer, see figures 8.3(b) and 8.6(b). Data suggests that the 175kHz transducer was more highly damped, limiting the responsiveness to produce a lower voltage across the piezoelectric material in response to similar stress wave signals.

When looking at the commencement of acoustic emission from the 10° and 45° material (figures 8.3(b) and 8.6(b)) the reduced response of the acoustic emission detection system is clear. The acoustic emission occurs at a much later time. However, while this appears the case the clustered data still responds to changes in the stress-strain response of the material. In the case of the 10° material Cluster 2 data appears at a point where a load drop occurs, with Cluster 3 data appearing as specimen stiffening occurs at about 7 minutes into the test. In the case of the 45° material acoustic emission starts to occur at a point when the specimen stiffens late in the test.

Testing using two different transducers resonances has demonstrated the need to optimise the test system to find the required information reliably, since the 175kHz transducer has not detected the early modulus changes detected by the 375kHz transducer. These are issues that need further investigation.

It is worth commenting that the cluster analysis for the various composite materials show strong similarities even though the time dependent behaviour differs markedly.

An important part of the experiment was the monitoring of damage preceding the failure point. One of the aims of the investigation was to observe changes in the acoustic emission that indicated the imminent failure of the specimen. It is reported in other work [Holt and Worthington (1981)] that near failure the count rate of acoustic emission events dramatically increases as the number of defect locations multiplies. These experiments were not able to respond to the dramatic increase in the number of events due to the limit imposed on the capture rate by a computer controlled acquisition system. So the interest

was focused on the cluster data results. The proportion of Cluster 1 events in the total population of acoustic emission events would suggest more severe damage occurring.

A trend in the average parameter data per cluster was observed to be correlated to the changing angle of the fibre reinforcement. The average peak amplitude reduced as the fibre angle increased. If the source mechanisms are assumed to be similar in all composite material, then the difference in magnitude is due to a variation in the material properties along the path from source to transducer. For the larger fibre angles the stress wave was scattered and dispersed by the oblique fibre sides compared to the possible wave guide effect of travelling in a parallel direction to the fibre length encountered in 0° composite material.

The serrated shape of the stress graph for the 10° material (figure 8.3), was due to the grips slipping and relaxing the stress level in the specimen rather than due to material failure. The absence of bursts of acoustic emission associated with each load drop indicates that it is not serious material failure causing the load changes. The use of a less sensitive transducer (175kHz) meant that most of the noise produced by the grips moving was not detected and misinterpreted as acoustic emission from fracture within the composite material. The increase in the rate of acoustic emission is pronounced, particularly for Cluster 1 events, in the period prior to the failure point when fibre debonding and failure are dominant.

Figure 8.8 is a summary of the cluster data plotted against load for materials with fibre angles 10°, 20°, 30° and 45° The spread of the results across the range of stresses follows the expectation that acoustic emission occurs at different loads depending on the material strength.

The trend in the occurrence of acoustic emission with respect to the increasing load changes with fibre angle. Composite material with smaller fibre angles has a much larger stress range for damage initiation than material with larger fibre angles. This implies that more load was required to induce damage in the stronger fibres within the resin. The fibres when aligned with the load bear the stresses with relatively small strain. The small extensions in the fibres result in less crack propagation in the surrounding matrix material.

The results for the 10° material (figure 8.8) has a staggered progression due to the stress relaxation as the grips slipped. The almost linear increases in the number of events for clusters is miss leading since there was significantly more acoustic emission emitted than detected and recorded in these experiments. Exploratory experiments using the electronic AECL capture system that counts hits rather than digitising the complete waveform, registered many thousands of events compared to the hundreds recorded in this work.

8.4   Conclusions

Acoustic emission monitoring is the detection of real-time deformation in the composite material. Acoustic emission has provided a physical measurement technique for assessing the amount of damage occurring within a material without visual confirmation. The summation of the number of events from different clusters for a given time period, rapidly increases at significant points of material deformation, such as the period when the elastic modulus changes.

From the experiments carried out in the work reported here, it has been shown that the acoustic emission waveform contains information about the source mechanism. The fracture mechanism imparts a characteristic amount of energy which is translated into a detectable acoustic emission waveform of a standardised form. The acoustic emission was clustered into groups depending on the magnitude, risetime and ringdown count of the waveform. The occurrence of Cluster 1 events was consistently at higher stress levels, prior to the failure point of the material when significant damage was occurring in the material. These acoustic emission events were larger amplitude and with longer risetimes and more ringdown counts than the other two cluster events. The rate of acoustic emission prior to failure may not reflect the rapid increase seen in work by others, due to the limits of the refresh rate of the computer controlled capture system. The increased proportion of Cluster 1 events from the total population, does indicate a shift in emphasis towards more energetic stress waveforms.

An important observation was the occurrence of acoustic emission at points where the material modulus changed. The permanent damage associated with the material being stressed beyond the elastic region was accompanied by a significant increase in the level of

detected acoustic emission. During the use of a composite material there are significant amounts of acoustic emission. The presence of acoustic emission does not signify that the material is about to fail. From these studies a background level of acoustic emission comes from acceptable amounts of material movement and micro cracking as stresses are redistributed in the early stages of material testing. The importance of studying the acoustic emission waveforms was to distinguish the acoustic emission events that are no longer the background flexing of the material, but important deformation of the material. Cluster analysis grouped these important events into Cluster 1.

From the digitised waveform outlines, trends in the magnitude of the acoustic emission waveform were seen to correlate with the amount of irreversible damage occurring in the material. The average per cluster for the three parameters changed with changing fibre orientation in the composite material. The most obvious change was the peak amplitude for 0°, 20° and 30° material. The amplitude of the Cluster 1 acoustic emission reduced with increasing fibre angle to the loading direction. Assuming that the types of fracture mechanisms do not change with increasing fibre angle only the proportions, then an explanation for the amplitude change could be increased attenuation of the stress wave in the material. With more damage within a composite material having a larger fibre angle, the acoustic emission would be reduced in magnitude due to more internal scattering points deflecting part of the acoustic emission wave. Other workers have noted this observation.

The position of the defect relative to the transducer does have an affect on the acoustic emission data. For instance similar damage mechanisms such as matrix cracking occurring at different positions within the structure of the composite material will produce different magnitude acoustic emission waveforms. The variation would be more pronounced if the attenuating path length was long between source and transducer. With the use of more than one transducer and a triangulation method it would be possible to map a limited area of active deformation producing serious Cluster 1 acoustic emission. Future detailed mathematical work could investigate the minimisation of errors due to the anisotropic nature of composite material. The multiple layers of glass and resin rich areas, as well as point inclusions such as voids or foreign matter, all act as reflectors of the acoustic emission energy. Using techniques that are developing for ultrasonic inspection of

composite materials and geophysical seismic surveys, the deconvolution of the attenuating path travelled by the acoustic wave will enhance the identification of characteristics for different source mechanisms. However there are penalties to be paid in adopting more complex signal analysis, more time and resources are required.

Future work on improving the data acquisition system could investigate further the influence the choice of transducer and digitising regime has on the data set. The experiments reported here included observations on how the frequency of the resonant transducer can change the observed acoustic emission. The centre frequency of the two transducers used was different, which influenced the amount and time (stress) at which acoustic emission was detected. The choice of transducer frequency also affected the average values for the three parameters measured and subsequently used in the cluster analysis. Extending the waveform analysis to measure other characteristic parameters of the acoustic emission stress wave, could add more parameters to the data set used, thus improving the certainty of correctly clustered events.

The frequency of the transducers used in this work influenced the waveform outline and the values of the resulting waveform parameters. The ringdown count values did not preserve the true high or low frequencies in the acoustic emission event outside the narrow band of the resonant transducer. The digitising system, the A to D board and computer capture program, influenced the precision of the acoustic emission waveform and the number of events possible to capture.

Due to the ringing in the transducer and the time limit set by the digitising window, the occurrence of any deformation source mechanism with a long emission time was not clearly captured. The ringdown count for large burst events was limited by the User-set time limit of 200µs after the trigger time. Events that took time to emit the energy from the defect were poorly represented. Therefore there would be confusion between medium magnitude events of long duration and large magnitude, shorter duration events that have a long ringdown time due to the characteristics of the transducer. More parameters including frequency content information would help resolve the differences.

Future improvements to the clustering analysis technique could include the addition of more waveform parameters or the use of different criteria for accepting membership to a certain cluster. Expanding the number of parameters from three would strengthen the separation of events that have similar general waveform characteristics but originate from different source mechanisms. For example neural network analysis uses many parameters in a learning data set to form links between events, that uniquely describe the known source mechanism. When applied to experimental data, the multitude of relationships between waveform parameters is used to sift the events in to categories.

Having investigated the acoustic emission from glass fibre reinforced composite material a change in the fibre or matrix composition may show as a change in the characteristic acoustic emission detected. Changing the material used to make the specimens could be used to monitor the affects of the fibre type and the interface bond with the resin matrix. Due to the different fracturing nature of carbon and aramid fibres, it is expected there would be a difference in the acoustic signature when compared to the brittle fracture associated with a glass fibre. If there are detectable differences in the amplitude and frequency content of the acoustic emission according to fibre type, then the monitoring of hybrid composite material may reveal the damage accumulation in the different composite layers. The influence of changing the sizing coating on the fibre has been investigated using simple single bundle dogbone samples and acoustic emission monitoring (Okoroafor *et al*, 1996). The failing interface emitted acoustic emission at different loads depending on the strength of the bond. The energy content of an acoustic emission waveform may be proportional to the amount of energy required to fracture the interface bonds.

The waveform processing was influenced by the system that detected the acoustic emission. Further work in the area of acoustic emission waveform analysis would need to extend the narrow frequency band of the resonant transducer to broad band analysis. Upgrading and matching the capabilities of the digitising equipment would improve the precision of the acoustic emission waveform saved. The improved quality of the analysis of the acoustic emission waveform would then be able to provide more details about the source mechanism in the time and the frequency domains.

9   Theoretical Damage Model Development

9.1   Introduction

Modelling the accumulation of damage in a composite material is complicated by the contrasting material properties of the fibre and matrix. The chosen model by Ladeveze and Le Dantec (1992), represents damage as two simple damage parameters. These damage parameters refer to the damage developing as a result of increasing transverse and shear stresses within the material. The magnitude of the damage parameters is proportional to the amount by which the transverse and shear moduli reduce, caused by the damage weakening the material. The sections that follow describe the thermodynamic continuum equations that are the basis for the model and the empirical calculations of the constants of damage growth in a glass fibre composite material. All symbols are defined in the nomenclature at the beginning of this thesis. Programming details for the model are given in Chapter 10 and experiments using the model are discussed in Chapter 11.

9.2   Original Ladeveze and Le Dantec Equations

The mathematical model chosen to predict how a composite material deforms is taken from work by Ladeveze and Le Dantec (1992). The model predicts in a simple set of equations the effects of matrix cracking and fibre debonding at the lower stress levels. The continuum equations represent the damage development as increasing damage parameters, d and d'. These increasing damage parameters reduce the material properties in the transverse and shear directions relative to the fibre direction, respectively.

Models for composite material are complicated by the many failure mechanisms as discussed in Chapter 4. Therefore the model incorporates more than one failure criterion [Allix *et al* (1990)]. The material degradation considered in this work is the result of matrix cracking and the fibre debonding from the matrix at low loads. The effect of fibre breaking is not considered since this effect dominates at higher stresses near the sample failure point. Therefore the model used here is only applicable to the low load regime when damage is initiated.

The thermodynamic state equations are developed to separate the transverse and shear stresses that later control the damage development. The degree of damage is

progressive and is reflected by the magnitude of two parameters associated with the level of damage in the transverse and shear directions.

The model equations from the original paper applied to carbon fibre laminated material. The material was tested under tension and compression. This present study investigated the more widely used and available glass fibre reinforced polyester resin composite, tested in tension. The material characteristics are different for glass-fibre and carbon-fibre composite. Therefore the model development had to reflect these variations.

The main difference between the two composite materials derives from the transverse stresses developed in the $[\pm 45^{\circ}]_{2s}$ cross ply materials tested. Carbon composite has negligible levels of fibre orientated transverse stress compared to shear stresses because of the higher relative material shear modulus to transverse modulus. In the glass composite used in this work the transverse stresses across the fibres are significant and therefore could not be ignored when simplifying the calculation of the material damage constant used in the model equations.

9.2.1 Model Equations

The thermodynamic continuum equations are derived from work by Katchanov (1958), which develops damage as the progression of micro-cracks. The model includes cracks that are oriented parallel to the fibres (longitudinal) and are affected by positive opening transverse stresses and shear stresses (figure 9.1). A compressive-transverse stress relative to the fibre closes the crack and inhibits the crack propagation. Cracks orientated perpendicular to the fibres are not accounted for since the strength of the fibre will dominate the degradation in the longitudinal direction. The following analysis follows that of Ladeveze and Le Dantec (1992).

The elastic strain energy equation for a homogenised ply separates the positive and negative components of σ_{22}, the transverse stress:

$$E_D = \frac{1}{2}\left[\frac{\sigma_{11}^2}{E_1^0} - \frac{2v_{11}^0\sigma_{11}\sigma_{22}}{E_1^0} + \frac{\langle\sigma_{22}\rangle_+^2}{E_2^0(1-d')} + \frac{\langle\sigma_{22}\rangle_-^2}{E_2^0} + \frac{\sigma_{12}^2}{G_{12}^0(1-d)} \right] \qquad (9.1)$$

94
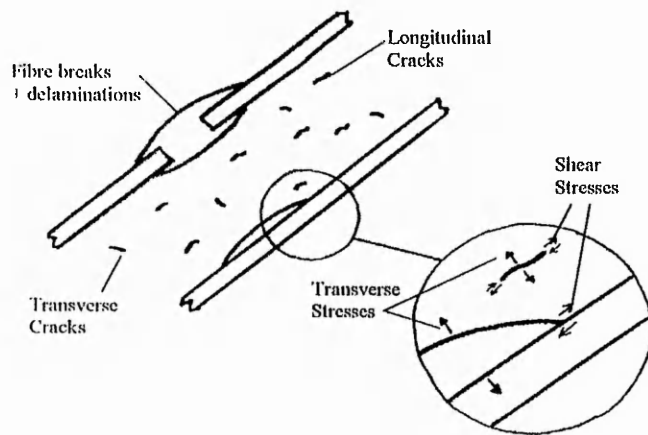
Figure 9.1 Failure modes in a composite material related to the fibre and the matrix.

Where E_D is material strain energy,

σ_{11}, σ_{22} and σ_{12} are ply stresses,

E_1^0, E_2^0 and G_{12}^0 are initial material moduli,

d and d′ are scalar variables for shear and transverse damage respectively, and

ν_{11} is the Poisons ratio.

By partial differentiation of equation 9.1 the changing state of the material strain energy relative to the parameters d and d′ can be calculated as follows;

$$Y_d \qquad \left.\frac{\partial E_D}{\partial d}\right|_{\overline{\sigma},d'} = \frac{1}{2}\frac{\sigma_{12}^2}{G_{12}^0(1-d)^2} \qquad (9.2)$$

$$Y_{d'} \qquad \left.\frac{\partial E_D}{\partial d'}\right|_{\overline{\sigma},d} = \frac{1}{2}\frac{\langle\sigma_{22}\rangle_+^2}{E_2^0(1-d')^2} \qquad (9.3)$$

Where Y_d and $Y_{d'}$ is the damage development separated into the two parts for d and d′, and the effective stress affecting the composite material when separated into the three components is:

$$\overline{\sigma} = \begin{bmatrix} \sigma_{11} \\[2mm] \dfrac{\langle\sigma_{22}\rangle}{1-d'} + \langle\sigma_{22}\rangle_- \\[2mm] \dfrac{\sqrt{2}\sigma_{12}}{(1-d)} \end{bmatrix}$$

The model distinguishes two failure modes in the material using the variables $\underline{Y}$ for matrix cracking and $\underline{Y'}$ for fibre debonding. The two damage mechanisms develop via changes in these variables as follows,

$$\underline{Y} = \sqrt{Y_d + bY_{d'}} \qquad (9.4)$$

$$\underline{Y}' = \sqrt{Y_{d'}} \qquad (9.5)$$

Where b controls the proportion of transverse stress induced damage to shear stress induced damage. From experimental evidence, Ladeveze and Le Dantec increase the damage in a composite material by the square root increase in stress, for good theoretical agreement with the material failure.

Matrix cracking damage ($\underline{Y}$) increases when one or both the transverse and shear stresses increase. The transverse stress dilates the crack and promotes the crack tip position, whilst the shearing stresses extend the crack by moving the two sides of the crack past each other producing stress concentrations at the crack tip. Fibre debonding ($\underline{Y}'$) is controlled by shear stress only. The maximum limit for transverse stress before complete fibre debonding is controlled by the brittle limit of the fibre/matrix interface tested under tension, Y_s'.

The change in damage parameters d and d′ are the result of the matrix damage accumulating due to shear and transverse stressing respectively. There are different initial requirements for loading and rates of increase of damage depending on the stress orientation and the material properties. These are controlled by the material constants, Y_o, Y_c, Y_o' and Y_c' in the equations below,

$$d = \frac{\left\langle \underline{Y} - Y_o \right\rangle}{Y_c} \qquad (9.6)$$

If d is less than 1 and $\underline{Y}'$ less than Y'_s, otherwise d equals 1.

$$d' = \frac{\left\langle \underline{Y} - Y_o' \right\rangle}{Y_c'} \qquad (9.7)$$

If d′ is less than 1 and $\underline{Y}′$ less than Y′ₛ otherwise d′ equals 1.

The constants Y_o and $Y′_o$ are the initial damage constants, Y_c and $Y′_c$ measure the rate of damage accumulation, and $Y′_s$ is the maximum allowed before the brittle failure of the fibre-matrix interface.

9.3   Experimental Determination of the Model Equation Constants

The damage constants for glass polyester composites (Y_o, Y_c, $Y′_o$, $Y′_c$, and b) are calculated from experimental results from tensile testing of symmetric angle ply materials. The materials used were [±45°]₂ₛ and [±67.5°]₂ₛ, which have symmetry about the midplane of the 8-ply lay-up. The symmetric material ensures that there is a plane stress condition within each ply, except at the edge of boundary layers, which have complex 3-dimensional stresses. The two materials with ±45° and ±67.5° arrangements of the ply, develop differing amounts of matrix cracking and fibre debonding. Therefore the results provide two sets of experimental data for the calculation of the initial constants and the rate of increase of damage in glass/polyester composite materials.

9.3.1   Tensile Testing of [±45]₂ₛ and [±67.5]₂ₛ Composite Material

The composite material tests were conducted on rectangular specimens, approximately 200 x 25 x 5 mm dimensions. Details of the material fabrication and testing method are given in Chapter 5.

The laminate stresses and strains measured in the experiments tensile stress σ^*_L, transverse strain ε^*_y and longitudinal strain ε^*_x, were resolved through the fibre angle to give the ply stresses with respect to the fibre orientation.

Classical laminate theory [Tsai and Hahn (1980)] is reported to have been used in the Ladeveze and Le Dantec paper. It is also the basis for a teaching program [Brooks (1992)] used to establish the differences in the stress regimes for carbon fibre and glass fibre composite materials. Table 9.1, gives a summary of the ply stress and strain as reported by the Ladeveze and Le Dantec paper (1992) for carbon fibre composite compared to that calculated by the teaching program for glass fibre composite. The

different material moduli used produce significantly different stresses in the laminates. The teaching program values are used in the computer programs used by the model reported here to develop the damage accumulation.

Laminate	Stress Strain	Ladeveze and Le Dantec	Teaching Program
		Carbon fibre composite	Glass fibre composite
$\theta=[\pm45]_{2s}$	σ_{22}	0	$0.2037\sigma^*_L$
	σ_{12}	$0.5\sigma^*_L$	$0.5\sigma^*_L$
	ε_2	$(\varepsilon_x+\varepsilon_y)/2$	$(\varepsilon_x+\varepsilon_y)/2$
	ε_{12}	$\varepsilon_y-\varepsilon_x$	$\varepsilon_y-\varepsilon_x$
$\theta=[\pm67.5]_{2s}$	σ_{22}	$0.8536\sigma^*_L$	$0.8068\sigma^*_L$
	σ_{12}	$0.3536\sigma^*_L$	$-0.4004\sigma^*_L$
	ε_2	$0.1464\varepsilon_x + 0.8536\varepsilon_y$	$0.8536\varepsilon_x + 0.1464\varepsilon_y$
	ε_{12}	$0.3536(\varepsilon_x-\varepsilon_y)$	$0.7071(\varepsilon_y-\varepsilon_x)$

Table 9.1 Summary of the calculations used by Ladeveze and Le Dantec compared to classical laminate theory as used by the teaching program (Brooks, 1992).

The discrepancy between the formulations is significant for the $\pm45°$ material in the transverse stress direction (σ_{22}). Ladeveze and Le Dantec were able to assume the damage in the carbon fibre composite material was due to pure shear stresses since transverse stresses were negligible. This is not the case for glass fibre composite materials. Other work has also drawn attention to these differences [Kellas *et al* (1991), Wisnom (1995)]. The modes of failure observed by Rotem and Hashin (1975) suggest that failure in $\pm45°$ material is not limited to shear interlaminar cracking only. Due to the accumulation of

cracks throughout the ply and the debonding of fibres allowing the fibres to pull out, transverse stresses are also significant.

During the Ladeveze and Le Dantec experiments, the calculation of $\underline{Y}$ from equation 9.4, was simplified due to shear stresses being far more significant than transverse stresses, so that;

$$\underline{Y} = \sqrt{Y_d} = \frac{\sigma_{12}}{(1-d)\sqrt{2\,G_{12}^0}} \qquad (9.8)$$

This then allowed the calculation of the value of the constant b. Rearranging equations 9.4 and 9.6, the constant can be calculated thus:

$$b = \frac{(Y_c d + Y_o)^2 - Y_d}{Y_{d'}} \qquad (9.9)$$

Since transverse stresses were to be accounted for in $\pm 45^\circ$ glass fibre composite materials a value for the constant b used in equation 9.4, had to be assumed.

The constant b controls the proportion of shear and transverse energy in equation 9.4. The shear stress component is larger than the transverse stress, so the value of b was chosen to be 4, making the shear approximately four times larger than the transverse stresses. The Ladeveze and Le Dantec value was 2.5. From the proportions of the loading tensile stress in Table 9.1, (approximately $0.2\sigma_L^*$ for the transverse and $0.5\sigma_L^*$ for the shear), a value of 4 for b may be larger than the correct value. The shear stresses are approximately 3 times larger than the transverse stresses in $\pm 45^\circ$ material, which will also be affected by the differences in the material moduli. More investigation into the effects of b on the equations is required; however the value of 4 chosen is a realistic starting value.

The averaged stress/strain results from 4 specimens for each of the two angles, $[\pm 67.5^\circ]_{2s}$ and $[\pm 45^\circ]_{2s}$, are shown in figures 9.2 and 9.3 respectively. The results show that the smaller transverse stresses in either laminate material are still significant in a glass fibre
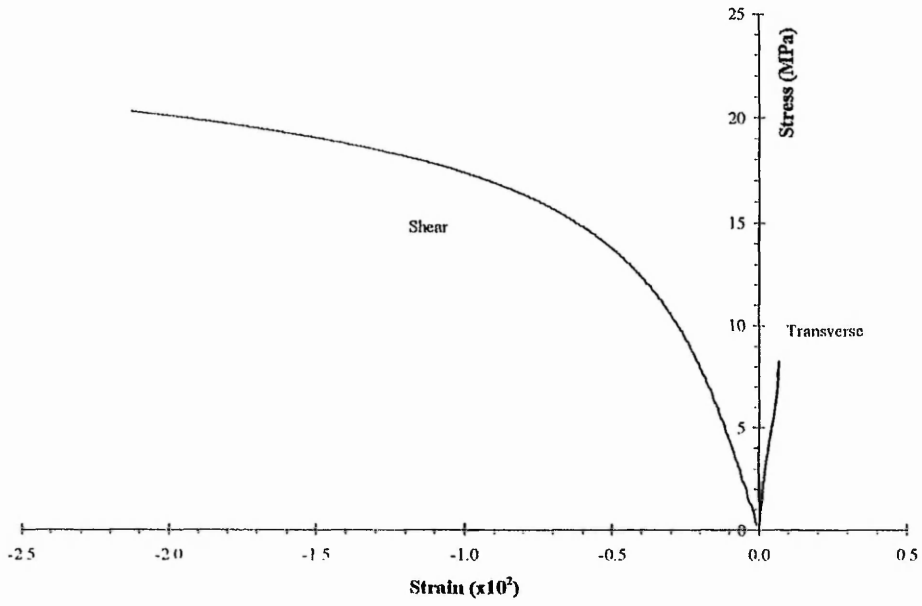
Figure 9.2 Average stress/strain diagrams for $[\pm45^{\circ}]_{2s}$ cross ply material.
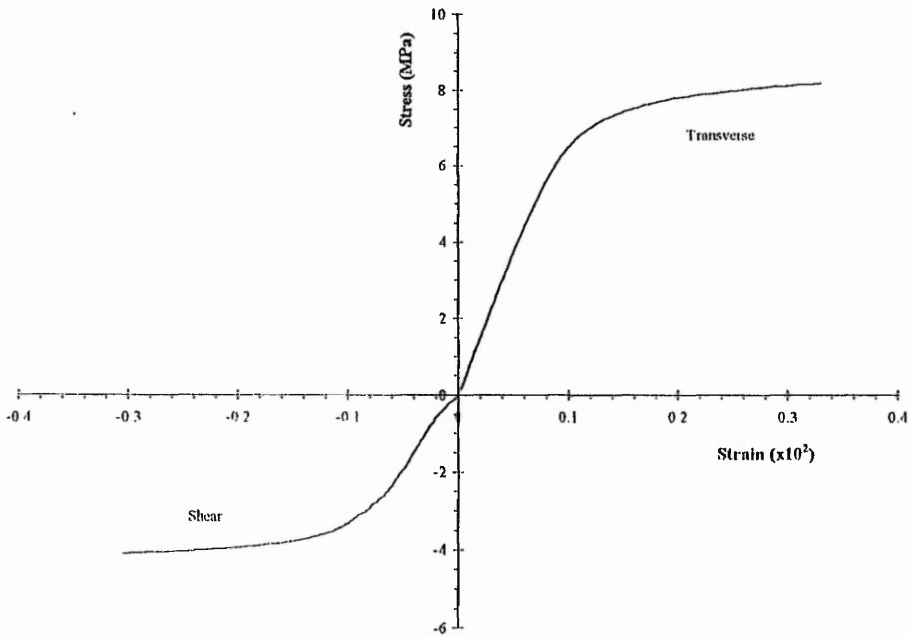
Figure 9.3 Stress/strain diagrams for $[\pm67.5^{\circ}]_{2s}$ cross ply material tested for the damage model.
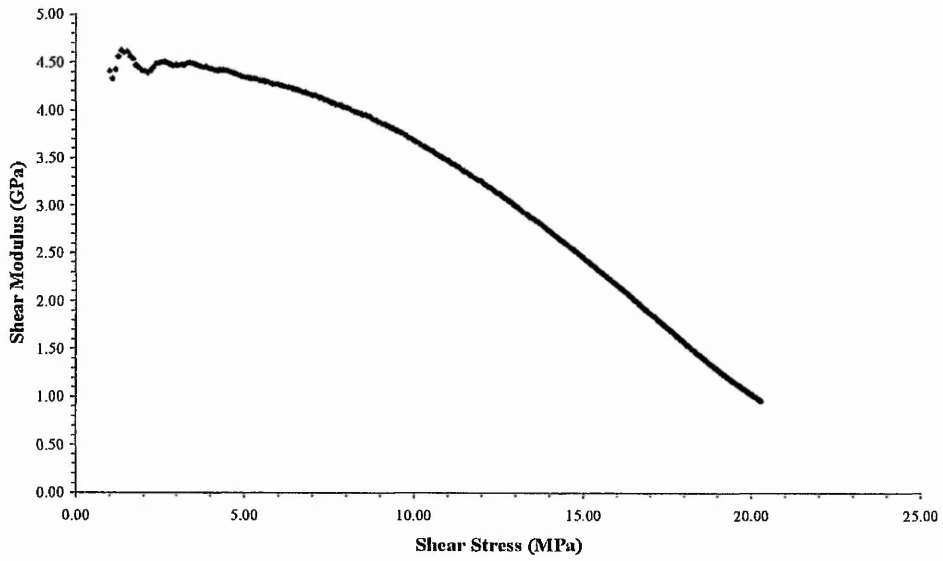
Figure 9.2.1 Changing shear modulus (G_{12}) against increasing shear stress.
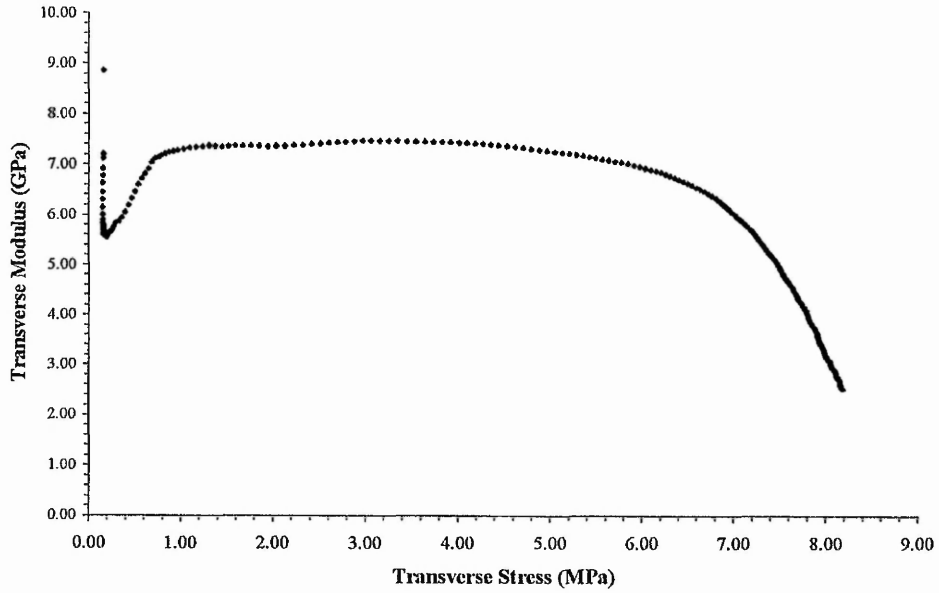
Figure 9.3.1 Changing transverse modulus (E_2) against increasing transverse stress.

composite. The moving tangent moduli for the shear and transverse stress/strain of the $[\pm45^\circ]_{2s}$ and $[\pm67.5^\circ]_{2s}$ were used for the experimental calculation of d and d′ respectively (Figures 9.2.1 and 9.3.1). A running 30-point best fit line calculated the initial moduli change of the transverse and shear graphs. This method involved taking thirty points to recalculate the gradient, one point was taken from the end of the line and one point added to the front, with the gradient calculated for the new centre point. The largest gradient values were equivalent to the initial undamaged material moduli, E^o_2 and G^o_{12}. The changing gradients of E_2 and G_{12} were then used to calculate the changing experimental values for d′ and d respectively, using the following equations:

$$d = \frac{(G^o_{12} - G_{12})}{G^o_{12}} \qquad (9.10)$$

$$d' = \frac{(E^o_2 - E_2)}{E^o_2} \qquad (9.11)$$

The values of d, d′, the shear (σ_{12}) and transverse (σ_{22}) stresses were used in equation 9.2 and 9.3 and subsequently in equation 9.4 to calculate $\underline{Y}$. By rearrangement of equation 9.6,

$$d = \frac{Y}{Y_c} - \frac{Y_o}{Y_c} \qquad (9.12)$$

The gradient of the graph in figure 9.4 gives $1/Y_c$ and the y-axis intercept gives $-Y_o/Y_c$. Thus, Y_c and Y_o can be determined.

In a similar fashion the constants Y'_o, and Y'_c were calculated using the experimental data from tensile testing of the $[\pm67.5^\circ]_{2s}$ material. Figure 9.3 shows the graph for the transverse and shear stresses resolved from the measurement of the specimen's longitudinal stress, transverse and longitudinal strain (Table 9.1). Figure 9.5 displays the damage curve for d′ vs. $\underline{Y}$ calculated in a similar fashion as the previous
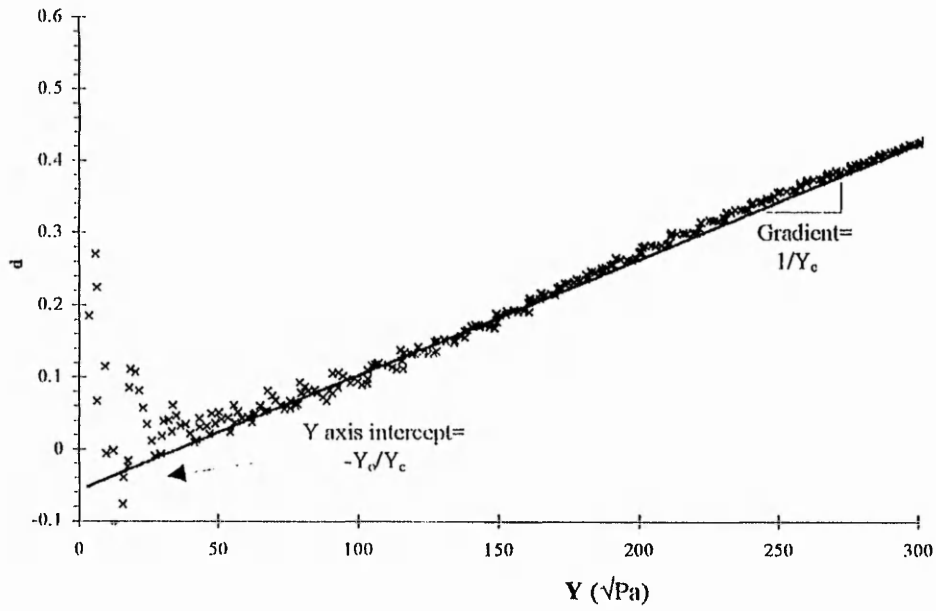
Figure 9.4 Damage development graph using data from $[\pm 45^\circ]_{2s}$ material.
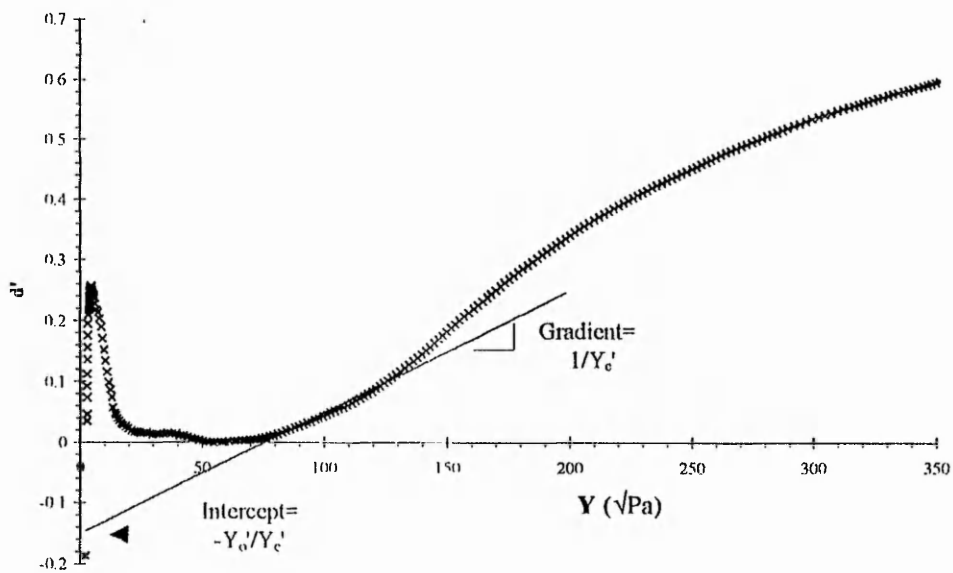
Figure 9.5 Damage development graph using data from $[\pm 67.5^\circ]_{2s}$ material.

d-$\underline{Y}$ damage graph (figure 9.4) for the shear damage. The constant values calculated are summarised in Table 9.2. The gradient line was fitted to data that occurred after the maximum material modulus. Prior to this point the material moduli fluctuated and caused the damage calculation of $\underline{Y}$ to vary as well.

The theoretical failure point in the model was reached when either of the damage parameters d or d' became equal to 1, or the parameter $\underline{Y}'$ became equal to the constant Y'_s for failure by fibre debonding. The value for Y'_s was measured from the corresponding point on the damage graph when failure occurred in the $[\pm 67.5^\circ]_{2s}$ material. In figure 9.6(a), the maximum stress point (9.7MPa) on the graph was projected on to the damage graph (figure 9.6(b)). The square marks the maximum load point and the triangle the maximum transverse damage level. This is the value for the fibre debonding limit, Y'_s, approximately $83\sqrt{Pa}$. The damage graph (figure 9.6(b)) retraces the line because of the decreasing stress/strain gradient after the stress maximum. This produces decreasing levels of damage or improving material strength! For the three material angles subsequently tested (results given in Chapter 11), the load was increased until an element reached the fibre debonding level of $\underline{Y}' = 83\sqrt{Pa}$.

9.4   Discussion of the Determination of Constants

The graph of d against $\underline{Y}$, (figure 9.4), when extended to higher loading stresses does not have the linear shape reported by Ladeveze and Le Dantec (1992). This suggests that the damage development after the initial stages, does not accumulate in a linear fashion. At higher stresses the damage rate increases rapidly in glass fibre composite materials. This non-linear increase in the damage accumulation is consistent with the results from acoustic emission experiments [Holt and Worthington (1981), Kander (1991)]. The rate of acoustic emission rises quickly with higher stress. The acoustic emission results reported in this work, do not show the rapid increase due to the limit imposed by the maximum capture rate of the computer system. Further work is required to investigate the possible changes in the damage parameter equations needed to account for the non-linear damage accumulation at higher stress levels.

The constants, Y_o, Y_c, Y'_o, Y'_c, and b, used in the calculation of damage initiation and growth are in Table 9.2. These values only reflect the damage at the low stress. It can
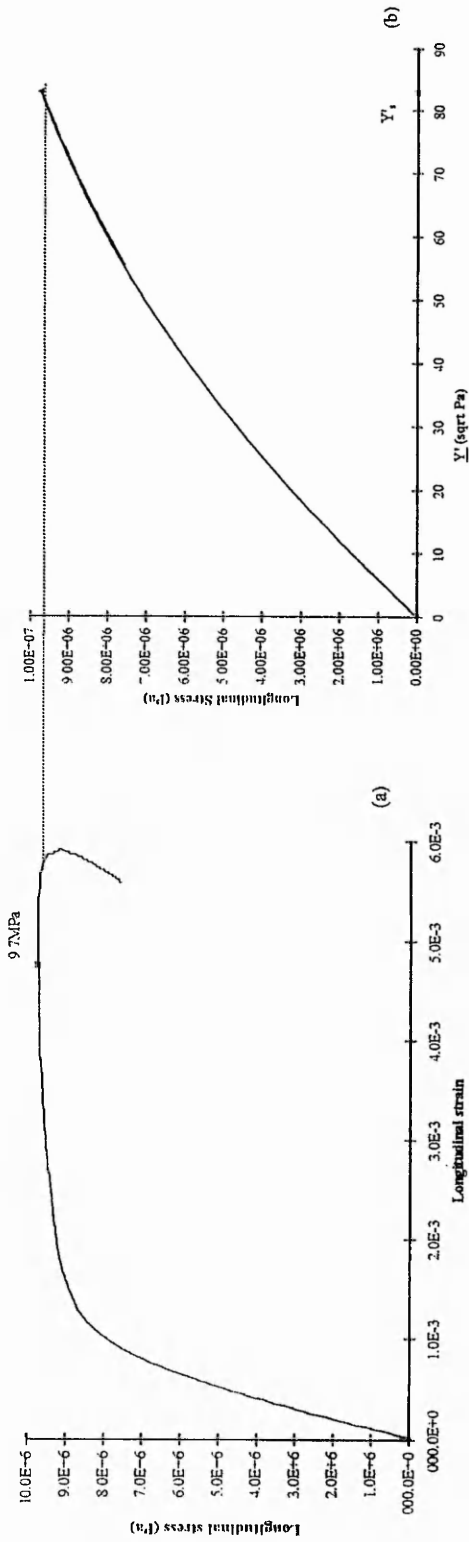
Figure 9.6 Calculation of Y'_s, the fibre debonding failure value, (a) the specimen failure stress projected on to (b) the maximum damage Y'.

be seen from Table 9.2 that both the threshold parameters (Y_o and Y_o') and the damage growth rate parameters (Y_c and Y_c') are significantly lower in glass fibre than carbon fibre composites. This reflects the lower moduli and stresses in the glass fibre material. The effects of the reinforcing fibres breaking have been ignored in this model. However most uses of composite material extend the material beyond the lower strength regimes, so it is important the model has an additional function to account for the brittle fibre breakage. The work by Ladeveze and Le Dantec (1992) and Allix *et al* (1989), suggest additional functions to accommodate non-linear plastic deformation, brittle fibre breakage and compressional stress damage. These would have to be critically analysed for their compatibility with glass fibre composites and built into the model.

Model Constant	Units	Ladeveze and Le Dantec	Present Model
		Carbon Fibre Composite	Glass-Fibre Composite
Y_o	$\sqrt{Pa}$	150	7.99
Y_c	$\sqrt{Pa}$	2770	493.58
Y_o'	$\sqrt{Pa}$	240	19.74
Y_c'	$\sqrt{Pa}$	3780	518.13
b	-	2.5	4
Y_s'	$\sqrt{Pa}$	700	83
E_1^o	GPa	170	37.0
E_2^o	GPa	10.8	9.1
G_{12}^o	GPa	5.8	5.6

Table 9.2 A comparison of damage constants and material moduli for glass- and carbon-fibre composite materials.

The constant b controls the relative proportions of transverse to shear stresses required in the model for damage to occur. The b value also has an effect on the development of d and d' via the calculations of $\underline{Y}$ and $\underline{Y}'$. This in turn controlled the

106

magnitude of the damage parameter values. The method for calculating the exact value of b requires more study to assess the proportion of damage accumulation due to shear and transverse stresses, which in turn may require the fabrication of composite material with different fibre orientations to stimulate different stress regimes.

The experimental limit for the damage model was the theoretical failure point due to fibre debonding or the total degradation of the material moduli. For the three material angles tested, the load was increased until an element reached the fibre debonding level of Y' equal to $83\sqrt{Pa}$ (Y'_s). The results for the 10° experiments were stopped at $210MPa$, for the 20° at $66MPa$ and for 45° at $16.5MPa$ load on the finite element mesh.

9.5   Conclusion

The damage model chosen was originally developed for the accumulation of damage in carbon fibre composite material. From experimental and theoretical calculations the damage development is different in glass fibre composites, so the basis of the model had to be carefully and critically reassessed to match the changes in material to the equations generated. The assumption of zero transverse stress in $[\pm45^o]_{2s}$ carbon composite material and hence the calculation of equation constants could not be applied to glass fibre composite experiments. Therefore the value of the constant b, that controls the proportion of shear and transverse damaging stresses, was an informed choice. The affects of the value of b on the resulting damage accumulation needs to be studied in depth before this model can be used to monitor damage accumulation at higher stresses or in more complex geometries than a simple single ply.

The choice of the laminate angles, 45° and 67.5^o, was guided by the material used by Ladeveze and Le Dantec. A systematic theoretical study of the stresses developed in glass fibre composite material may reveal more useful orientations for initially calculating the damage constants. The differences between carbon and glass material moduli will affect the degree and the location of damage accumulation in the structure, but it is the shape, the lay-up of the composite material that has a significant affect on the initiation and the propagation of damage. The design of non-symmetrical laminate models, using finite element analysis, may extend the appreciation of the complex development of damage in composite materials.

10 Damage Model Programs

10.1 Introduction

To apply the theoretical model discussed in Chapter 9, to predict the accumulation of damage in a real composite, the calculation of the damage development was incorporated into a suite of Fortran computer programs. A finite element package was used to calculate the changing material stress response to damage giving indications of the severity of damage growth and the location of material degradation.

The following sections give details of the finite element model (Section 10.2) and the programs used to calculate damage (Section 10.3). In particular PROGRAM.FOR is described which calculates the changing damage level per element of the model. Figure 10.1 shows the flow diagram for the programs used to theoretically calculate damage in a composite material.

10.2 Finite Element Model

The finite element package, called PAFEC74 (Pafec Ltd.), was used to develop a simple, single ply composite material model for use with the theoretical damage prediction equations discussed in Chapter 9. The package requires the submission of a data file, NEWMESH.DAT, to the finite element package, which contains commands and details of the type of analysis to perform. The NEWMESH.DAT file contained detailed descriptions of the node locations, the element topology, element material properties and the loading/restraining of the mesh. An outline of the contents of this file is given in Appendix A.1.

There were two mesh designs used to model the composite material with elements of different sizes. Both 2-D meshes comprised 2500 plane stress, orthotropic quadrilateral, 8-noded elements. The overall model dimensions were 200mm by 25mm by 4mm, which was similar to the tested composite material. Figure 10.2 shows a schematic diagram of the model, including the loading position (arrows) and the restrained ends of the model (hatched region). The load was applied to the model as a stress applied to the nodes along one of the short ends, in the x direction only. The opposite restrained end had the nodes in
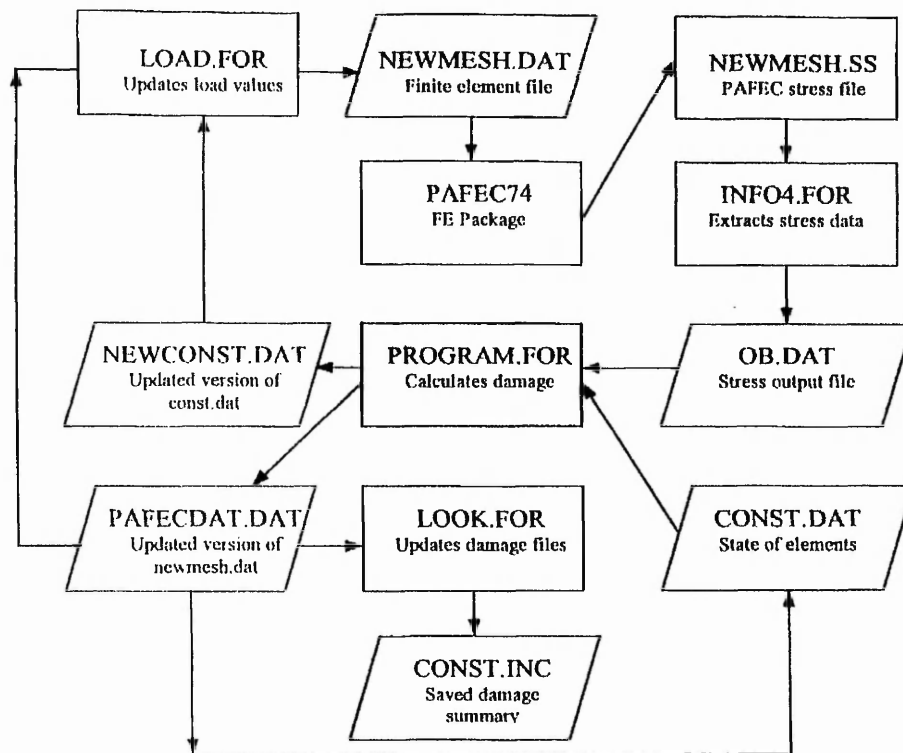
Figure 10.1 Flow diagram of the steps through the programs and data files used in the damage model experiments.

(a)

Restrained movement
in x direction

Loading direction

(b)

← 100 elements →

25mm

25
elements

← 200mm →

"Damaged" element

Large, rectangular element mesh

(c)

25 elements — 50 elements — 25 elements

25
elements

← 75mm — 50mm — 75mm →

Three zone mesh with central square elements
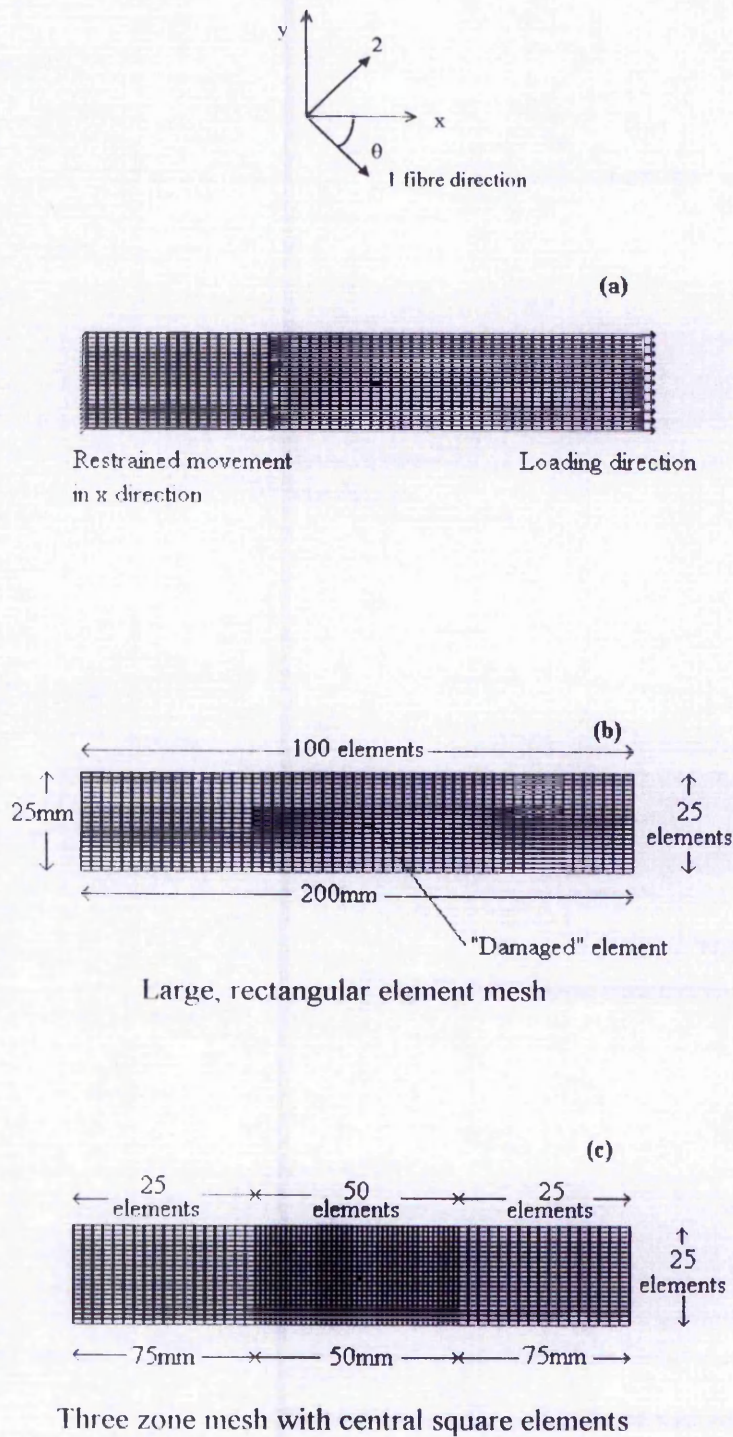
Figure 10.2 Finite element mesh showing a) the loaded and restrained ends of the mesh and the fibre direction, b) the rectangular mesh and c) the three zone mesh with the smaller square elements in centre zone.

110

the end plane restricted in movement in the x direction. Movement of the short end nodes was not restricted in the y and z directions.

The first mesh had similar rectangular elements (figure 10.2 (b)), 2.0 x 1.0mm. The second mesh design had three zones - a central dense mesh with outer mesh zones containing larger sized elements (figure 10.2 (c)). The central zone had elements 1.0mm x 1.0mm, compared to the outer zones of 2.0mm x 1.0mm. There were 1250 elements in the central zone and 625 in each of the outer zones.

To promote the damage in the central area of the mesh, an element at the centre was designated to have different properties to the initial surrounding material. The centre element was made twice as stiff in all three property directions i.e. longitudinal, transverse and shear. This stiffer element caused a high stress concentration to occur so initialising the damage from this point. If there was no stronger central element then the grip zones, i.e. the loaded and restrained short ends of the mesh, would have higher stress concentrations than the bulk of the material caused by the restraints on movement. Higher stress concentrations at the ends of the mesh would simulate the model for the undesirable situation of damage proliferation in a specimen at the grips.

The initial PAFEC input file, NEWMESH.DAT, was written using a program ARRAY.FOR. An automatic method was needed to accurately write the 2500 lines of detail required for each element in the mesh, as well as approximately 80 different damaged material combinations for the changing shear and transverse material moduli. The material property list contained all possible combinations of material degradation due to the effects of d and d′ on the initial shear and transverse material values. The value for longitudinal modulus, E_1, was initially set to be constant. Each element had a material property number, set initially all the same except for the central 'damaged' element. This detailed description of the material properties per element was necessary if the damage equations were to alter the individual element properties as the result of accumulating damage. The state of an element was rewritten with a new property number if the damage equations calculated that damage had progressed sufficiently to reach the next damage level. More details on the computer program, PROGRAM.FOR, which calculates the damage accumulation, are described in Section 10.3.

111

To simulate the different orientations of fibres in the composite materials, the major axis of the material was rotated through an angle equivalent to experimental angles used (ANG1). The stresses retrieved from the PAFEC stress output file using the program INFO4.FOR, were originally relative to the main axis of the mesh. These stresses were resolved to be relative to the fibre orientation before being used in the calculations of damage.

10.3   Computer Program Control of the Damage Model.
10.3.1   PROGRAM.FOR - Damage Program

Due to reported experimental localisation of stress around sites of cracking in a composite material, the use of discrete finite element analysis was a practical tool for analysing the stresses in a deforming composite material. The partitioning of a material into elements allowed for the spatial study of the progression of damage through the finite element mesh. The discrete method for calculating the damage parameters in the model was then performed at the element level.

A series of Fortran programs were written to integrate the output stress data file (NEWMESH.SS) produced by the commercial FE program, with a routine that calculated the new damage parameter values per element (PROGRAM.FOR). The flow diagram (figure 10.1) shows the analysis path. For automatic submission of all the stages of processing, checking and changing of parameters, the process was controlled for the VAX system using a procedure file. The procedure file (FINITE.COM) synchronised the finite element analysis of the input file NEWMESH.DAT, with the damage calculating program, PROGRAM.FOR. Details of the procedure file are given in Appendix A6.

PROGRAM.FOR used an input file containing the current state of the elements, (CONST.DAT), which were compared to the new calculated damage values for damage parameters d and d'. This file contained in three columns, the element number and the current values for the damage parameters. Other input files included the stresses per element retrieved from the PAFEC stress file, NEWMESH.SS, using the program INFO4.FOR which were saved to the file OB.DAT.

The equations and constant values used in the program PROGRAM.FOR were as reported in Chapter 9.

Changes to the damage parameters for each element were automatically checked with the previous run using the program LOOK.FOR. After each load increment a permanent summary of the magnitude of the damage parameters for a given load was saved as an output file, CONST.INC.

10.3.2 Process Control Programming

The load applied to the mesh was along one of the short ends of the mesh. The value, in Pascal, was increased after each damage cycle. The load value could have been kept constant until there was no further change in the damage calculations. This would have been similar to experiments were the load is increased and held until very few acoustic emission events are monitored. The experiments reported here did not dwell on the same load. Small load increments were controlled by the program LOAD.FOR and the present magnitude of the load recorded in another data file LOADVAL.DAT. Using the data file LOADVAL.DAT it was possible to change the starting load and the load increment.

The procedure file, FINITE.COM, used by the VAX operating system, co-ordinated the run times of the Fortran programs involved in the damage analysis. The synchronised running of the damage program after the lengthy finite element analysis was possible without the need for User prompting. An estimate of the time for one experiment involving 20 load steps was between 5 and 48 hours.

10.4 Data Representation

Pictorial contour plots (Microsoft SLIDEWRITE) of the central portion of the mesh with highlighted areas of damage accumulation and change are presented in figures 11.1 to 11.6. The data was taken from the files saved by the program LOOK.FOR. The damage parameters d and d' changed in small increments, 0.1, about the central 'damaged' element of the mesh. The pair of plots for d and d' are presented for increasing loads where the increase in stress on the mesh has caused a significant change in the overall level of damage, or produced a definite progression of damage across the mesh. The elements

around the centre changed their values of d and d′ normally by only one increment of 0.1. These adjacent elements with slightly higher damage levels were more likely to change damage state. Extended limb patterns of damaged elements radiated out from the centre. At certain loads the majority of the elements show an increase in the damage level for the whole mesh. The change did not occur at the same load for the d and d′ damage parameters. Rather the d′, shear modulus modifier, occurred at lower stresses than the d transverse damage parameter. A small number of elements did not undergo this rise in damage level and remained at a lower threshold. This produced wells of less damaged material that occupied areas between previously extended limbs of more damaged elements. As the load increased, more of these less damaged elements increased their damage level and the wells shrank in size.

11   Damage Modelling - Results and Discussion

11.1   Introduction

The theoretical damage model, discussed in Chapter 9, was integrated within a two dimensional finite element model of a composite material, to investigate the evolution of damage and the effect of load and fibre orientation on this damage growth. The model was tested for fibre orientations 10°, 20° and 45°, the angle measured between the load and the fibre axes. The dependence of the damage growth pattern on the element dimensions is discussed. Results of the growth pattern for the rectangular element mesh are discussed in detail. This is followed by a comparison of the results from the 3 zoned mesh, reported for the three angles which highlight only slight differences in pattern at the different load levels due to element dimension changes.

The results are displayed as contour plots in the region of the central portion of the finite element mesh about the central damaged element. The left hand column of each figure shows the d' parameter, the transverse modulus modifier, along side the development of d, the shear modulus modifier. At certain loads almost all the elements in the mesh change to the next damage level except for a few central elements. These few elements are left as shrinking wells of less damaged elements in a sea of damage. The contour plots do not always show clearly the location of these less damaged elements, and so are shaded for clarity.

Each figure for a particular material angle and element shape has many parts to show the damage pattern development with increasing load. The 10° results are in figure 11.1 for the rectangular element mesh and figure 11.4 for the 3 zoned mesh. The 20° results for the rectangular mesh are in figure 11.2 and for the 3 zoned mesh in figure 11.5. The 45° results are figures 11.3 and 11.6 for rectangular and 3 zoned mesh respectively. The detail shows the changes at the significant points of rapid damage growth due to matrix cracking $\underline{Y}$ and fibre debonding $\underline{Y'}$. A summary of the damage levels for matrix cracking and fibre debonding can be seen in figures 11.7 and 11.8.
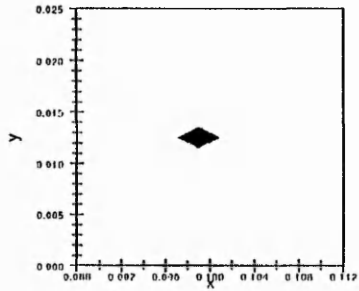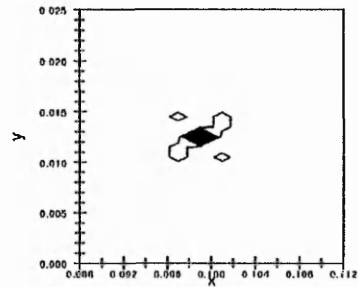
105MPa (a)
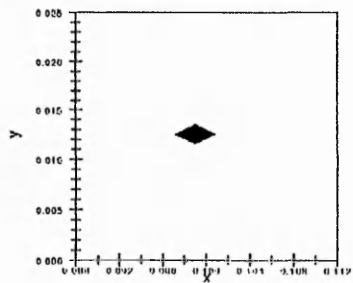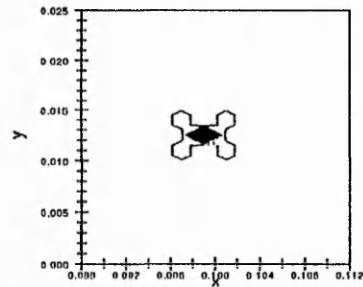
115MPa (b)
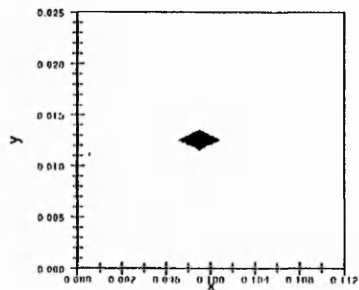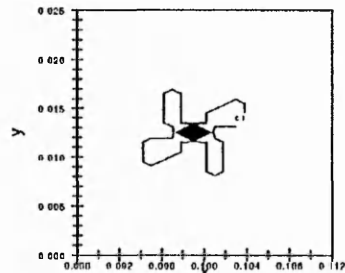
120MPa (c)
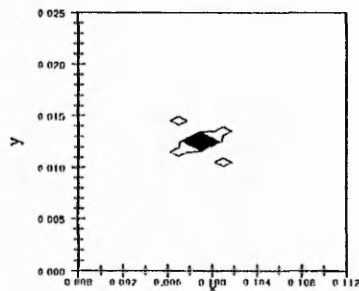
125MPa (d)
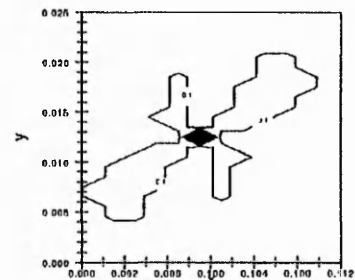
d' - transverse damage   d - shear damage

Figure 11.1 Damage development for 10° material using the rectangular element mesh.
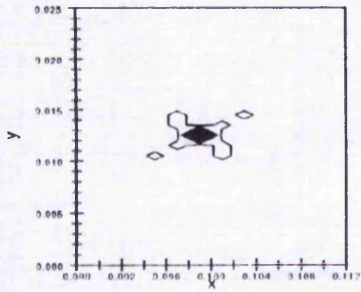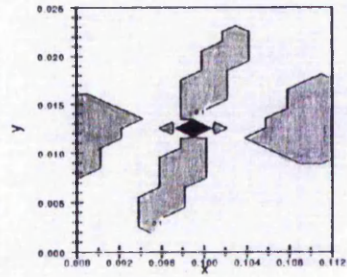
130MPa (e)
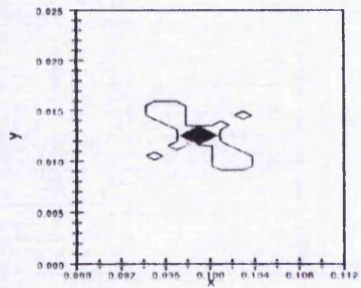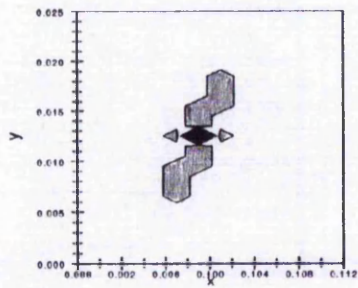
145MPa (f)
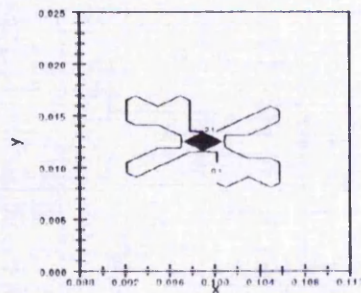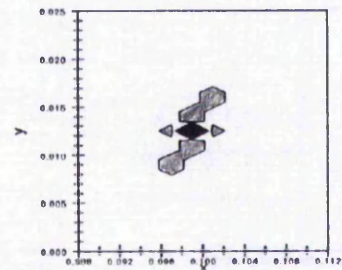
150MPa (g)
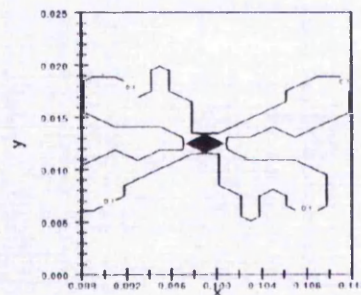
155MPa (h)
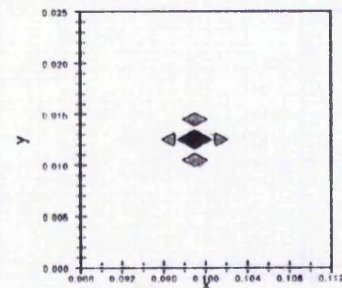
d´ - transverse damage   d - shear damage

Figure 11.1 continued. Damage development for 10° material using the rectangular element mesh.
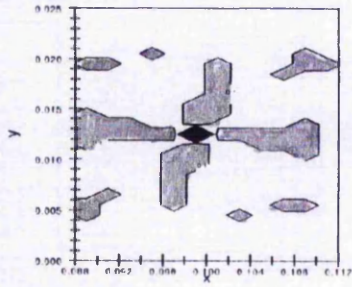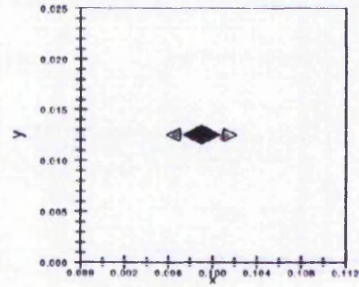
160MPa   (i)
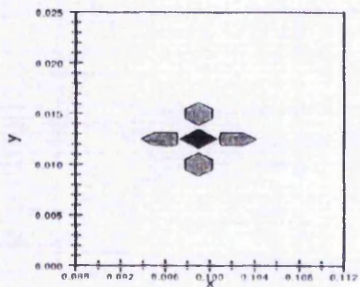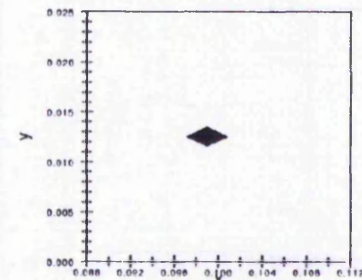
165MPa   (j)
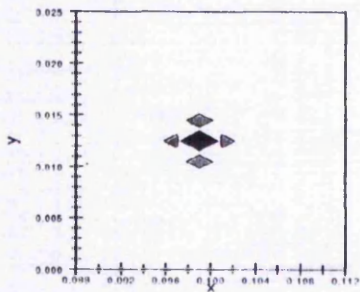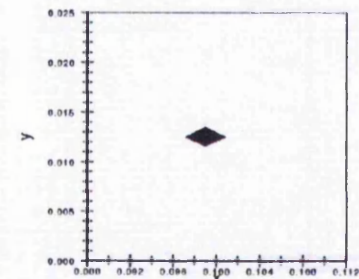
170MPa   (k)
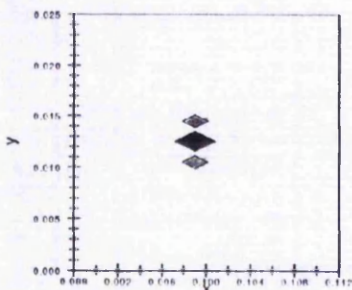
180MPa   (l)
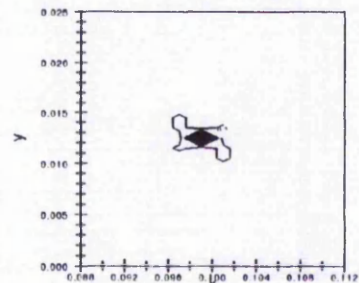
d' - transverse damage   d - shear damage

Figure 11.1 continued. Damage development for 10° material using the rectangular element mesh.

118
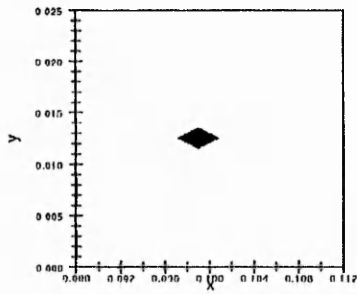
30MPa   (a)
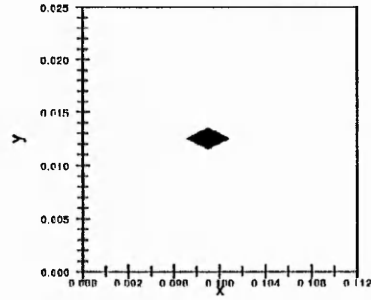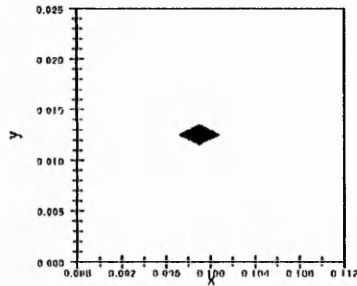
32MPa   (b)
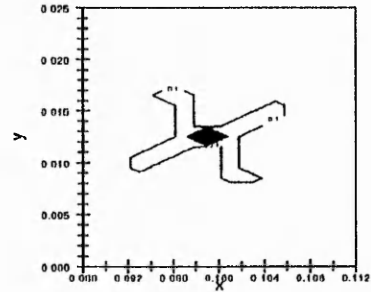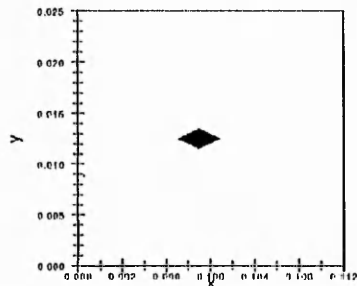
34MPa   (c)
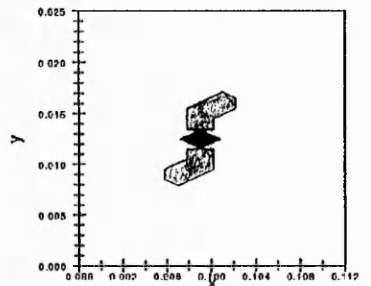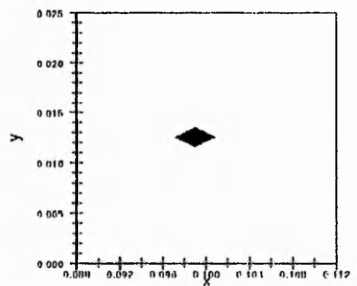
36MPa   (d)
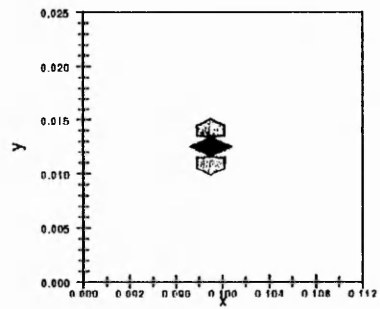
d´ - transverse damage   d - shear damage

Figure 11.2 Damage development for 20° material using the rectangular element mesh.
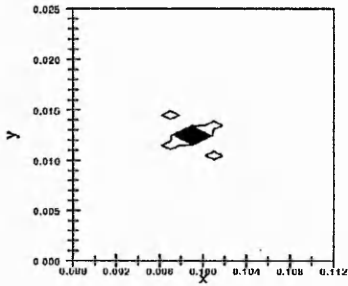
38MPa   (e)
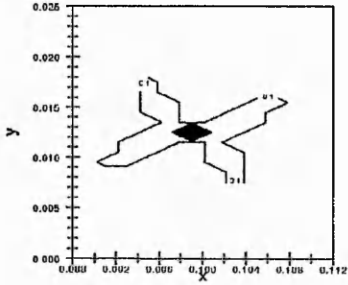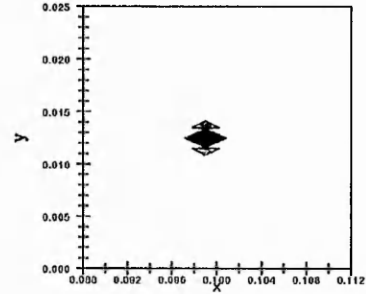
40MPa   (f)
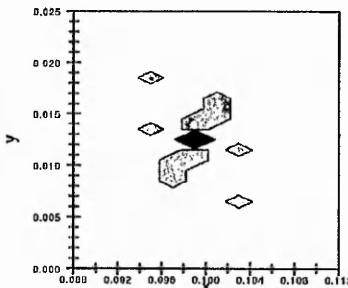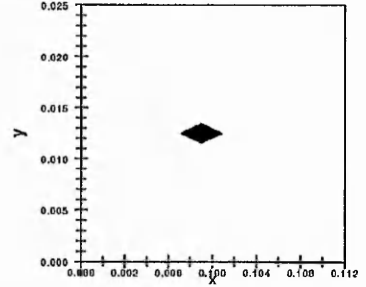
42MPa   (g)
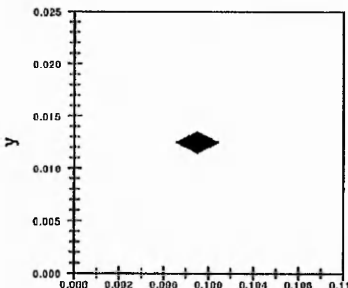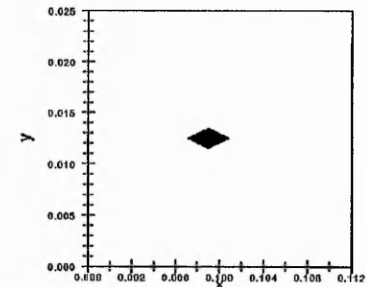
44-50Pa   (h)
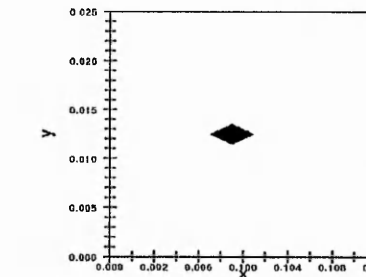
d´ - transverse damage   d - shear damage

Figure 11.2 continued. Damage development for 20° material using the rectangular element mesh.
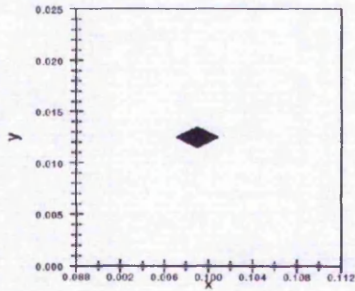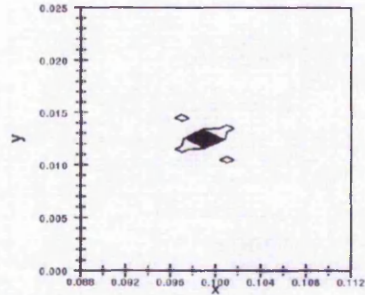
52MPa (i)
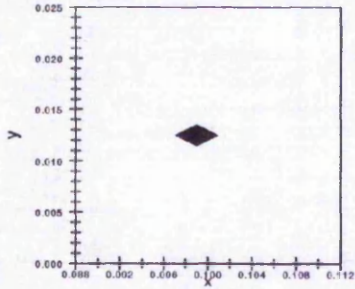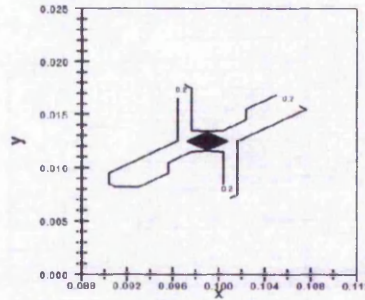
54MPa (j)
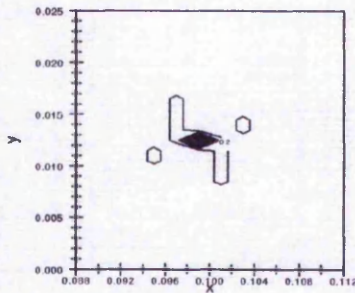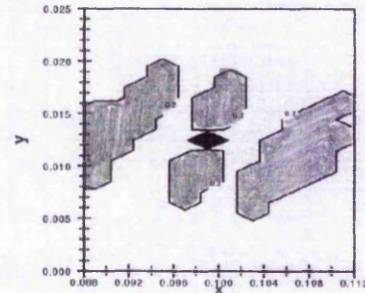
56MPa (k)
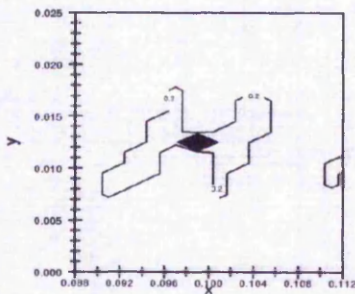
58MPa (l)
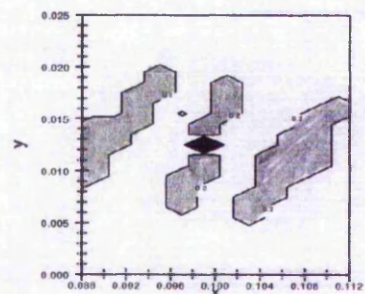
d´ - transverse damage   d - shear damage

Figure 11.2 continued. Damage development for 20° material using the rectangular element mesh.
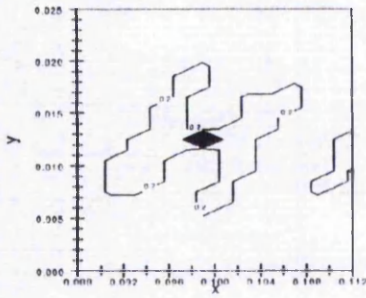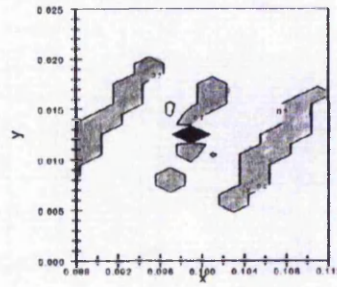
60MPa   (m)
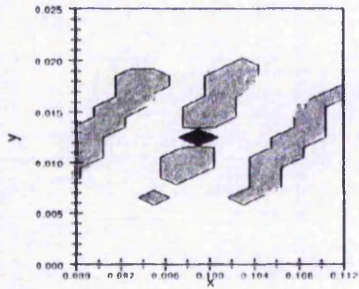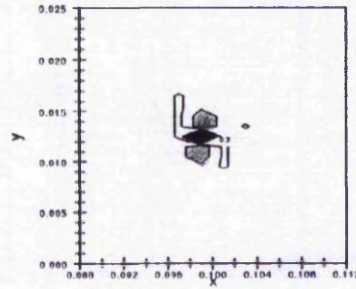
64MPa   (n)
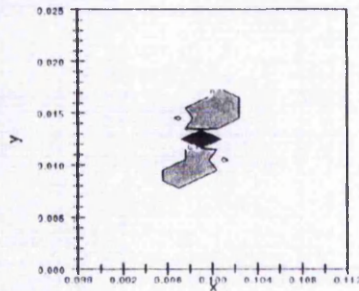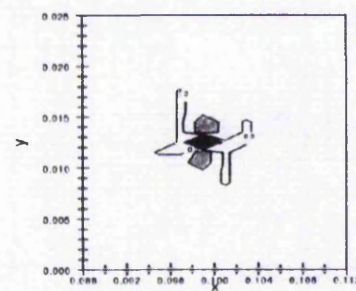
66MPa   (o)

d´ - transverse damage   d - shear damage

Figure 11.2 continued. Damage development for 20° material using the rectangular element mesh.
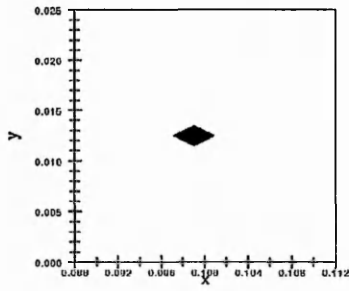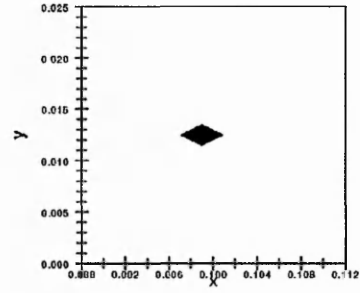
7.0MPa   (a)
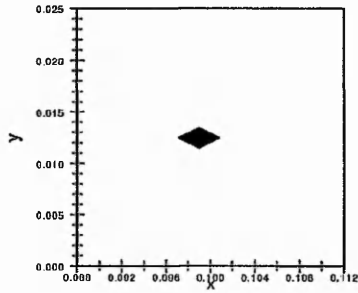
7.2MPa   (b)
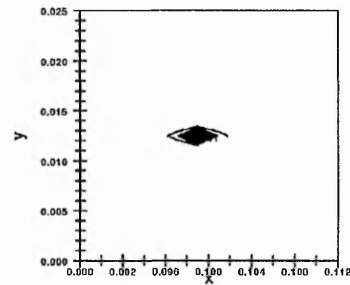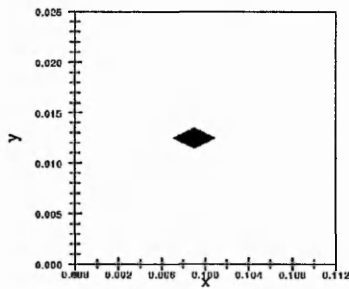
7.4MPa   (c)
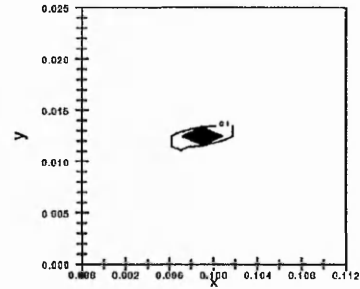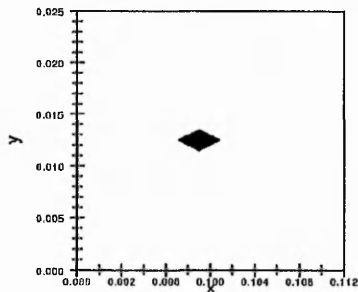
7.6MPa   (d)
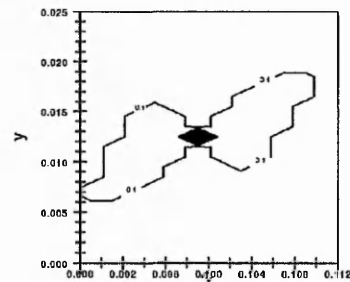
d′ - transverse damage   d - shear damage

Figure 11.3 Damage development for 45° material using the large rectangular element mesh.
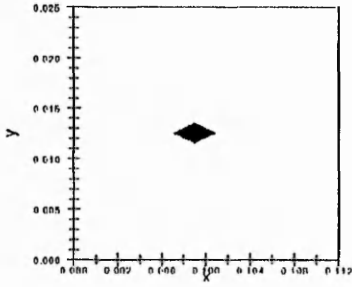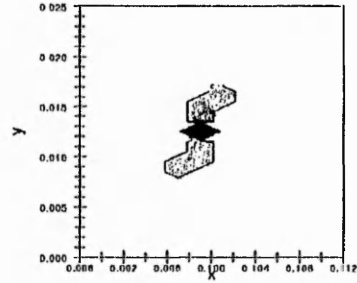
7.8MPa   (e)
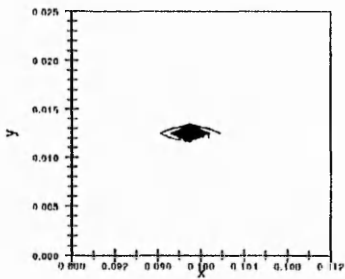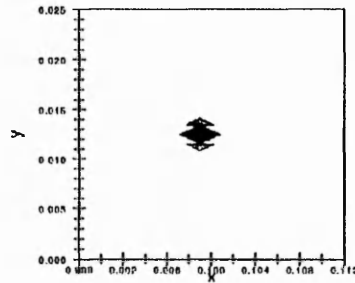
8.8MPa   (f)
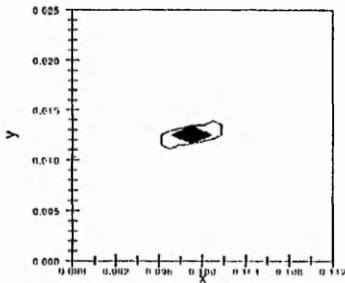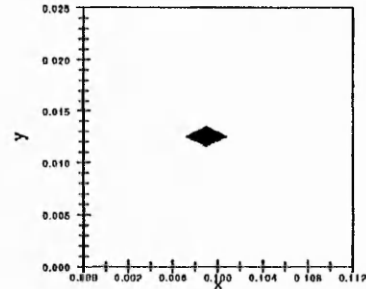
9.2MPa   (g)
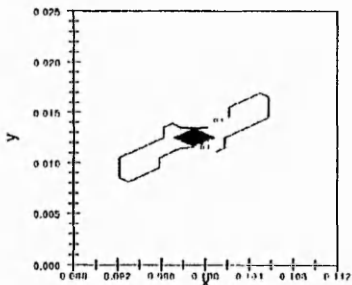
9.4MPa   (h)
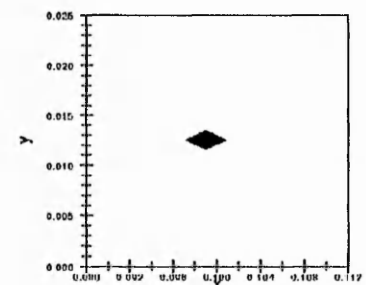
d′ - transverse damage   d - shear damage

Figure 11.3 continued. Damage development for 45° material using the large rectangular element mesh.
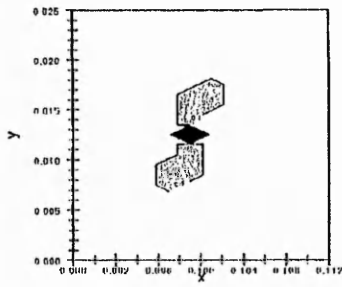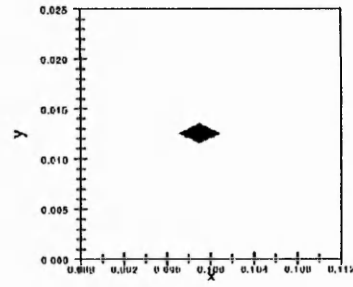
9.6MPa (i)
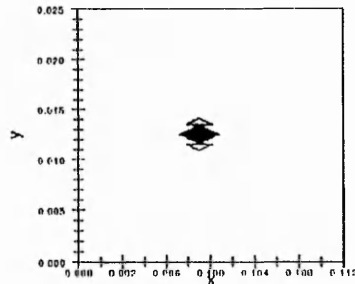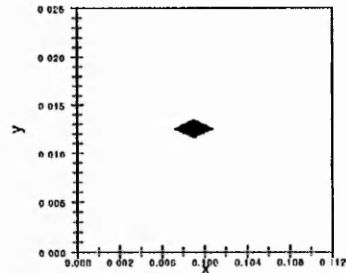
10.0MPa (j)

d' - transverse damage   d - shear damage

Figure 11.3 continued. Damage development for 45° material using the large rectangular element mesh.
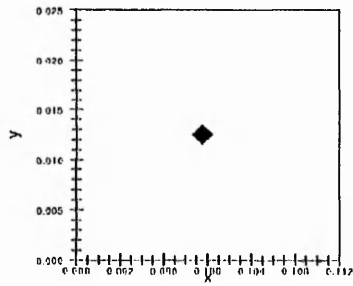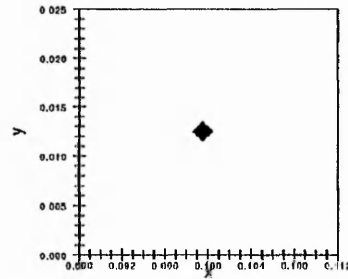
95MPa   (a)
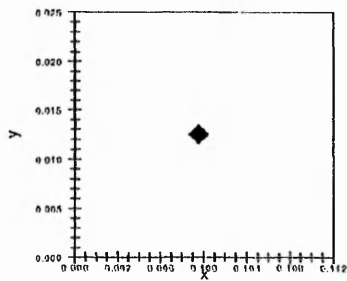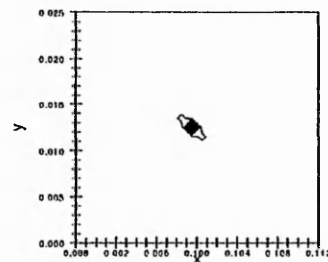
100MPa   (b)
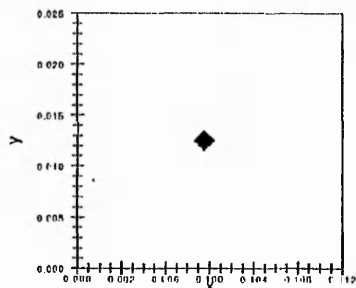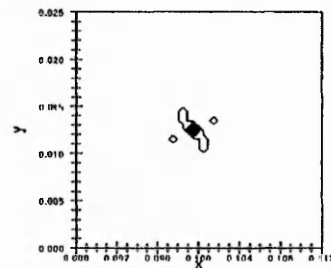
115MPa   (c)
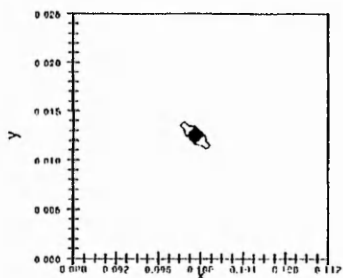
120MPa   (d)
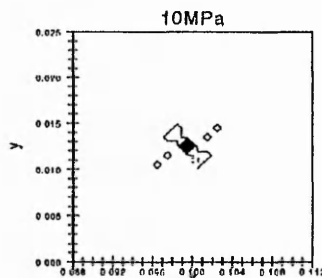
d′ - transverse damage   d - shear damage

Figure 11.4 Damage development for 10° material using the three zone mesh.
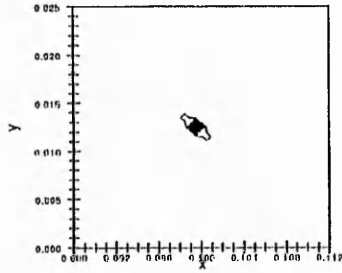
125MPa   (e)
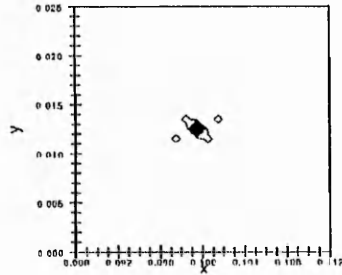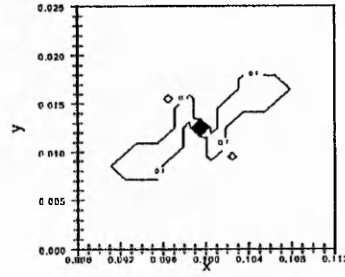
135MPa   (f)
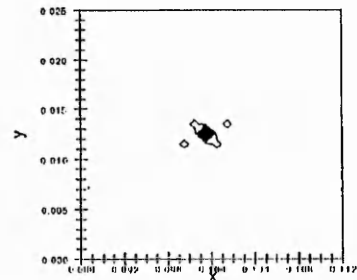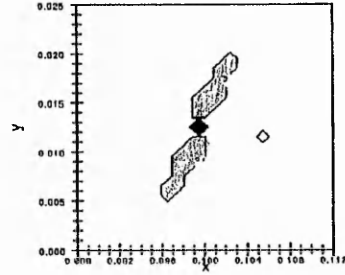
140MPa   (g)
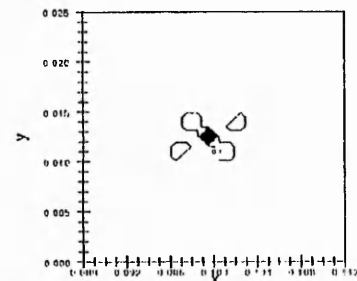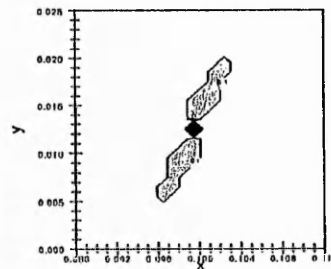
145MPa   (h)
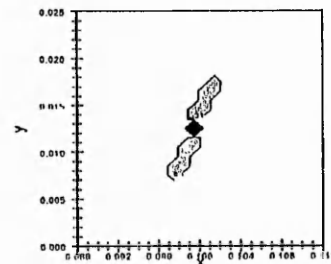
d' - transverse damage   d - shear damage

Figure 11.4 continued. Damage development for 10° material using the three zone mesh.
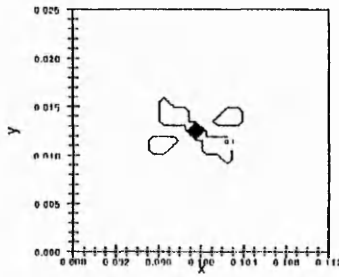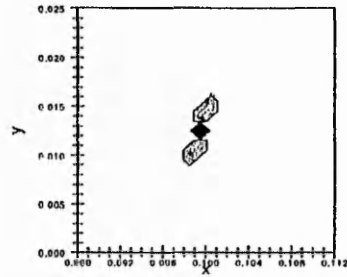
150MPa (i)
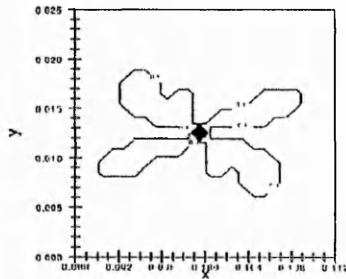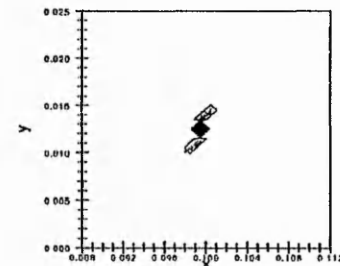
155MPa (j)
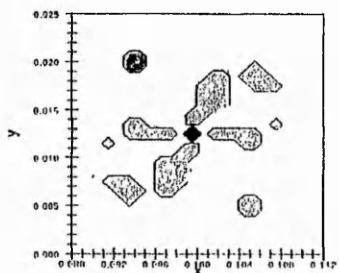
160MPa (k)

165MPa (l)

d´ - transverse damage   d - shear damage

Figure 11.4 continued. Damage development for 10° material using the three zone mesh.

30MPa   (a)

32MPa   (b)

34MPa   (c)

36MPa   (d)

d´ - transverse damage   d - shear damage
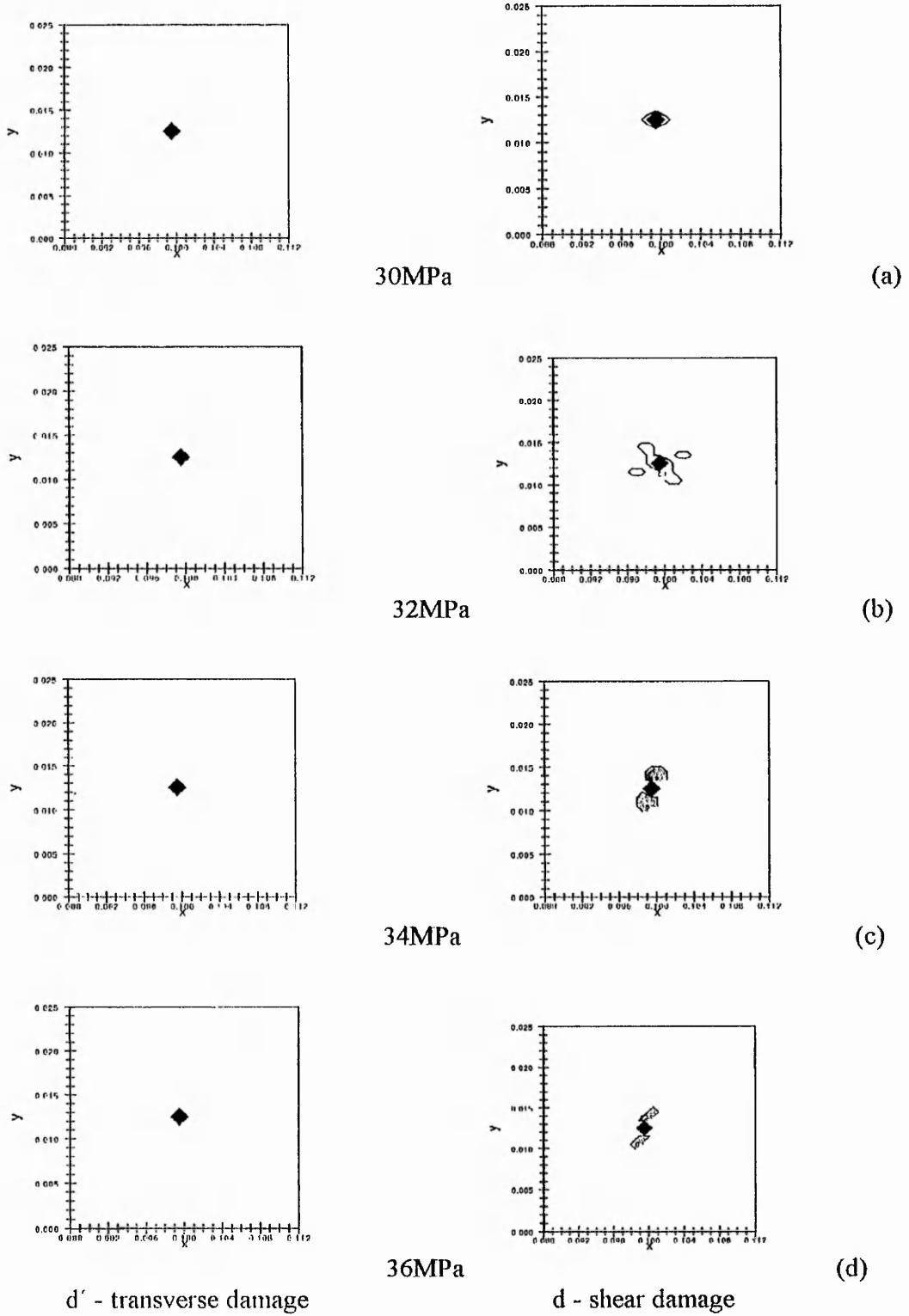
Figure 11.5 Damage development for 20° material using the three zone mesh.
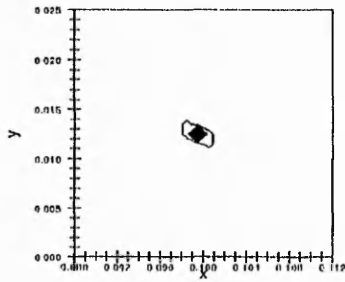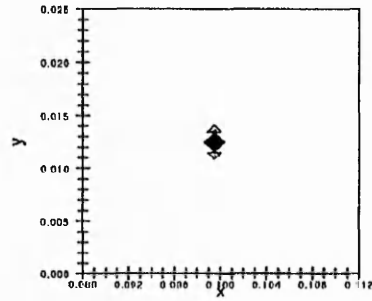
38MPa   (e)
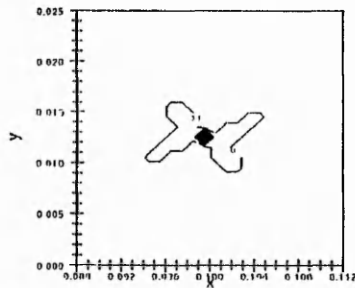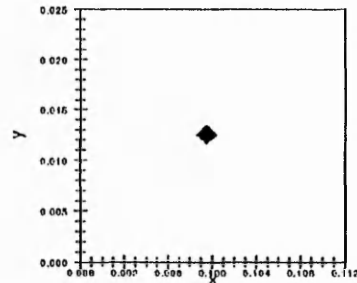
40MPa   (f)
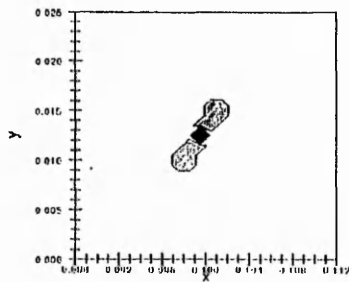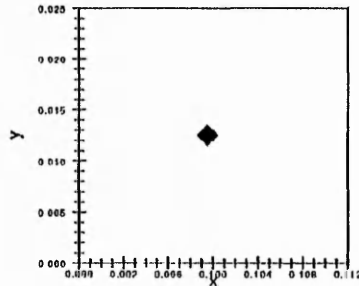
42MPa   (g)
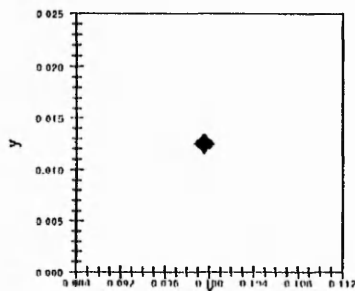

52MPa   (h)
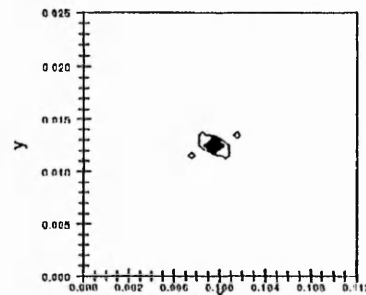
d′ - transverse damage   d - shear damage

Figure 11.5 continued. Damage development for 20° material using the three zone mesh.
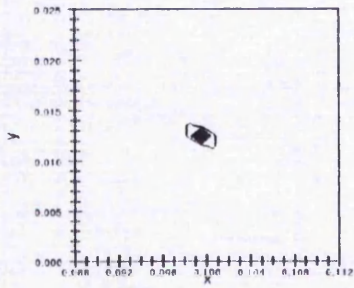
54MPa (i)
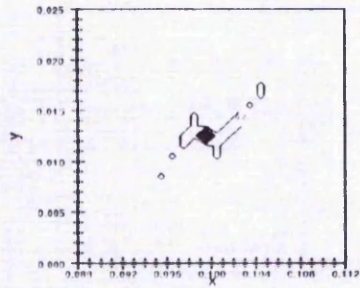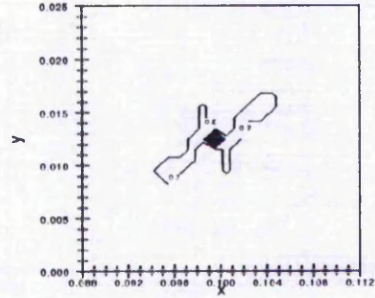
56MPa (j)
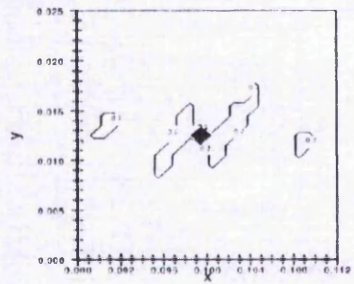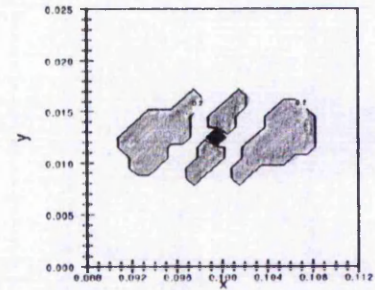
58MPa (k)
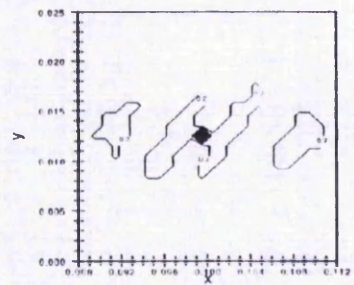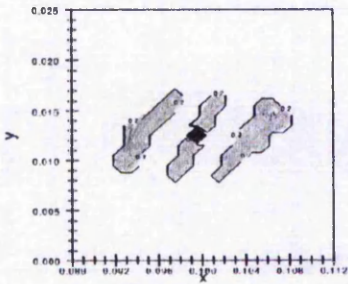
60MPa (l)
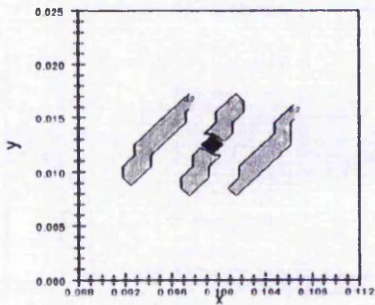
d´ - transverse damage   d - shear damage

Figure 11.5 continued. Damage development for 20° material using the three zone mesh.

132
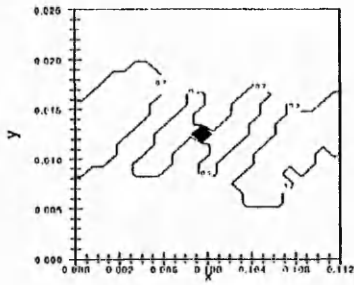
62MPa   (m)
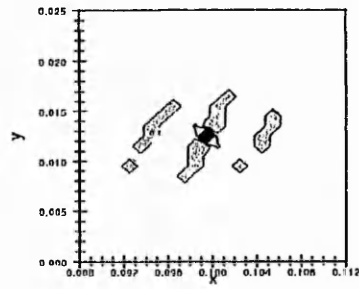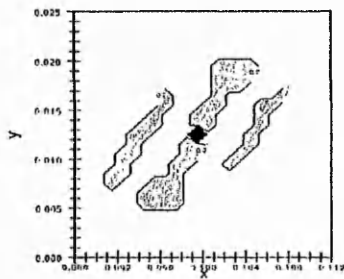
64MPa   (n)
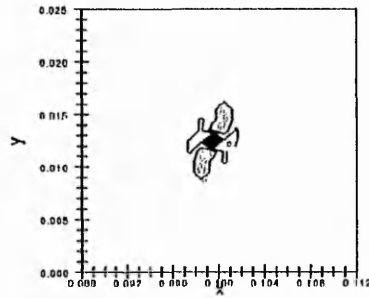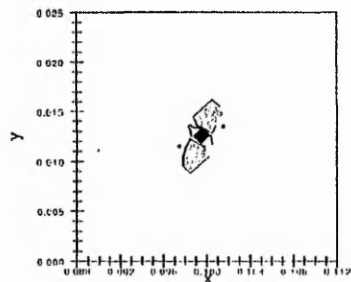
66MPa

d′ - transverse damage   d - shear damage
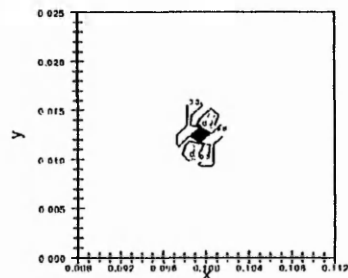
Figure 11.5 continued. Damage development for 20° material using the three zone mesh.
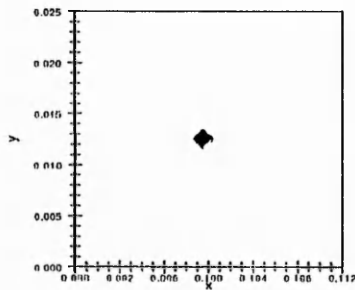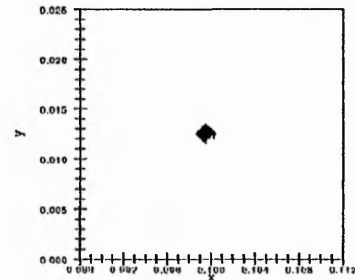
6.8MPa   (a)
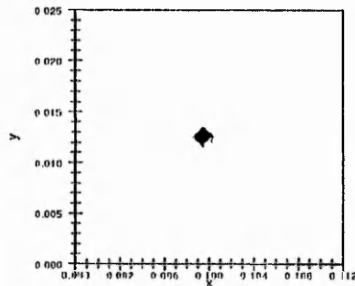
7.0MPa   (b)
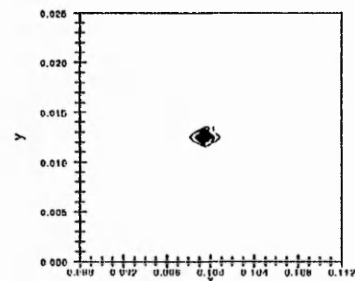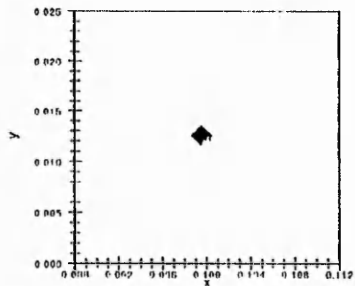
7.4MPa   (c)
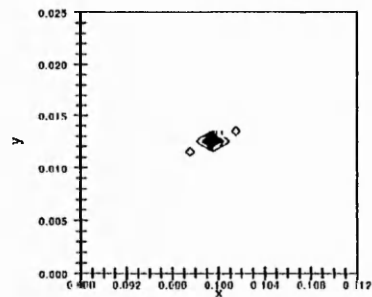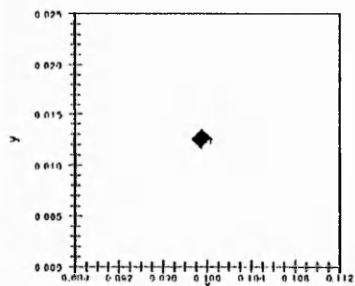
7.6MPa   (d)
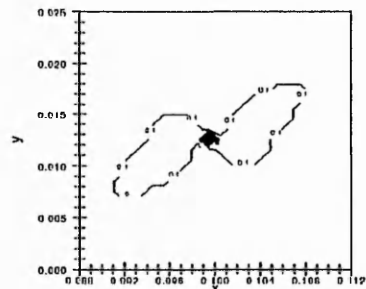
d´ - transverse damage   d - shear damage

Figure 11.6 Damage development for 45° material using the three zone mesh.
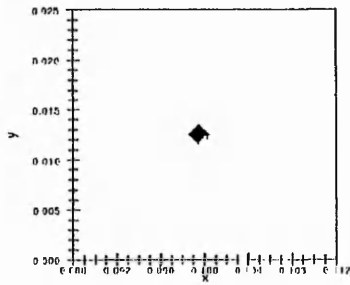
7.8MPa   (e)
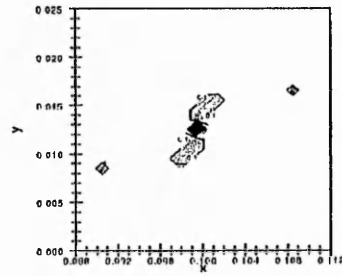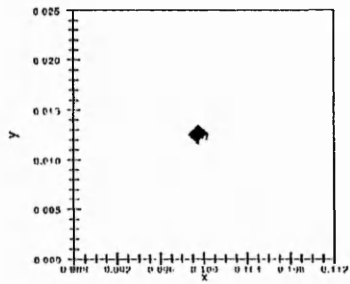
8.0MPa   (f)
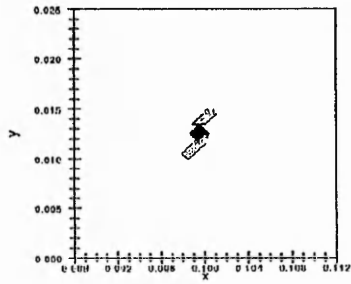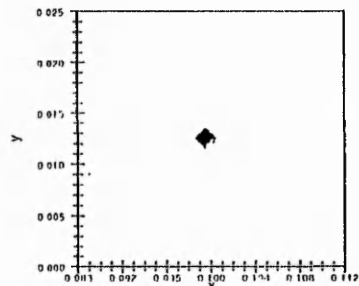
8.2MPa   (g)
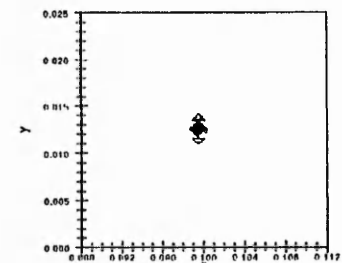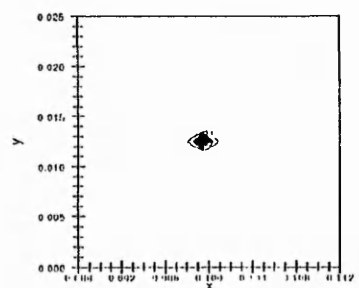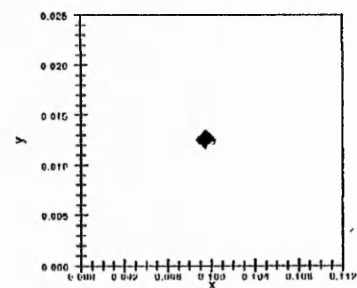
8.8MPa   (h)

d' - transverse damage   d - shear damage

Figure 11.6 continued. Damage development for 45° material using the three zone mesh.
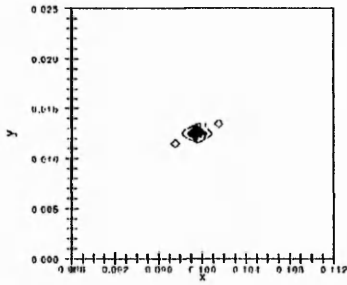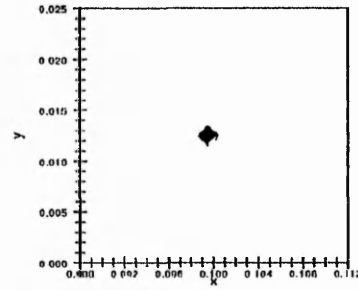
9.2MPa (i)
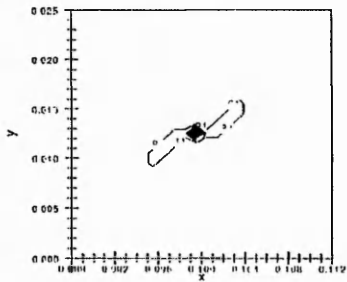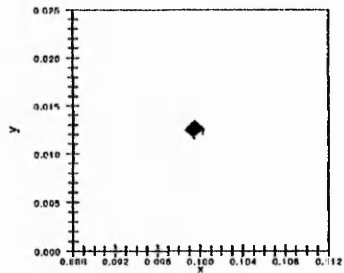
9.4MPa (j)
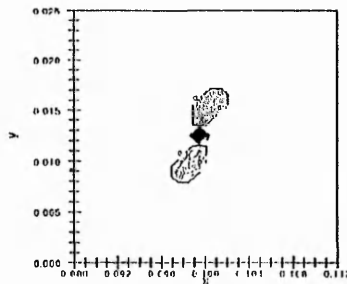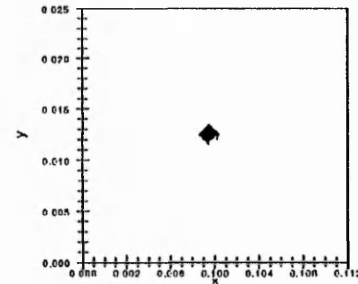
9.6MPa (k)
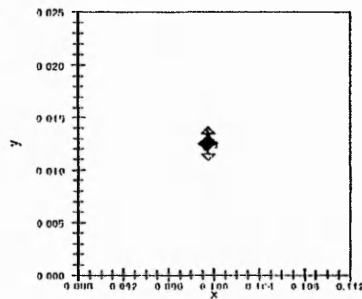
10.0MPa (l)
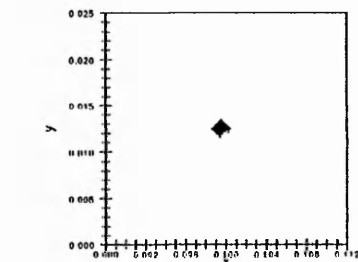
d´ - transverse damage   d - shear damage

Figure 11.6 continued. Damage development for 45° material using the three zone mesh.
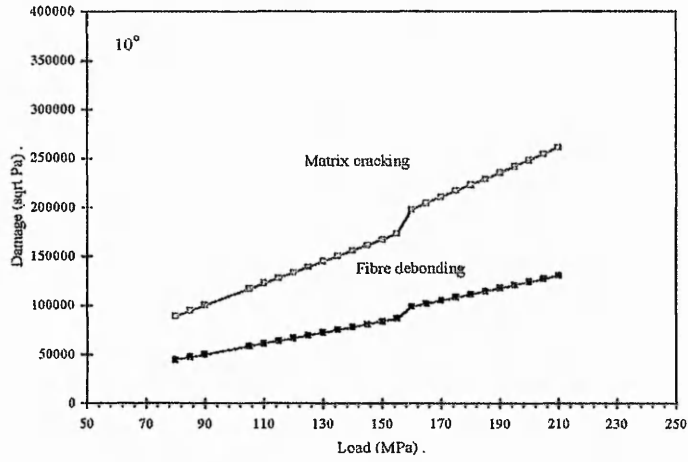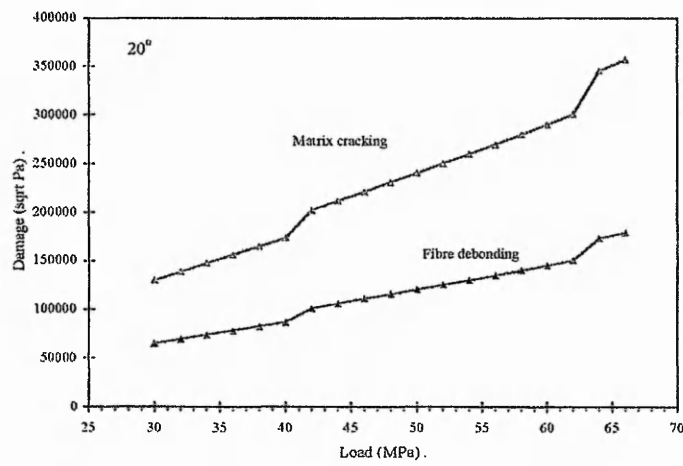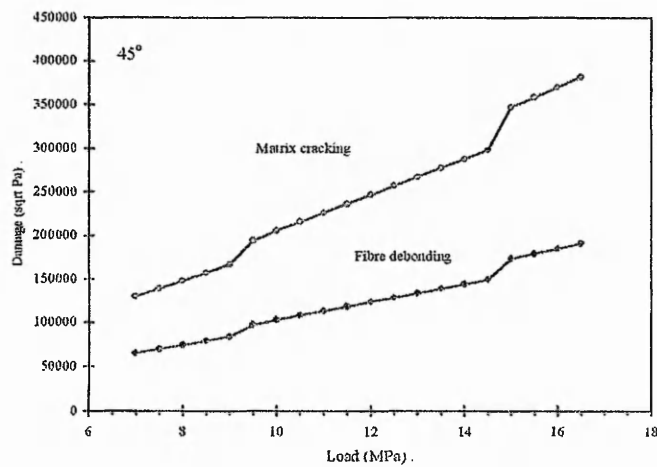
Figure 11.7 Damage levels for a) 10° b) 20° and c) 45° models, showing matrix cracking (pink) and fibre debonding (blue).
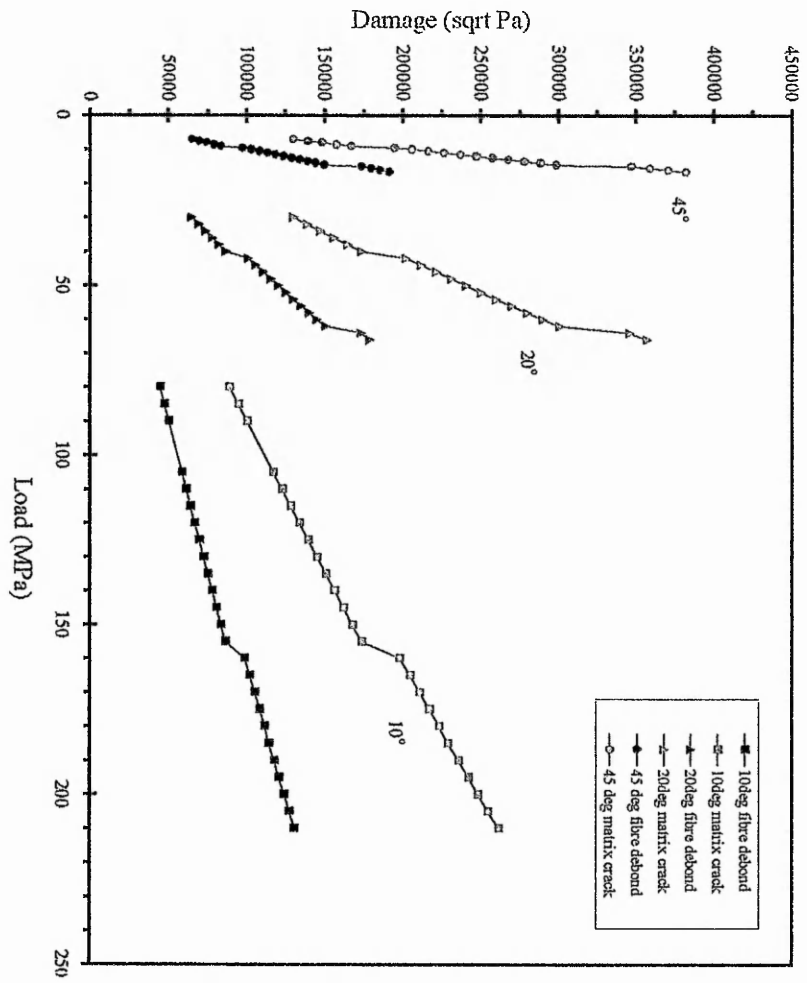
Figure 11.8 Damage graphs for 10°, 20° and 45° damage models.

Damage (sqrt Pa)

Load (MPa)

45°

20°

10°

10deg fibre debond
10deg matrix crack
20deg fibre debond
20deg matrix crack
45 deg fibre debond
45 deg matrix crack

138

11.2 Comparison of Damage Growth for Various Material Angles

The difference between each simulation was the angle of the main material axis with respect to the loading direction (x direction). The material properties had equivalent fibre directions of 10°, 20° and 45°. The same principal material property values used are summarised in Table 9.2 in Chapter 9.

The load level at which the first damage occurs differs predictably for the three material angles. The 'stronger' material, (10° orientation), shows damage development at 105MPa (figure 11.1(a)), compared to 20° at 32MPa (figure 11.2(b)) and 45° at 7.2MPa (figure 11.3(b)). The significantly higher stress required to develop damage in the 10° material compared to 45° is as observed in experimental results for composite material. The alignment of the strong fibres to the load requires a higher loading before damage occurs in the surrounding matrix or the fibres themselves.

The damage growth pattern can be summarised as localised increases of damage in the elements about the central 'damaged' element and corresponding reductions in material moduli followed by a near universal increase of damage level in all elements of the mesh at specific loads. As an example of the damage development pattern a description of the d (shear) damage change for the 10° experiment using the rectangular element shape, will be given (figure 11.1).

The first load at which elements are sufficiently stressed to induce damage is at 105MPa (figure 11.(a)). The area is confined to elements changing northeast (NE) to southwest (SW), and isolated elements NW-SE. The damage has reduced the shear modulus by 0.1. The damage area enlarges to have symmetrical NE-SW and NW-SE extensions from the centre. The damage growth pattern enlarges and broadens the area of elements affected in the NE-SW directions for the 120MPa load. The other two limbs extend the damaged area north and south across the width of the specimen at the 120MPa and 125MPa loads (figure 11.1(c) and (d)). With the next load increment to 130MPa the majority of the elements increase their shear damage state from 0.0 to 0.1 (figure 11.1(e)). The pattern observed in figure 11.1(e), is the outline of the elements that remain at the d=0.0 level. These elements are at positions north and south (long relatively thin limbs), broad areas east and west, and single elements east and west of the central element. At

139

increasing loads, figure 11.1(f) for example, the wells of less damaged elements (d=0.0) diminish as the elements deform to the damage level d=0.1. Over the following 35-40MPa the shear damage equilibrates at d=0.1 for all elements. Then at 180MPa (figure 11.1(l), the damaged state of elements near the centre increases to the next damage level of d=0.2. The damage pattern repeats the growth directions NE-SW and N-S from the centre. This time the more damaged elements extend the width of the specimen (y axis direction). Superimposed over the centre portion of the mesh are elements that have been damaged to even higher levels (d=0.3), figure 11.1(o). The final picture of the shear damage at 220MPa, figure 11.1(p), is the damage pattern when the fibre debonding limit (failure) was reached. The majority of the elements are at the d=0.2 level, with the presence of wells at d=0.1 (broad rings east and west and two thin, long limbs north and south of the centre). In the sloping 'H' shaped area of damage there are elements that have reached the level of damage where d=0.4. The final shear modulus for these elements has reduced by 40% from it initial value.

An obvious result of the damage pattern is the elements immediately around the central element are the first to change for all three angles. Of the eight elements that surround the central one, it is not clear if there is a certain element that changes first for a particular fibre angle. There are no other stress concentrations sufficiently high to change the moduli, this includes the restrained grip positions along the short sides of the mesh. There are element positions that do not change initially for any of the angles, these are north (N) and south (S) of the centre- tangential to the maximum stress direction.

Looking at the transverse damage parameter d', changes up to the point when the whole mesh changes, the pattern of growth is different for the angles. The figures of particular interest are figure 11.1(h) for 10°, figure 11.2(f) for 20° and figure 11.3(h) for 45°. The damaged area for each fibre angle reduces with increasing angle. The shape and number of damaged arms radiating out from the centre element also reduces. The damage zone for the 10° material extends 6 to 7 elements away from the centre, in the form of four arms. The 20° material has the four arms, but the pattern is not as extensive, only extending 4 elements away. The 45° material has the smallest extension of ENE-WSW limbs, and the other two arms (NW-SE) are only just visible as a damaged area around the central element.

The transverse damage parameter (d') contour plots in figures 11.1(p), 11.2(m) and 11.3(h) for the 10°, 20°, and 45° experiments respectively, show the damage accumulation pattern prior to the end of the simulations. The larger angle material, 45°, has a less extensive damage pattern at the end compared to the extended pattern for the 10° experiment. The 20° material has damage at the d'=0.2 level, and the 45° material at only d'=0.1, which is dramatically different to the state of the 10° material. The 10° experiment calculated elements with damage at d'=0.4, a difference of d'=0.2 above the general level of the mesh. This indicates that the smaller angle model was able to develop degradation in the mesh to a higher level before failure. The material strength characteristic allows for highly damaged elements in the mesh before the failure stress level is reached.

11.3   Changing Angle of Damage Growth Pattern

The direction of the extending arms of damage also change with changing material angle. A summary figure of the contour plots for the three angles is shown in figure 11.9 for the loads that show increasing damage lobes extending from the central element. The 10° picture, from figure 11.1(o), has the edge of the sloping damage area at 64°/62° to the x-axis, compared to 20° at 58°/52° (figures 11.2(m) and (j)) and 45° at 39°/58° (figures 11.3(h) and (d)). The changing orientation of the damaged zones will depend on the angle of the fibres in the models and the material properties for the ply. As the fibre angle increases the material stiffness in the transverse and shear directions also increase but not at the same rate. The shear modulus peaks at 45°, compared to the transverse modulus that still increases until 90°. Within the damage model the damage constants (Y_c and Y_c') also influence the rate at which damage accumulates, therefore a complex mixture of parameters need to be further investigated to analytically solve the angle at which the damage will grow from the central element.

11.4   Matrix Cracking and Fibre Debonding Development

Comparing the results for all angles, the damage develops first in the d parameter (shear). The d parameter is associated with the shear stresses and damage development using equation 9.6 in Chapter 9. The equation constants used Y_o and Y_c, are smaller than for the transverse constants Y_o' and Y_c' (Table 9.2). This leads to the more rapid
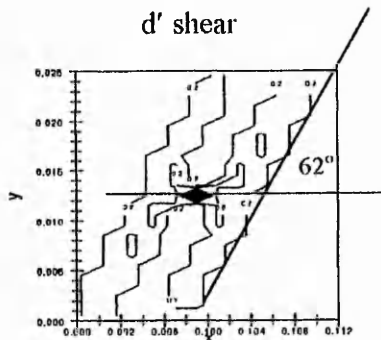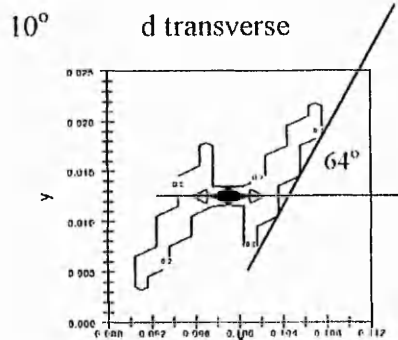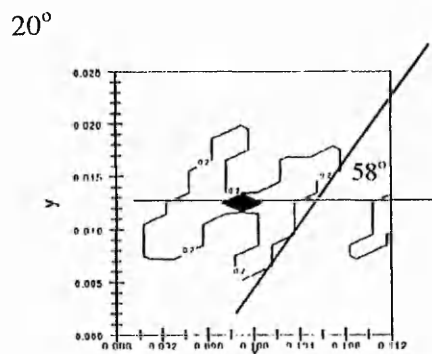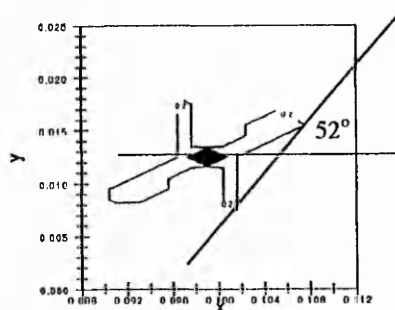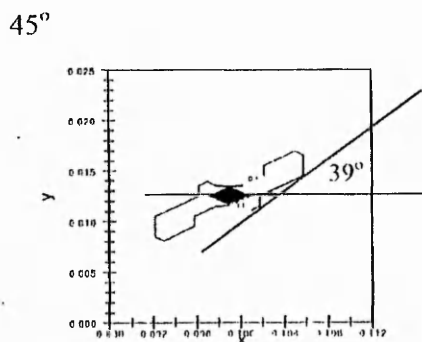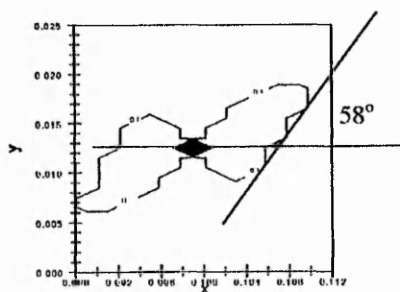
Figure 11.9 Summary of the damage extensions from the central element for the three material angles.

142

development of matrix cracking rather than fibre debonding. The matrix cracking dominance is principally due to the larger constant b term involving four times the transverse damage value, $Y_{d'}$, calculated in Equation 9.4. The smaller shear term, Y_d, does not have a large influence on the growth pattern of matrix cracking. The modification of d' the transverse modulus modifier, in Equation 9.7, uses the larger constant values, Y'_o and Y'_c, which require a higher stress level to initiate damage so occur at higher stresses.

The contour plots at low load levels show damage radiating away from the centre for the shear damage parameter (d) but no change in the transverse damage parameter (d') value. The level of the transverse damage parameter d', rises to the next level at a higher load. This change corresponds to a gradient change in the graphs in figures 11.7 and 11.8, of the matrix cracking damage (**Y**) and the fibre debonding (**Y'**). For all three angles there is a change of gradient when the general transverse damage level changes for the majority of the mesh elements. The damage value (y axis figure 11.8) at the step is the same for the matrix cracking and the fibre debonding for the three angles. The first step in the matrix cracking is at about 170000√Pa and the fibre debonding at 90000√Pa.

The graphs for the 20° and 45° experiments also show another step (figure 11.7). The matrix cracking damage level is at about 300000√Pa and fibre debonding at 150000√Pa. The 10° experiment does not reach this point of damage development in the damage parameters d and d', before an element is calculated as having reached the failure limit (Y_s') and the experiment is stopped.

The shear modulus modifier, d parameter, has a sequence of growth patterns for the different angles, but has no noticeable affect on the matrix cracking or fibre debonding development (figure 11.7). This is due to the small magnitude of the Y_d term in Equation 9.4 for matrix cracking, and the shear term present in the fibre debonding calculation (Equation 9.5).

The rate of damage accumulation between the different material angle simulations increases with increasing angle, as seen in figure 11.7. The gradient of the lines for both matrix cracking and fibre debonding increase for larger fibre angles to the load. This is

observed in SEM pictures of small angle composite material where the fibres take the majority of the load in preference to the matrix, therefore reducing the amount of damage observed in the matrix and fibre interface region.

An extension to the above relationship for calculated damage development is to relate the damage rate value to a matrix crack length or a fibre debond length, and then to the different acoustic emission emitted by a composite material. This additional analysis could be considered in future work.

11.5   Damage Responses to Different Element Dimensions

For a realistic response, a damage model using finite element analysis must not have the damage development influenced by the mesh dimensions. The degree of damage in the model must be independent of the size of the elements used. The detailed spatial development of the damage pattern will be influenced by the size of the element. However there should be comparable responses at similar stages in the loading of the model.

This damage model was independent of the mesh dimensions for the development of damage. The results from the three experimental angles, 45°, 20° and 10°, were recalculated using the different mesh described in Chapter 10.2, with three zones of different sized elements.

The 10° model with the central zone of smaller, square elements, does mirror the damage accumulation seen in the rectangular mesh. In figure 11.4(d), the transverse damage parameter d', shows the first changing elements at a load level of 120MPa. This is comparable with the start in the rectangular element model at 125MPa. The step in d' parameter level from d'=0 to d'=0.1, is at the same load level (160MPa) for the two meshes. The damage development between these two points generally follows a similar pattern for the different sized element. There are arms of more damaged elements radiating out from the central element at ENE-WSW and NW-SE directions. The shear damage starts to modify elements at a similarly early 100MPa. The shape of the damaged area prior to the shear damage level for the mesh rising, is likewise at the 125MPa load, with the common N-S smaller limbs, between broader NE-SW zones of damage.

144

The 20° experiments compare favourably with the starting load for changes in the transverse and shear parameters, d (shear) starts at 32MPa and d' (transverse) being at 38MPa for both models. The shapes of the damage zones are similar, with the square element model (3 zone) producing a slightly smaller zone of influence.

The 45° experiments have the same changing loads for the parameters d and d' in the 3 zoned mesh and the rectangular element mesh. The shape of the damage zone for the transverse parameter d' at 9.4MPa is similar - a narrow NE-SW area of more damaged elements (figures 11.3(h) and 11.6(j)). The next load step, 9.6MPa has most of the elements raising the d' level to 0.1, except for two wells north and south of the central element. The shear modulus modifier, d, has a similar growth pattern for both mesh. For example at 7.6MPa (figure 11.3(d) and figure 11.6(d)), both experiments produced a broad pair of damage arms, NE-SW of the central element.

11.6   Conclusion

The damage model was used in conjunction with the finite element analysis to simulate the accumulation of damage in a stressed composite material. The damage manifests its self as a reduction in the shear and transverse material moduli relative to the fibre orientation. The stresses within the finite element model were higher around the central stiffened element. This stress concentration enabled the seeding of damage in the centre of the mesh rather than at the extremities. The load at which the first level of damage was attained was different depending on the fibre angle. The stronger 10° material required a higher load than the 20° which in turn was higher than for the 45° material.

The first damage to appear was the modification to the shear modulus caused by changes of the d damage parameter. The changes were due to the lower constant values used in the damage model equations. This early decrease in strength was not obvious in the damage graphs for matrix cracking or fibre debonding because of the relatively small affect shear modulus changes had on the calculated damage levels. Changes to the transverse damage parameter d' on an overall mesh scale produced significant increases in the matrix cracking and the fibre debonding damage levels.

The angle of the fibre in the model composite material had an affect on the area of material with above average damage and also the orientation of these zones of damage.

145

The small angle 10° material had a pronounced highly damaged area with elements at a damage level of d=0.4 before failure. This contrasts with the 45° model that had only just reached d=0.1 before failure. The 10° damage zone extended across the central zone of the mesh at a greater angle relative to the main material axis, compared to the 45° material which was broader and the damage zone showed a closer orientation to the material axis. These differences are due to the interaction of the changing material moduli and the constants used in the damage model equations.

The finite element simulations using two different element sizes and shapes, square and rectangular produced similar damage growth patterns in the area around the central element. The degree of damage, as calculated by the changing value of the damage parameters d and d', are similar for the different mesh. Therefore it can be concluded that the finite element mesh used did not significantly influence the model.

Drawing together the results from the damage modelling experiments reported here in this chapter and the practical results from the acoustic emission monitoring reported in Chapter 8, there are similarities. The comparison is shown in the summary figure (figure 11.10), which is a combination of figure 11.8 and a modified figure 8.8, for damage model and acoustic emission results respectively. The relative positions of the damage model results are comparable with the acoustic emission on a common stress axis.

The 10° material results are separated from the other material results for both experimental procedures. The impression given by both sets of results is that the 10° material required the higher stresses for damage to accumulate. The 45° damage model results are compared with the 30° acoustic emission results because of the distorted stress values for the 45° acoustic emission results. The rapid rise in damage development with stress is reflected for both the practical and theoretical experiments. Both results requiring relatively lower stresses to produce material failure.

The summation of Clusters 1 and 2 produces a total for matrix dominated acoustic emission and Cluster 1 reflects the damage associated with the fibre, fibre debonding. The gradients of the acoustic emission rate and the accumulation of the damage model are comparable. The energy bursts released by over stressed material and detected as acoustic
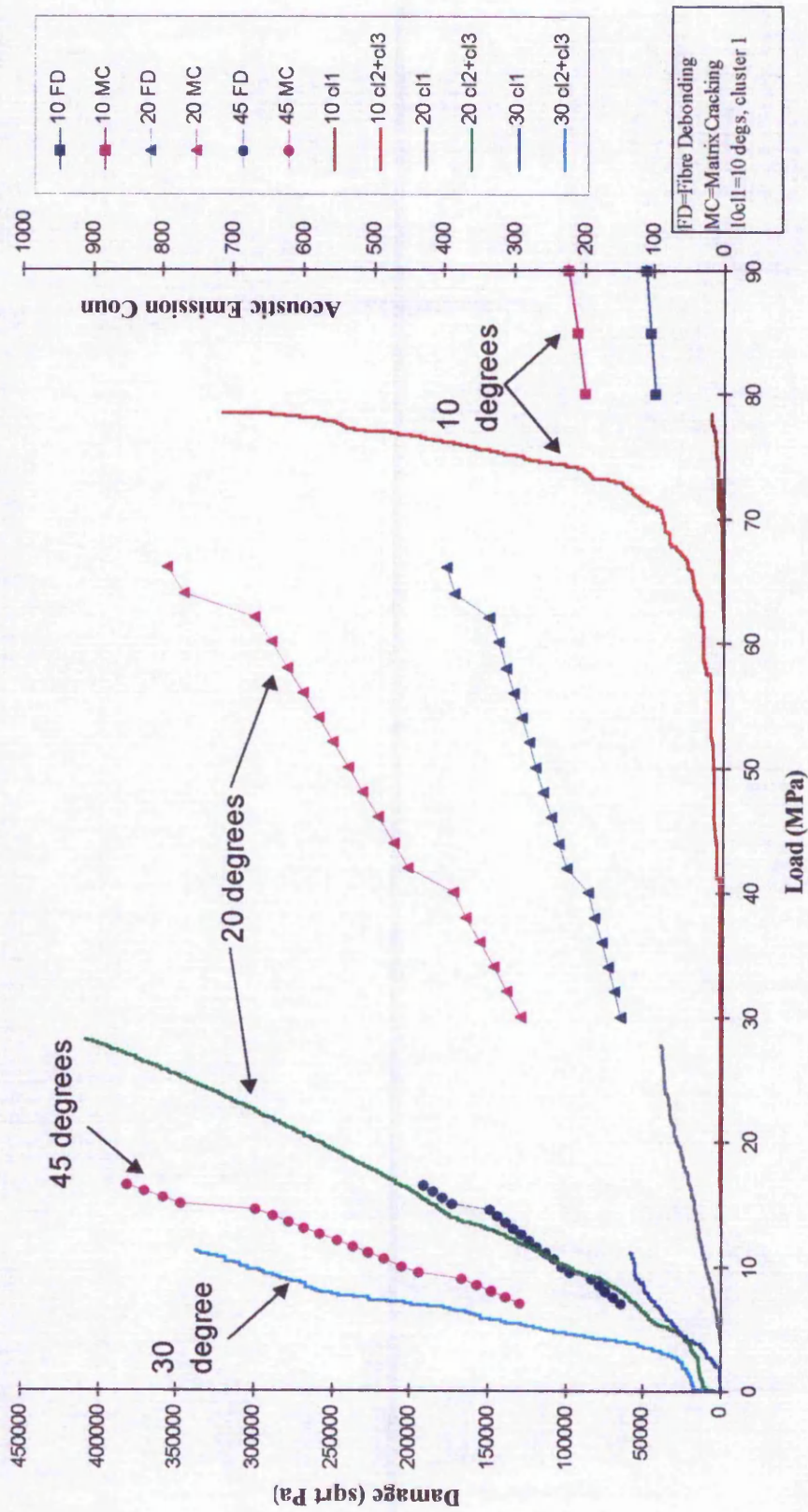
Figure 11.10 Summary of the damage model and acoustic emission results with respect to the loading.

emission stress waves, may be compared to the discrete increases in the damage parameters per element in the finite element mesh. Both model and practical experiment related damage with the increasing stress in the material. This result indicates that the two experiments are modelling or monitoring the same phenomena of damage accumulation in a composite material.

12   Conclusions and Future Work

12.1   General Conclusions

An initial aim of this work was to develop an acoustic emission detection system to investigate the damage occurring in a composite material. The material deforms and releases part of the stored strain energy within the material as sudden bursts of acoustic emission. The experimental system used to monitor the acoustic emission was simple and robust, which allowed the investigation of damage without the need for visual confirmation and the sectioning of the specimen. The acoustic emission was detected at the surface by a single piezoelectric transducer and transformed into an oscillating voltage. This voltage signal was digitised and post processed using dedicated computer programs to extract acoustic emission waveform characteristics. Due to the computer integrated storage recovery rate, the number of events captured was a small proportion of the total emitted by the deforming composite material but a representative sample of the total population of events. The digitising rate for the A to D board was adequate for the transducers used, since they were resonant transducers with a limited sensitive frequency range.

Analysis of the acoustic emission from experimental work performed here, revealed groups of events with similar characteristic waveform parameters. The use of cluster analysis brought together events with similar waveform amplitudes, risetimes and ringdown counts. To promote the development of different ratios of the damage mechanisms in a composite material, the test was performed on unidirectional material with different fibre orientations relative to the loading axis. The small angle material such as 0° and 10° orientations to the load, produced the larger acoustic emission events (Cluster 1) predominantly at the latter, high load stages of the experiment. The smaller events (Cluster 2 and 3) were occurring throughout the experiments which relates to the continuous background damage occurring in the matrix. There were changes in the rate of occurrence of the matrix associated acoustic emission about the failure point. This increase in matrix cracking and the occurrence of the Cluster 1 events was associated with fibre related damage, and was responsible for the change in the material strength seen as a material modulus decrease.

149

The composite material with fibres at larger angles (20° and 30°) to the load direction developed early damage at lower loads in the form of fibre debonding and matrix cracking as expected. Since the strong glass fibre axis was not parallel to the load, the material stresses were directed across the fibre-matrix interface. This weaker component of the composite material failed at a lower load. The acoustic emission coincided with the earlier start of fibre debonding along the stressed interface zones, and hence the occurrence of Cluster 1 events relatively earlier in the experiments. In the experimental results shown in Figure 11.10, the numbers of Cluster 1 events are significantly lower than the combined Clusters 2 and 3. The relationship with respect to the loading is as expected – the small angle material producing acoustic emission or damage initiation, at the higher load levels.

The largest interference to effectively analysing acoustic emission waveforms are the errors incurred due to the complicated attenuation paths between damage mechanism sources and the transducer. This is due to the anisotropic composite material. The attenuating path through the composite material and the type of transducer will modify the results. Since the dimensions of the composite material under test were only a few multiples of the size of the transducer piezoelectric face, this limitation was not expected to influence the results greatly. However, results of the average acoustic emission amplitudes per cluster did show a decrease in value with increasing fibre angle in the composite material. This may have been due to the increased attenuation caused by more damage in the weaker material producing scattering of the stress wave.

The damage model investigated here simulated a single ply composite material with fibre orientations similar to those in the experimental acoustic emission experiments. The damage was modelled to represent matrix cracking and fibre debonding. The model predicted the early onset of damage at low loads for material with larger fibre angles relative to the loading direction, as seen in the summary figure 11.8. The results from the three angles examined, (10°, 20° and 45°) showed that matrix cracking (pink lines) was more pronounced than fibre debonding (dark blue), with greater increases in the damage level. As the stress on any of the composite materials modelled was increased, the matrix cracking deformation was greater than for the fibre debonding. The greater amount of

matrix damage was consistent with that observed in the practical acoustic emission monitoring, where there were more events in Clusters 2 and 3 compared to Cluster 1.

Representation of the damage development in the theoretical model was seen as changes in the shape and the magnitude of the contour plots for the shear and transverse moduli modifiers (d and d'). Due to the choice of the magnitude of the constant b, used to calculate matrix cracking damage (equation 9.4), the transverse damage parameter d', had a greater influence on the accumulation of damage in this model. However the shear damage was the first to modify its material modulus at lower loads than the transverse modifier. This was due to the smaller equation constant values (Y_o and Y_c) which controlled initiation and rate of increase in shear modulus modification.

The damage zones radiating from the central damaged element varied in orientation with respect to the main material axis due to the relative material moduli. The direction of damage extension was probably already set at the start of the experiment by the equation constants used in the model including the material moduli.

The damage model consisted of a series of computer programs that sequentially ran the damage equation calculations, made the changes to the finite element model and resubmitted the updated model for reanalysis. This damage analysis loop enabled more than one principal material axis angle to be automatically tested at many different load levels. The development of matrix cracking, fibre debonding and moduli reductions were studied for different element dimensions and material properties. The results from studies using rectangular elements (1 x 2mm) compared with square elements (1 x 1mm) produced similar damage development and magnitude.

From the initial study here, it has been shown that the different damage mechanisms have different acoustic emission waveform characteristics that can be grouped into clusters. The parameters used for the cluster analysis can be simple amplitude variations in the time domain, but with improved quality of data, information from the frequency domain could be used. Further improvements in the quality and variety of the cluster variables will come with improved data capture equipment. The results of this work highlight the usefulness of acoustic emission analyse and differentiate the many damage

mechanisms in composite material. The damage model used damage parameters which modified the material moduli to represent progressive failure, and likewise matched the observed damage accumulation of fibre debonding and matrix cracking in composite material. The comparison of the experimental with the theoretical development of damage in a composite material revealed similarities in growth rate with respect to the stresses within the material.

12.2   Future Work

The amplitude of the acoustic emission waveform was characteristic of the total energy content of the damage mechanisms occurring. Differences in the waveform were related to the fracture and debonding nature of strong glass reinforcing fibres and the cracking of the surrounding resin matrix. Successful multivariate analysis to differentiate groups of similar source mechanisms relied on the quality and the number of parameters in the input data set. The present simple equipment would benefit from improved rates of acoustic emission capture since the increased rates nearing specimen failure were not reflected in the increased acoustic emission monitored by this system. This would entail a much faster storage system with a larger storage capacity. The quality of parameter data is closely related to the number of digitising points representing the waveform. If the transducer was changed to a wide frequency band transducer this would provide more information about the damage mechanisms in the frequency and time domains, requiring a more sophisticated and therefore more expensive digitising system.

An enhancement of the system would be to integrate the acquisition of acoustic emission with the automatic measurement of the waveform parameters and then the placement in a suitable cluster. This will speed up the classification and the monitoring of acoustic emission events with critical affects on the composite material integrity. The occurrence of Cluster 1 events associated with detrimental fibre debonding or fracture could be monitored more closely than the general non-critical background occurrence of minor matrix cracking. The choice of the clustering program may also influence the degree of grouping of similar events. Other programs using different selection criteria and quantity of data may place boundary events in different final positions.

With the use of a relatively smaller transducer and a triangulation method, it could be possible to locate specific areas of active damage with a degree of accuracy that is lost using the large faced transducer. A detailed acoustic emission investigation of important parts of a structure could be included in the continual monitoring for structural integrity. Automatic acoustic emission monitoring could then provide information of damage occurrence, with cluster analysis indicating the degree of severity.

An advanced use of acoustic emission monitoring could be the monitoring of damage in hybrid composite material with different fibres such as aramid or carbon, or different degrees of matrix cure and sizing, which are likely to produce subtle differences in the waveform characteristics. Therefore, after initial tests to characterise the damage sources, the monitoring of acoustic emission would allow the possible detailed monitoring of damage progression through hybrid laminates with different ply materials, as previously reported by Short and Summerscales (1984).

The finite element model could be extended to represent more complicated ply combinations. The development of a laminate model with various fibre angle and changes in material moduli for hybrid composite materials, could be analysed. The future study of damage accumulation in composite material will develop more rapidly as the means to process huge quantities of computer data becomes cheaper and more available. The inclusion of other damage mechanisms such as fibre breakage and plastic deformation of the matrix, will extend the usefulness of the models.

13   Acknowledgements

I would like to thank Lewis Morgan and Gordon Stirling from the sponsoring company British Gas, for their assistance and the chance to work in the very dynamic subject of composite material testing.

Due to the diverse contents of the project it was helpful having two supervisors, Dr Roger Hill and Dr Richard Brooks, who were experts in their fields. It was also useful working at both The Nottingham Trent University and The University of Nottingham, and having the availability of quality resources and assistance.

There are many people at both universities, who helped me on technical matters small and large, who I thank very much. I single out for special thanks Emmanuel Okoroafor, Peter Hooper, Roger Smith and Howard Rees.

The writing up of my work would not have been possible without the loan of equipment and time given by friends, thanks.

14   References

Agarwal, B.D., Bhushan, B., and Mazkumdar, S.K., 'Damage propagation during flexural and axial fatigue of unidirectional kevlar fabric reinforced epoxy composites', Proceeding of 7th ICCM, Eds.: Wu, Gu and Wu, 1989, Vol 2, pp.367

Allen, D.H., Harris, C.E. and Groves.S.E., 'A thermomechanical constitutive theory from elastic composites with distributed damage- I. Theoretical development', Int. Journ. Solids. Structures, 23(9), 1987, pp.1301-1318.

Allen, D.H., Harris, C.E and Groves, S.E., 'Damage modelling in laminated composites', Yielding, Damage and Failure of Anisotropic Solids, EGF5 (Ed. J.P. Boehler) 1990, Mechanical Engineering Publications, London, pp.535-549.

Allen, D.H., Groves, S.E. and Harris, C.E., 'A cumulative damage model for continuous fibre composite laminates with matrix cracking and interply delaminations', Composite Materials: Testing and Design (8th conf.), ASTM STP 972, J.D. Whitcomb, Ed., American Society for Testing and Materials, Philadelphia, 1988, pp.57-80.

Allix, O. and Ladeveze, P., 'Interlaminar interface modelling for the prediction of delamination', Composite Structures, Vol.22, 1992, pp.235-242.

Allix, O, Ladeveze, P, Gilletta, D., and Ohayon, R, 'A damage prediction method for composite structures', Int. J. for Numerical Methods in Engineering, Vol. 27, 1989, pp.271-283.

Almeida, A. and Hill, E.K., 'Neural network detection of fatigue crack growth in riveted joints using acoustic emission', Materials Evaluation, 1995, Vol.53(1), pp.76-82.

Awerbuch, J, Gorman, M.R. and Madhukar, M., 'Monitoring acoustic emission during quasi-static loading-unloading cycles of filament-wound graphite-epoxy laminate coupons', Materials Evaluation, Vol. 43, 1985, pp.754.

Barre, S. and Benzeggagh, M.L., 'On the use of acoustic emission to investigate damage mechanisms in glass-fibre-reinforced polypropylene', Composite Science and Technology, Vol. 52, 1994, pp.369-376.

Belchamber, R.M., Betteridge, D., Chow, Y.T., Lilley, T., Cudby, M.E.A. and Wood, D.G.M., 'Evaluation of pattern recognition analysis of acoustic emission from stressed polymers and composites', Journal of Acoustic Emission, Vol.4(4), 1985, pp.71-83.

Bhat, M.R. and Murthy, C.R.L., 'Fatigue damage stages in unidirectional glass-fibre-epoxy composites: identification through acoustic emission technique', Int. J. Fatigue, Vol.15(5) 1993, pp.401-405.

Bhat, M.R., Majeed, M.A. and Murthy, C.R.L., 'Characterization of fatigue damage in unidirectional GFRP composites through acoustic emission signal analysis', NDT & E International, Vol.27(1), 1994, pp.27.

Bouadi, H and Sun, C.T., 'Hygrothermal effects on structural properties of unidirectional glass-epoxy composites', Proceeding of 7th Int. Conf. Composite Materials, Tokyo, Eds. Wu, Gu and Wu, Vol. 2, 1989.

Brindley, B.J., Holt, J. and Palmer, I.G., 'Acoustic Emission - 3 The use of ring-down counting', Non-Destructive Testing, December, 1973, pp.299.

Brooks, R, Laminate analysis program from a short course, 'Introduction to Engineering with Composites', The University of Nottingham, Mechanical Engineering Department, 1992.

Budiansky.B and N.A.Fleck, 'Compressive failure of fibre composites', J.Mech.Phys.Solids, 41(1), 1993, pp.183-211.

Cantwell,W.J. and J.Morton, 'The significance of damage and defects and their detection in composite materials: a review.', J.Strain Anal.Eng.Design. **27**(1), 1991, pp.29-42.

Caprino, G. and Teti, R., 'Residual strength evaluation of impacted GRP laminates with acoustic emission monitoring', Composites Science and Technology, Vol. 53, 1995, pp.13-19.

Caprino, G. and Teti, R., 'Quantitative acoustic emission for fracture behaviour of centre-hole GFRP laminates', Journal of Composite Materials, Vol.28 (13), 1994, pp.1237.

Carlsson, L.A, Gillespie, Jr., J.W. and Pipes, R.B., 'On the analysis and design of the end notched flexure (ENF) specimen for mode II testing.', J.Composite Materials, **20**, 1986, pp.594-604.

CARP Code, 'Recommended Practice for acoustic emission testing of fiberglass Tanks/vessels', Corrosion-Resistant Structures Committee, Reinforced Plastics/Composites Institute, The Society of the Plastics Industry, USA, 1982.

Chang, F.K. and Chang, K.Y., 'A progressive damage model for laminated composites containing stress concentrations', J.Composite Materials, **21**, 1987, pp.834-855.

Chen, F., Bazhenov, S., Hiltner, A. and Baer, E., 'Flexural failure mechanisms in unidirectional glass fibre-reinforced thermoplastics', Composites, Vol 25(1), 1994, pp.11.

Cherfaoui, M, Roget, J., Lemascon, A. and Jeanville, M., 'The study of acoustic emission from composites by means of multivariate analysis', 6th International Conference on Composite Material, Imperial College, London, 1987, pp.1/424.

Chow, T.M., Hutchins, D.A. and Mottram, J.T., 'Simultaneous acoustic emission and ultrasonic tomographic imaging in anisotropic polymer composite material', J. Acoust. Soc. Am. Vol.94 (2/1), 1993, pp.944.

CRAG , Composite Research Advisory Group, 'Test methods for the measurement of the engineering properties of fibre reinforced plastics', editor: P.T. Curtis, Technical Report 88012, February 1988, Procurement Executive, Ministry of Defence, Farnborough, UK.

Crostack, H.A., 'Basic aspects of the application of frequency analysis', Ultrasonics, November, 1977, pp.253.

Cui, W.C., Wisnom, M.R. and Jones, M., 'Failure mechanisms in three and four point bending tests of unidirectional glass/epoxy', Journal of Strain Analysis, Vol 27 (4) 1992, pp.235.

Dai, Z.Z. and Harris, B., 'Acoustic emission study of impact-damaged GRP pipes', NDT International, Vol. 21(4), 1988, pp.259.

Devries, F., Dumontet, H., Duvaut, G. and Lene, F., 'Homogenization and damage for composite structures', Int.J.for Numerical Methods in Engineering, 27, 1989, pp.285-298.

Dharan, C.K.H., 'Delamination fracture and acoustic emission in carbon, aramid and glass-epoxy composites', 6th International Conference on Composite Materials, Imperial College, UK, 1987, pp.1/405.

Drobot, Y.B, 'A priori evaluation of the speed and the attenuation of acoustic emission signals', Russian Journal of Nondestructive Testing, 1993, Vol.28(9), pp. 526-529. Far Eastern Standard Scientific and Production Union, Khabarovsk. Translated from Defektoskopiya, No. 9, pp.17-21, September 1992.

Dumont, J.P., Ladeveze, P., Poss, M., and Remond, Y., 'Damage mechanics for 3-D composites', Composite Structures, **8**, 1987, pp.119-141.

Elsley, R.K. and Graham, L.J., 'Pattern recognition in acoustic emission experiments', Invited Paper, SPIE, Vol.768, International Symposium on Pattern Recognition and Acoustical Imaging, 1987, pp.285.

Everitt, B.S., 'Cluster Analysis', publishers: Edward Arnold, Hodder & Stoughton, London, 1993, 3rd Edition.

Everitt, B.S. and Dunn, G, 'Applied Multivariate Data Analysis', publishers: Edward Arnold, Hodder & Stoughton, London, 1991.

Fan, C.F. and Hsu, S.L., 'A study of stress distribution in model composites by finite element analysis. II. Fiber/matrix interfacial effects', Journal of Polymer Science, Part B:Polymer Physics, Vol.30, 1992, pp.619-635.

Faudree, M., Baer, E., Hiltner, A. and Collister, J., 'Characterisation of damage and fracture processes in short fibre BMC composites by acoustic emission', Journal of Composite Materials, Vol. 22, 1988, pp.1170.

Favre, J.P. and Laizet, J.C., 'Amplitude and counts per event analysis of the acoustic emission generated by the transverse cracking of cross-ply CFRP', Composite Science and Technology, Vol. 36, 1989, pp.27-43.

Fowler, T.J, 'Chemical industry application of acoustic emission', Material Evaluation 50(7), 1992, pp875-882

Fukunaga, H., Chou, T.W., Peters, P.W.M. and Schulte, K., 'Probabilistic failure strength analysis of graphite/epoxy cross-ply laminates', J.Compos.Materials **18**, 1984, pp.339-356.

158

Galiotis, C, Melanitis, N, Vlattas, C, and Wall, A, 'Interfacial measurements in single fibre model composites', 2nd International Conference on Deformation and Fracture of Composites, UMIST, Manchester, March 1993, paper 14.

Gent, A.N. and Wang, C., 'Matrix cracking initiated by fibre breaks in model composites', Journal of Material Science, 27, 1992, pp.2539-2548.

Ghorbel, I., Valentin, D., Yrieix, M.C. and Grattier, J., 'The influence of matrix rheological properties on acoustic emission and damage accumulation in GRP tubes', Composite Science and Technology, Vol. 41, 1991, pp.221-236.

Gillespie.J.W.,Jr, Carlsson, L.A. and Pipes, R.B, 'Finite element analysis of the End Notched Flexure specimen for measuring mode II fracture toughness', Composites Science and Technology, 27, 1986, pp.177-197.

Glennie, A.M.G., Gulley, T.J. and Summerscales, J., 'Acoustic emission modulus determination and source location in unidirectional fibre reinforced polymer composites', J. Acoustic Emission, Vol.4(2/3), 1985, Lake Tahoe, Navada, pp.s170-173.

Graham, L.J. and Alers, G.A., 'Acoustic emission in the frequency domain', Monitoring Structural Integrity by Acoustic Emission, ASTM STP 571, American Society for Testing and Materials, 1975, pp.11-39.

Gregory, M.A, and Herakovich, C.T., 'Predicting crack growth direction in unidirectional composites', J.Comp.Materials, 20, 1986, pp.67-85.

Hahn, H.T. and Kim, R.Y, 'Proof testing of composite materials', J. Composite Materials, Vol 9, 1975, pp.297.

Hamstad, M.A., Whittaker, J.W. and Brosey, W.D., 'Correlation of residual strength with acoustic emission from impact-damaged composite structures under constant biaxial load', Journal of Composite Materials, Vol. 26(15), 1992, pp.2307-2328.

Hamstad, M.A., 'Acoustic emission from filament-wound pressure bottles', Proceedings 4th SAMPE Conference, 1972, pp.321-331.

Harlow, D.G and Phoenix, S.L, 'Bounds on the probability of failure of composite materials', Int.Journ. of Fracture, 15(4), 1979, pp.321-336.

Harlow, D.G and S.L.Phoenix, 'Probability distributions for the strength of composite materials I:two-level bounds', Int. J. Fracture, Vol. 17(4), 1981, pp.347.

Hashin, Z., 'Analysis of damage in composite materials', Yielding, Damage and Failure of Anisotropic Solids, EGF5 (Ed. J.P. Boehler) 1990, Mechanical Engineering Publications, London, pp.3-31.

Herrera-Franco.P.J. and Drzal, L.T., 'Comparison of methods for the measurement of fibre/matrix adhesion in composites', Composites, 23(1), pp.2-27, 1992.

Herrmann, K.P. and Ferber, F., 'Numerical modelling of elementary failure mechanisms and associated caustics in two-phase composite structures', Computers and Structures, Vol 44(1/2), 1992, pp.41-53.

Higo, Y., Takashima, K., Nunomura, S., Nakamura, H. and Wada, A., 'On a new real-time calibration method for the acoustic emission measurement system with transducer, specimen and waveguide', The 5th International Acoustic Emission Symposium, Tokyo, 1980, pp.103-114.

Holt, J. and Worthington, P.J., 'A comparison of the fatigue damage detection in carbon and glass fibre/epoxy composite materials by acoustic emission.' Int.J. Fatigue, January, 1981, pp.31.

Hsu, N.N. and Eitzen, D.G., 'AE signal analysis - laboratory experiments examining the physical processes of acoustic emission', The Fifth International Acoustic Emission Symposium, Tokyo, 1980, paper 1-1, pp.67-78.

Hull, D., 'An Introduction to Composite Materials', Cambridge Solid State Science Series, Cambridge University Press, 1993.

Ikegami, K and Yoshida, M, 'Macroscopic failure conditions of hybrid laminates of fibre reinforced plastics', Yielding, Damage and Failure of Anisotropic Solids, EGF5 (Ed. J.P. Boehler) 1990, Mechanical Engineering Publications, London, pp.777-790.

Ivanov, V.I. and Mirgazov, V.A., 'Special features of the frequency and impulse characteristics of acoustic emission transducers', The Russian Journal of Non-destructive Testing, Vol. 29(1), 1993, pp.42-49, translated from Defektoskopiya, No. 1, pp.51-58, January 1993.

Janankhani, H. and Galiotis, C., 'Interfacial studies of Aramid/epoxy systems', Proc. of 7th Int. Conf. on Composite Materials, Vol 2, Pergamon Press, 1989.

Kachanov, L.,M., 'Time of the rupture process under creep conditions', Izv. Akad. Nauk SSR Otd. Tech. Nauk, 8, 26-31, 1958.

Kander, R.G., 'A study of damage accumulation in unidirectional glass reinforced composites via acoustic emission monitoring', Polymer Composites, Vol. 12(4) 1991, pp. 237-245.

Kaw A.K., Selvarathinam, A.S. and Besterfield, G.H., 'Comparison of interphase models for a crack in fibre reinforced composite.', Theoretical and Applied Fracture Mechanics, Vol 17, 1992, pp.133-147.

Kawamoto, K. and Ono, K., 'Pattern recognition analysis of acoustic emission signals from carbon fibre/epoxy composites', 35th International SAMPE, Symposium and Exhibition Society for Advancement of Materials and Process Engineering. 1990, pp.230-239.

Kim, K.S. and Hong, C.S., 'Delamination growth in angle-ply laminated composites', J. Composite Materials, 20, 1986, pp.423-438.

Kim, Y.W. and Hong, C.S., 'Progressive failure model for the analysis of laminated composites based on finite element approach', Journal of Reinforced Plastics and Composites, Vol. 11, 1992, pp.1078-1092.

Kimpara,I., Tsushima, E. and Ishida, Y., 'Tensile failure mechanisms of unidirectional pitch-based CFRP with different interfacial strength', Proceedings of 7th International Conference of Composite Materials, 1989, Wu, Gu and Wu, Eds., Vol 2, pp.73-78.

Kline, R.A. and Ali, S.S., 'Attenuation and dispersion in AE waveforms: a comparison of theory and experiment', J Acoustic Emission, Vol.4(2/3), 1985, pp.42.

Kondo, K. and Aoki, T., 'An energy release rate approach for free-edge delamination problem in composite laminates', Proc. 4th Int. Conf Composite Structures, Paisley, Scotland, 1987, pp.241-257

Kortschot, M.T and Beaumont, P.W.R., 'Damage mechanics of composite materials:I-Measurements of damage and strength.', Composite Sci. Technology, 1990, pp.289-301.

Kwon, Y.W., 'Analysis of composite plates containing cracks.' Journal of Pressure Vessel Technology 114, 1992, pp.358-363.

Kwon, Y.W. and Byun, K.Y. 'Development of a new finite element formulation for the elasto-plastic analysis of FRC.' Computers and Structures, 35, 1990, pp.563-570.

Ladeveze, P. and Le Dantec, E., 'Damage modelling of elementary ply for laminated composites', Composite Science and Technology Vol 43, 1992, pp.257-267.

Ladeveze, P., 'A damage computational method for composite structures', Computers and Structures, Vol.44(1/2), 1992, pp.79-87.

162

Laksimi, A., Gong, X.L. and Benzeggagh, M.L., 'Analysis of damage mechanisms in a centrally notched glass-fibre/epoxy plate', Composite Science and Technology, Vol. 52, 1994, pp.85-91.

Laws, N., Dvorak, G.J. and Hejazi, M., 'Stiffness changes in unidirectional composites caused by crack systems', Mechanics of Materials, Vol 2, 1983, pp.123-137.

Lee and Priston, A-M, Work under taken by visiting 6th form student, 1995

Li, S., Jiang, C. and Han, S., 'Modelling of the characteristics of fibre reinforced composite materials damaged by matrix-cracking', Composite Science and Technology, Vol 43, 1992, pp.185-195.

Li, Y.L., Ruiz, C. and Harding, J. 'Failure analysis of woven Hybrid composite using finite element method', Report: OUEL 1784/89, 'Modelling of the impact response of fiber reinforced composites', Technomic Publications, 1992.

Lorenzo, L. and Hahn, H.T., 'Damage assessment by acousto-ultrasonic technique in composites', Composite Materials: Testing and Design (8th Conference), ASTM STP 972, J.D. Whitcomb. Ed., American Society for Testing and Materials, Philadelphia, 1988, pp.380-397.

Manders, P.W., Chou, T., Jones, F.R. and Rock, J.W., 'Statistical analysis of multiple fracture in 0°/90°/0° glass fibre/epoxy resin laminates', J. Material Science, Vol 18, 1983, pp.2876-2889.

Maslouhi, A., Roy, C., Proulx, D., Cherfaoui, M. and Zimcik, D.G., 'Statistical analysis of acoustic emission signals associated with fatigue damage in CFRP composites', 35th International SAMPE, Symposium and Exhibition Society for Advancement of Materials and Process Engineering. 1990, pp.250-258.

Meissner, M. and Ranachowski, Z., 'Modelling of acoustic emission sources', Acustica, Research Notes, Vol. 79, 1993, pp.186-189.

Mielke, W., Hampe,A, Hoyer, O. and Schumacher, K. 'Analysis of AE-events from single fibre pull-out experiments', 35th International SAMPE, Symposium and Exhibition Society for Advancement of Materials and Process Engineering. 1990, pp.223-331.

Mittelman, A. and Roman, I., 'Monitoring the tensile deformation in real unidirectional Kevlar-epoxy composites', NDT & E International, Vol. 24(2), 1991, pp.85.

Mori, T., Tanimoto, T., Hamada, H., Maekawa, Z-I., Hirano, T. and Kiyosumi, K., 'Fracture and acoustic emission characteristics of glass fibre reinforced plastic panels for hot water', Polymer Composites, Vol. 15(3), 1994, pp.206.

Mori, Y. and Obata, Y., 'Characteristics of acoustic emission source in a fatigue crack', Nondestructive Testing Communications, Vol.4, 1988, pp.11-21.

Murakami, S., 'A continuum mechanics theory of anisotropic damage', Yielding, Damage and Failure of Anisotropic Solids, EGF5 (Ed. J.P. Boehler) 1990, Mechanical Engineering Publications, London, pp.465-482.

Murtagh, F and Heck, A, 'Multivariate Data Analysis', D Reidel Publishing Company, Kluwer Academic Publishers, Norwell, USA, 1987.

Murthy, P.L.N. and Chamis, C., 'Composite interlaminar fracture toughness: three-dimensional finite element modelling for mixed mode I, II and fracture.', Composite Materials: Testing and Design, 8th conference, ASTM STP 972, J.D. Whitcomb, Ed., American Society for Testing and Materials, Philadelphia, 1988, pp.23-40.

Murthy, C.R.L, Majeed, M.A., Pathak, S.C. and Rao, A.K., 'In-flight monitoring for incipient cracks in an aero engine mount: an approach through pattern recognition', J. Acoustic Emission Vol.4(2/3), 1985, pp.s147.

Ni, Q-Q. and Jinen, E, 'Acoustic emission and fracture of carbon fibre reinforced thermosoftening plastic (CFRTP) materials under monotonous tensile loading', Engineering Fracture Mechanics, Vol. 45(5), 1993, pp.611-625.

Ohtsu, M., 'Source kinematics of acoustic emission based on a moment tensor', NDT International, Vol. 22(1), 1989, pp.14.

Okoroafor E.U. and Hill, R, 'Determination of fibre-resin interface strength in fibre reinforced plastics using the acoustic emission technique', Journal of Physics D - Applied Physics, 1995, Vol. 28 (9), pp.1816-1825.

Okoroafor, E.U., Priston, A.M. and Hill, R., 'Evaluation of the interfacial tensile strength of composite materials using acoustic emission', Proceedings of the 3rd International Conference on Deformation and Fracture of Composites, University of Surrey, 1995, pp.518-525.

Okoroafor, E.U., Priston, A.M. and Hill, R., 'Adhesion in fiber-reinforced plastics investigated by means of acoustic emission', Int. J. of Adhesion and Adhesives, 1996, Vol. 16(3), pp.141-146.

Ono, K and Huang, Q., 'Pattern recognition analysis of acoustic emission signals', Progress in Acoustic Emission VII, The Japanese Society for NDI, 1994, pp.69.

Petitpas, E. and Valentin, D., 'Edge effect on unidirectional composite observed during acoustic emission monitoring of damage', Journal of Material Science Letters, Vol. 11, 1992, pp.63-66.

Petrovskii, O.L. and Shalygin, V.N., 'Acoustic emission instrument system for monitoring the heat treatment of polymer composites', Measurement Techniques USSR, Vol. 34, 1991, pp.499-503. Translated from Izmeritel'neya Tekhnika, 1991, No.5, 41-43.

Pollock, A.A., 'Acoustic emission - 2 Acoustic emission amplitudes', Non-Destructive Testing, October, 1973, pp.264-269.

Ponsot, B., Valentin, D. and Bunsell, A.R., 'The effects of time, temperature and stress on the long term behaviour of CFRP', Composite Science and Technology, Vol 35, 1989, pp.75-94.

Poursartip, A., 'The modelling of damage processes in composite materials', Ashby Symp.:The modelling of material behaviour and its relation to design. Ed. J.D.Embury and A.W.Thompson, The Minerals, Metals and Materials Society, 1990.

Priston, A, Hill, R and Brooks, R, "Damage prediction using associated acoustic emission from composite materials", Proceedings of 10th International Conference on Composite Materials, Vancouver, Canada, August 1995, Volume 5, pp 389-395

Prosser, W.H., Jackson, K.E., Smith, B.T., McKeon, J. and Friedman, A., 'Advanced waveform-based acoustic emission detection of matrix cracking in composites', Materials Evaluation, September 1995, pp.1052-1058.

Pyrz, R., 'A micromechanically based model for composite materials with matrix cracks', Composites Engineering, Vol 2(8), 1992, pp.619-6629.

Pyrz, R., 'Quantitative description of the microstructure of composites. Part I: morphology of unidirectional composite systems', Composites Science and Technology, Vol 50, 1994, pp.197-208.

Reddy, J.N. and Pandey, A.K. 'A first ply failure analysis of composite laminates' Comput. Struct. 25, 1987, pp.371-393.

Reifsnider, K.L., 'The critical element model: a modelling philosophy', Engineering Fracture Mechanics, Vol 25(5/6), 1986, pp.739-749.

Rosen, B.W., 'Fibre composite materials', American Society for Metals, Metal Park, Ohio. 1964.

Rosensaft, M. and Marom, G., 'Evaluation of bending test methods for composite materials', Journal of Composite Technology and Research, Vol 7, (1), 1985, pp.12-16.

Rotem A. and Altus, E., 'Fracture modes and acoustic emission of composite materials', Journal of Testing and Evaluation, Vol.7(1), 1979, pp.33-40.

Rotem, A. and Hashin, Z., 'Failure modes of angle ply laminates', J. Composite Materials, Vol 99, 1975, pp.191-206.

Sallehh, R., Day, R. and Taylor, R., 'Correlation between the acoustic emission and damage modes during splitting of carbon fibre reinforced poly-ether-ether-ketone composites', Journal of Materials Science Letters, Vol.14, 1995, pp.398-400.

Sato, N., Kurauchi, T. and Kamigaito, O., 'Detection of damage in composite materials by thermo-acoustic emission measurement', Journal of Composite Materials, Vol.22, 1988, pp.447-458.

Schiavon, I., Fougeres, R., Rouby, D. and Fleischmannn, P., 'Mechanical parameters and acoustic emission as damage indicators during fatigue of one dimensional glass/epoxy composites', Progress in Acoustic Emission IV, The Japanese Society for NDI, 1988, pp.788-794.

Scott, F, 'Processing characteristics of polymer resins for the resin transfer moulding process', Ph.D. Thesis, Department of Mechanical Engineering, The University of Nottingham, X-76-0303557-5, 1988.

Scruby, C.B., 'An introduction to acoustic emission', J. Phys. E: Sci. Instrum., Vol. 20, 1987, pp.946-953.

Short, D. and Summerscales, J., 'Amplitude distribution acoustic emission signatures of unidirectional fibre composite hybrid materials', Composites, Vol.15(3), 1984, pp.200-206.

Siegmann, A. and Kander, R.G., '*In-situ* acoustic emission monitoring during electron microscopy of a model composite material', Polymer Composites, Vol. 13(2), 1992, pp.108-120.

Spearing, S.M. and Beaumont, P.W.R., 'Fatigue damage mechanics of composite materials. I: Experimental measurement of damage and post-fatigue properties', Composite Science and Technology, **44**, 1992, pp.159-168.

Steiner, K.V., Eduljee, R.F., Huang, X. and Gillespie Jr, J.W., 'Ultrasonic NDE techniques for the evaluation of matrix cracking in composite laminates', Composite Science and Technology, Vol. 53, 1995, pp.193-198.

Stijnman, P.W.A., 'Determination of the elastic constants of some composites using ultrasonic velocity measurements', Composites, Vol. 26, 1995, pp.597-604.

Styles, P, Rouse, C and Wilson, S, 'Microseismic monitoring of landslip movement in South Wales', Welsh Office Research Contract Report, WEP/100/154/2, 120 pages.

Sun, C.T. and Chung, I., 'An oblique end tab design for testing off-axis composite specimens', Composites, Vol 24(8), 1993, pp.619-623.

Suzuki, H, Takemoto,M., and Ono, K., 'AE source wave characterization to study the fracture dynamics in a dissipative glass fibre/epoxy model composite', Progress in Acoustic Emission VII, The Japanese Society for NDT, 1994, pp.457-462

Talreja, T., 'Internal variable damage mechanics of composite materials', Yielding, Damage and Failure of Anisotropic Solids, EGF5 (Ed: J.P. Boehler), 1990, Mechanical Engineering Publications, London, pp.5509-533.

Tan, S.C. 'A progressive failure model for composite laminates containing openings', J.Composite Materials, **25**, 1991, pp.556-577.

Thomason, J.L, 'The interface region in glass-reinforced epoxy resin composites:1. Sample preparation, void content and interfacial strength', Composites, Vol. 26(7), 1995, pp.467-475.

Thomason, J.L, 'The interface region in glass-reinforced epoxy resin composites:2. Water absorption, voids and the interface', Composites, Vol 26(7), 1995, pp.477.

Thomason, J.L, 'The interface region in glass-reinforced epoxy resin composites:3. Characterisation of fibre surface coatings and the interphase', Composites, Vol 26(7), 1995, pp.487.

Tissington, B., Pollard,G and Ward, I.M., 'A study of the influence of fibre/resin adhesion on the mechanical behaviour of ultra-high modulus polyethylene fibre composites.', J.Material Science, **26, 1991**, pp.82-92.

Uenoya, T, 'Acoustic emission analysis on interfacial fracture of fabric laminated polymer matrix composites', Progress in Acoustic Emission, Japanese Society for NDI, 1994, pp.387-392.

Valentin, D, 'A critical analysis of amplitude histograms obtained during acoustic emission tests on unidirectional composites with epoxy and a PSP matrix', Composites, Vol. 16(3) 1985, pp.225-230.

Valentin, D., Bonniau, P and Bunsell, A.R., 'Failure mechanism discrimination in carbon fibre- reinforced epoxy composites', Composites, Vol. 14(4), 1983, pp.345-351.

Wagner, J.W. and Huber, R.D., 'Optical methods for detection of acoustic emission', Progress in Acoustic Emission VII, The Japanese Society for NDI, 1994, pp.1-8.

Wagner, P, Ray, R, Hart, K and Little, B, 'Microbiological degradation of stressed fiber-reinforced polymeric composites', MP, vol. 35, Feb. 1996, pp.79-82.

Wang, S.S. and Choi, I., 'The interface crack behaviour in dissimilar anisotropic composites under mixed-mode loading', Journal of Applied Mechanics, Vol.50 1983, pp.179.

Warrender, A.J., Wood,J., Tooth, A.S. and Banks, W.M., 'The support of horizontal cylindrical GRP vessels - saddles or longitudinal beams?', Proceedings, 4th International Conference on Composite Structures, Paisley College of Technology, Scotland, 1987, pp.1.235.

Waschkies, E. and Holler, P., 'Interpretation of acoustic emission signals', Int. J. Pres. Ves. & Piping, Vol 15, 1984, pp.151-157.

Watson, A.S. and Smith, R.L, 'An examination of statistical theories for fibrous materials in the light of experimental data', J.Material Science, 20, 1985, pp.3260-3270.

Whitney, J.M., 'Elasticity analysis of orthotropic beams under concentrated loads', Composite Sci. Technology, 22, 1985, pp.167-184.

Wishart, D., 'Clustan User Manual', 4th Edition, Computing Laboratory, University of St.Andrews, Scotland.

Wisnom, M.R. and Green, D., 'Tensile failure due to interaction between fibre breaks', Composites, 26, 1995, pp.499-508.

Wolstenholme, L.C. and Smith, R.L., 'Statistical inference about stress concentrations in fibre-matrix composites', J.Material Science, 24, 1989, pp.1559-1569.

Wu, T.T. and Gong, J.H., 'Application of transient elastic waves to the nondestructive evaluation of plate structure with cavity or inclusion', J. Acoust. Soc. Am., Vol. 94(3,1), 1993, pp.1453.

Yamaguchi, K., Oyaizu, H., Johkaji, J. and Kobayashi, Y., 'Acoustic emission technology using multi-parameter analysis of waveform and application to GFRP tensile tests', Acoustic Emission: Current Practice and Future Directions, ASTM STP 1077, Eds., W. Sachse, J. Roget and K. Yamaguchi , American Society for Testing and Materials, Philadelphia, 1991, pp.123-145.

Young, R.J., 'Composite micromechanical test methods and their interpretation', 2nd International Conference on Deformation and Fracture of Composites, UMIST, Manchester, March 1993, pp.k1-k10.

Zhou, L.M., Kim, J.K. and Mai, Y.W., 'Interfacial debonding and fibre pull-out stresses 2) A new model based on the fracture mechanics approach', J.Materials Science, 27(12), 1992, pp.3155-3166.

Zhu, Y., Zhou, B., He, G. and Zheng, Z., 'A statistical theory of composite materials strength', J.Composite Materials, 23, 1989, pp.280-287.

Zweben, C. and Rosen, B.W, 'A statistical theory of material strength with application to composite material', J. Mech. Phys. Solids, Vol.18, 1970, pp.189-206.

Appendix A   Computer Programs

A   Damage Model

A.1   NEWMESH.DAT   *Summary of input control program for PAFEC74 finite element package*

```
CONTROL              control module allows certain phases to work
FULL.CONTROL
PHASE=1,2,4,6,7,9
USE.R86010           program to replace faulty original version
STRESS               plane stress calculations
CONTROL.END
```

```
NODES                node positions x and y, z is constant
Z=      0.00000
```

NODE	X	Y
1	0	0
2	0.2	0
3	0	0.025
4	0.2	0.025

....

```
ELEMENTS             element number and the surrounding nodes
GROUP=1
ELEMENT= 36215   element type - orthotropic, 8 nodes etc.
```

NUMBER	PROPERTY.NUMBER	TOPOLOGY
1	12	1 9 10 11 12 13 14 15
2	12	9 16 11 17 18 14 19 20
3	12	16 21 17 22 23 19 24 25

....

```
ORTHOTROPIC.MATERIAL      material properties
```

NUMBER	SXX	SYY	SHXY	
1	0.27E-10	0.11E-09	0.18E-09	*initial properties*
2	0.27E-10	0.11E-09	0.19E-09	

....

	SXX	SYY	SHXY	
90	0.13E-10	0.57E-10	0.88E-10	*'damaged' element*
100	0.27E-09	0.11E-08	0.18E-08	*failed element*

```
LAMINATES            laminates required because of orthotropic material
```

NUMBER	ORTH	LOWER		UPPER	ANG1	STORE
1	1	-0.002	0.002	10	1	*ang1 = 10°*
2	2	-0.002	0.002	10	1	*STORE saves the*
3	3	-0.002	0.002	10	1	*stress data (.o09)*

....

```
SURFACE.FOR.PRESSURE
PRESSURE.VALUE=  -230000000.0        230MPa tension (dilational)
LOAD.CASE   NODE  PLANE  AXIS        applied to the plane through
1       3    1     1                 node 3 with constant x
```

```
RESTRAINTS                                    mesh restraint in x
NODE.NUMBER      PLANE      DIRECTION         direction at node 1.
   1               1            1
```

```
END.OF.DATA                                   end of data file
```

A.2   PROGRAM.FOR

```
C   PROGRAM TO CONTROL ALL PARTS OF THE MODELLING CALCULATION
C

      REAL LOAD,E20,G120,SIGXX,SIGYY,SIGXY,OLDDT,OLDDS
    +,NEWDT,NEWD
      INTEGER L1,ELEM,MAT,OLDELE,C,PROPNUM,PROP,RUNNUM
      CHARACTER*55 TOPO,TITLE
      CHARACTER*18 WORDS,TI
      CHARACTER*70 LINE,ANS

C   READING IN THE FILES PRODUCED BY A PAFEC RUN

      OPEN(20,FILE='OB.DAT',STATUS='OLD')
      OPEN(30,FILE='NEWMESHH.DAT',STATUS='OLD')
      OPEN(40,FILE='CONST.DAT',STATUS='OLD')
      OPEN(50,FILE='NEWCONST.DAT',STATUS='NEW')
      OPEN(60,FILE='PAFECDAT.DAT',STATUS='NEW')

C   NOW TO THE CALCULATIONS OF THE 'D' PARAMETERS
C
C   READ IN THE OLD VALUES FOR D1 (D') AND D2 (D)
C   FROM CONST.DAT FILE. THIS FILE KEEPS A RECORD

      DO 500 I=1,2500

   PROPNUM=0

      READ(20,2000)ELEM,MAT,SIGXX,SIGYY,SIGXY
   READ(40,3000)OLDELE,OLDDT,OLDDS,C

C       CHECKS FOR FAILURE IN THE ELEMENT BY LOOKING AT THE
C       PROPERTY ENTRY. 100= FAILURE
C       YC1-YC"
C       Y10-Y0'

      YC1=518.13
      Y10=19.74
      YC2=493.58
      Y20=7.99
      B=4

C TSAI AND HAHN MATERIAL VALUES
C   E10=3.8E10
C   E20= 0.827E10
C   G10  0.41E10

C   /-45 PLY VALUES
```

```
C
      E10=3.71E10
      E20=0.88E10
      G10=0.57E10

C CHECKING FOR FAILED ELEMENT

      IF(C.EQ.100.OR.C.EQ.90.OR.OLDDT.EQ.1.OR.OLDDS.EQ.1)THEN
      NEWDT=1.0
      NEWDS=1.0
      PROPNUM=C
      GOTO 201
      ENDIF

C TRANSVERSE STRESSES IN TENSION ONLY, NO COMPRESSION

      IF(SIGYY.EQ.0.OR.SIGYY.LT.0)THEN
      YD1=0.0
      GOTO 50
      ENDIF

   YD1 = (SIGYY**2)/(2*E20*((1-OLDDT)**2))

50    CONTINUE

      YDS=(SIGXY**2)/(2*G10*((1-OLDDS)**2))

C  TRANSVERSE DAMAGE

      Y1=(YDS)**0.5

C  SHEAR DAMAGE

   Y2 = (YDS+(B*YD1))**0.5


C  MUST HAVE POSITIVE NUMERATORS FOR D1 AND D2

      IF(Y1.EQ.Y10.OR.Y1.LT.Y10)THEN
      NEWDT=OLDDT
      GOTO 60
      ENDIF

      NEWDT = (Y1-Y10)/YC1

60    CONTINUE

      IF (Y2.EQ.Y20.OR.Y2.LT.Y20)THEN
      NEWDS=OLDDS
```

175

```fortran
        GOTO 70
        ENDIF

    NEWDS = (Y2-Y20)/YC2

70      CONTINUE

C CHECKING THE DAMAGE PARAMETER INTERVAL VALUE

        IF(NEWDT.LT.OLDDT)THEN
        NEWDT=OLDDT
        GOTO 100
        ENDIF

        IF(NEWDT.LT.0.1)THEN
        NEWDT=0.0
        GOTO 100
        ELSE IF(NEWDT.EQ.0.1.OR.NEWDT.LT.0.2)THEN
        NEWDT=0.1
        GOTO 100
        ELSE IF(NEWDT.EQ.0.2.OR.NEWDT.LT.0.3)THEN
        NEWDT=0.2
        GOTO 100
        ELSE IF(NEWDT.EQ.0.3.OR.NEWDT.LT.0.4)THEN
        NEWDT=0.3
        GOTO 100
        ELSE IF(NEWDT.EQ.0.4.OR.NEWDT.LT.0.5)THEN
        NEWDT=0.4
        GOTO 100
        ELSE IF(NEWDT.EQ.0.5.OR.NEWDT.LT.0.6)THEN
        NEWDT=0.5
        GOTO 100
        ELSE IF(NEWDT.EQ.0.6.OR.NEWDT.LT.0.7)THEN
        NEWDT=0.6
        GOTO 100
        ELSE IF(NEWDT.EQ.0.7.OR.NEWDT.LT.0.8)THEN
        NEWDT=0.7
        GOTO 100
        ELSE IF(NEWDT.EQ.0.8.OR.NEWDT.LT.0.9)THEN
        NEWDT=0.8
        GOTO 100

C       ELSE IF(NEWDT.EQ.0.9.OR.NEWDT.LT.1.0)THEN
C       NEWDT=0.9
C       GOTO 100
C       ELSE IF(NEWDT.GT.1.0)THEN

        ELSE IF(NEWDT.GT.0.9)THEN
C       WRITE(6,*)' BUSTED ELEMENT',I
```

```
      PROPNUM = 100
      NEWDT=1
      GOTO 100
      ENDIF

100   CONTINUE

C     FINDING THE INTERVAL FOR THE DAMAGE PARAMETER

      IF(NEWDS.LT.OLDDS)THEN
      NEWDS=OLDDS
      GOTO 200
      ENDIF

      IF(NEWDS.LT.0.1)THEN
      NEWDS=0
      GOTO 200
      ELSE IF(NEWDS.EQ.0.1.OR.NEWDS.LT.0.2)THEN
      NEWDS=0.1
      GOTO 200
      ELSE IF(NEWDS.EQ.0.2.OR.NEWDS.LT.0.3)THEN
      NEWDS=0.2
      GOTO 200
      ELSE IF(NEWDS.EQ.0.3.OR.NEWDS.LT.0.4)THEN
      NEWDS=0.3
      GOTO 200
      ELSE IF(NEWDS.EQ.0.4.OR.NEWDS.LT.0.5)THEN
      NEWDS=0.4
      GOTO 200
      ELSE IF(NEWDS.EQ.0.5.OR.NEWDS.LT.0.6)THEN
      NEWDS=0.5
      GOTO 200
      ELSE IF(NEWDS.EQ.0.6.OR.NEWDS.LT.0.7)THEN
      NEWDS=0.6
      GOTO 200
      ELSE IF(NEWDS.EQ.0.7.OR.NEWDS.LT.0.8)THEN
      NEWDS=0.7
      GOTO 200
      ELSE IF(NEWDS.EQ.0.8.OR.NEWDS.LT.0.9)THEN
      NEWDS=0.8
      GOTO 200
C     ELSE IF(NEWDS.EQ.0.9.OR.NEWDS.LT.1.0)THEN
C     NEWDS=0.9
C     GOTO 200
C     ELSE IF(NEWDS.GT.1.0)THEN
      ELSE IF (NEWDS.GT.0.9)THEN
C     WRITE(6,*)' DAMAGE PARAMETER D2>1.0 FOR ELEMENT = ',I
      PROPNUM = 100
      NEWDS=1
```

177

```
            GOTO 201
            ENDIF


  200   CONTINUE

            IF(PROPNUM.EQ.100)THEN
            GOTO 201
            ENDIF

C     FINDING THE NEW MATERIAL PROPERTIES NUMBER FOR PUTTING
C        BACK INTO THE PAFEC FILE. *100=10*0.1+10 SEPARATE LEVELS
C
C     HAD TO CHANGE THE PROPNUM CALC DUE TO HAVING ONLY D=0
C        TO 0.8 VALUES
C
C     PROPNUM - NEWDT*100+NEWDS*10+1    THIS ONE IS FOR D=0 TO 0.9
C        VALUES

            PROPNUM = NEWDT*100-NEWDT*10+NEWDS*10+1
            IF(C.EQ.90.AND.PROPNUM.EQ.1)THEN
            PROPNUM=90
            ENDIF

            IF(PROPNUM.GT.81)THEN
            PROPNUM=100
            ENDIF

  201   CONTINUE

C     WRITING TO THE NEW CONSTANTS FILE

            WRITE(50,3000)ELEM,NEWDT,NEWDS,PROPNUM
  500   CONTINUE

            REWIND(50)

C     WRITING THE NEW VALUES TO THE PAFEC INPUT.DAT FILE
 1500   CONTINUE

C        TITLE LINE
            READ(30,7000)LINE
            WRITE(60,10000)LINE

C     WRITING THE CONTROL AND ELEMENTS TO PAFECDATB.DAT FILE(60)
C     FROM NEWMESHH.DAT FILE(30)

            DO 600, K=1,7768
            READ(30,7000)LINE
            WRITE(60,7000)LINE
```

```
600     CONTINUE

C       READING FROM NEWMESHH.DAT(30) AND PROPERTY FILE MADE C
        ABOVE NEWCONST.DAT (50)  AND WRITING UPDATED PROPERTY C
        VALUES INTO THE PAFEC INPUT FILE PAFECDAT.DAT

        DO 700, I=1,2500
        READ(30,4000)L1,PROP,TOPO
        READ(50,3000)ELEM,D1,D2,PROPNUM
        WRITE(60,4000)ELEM,PROPNUM,TOPO

700     CONTINUE

C       WRITING OUT THE REST OF THE PAFEC FILE UPTO LOAD:
C       MATERIAL PROPERTIES,LAMINATES LOAD HEADINGS

        DO 800, I=1,174
        READ(30,7000)LINE
        WRITE(60,7000)LINE
800     CONTINUE

        READ(30,6000)WORDS,LOAD
        LOAD=LOAD
        WRITE(60,6000)WORDS,LOAD

C       THE REST OF THE FILE
        DO 900,I=1,18
        READ(30,7000)LINE
        WRITE(60,7000)LINE
900     CONTINUE

2000    FORMAT(I6,5X,I4,3(2X,F13.1))
3000    FORMAT(I4,6X,F3.1,2X,F3.1,2X,I4)
4000    FORMAT(5X,I4,1X,I4,1X,A50)
5000    FORMAT(I4)
6000    FORMAT(A18,F13.1)
7000    FORMAT(A70)
8000    FORMAT(F12.1)
9000    FORMAT(A40)
10000   FORMAT(A6,A40)

        CLOSE(20)
        CLOSE(30)
        CLOSE(40)
        CLOSE(50)
        CLOSE(60)

        STOP
        END
```

A.3   INFO4.FOR

```
C      MODIFIED PAFEC PROGRAM TO EXTRACT STRESSES FROM PHASE 9 DATA
C      FILE. CORRECTING FOR THE FIBRE ORIENTATION.
C

C------PAFEC AND VAX VMS SETTINGS
      DIMENSION ST(500)
          REAL ANGLE,N2,M2
C------ICNL AND ICNLP ARE COMMON BLOCKS REQUIRED BY THE I/O ROUTINES
      COMMON/ICNL/ICOUT,ICERW,ICNL(2,150)
      COMMON/ICNLP/ ICNLS,ICNLM
      CHARACTER FILE*6
      ICNLS = 121
      ICNLM = 150
C------INITIALIZE PUMAS
      CALL ZZUINI


          FILE = 'MEB.SS'
C------OPEN THE STRESS FILE CALLED 'MEB.SS', THIS IS THE .SS FILE
C------FROM PHASE 9
      CALL YYFOPE(2,FILE,6,1,1,500,2,1,0,1,0,NFID13,NST13)


C------OPEN OUTPUT FILE CALLED 'OB', REARRANGED STRESSES
      CALL YYFOPE(2,'OB.DAT',6,1,1,80,0,0,2,1,0,NFID6,NSTAT6)


C------DETERMINE CHANNEL NUMBER OF STRESS FILE AND SET IN ICNL
      CALL ZZFINQ(1,NFID13,1,IC13,NST13)
      ICNL(1,13) = NFID13
      ICNL(2,13) = IC13
C------DETERMINE CHANNEL NUMBER OF OUTPUT FILE AND SET IN ICNL
      CALL ZZFINQ(1,NFID6,1,IC6,NSTAT6)
      ICNL(1,6) = NFID6
      ICNL(2,6) = IC6
      ICERW   = IC6
      ICOUT   = IC6
      ICONT1  = 0
      ICONT2  = 0


C------CALL R70000 WITH IOPT=10 TO RETRIEVE ALL UNAVERAGED STRESSES
  110 CALL R70000(ST,-1.0,0,0,0,0,0,0,100,ICONT1,ICONT2,10,13)

C---------LOOP THROUGH STRESS RECORDS IN ST
          DO 120 L1 = 1,77,19
          IELEM = ST(L1)+0.1
          IF(IELEM.EQ.0) GOTO 130
          IGRP=ST(L1+1)
          IMAT = ST(L1+2)
          IERN=ST(L1+3)
```

```
      ILO=ST(L1+4)
      NODE1=ST(L1+5)
      NODE2=ST(L1+6)
      NODE3=ST(L1+7)
      NODE4=ST(L1+8)
      SIGXX = ST(L1+9)
      SIGYY = ST(L1+10)
      SIGZZ=ST(L1+11)
      SIGXY = ST(L1+12)
      SIGYZ =ST(L1+13)
      SIGZX=ST(L1+14)
      SIGE=ST(L1+15)
      XX =ST(L1+16)
      YY=ST(L1+17)
      ZZ =ST(L1+18)

C-----CALCULATING MATERIAL STRESSES FOR THE FIBRE ANGLE

      ANGLE=10.0
      M=COSD(ANGLE)
      M2=(COSD (ANGLE))**2
      N=SIND(ANGLE)
      N2=(SIND(ANGLE))**2
      STX=(M2*SIGXX)+(N2*SIGYY)+(2*M*N*SIGXY)
      STY=(N2*SIGXX)+(M2*SIGYY)-(2*M*N*SIGXY)
      STXY=(-M*N*SIGXX)+(M*N*SIGYY)+((M2-N2)*SIGXY)

C      WRITE(6,*)IELEM,STX,STY,SIGYY,STXY,SIGXY


      IF(NODE2.GT.0)THEN
C-----WRITES COMPLETE HISTORY USING THIS WRITE STATEMENT
C      WRITE(ICOUT,1)IELEM,IGRP,IMAT,IERN,ILO,NODE1,NODE2,NODE3
C     + ,NODE4,SIGXX,SIGYY,SIGZZ,SIGXY,SIGYZ,SIGZX,SIGE,XX,YY,ZZ

C      WRITE(ICOUT,3)IELEM,IMAT,SIGXX,SIGYY,SIGXY

C-----WRITES A LIMITED NUMBER OF STRESSES
       WRITE(ICOUT,4)IELEM,IMAT,STX,STY,STXY

      ENDIF
C-------SET IADR TO POINT TO THE NODE CODE FOR THIS RECORD
C      FOR A SHELL ELEMENT IF THIS SHELL ELEMENT RECORD
C      FOR THE UPPER (LOWER) SURFACE THIS WILL BE IN THE
C      NEXT (LAST) RECORD
      IADR = L1+5
      T    = ST(IADR)
      IF(ABS(T-0.5).LT.0.1) IADR = IADR+19
      IF(ABS(T+0.5).LT.0.1) IADR = IADR-19
      NODE1 = ST(IADR)+0.1
```

```
          NODE2 = ST(IADR+1)+0.1

120    CONTINUE
C------CALL R70000 AGAIN IF MORE RECORDS ARE TO BE FETCHED
130    IF(ICONT1.NE.0) GOTO 110
C------CLOSE DOWN PUMAS
       CALL ZZUEND(-1)
       STOP

4      FORMAT(I6,5X,I4,3(2X,F13.1))
3      FORMAT(I6,5X,I4,2X,E8.2,2X,E8.2,2X,E8.2)
       END
```

A.4   LOOK.FOR

```
C       PROGRAM TO LOOK AT EACH LINE OF THE FILES
C       CONST.DAT  AND   NEWCONST.DAT   FOR THE CHANGES IN THE
C       DAMAGE VALUES.
C

        CHARACTER*40 LINE
        CHARACTER*13 NEWFILE
        CHARACTER*6 FRONT
        CHARACTER*3 END
        REAL D1,D2,LOAD,F1,F2,X,SL,ST,SS
        INTEGER ELEM1,ELEM2,PROP1,PROP2,ENDVAL,VAL,A,B

        OPEN(10,FILE='LOAD.DAT',STATUS='OLD')
        OPEN(20,FILE='CONST.DAT',STATUS='OLD')
        OPEN(30,FILE='NEWCONST.DAT',STATUS='OLD')
        OPEN(50,FILE='LOADVAL.DAT',STATUS='OLD')
        OPEN(70,FILE='OB.DAT',STATUS='OLD')

        LOADVAL=0

        READ(10,1000)LOAD

C       READING IN DAMAGE PARAMETERS
10      READ(20,2000,END=100)ELEM1,D1,D2,PROP1
        READ(30,2000)ELEM2,F1,F2,PROP2

C       COMPARING CONSTB WITH NEWCONSTB
        IF(D1.EQ.F1.AND.D2.EQ.F2)THEN
        GOTO 10
        ENDIF

        LOADVAL=1
        GOTO 10

100     CONTINUE

        READ(50,6000)VAL,ENDVAL

C       INCREMENTING LOAD EVERY TIME

        LOADVAL=0

        IF(LOADVAL.EQ.1.AND.LOADVAL.EQ.VAL)THEN
        ENDVAL=ENDVAL+1
        GOTO 120
        ENDIF
```

```
C       ENDVAL=(((LOAD**2)**0.5)/1E5)+1
        ENDVAL=(((LOAD**2)**0.5)/1E6)
120     CONTINUE

        REWIND 50
        REWIND 30
        WRITE(50,6000)LOADVAL,ENDVAL
        REWIND 50
        READ(50,3000)LOADVAL,END

        IF(LOADVAL.EQ.1) THEN

        FRONT='M10B'
        NEWFILE= FRONT//END//'.DAT'
        OPEN(40,FILE=NEWFILE,STATUS='NEW')
        WRITE(40,*) LOAD,'Pa    PROG B'

        OPEN(60,FILE='NEWMESHH.O07',STATUS='OLD')

        DO 50 I=1,80
        READ(60,225)LINE
50      CONTINUE

        WRITE(40,*)' NODE    UX    UY  STRESS LONG  STRESS TRANS
     +   STRESS SHEAR'
        DO 60 J=1,10
        READ(60,225)LINE
        WRITE(40,225)LINE
60      CONTINUE

150     READ(30,2000,END=200)ELEM1,D1,D2,PROP1
        READ(70,7000,END=200)A,B,SL,ST,SS
        WRITE(40,8000)ELEM1,D1,D2,PROP1,SL,ST,SS
        GOTO 150

        ENDIF

C       THE NAME OF THE OUTPUT FILE
        FRONT='M10B'
        NEWFILE= FRONT//END//'.INC'
        OPEN(40,FILE=NEWFILE,STATUS='NEW')

        WRITE(40,*)'PROG B. NO CHANGE TO DAMAGE PARAMETER
     + VALUES AT ',LOAD,'Pa'

        OPEN(60,FILE='NEWMESHH.O07',STATUS='OLD')

        DO 53 I=1,80
        READ(60,225)LINE
```

```
53      CONTINUE

        WRITE(40,*)' NODE    UX    UY STRESS LONG   STRESS TRANS
+ STRESS SHEAR '
        DO 63 J=1,10
        READ(60,225)LINE
        WRITE(40,225)LINE

63      CONTINUE

153     READ(30,2000,END=200)ELEM1,D1,D2,PROP1
        READ(70,7000,END=200)A,B,SL,ST,SS
        WRITE(40,8000)ELEM1,D1,D2,PROP1,SL,ST,SS
        GOTO 153

200     CONTINUE

225     FORMAT(A40)
250     FORMAT(I6,7X,A8,1X,A8,13X,F8.2,24X,F6.3,1X,F6.3,1X,F6.3)
350     FORMAT(I6,2X,A8,2X,A8,2X,F8.2,2X,F6.3,2X,F6.3,2X,F6.3)
1000    FORMAT(F13.1)
2000    FORMAT(I4,6X,F3.1,2X,F3.1,2X,I4)
3000    FORMAT(I5,2X,A4)
5000    FORMAT(I5)
6000    FORMAT(I5,2X,I4)
7000    FORMAT(I6,5X,I4,3(2X,F13.1))
8000    FORMAT(I4,6X,F3.1,2X,F3.1,2X,I4,3(2X,F13.1))

        CLOSE(10)
        CLOSE(20)
        CLOSE(30)
        CLOSE(40)
        CLOSE(50)
        CLOSE(60)
        CLOSE(70)

        STOP
        END
```

A.5   LOAD.FOR

```
C     PROGRAM TO UPDATE THE LOAD VALUES IN NEWINPUT.DAT
C     FOR THE FINITE ELEMENT PROGRAM USING RECTANGULAR
C     ELEMENTS

      REAL VAL,INT,NEWVAL
      CHARACTER*70 LINE
      CHARACTER*17 WORD

      OPEN(20,FILE='LOAD.DAT',STATUS='OLD')
      OPEN(30,FILE='NEWMESHH.DAT',STATUS='OLD')
      OPEN(40,FILE='NEWLOAD.DAT',STATUS='NEW')
      OPEN(50,FILE='NEBNEWMESHH.DAT',STATUS='NEW')
      OPEN(60,FILE='LOADVAL.DAT',STATUS='OLD')

C     READING IN LOAD USED PREVIOUSLY
      READ(60,4000)LOADVAL
C     READ IN THE NEW LOAD VALUE AND THE LOAD INCREMENT (INT)
      READ(20,1000)VAL,INT

C IF LOADVAL  1 THEN DO NOT INCREASE THE LOAD
      IF(LOADVAL.EQ.0)THEN
      NEWVAL= VAL-INT
      GOTO 50
      ENDIF

      NEWVAL=VAL

50    CONTINUE

      WRITE(40,1000)NEWVAL,INT

      DO 100 I=1,10443
      READ(30,2000)LINE
      WRITE(50,2000)LINE

100   CONTINUE

      WORD='PRESSURE.VALUE='
      READ(30,2000)LINE
      WRITE(50,3000)WORD,NEWVAL

      DO 200 I=1,18
      READ(30,2000,ERR=300)LINE
      WRITE(50,2000)LINE
200   CONTINUE
300   CONTINUE
```

```
1000   FORMAT(F13.1,5X,F13.1)
2000   FORMAT(A70)
3000   FORMAT(A17,F13.1)
4000   FORMAT(I5)

       REWIND 20
       CLOSE(20)
       CLOSE(30)
       CLOSE(40)
       CLOSE(50)
       CLOSE(60)

       STOP
       END
```

A.6   FINITE.COM - *Procedure file for automatic submission of the model*

```
$ COUNTS=1                              counter
$ LOOP1:                                start of loop1
! $IF COUNTS.EQ.1 THEN GOTO CONT        to jump to the damage calcs.
$SYSRUN PAFEC                           initialise the PAFEC package
$LJ7 NEWMESHH BATCH$LONG                submit to batch queue on VAX
$SYNC/QUEUE=BATCH$LONG PAFEC_JOB_NEWMESHH   waits until
$ DEL NEWMESHH.BS;*              PAFEC finishes before proceeding
$ DEL NEWMESHH.FS;*
$ DEL NEWMESHH.ES;*                     Deletes large process files
$CONT:


$ @AMPLINK                             Links PAFEC data output files
$ WRITE SYS$OUTPUT "LINKING INFO4.FOR"
$ LINK INFO4,'AMPLINK'
$ RENAME NEWMESHH.SS MEB.SS
$ WRITE SYS$OUTPUT "RUNNING INFO4.FOR"
$ RUN INFO4              Extracting stress data for elements


$ WRITE SYS$OUTPUT "RUNNING PROGRAM"
$ RUN PROGRAM                   Calculating damage per element
$ WRITE SYS$OUTPUT " RUN=",COUNTS


$ RUN LOOK       Compares the old and new element damage values for changes
$ RENAME NEWCONST.DAT CONST.DAT
$ RENAME PAFECDAT.DAT NEWMESHH.DAT Updates files
$ WRITE SYS$OUTPUT "RUN LOOK.FOR,  RUNNING LOAD.FOR"


$ RUN LOAD                      Updates load in FE model
$ WRITE SYS$OUTPUT "FINISHED LOAD.FOR"
$ RENAME NEBNEWMESHH.DAT NEWMESHH.DAT
$ RENAME NEWLOAD.DAT LOAD.DAT Renames files so not to overwrite


$ COUNTS=COUNTS+1                       Updates counter
$ WRITE SYS$OUTPUT "LOOP=",COUNTS
$ TYPE LOAD.DAT
$ DEL MEb.SS;*                          Removes old files
$ DEL NEWMESHH.O0*;*
! $ DEL RUB.DAT;*
$ PURGE
$ SH TIME                               Time at end of iteration
$ IF COUNTS.LE.30 THEN GOTO LOOP1       Loops around again
$ SH TIME                               Experiment end time


$ EXIT
$ STOP
```

Appendix B Published Papers

1. Okoroafor, E.U, Priston, A.M. and Hill, R., 'Interfacial Adhesion in fiber-reinforced plastics investigated by means of acoustic emission', Int. J. of Adhesion and Adhesives, 1996, Vol. 16(3), pp.141-146.

2. Priston, A, Hill, R and Brooks, R, "Damage prediction using associated acoustic emission from composite materials", Proceedings of 10th International Conference on Composite Materials, Vancouver, Canada, August 1995, Vol. V, pp389-395.

3. Hill, R, Okoroafor, E U and Priston, A, "Acoustic emission from composite and the relationship of damage induction", Ultrasonics International (and Ultrasonics) 1995, Edinburgh, July 1995, Ultrasonics, 34, 1994, pp321-325.

4. Priston, A, Hill, R and Brooks, R, "Damage Mechanisms, Damage Modelling and Associated Acoustic Emission from Composites", poster presentation, Proceedings of the 3rd International Conference on Deformation and Fracture of Composites, University of Surrey, Guildford 1995, pp500-507.

5. Okoroafor, E.U., Priston, A.M. and Hill, R., 'Evaluation of the interfacial tensile strength of composite materials using acoustic emission', Proceedings of the 3rd International Conference on Deformation and Fracture of Composites, University of Surrey, 1995, pp.518-525.

6. Okoroafor, E.U., Priston, A.M. and Hill, R., "Routine evaluation of interfacial adhesion in fibre reinforced plastics", Advanced Composites (Letters), December 1994.

I

Interfacial Adhesion in Fibre Reinforced Plastics Investigated by means of Acoustic Emission.

E.U.OKOROAFOR[*], A—M.PRISTON, R.HILL.

Department of Chemistry and Physics, The Nottingham Trent University, Clifton Campus, Nottingham NG11 8NS, UK.

The nature of fibre—matrix adhesion, the strength of the interface and the type of failure mode have been investigated via the acoustic emission(AE) technique. When unidirectional composites are subjected to transverse tension, the predominant fracture mechanism is interfacial failure events whose stress waves are detected as acoustic emission at ultrasonic frequencies by a piezoelectric transducer placed in intimate contact with the test specimen. The stress and strain range over which these AE events occur determine the strength of the fibre—matrix interface, while the relative total number of recorded AE events give indication as to the interfacial failure mode. The method developed here has been applied to a variety of composite systems and shows potential as a simple and convenient means of monitoring adhesion, interfacial strength and interfacial failure mode in fibre reinforced plastics.

1. Introduction:

The mechanical performance of composite materials depends, among other things, on the characteristics of the interface between the reinforcing fibres and the matrix, since a weak interface will certainly lead to a premature failure when substantial load sharing is expected via the interface. For stresses applied perpendicular to the fibre direction, the knowledge of the characteristic strength of the fibre—matrix interface becomes essential when tailoring performance to applications.

Previous studies of fibre—matrix adhesion in composites were based mainly on single fibre model methods, which are tedious, time consuming and prone to error due to the oversimplified representation of the state of stress occurring at the interphase. In fact, in a recent review, Drzal et al[1], pointed out that none of the single fibre models can offer a complete and unambiguous idea of the level of adhesion in fibre reinforced plastics.

On the other hand, measurement of the properties of the interface, using real composites, is not a simple task, due to interferences from a variety of failure mechanisms occurring during material testing. The complex state of stress developed during testing of such materials further complicates the situation. In this paper, employing simple multi—fibre composites, it becomes possible to reduce the failure mechanisms to that mainly associated with interfacial failure. This also facilitates the description of the state of stress at the interface region. The method differs from previous studies of fibre—matrix adhesion and has not previously, to our knowledge, been reported.

In a simple bundle of fibres composite(BFC) with the fibre axis perpendicular to the tensile direction, the interfacial adhesion between the matrix and the fibres has been investigated using acoustic emission(AE). The AE indicates the strain and stress level for failure at the interface as well as the failure mode. The method developed here has been applied to monitor the level of fibre—matrix adhesion in composite systems such as: E—glass/polyester; Kevlar—49/polyester; E—glass/epoxy and; Kevlar—49/epoxy. By varying the treatment of the fibre surface(as—received, lubricated), this changes the nature of the interfacial bonding and is reflected unambiguously in the acoustic emission, yielding the

2

characteristics of the interface. The simplicity and convenience of the method shows potential as a means of routine evaluation of adhesion in a variety of composite systems.

2. Experimentation:

2.1 Materials preparation;

Composite reinforcements used in this study include as—received Kevlar—49 (DuPont (UK) Ltd; Den 2160, Dtex 2400, finish—free) and E—glass (Fibre—Glass (UK) Ltd; Equerove, Silane—sized, EC13, 600 Tex). The matrix materials used were Crystic Polyester 272 resin, supplied by SCOTT Bader (UK) Ltd and Epoxy LY 5025 supplied by CIBA—Geigy Polymers (UK). Their preparation followed the recommended procedure for producing composite materials. For polyester: 100 parts of Crystic polyester 272 resin; 2 parts of Crystic catalyst M(methyl ethyl ketone peroxide); and 1 part of cobalt accelerator E in styrene were used. This was cured for 7 days at room temperature. For the epoxy, 100 parts of the resin LY 5025 and 38 parts of the hardener HY 5025 were used and cured for 8 hours at 80°C. These resins, after degassing, were then poured into a dog—bone shaped mould of silicon—rubber, containing a fibre bundle at its' centre that is oriented transverse to the longitudinal axis of the mould(TBFC). In the cases where the fibres were subjected to surface—treatment, this was accomplished simply by coating the fibres with a silicon oil. To establish the predominant failure mechanisms occurring during deformation of composites with various fibre orientations, some bundle of fibre composites were prepared with a longitudinal orientation(LBFC) of the fibre bundle. All composite gauge dimensions were 40x5x2.5mm.

2.2 Tests conditions;

All tensile tests were performed using a LLOYD—6000R tensile testing machine, at a constant crosshead movement rate of 0.5%/min or equivalently 0.2mm/min.

The AE technique was employed during the tests as a means of monitoring and discriminating the fracture mechanisms occurring during the deformation of the composites. Previously[2], the technique has been employed to monitor fibre failures and their mode(singlets $\equiv$ one fibre failure at a time, doublets, triplets, etc) during tensile testing of fibre bundles in air, yielding the stress—strain response. In another study[3], it has been possible to relate AE signal parameters to fracture stress and hence discriminate fibre systems from each other as well as composite fracture mechanisms. In this study, a commercial AE transducer (AC375L, resonant frequency 375kHz, supplied by Acoustic Emission Technology Corporation) was utilized. This transducer was spring clamped to the middle portion of the composite test specimen mounted in the grips of the tensile machine. Silicon grease was used as an acoustic couplant. The AE signals from the transducer, were preamplified by 60dB, using a preamplifier(AECL 2100/PA) with narrow band filtering (208—530kHz bandpass) around the transducer resonance, and processed using the AECL 2100M acoustic emission system. The processed signals are then extracted and analysed as detailed elsewhere[3]. Some of the possible AE signal parameters(initial peak voltage, event rise time, event duration and the ringdown counts per event or group of events, i.e., number of positive threshold crossings) can be related to the nature of the event. As the parameters are interdependent, choice of which one to use is often based on accessibility. The values obtained for these AE parameters are considered relative since they depend on the threshold voltage applied. In this study the ringdown count was used which is related to the relative acoustic energy[4] released by the fracture events. AE instrument settings were: dead time, 0.2ms and threshold of 0.2Volts. The threshold was chosen to eliminate electronic background noise, noise from the grips and the tensile machine, thus ensuring that received signals were from the fractures occurring in the composite being tested. Figure 1., shows the schematic diagram of the experimental system and specimen types.

3

3. Results/Analysis/Discussion:

The typical mechanical and AE test data from transverse(TBFCs) and longitudinal bundle of fibres composites(LBFCs) of Kevlar/polyester are presented in figures 2a and 2b respectively. In the former case, the fracture events occur at low strains and with relatively small ringdown counts per event. While in the latter case, the fracture events occur close to composite failure strain and possess higher ringdown counts per event, which exhibit an increasing trend with applied stress. This trend has previously been reported by us[3] in tests involving fibre bundles in air. From known mechanical effects and the AE ringdown patterns in both figures, the events recorded during tensile deformation of the TBFCs were associated with fibre—matrix interfacial failure, while for LBFCs, the events were mainly associated with fibre fractures, since in the stress range over which the events occurred, the main load bearing constituent of the composite are the fibres and their fracture led to the failure of the composite as a whole. Having established that it is possible with AE to monitor interfacial failure during tensile deformation of TBFCs, we now extend the method to compare the level of interfacial adhesion between a matrix material and different fibre systems and vice versa, including varying fibre surface condition.

Test data for TBFCs of Kevlar/polyester and E—glass/polyester are given in figures 3a and 3b respectively. Fibre surface conditions were as—received. The stress—strain response of the composites did not show any significant difference and this, in either case, is attributed to the low fibre volume fraction. Hence, the role played by the resin—fibre interface is not made manifest in relation to the composite stress—strain response. Nonetheless, examination of the failed composites revealed that failure occurred within the composite region containing the fibre bundle and nowhere else which clearly indicates that fibre—matrix interfacial failure initiated the composite failure.

Using the AE events—strain response as an indicator, since the recorded events are associated with interfacial failure, one can deduce that the interface characteristics in both composites are completely different: The Kevlar/polyester interface failed at low strains and within the elastic region of the matrix material, while E—glass/polyester interface failed well beyond the yield point of the matrix material. This clearly suggests that the E—glass/polyester interface is much stronger than the Kevlar/polyester interface. We note also, that there are fewer recorded events in the case of E—glass/polyester. In this case, unlike the case of Kevlar/polyester, there were very few fibres exposed after composite fracture, and these fibres were covered with the matrix material, indicating that interfacial failure, here, occurred predominantly in the interphase region. As the interphase is common to many fibres, it is therefore not surprising that there are fewer recorded events during interfacial failure of the E—glass/polyester system. For the Kevlar/polyester system, the exposed fibres were clean of the matrix material, consistent with failure occurring at the fibre—matrix interface. These information unambiguously show that E—glass used in this study, unlike Kevlar—49, adheres well to Crystic—polyester. This adhesion can be attributed to the interactions between the silane coupling agent and polyester[5]. Test data involving fibres treated with a silicon—oil prior to composite manufacture are presented in figures 4a and 4b for Kevlar/polyester and E—glass/polyester respectively. Comparing the AE event—strain data of similar composites in figures 4 and 3, it becomes apparent, particularly in the case of E—glass, that the silicon—oil treatment modifies the nature of the interfacial bonding. The interfacial failure strain decreased and the number of recorded interfacial failure events increased. This clearly demonstrates a case of reduced adhesion, with event recording starting at low strains in both composites. The small difference of interfacial failure strain in the case of Kevlar further indicates that Kevlar—49 used in this study, practically, does not adhere to the Crystic—polyester resin used. In these circumstances, adhesion between Kevlar—49 and polyester could only be physical and due to resin shrinkage onto the fibres.

Test data for TBFCs of Kevlar—49/epoxy and E—glass/epoxy are presented in figures 5a. and 5b. respectively. In figures 6a. and 6b., we show the test data when the fibre systems were pretreated with a silicon—oil prior to composite manufacture. While the stress—strain responses, for corresponding composites, in figures 5 and 6 appear identical,

4

the AE events–strain responses show again that the silicon–oil treatment reduces adhesion, so interfacial failure events start early in strain and at correspondingly lower stress values. One notes also a significant increase in the number of recorded events, which is consistent with failure occurring predominantly at the fibre–matrix interface. This variation of the AE response with level of adhesion due to fibre surface treatment is clearer in figure 7, which is a replot of the stress and AE event–strain data in figures 5a and 6a. Figure 7 clearly demonstrates that the our experimental approach using AE would give a clearer idea of the level of fibre–matrix adhesion than via a stress–strain method alone.

Since for the TBFCs tested, load sharing is about equal between the fibres and the matrix, the stress range over which the interfacial failure events occurred can be regarded as the range of the fibre–matrix interface strength. That failure occurts over a range of stress or strain may be attributed to non–uniform loading of the interface or interphase, due probably to some degree of misalignment of the fibres in the bundle,and edge effects, etc. However, as there appears to be a closer relationship between the commencement of interfacial failure events and the level of fibre–matrix adhesion, we propose, that the corresponding stress at the occurrence of the first few events be taken as the interfacial failure strength. Interfacial failure strength(IFS) values obtained in this way are presented in table 1.

Table 1. Interfacial failure strength(IFS) for as–received and for silicon–oil treated Kevlar and E–glass fibres embedded in polyester and epoxy resins.

Resin system	Fibre system	Fibre treatment	IFS (MPa)	N*
Polyester	Kevlar–49	Non	14.5	3
	''	S i–Oil	10.0	4
	E–glass	Non	26.5	5
	''	S i–Oil	14.0	5
Epoxy	Kevlar–49	Non	33.8	3
	''	S i–Oil	13.5	2
	E–glass	Non	28.5	3
	''	S i–Oil	12.7	2

N*: number of specimens tested. Non ≡ As–received and Si–Oil ≡ silicon–oil

It can be seen from table 1. that the interface failure strength of E–glass/polyester is twice that of Kevlar/polyester. E–glass/epoxy and Kevlar/epoxy systems exhibit similar interfacial failure strengths($\sigma_{glass} \simeq 28.5MPa$ and $\sigma_{kevlar} \simeq 33.7MPa$). Using this parameter as an indicator of level of adhesion, it can be said that there is better adhesion between Kevlar and epoxy than between Kevlar and polyester. This is probably as a result of interactions between Kevlar, the amine hardner and the epoxy resin. For E–glass, both resin systems gave similar levels of adhesion: the silane coupling agent is also known to interact with epoxy[5]. In all cases, silicon–oil treatment of the fibres prior to composite manufacture led to a reduction in the interfacial failure strength. The fact that a zero strength was not observed in these cases, could be due to the resins displacing some of the silicon–oil during wet–out of the fibres. From AE event–strain data, the indications are that the polyester resin displaces more of the silicon–oil than the epoxy. The origin of this is not quite clear.

4. Conclusion:

From the experimental results obtained during this study, the following conclusions can be drawn.

Information relating to composite interface properties can be deduced using simple composites which limits composite fracture mechanisms to those occurring mainly at the interface and also facilitates description of the stress field around the interface region.

Mechanical tests of such simple composites in conjunction with suitably adjusted AE instrumentation would provide a clear idea of the level of fibre—matrix adhesion, the strength of the interface and good indication of the dominant interfacial failure mode(i.e.,at the interface or in the interphase).

In the composite systems studied, the procedure presented in this paper showed clearly that silane—sized E—glass/polyester interface is stronger than the Kevlar—49/polyester interface, which is consistent with silane enhancing E—glass adhesion to polyester. The procedure did provide evidence also that in the Kevlar/polyester composite system, interfacial failure occurred mainly at the interface, while in the E—glass/polyester system, failure occurred largely in the interphase. However, in comparison to polyester, Kevlar exhibited a better level of adhesion with an epoxy matrix. In all cases, when the fibres are pretreated with a silicon—oil prior to composite manufacture, fibre—matrix adhesion is poor.

The simplicity of the method developed here implies that it can be used for routine evaluation of adhesion in a variety of composite systems and monitoring of degradation of the interface. In addition, when the transverse strength of unidirectional composite is dependent on the interface strength, the method would facilitate its estimation.

* *Enquiries should be directed to Dr E.U. Okoroafor*

References:

1. P.J. Herrera and L.T. Drzal " Comparison of methods for the measurement of fibre/matrix adhesion in composites ", Composites, 23, 1, 2–27, 1992.

2. E.U.Okoroafor and R.Hill, " Standardisation in the evaluation of composite fibres and quasi—composites using acoustic emission and mechanical testing.", pp 49–59, in Composites Testing and Standardisation, ECCM—CTS2. Edited by P.J.Hogg, K.Schulte, H.Wittich, Woodhead Publishing Limited, Cambridge, England, 1994.

3. E.U.Okoroafor and R.Hill, " Relating acoustic emission signal parameter to the strength of fibres used in the manufacture of polymeric composites ", (Accepted for publication in the journal, Ultrasonics).

4. A.G.Beattie, "Acoustic emission principles and instrumentation", J.Acoustic Emission, 2, 95, 1983.

5. E.P.Plueddemann, Silane Coupling Agents, Plenum Press, New York and London, 1982.

6

<u>Figure Captions:</u>

Figure 1. Schematic diagram of the experimental setup, including the acoustic emission system and specimen types.

Figures 2. Stress—strain responses of (a) transverse and (b) longitudinal bundle of fibres composites of Kevlar—49/polyester matrix, including the AE events—strain responses(N) and the associated ringdown counts/event(N_e).

Figures 3. Test data of transverse bundle of fibres composites of (a) Kevlar—49/polyester and (b) E—glass/polyester respectively, showing the stress—strain response, the AE events—strain response(N) and the associated ringdown counts/event(N_e).

Figures 4. Test data of similar composites as in figures 3a and 3b respectively, but with the fibres pretreated with a silicon—oil prior to composite manufacture.

Figures 5. Test data of transverse bundle of fibres composites of (a) Kevlar—49/epoxy and (b) E—glass/epoxy respectively, showing the stress—strain response, the AE events—strain response(N) and the associated ringdown counts/event(N_e).

Figures 6. Test data of similar composites as in figures 5a and 5b respectively, but with the fibres pretreated with a silicon—oil prior to composite manufacture.

Figure 7. Replot of stress—strain and events—strain data in figures 5a and 6a to illustrate the variation of AE response with level of adhesion due to fibre surface treatment.

<u>Table Captions:</u>

Table 1. Interfacial failure strength(IFS) for as—received and for silicon—oil treated Kevlar and E-glass fibres embedded in polyester and epoxy resins.

Figure 1. Schematic diagram of the experimental setup, including the acoustic emission system and specimen types.

Figures 2. Stress–strain responses of (a) transverse and (b) longitudinal bundle of fibres composites of Kevlar–49/polyester matrix, including the AE events–strain responses(N) and the associated ringdown counts/event(Ne).

Figures 3. Test data of transverse bundle of fibres composites of (a) Kevlar-49/polyester and (b) E-glass/polyester respectively, showing the stress-strain response, the AE events-strain response(N) and the associated ringdown counts/event(Ne):

Figures 4. Test data of similar composites as in figures 3a and 3b respectively, but with the fibres pretreated with a silicon—oil prior to composite manufacture.

Figures 5. Test data of transverse bundle of fibres composites of (a) Kevlar—49/epoxy and (b) E—glass/epoxy respectively, showing the stress—strain response, the AE events—strain response(N) and the associated ringdown counts/event(Ne).

Figures 6. Test data of similar composites as in figures 5a and 5b respectively, but with the fibres pretreated with a silicon-oil prior to composite manufacture.

Figure 7. Replot of stress–strain and events–strain data in figures 5a and 6a to illustrate the variation of AE response with level of adhesion due to fibre surface treatment.

DAMAGE PREDICTION USING ASSOCIATED ACOUSTIC EMISSION FROM COMPOSITE MATERIAL.

A-M Priston[1], R Hill[1]* and R Brooks[2]

1. Department of Chemistry and Physics, The Nottingham Trent University, Clifton Campus, Nottingham, NG11 8NS, UK.

2. Department of Mechanical Engineering, The University of Nottingham, Nottingham, NG7 2RD, UK.

*To whom enquiries should be addressed

ABSTRACT

The AE event waveforms from a deforming composite material contain a complex combination of frequencies reflecting the damage source mechanisms. It is possible to cluster AE events that have similar characteristics and may also have similar source mechanisms. Using the equations by Ladeveze and LeDantec [1], the stresses retrieved from a finite element model of a composite material are used to calculate the development of damage associated with matrix cracking and fibre debonding. Experimental results from the cluster analysis of AE event data are compared to the results from a theoretical of the accumulation of damage in a composite material.

INTRODUCTION

This work compares the acoustic emission (AE) emanating from a composite material and the predictions of a theoretical damage model. The AE events are grouped according to characteristic waveform parameters. This has separated events originating from differing fracture mechanisms by using a clustering technique, k-means test.

The damage mechanisms occurring in a glass fibre/polyester resin composite material will be due to a complex combination of matrix and fibre dominated fracturing mechanisms. A theoretical model is used which simplifies the composite material structure and allows damage parameters to be calculated to reflect the degree of material degradation. These damage parameters relate to the changes in the transverse and shear moduli as a result of fracture mechanisms reducing the strength of the material.

COMPOSITE MATERIAL TESTING

Composite material was fabricated to have unidirectional fibre orientation. The dry fibres (Silenka E-glass, 2400TEX, as received) were wound on to an open metal frame. The polyester resin (CVP6345.001, MEKP catalyst and cobalt accelerator) was hand impregnated into the fibres, and cured under pressure ($50kg/m^2$) at 80^oC for 10 hours. The specimens were cut to have the fibres at angles of 10°, 20°, and 30° to the loading direction. Tensile testing was performed using Instrom and Lloyd testing machines, loading under constant cross-head movement.

ACOUSTIC EMISSION MONITORING

Acoustic emission is the detected stress wave emitted by the composite material due to the impulsive development of damage sites. The released acoustic energy radiates away from the crack tip and is detected at the surface of the specimen as a very small surface movement. It is assumed that since the specimens were relatively small the transit distance for the AE stress wave was short, so the attenuation losses due to internal scattering and absorption and dispersion are minimal. The assumption is that similar mechanisms from different parts of the specimen will be detected as an AE event with comparable waveform characteristics.

The AE transducer was attached to the centre of the composite specimens, using a constant pressure spring clip and ultrasonic coupling gel. The transducer used was resonant at 175kHz. It is assumed that the transducer signal characteristics being evaluated reflect gross differences in fracture source mechanism distinguishable by narrow band transduction. The transducer signal was amplified (30dB 55kHz-550kHz preamplifier AECL). This amplified signal was digitised by an A-D board (1MHz sampling rate, Keithley DAS50) set to be triggered by the voltage level rising above a preset level. Two hundred data points (total time duration 200 s) were sampled per AE event. The sampled event waveform was rapidly stored on computer hard disk via direct memory access.

When the composite was deforming rapidly and the AE rate was high, the maximum rate of capture by the digitising system was about 20-25 events per second. No data capture system can digitise every event emitted, so it has to be assumed that the events captured are a representative selection of the total.

ACOUSTIC EMISSION WAVEFORM ANALYSIS

The AE parameters used included: the peak amplitude (PA) the difference between the maximum to minimum peaks (volts), the ringdown count (RD) the number of positive oscillations above a threshold value, and the risetime (RT) the time from the event start to the largest maximum or minimum peak (milliseconds). Other parameters, such as event duration and the energy were also calculated but not used in any further analysis.

Carrying out a qualitative visual inspection of AE waveforms suggested that there were different types of event occurring at certain times in the experiment. This would agree with our view that different mechanisms were still distinguishable after detection and digitisation.

The AE parameter data was subjected to different mathematical manipulations to extract the similarities and differences in the data. The principal component analysis (PCA) attempts to distinguish variations between the parameters, or variables, for each event. Clustering techniques, such as the k-means relocation or Ward's methods, group events with similar variable relationships into the same cluster.

PRINCIPAL COMPONENT ANALYSIS

Principal component analysis reduced the three parameter values to a single number representing the greatest linear variation between the events. The first component had the greatest variation, whilst the second component also had the greatest variation but with the condition that there was no correlation with the first component. These first two components (PC1 and PC2) accounted for the maximum amount of variation between all the events, so if plotted would separate events with different variable values in to distinct regions of the graph.

It was noted that PCA did group events with similar characteristics, but there was no clear demarcations between groups. Rather there was a "boomerang" shaped spread of the results.

CLUSTER ANALYSIS

The same event data was submitted to a mathematical package (CLUSTAN Ltd., UK) for cluster analysis in an attempt to separate and outline groups of events with strong similarities.

The cluster technique used was the k-means test of the Euclidean sum of squares. The Euclidean sum of squares is the sum of the distances between events in a cluster to the centre of the cluster. For an event to belong to a cluster the iterative k-means test removes and replaces events attempting to find the best cluster location that minimises the errors. A limit is set on the number of iterations possible if the calculations do not come to a natural minimum.

Due to the immense number of calculations required, the number of events were restricted to 999 events with three variables (peak amplitude, ringdown count and risetime).

The events were randomly allotted to a cluster at the start of the cluster analysis. The final cluster content did not depend on the event starting cluster. The number of clusters was reduced from 5 to 3 groups with the 4 cluster level reported.

FINITE ELEMENT DAMAGE MODEL

The theoretical model for the development of damage in a composite material, suggested by Ladeveze and LeDantec [1], predicts a level of damage dependant on the stresses experienced and hence the material moduli reductions in a theoretical composite.

Using the method of finite element analysis to segment a model into small volumes, or elements, it is possible to calculate the stress responses at the mesoscale for a loaded composite. The composite material response to subtle changes in the material properties can be studied without the need to fabricate every variation.
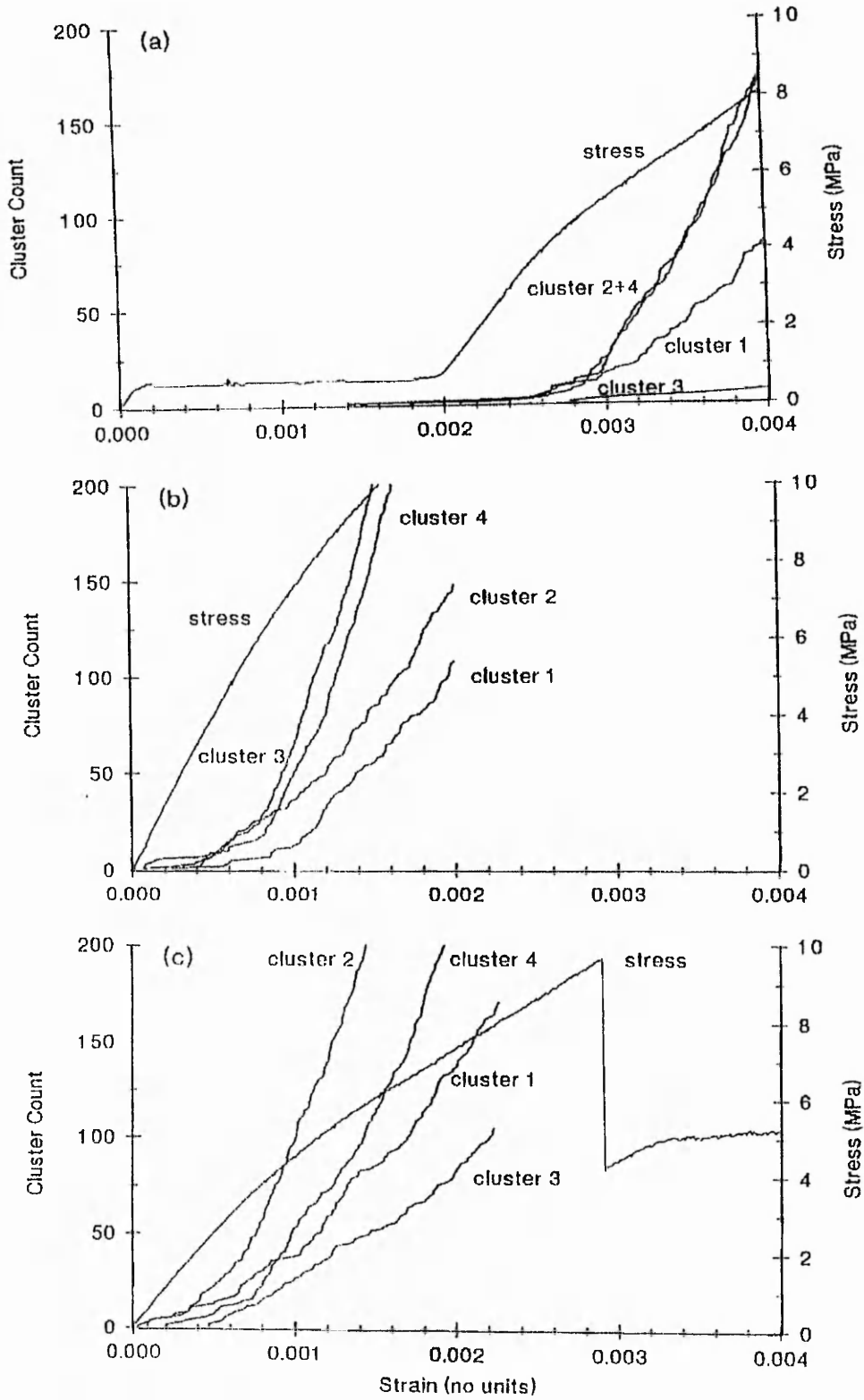
Figure 1: Cluster and stress plots for (a) 10°,(b) 20° and (c) 30° composite

The 2-D PAFEC finite element model consisted of 6 x 48 plane stress orthotropic quadrilateral elements (1 element was approximately 16 mm^2).

The FE model is loaded incrementally and the stresses from each element retrieved and used to calculate the damage values (d and d') for the composite material. These damage parameters d and d' increased as the damaged state developed, affecting both the transverse and shear moduli.

Initial constants for the material before deformation are determined using specimens made of similar fibres and matrix. These constants then control the degree of deformation given the damage calculated at each applied stress level.

RESULTS AND DISCUSSION

ACOUSTIC EMISSION DATA

Composite material with three fibre orientations were subjected to the PCA and cluster analyses. These orientations were 10°, 20° and 30° cut from glass/polyester unidirectional composite material.

Cluster 1 AE events were observed to have characteristically small amplitude, few ringdown counts and a short risetime. For the three composite material orientations, (figure 1,(a),(b),(c)) cluster 1 shows a gradual increase in event rate for increasing fibre angle.

For the 10° composite, clusters 2 and 4 are observed to be close together on the PCA plots and are seen to rise together in figure 1 (a). Both clusters have relatively few events until the modulus starts to change, after which both gradually rise.
Cluster 4 for both the 20° and 30° materials has a much more pronounced increase in AE just after the modulus knee. This sharp increase in the AE event rate is also present in the 10° composite (cluster 4 and 2).

The rapid change in the rate of occurrence of clusters 2 and 4 for all three material orientations, highlights a significant change in the way the material is deforming and fracturing. Cluster 2 and the early stages of Cluster 4, could be a general phase of material deformation where matrix cracks experienced in the early stages of testing are coalescing into significant cracks that are now impinging on to the fibre zone - reflected by the changing material modulus.

The first events appearing in cluster 3 occur as the clusters 2 and 4 event rate rises. Cluster 3 events are characteristically large amplitude with many ringdown counts, reflecting fracture processes that release larger amounts of energy than the other AE events.

With the associated modulus change, it would suggest that events in cluster 3 are fibre dependant. The process of fibre breakage and fibre debonding, would release larger amounts of energy than matrix cracking for example. This would agree with the cluster 3 events having larger peak amplitudes and many more ringdown counts.
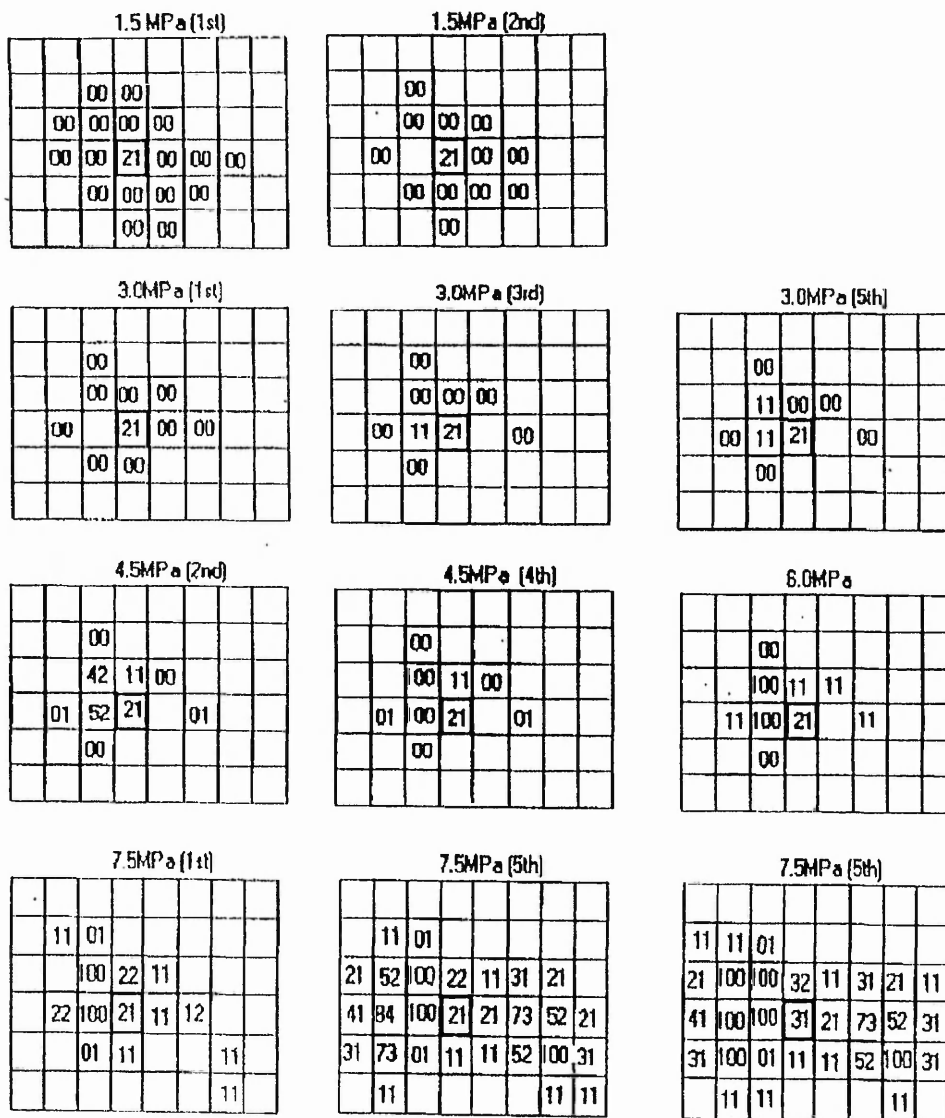
ALL BLANK SQUARES = 10   **Central Element =** ☐

| Key	d'	d		Key	d'	d
01	0.0	0.1		32	0.3	0.2
10	0.1	0.0		41	0.4	0.1
11	0.1	0.1		42	0.4	0.2
12	0.1	0.2		52	0.5	0.2
21	0.2	0.1		73	0.7	0.3
22	0.2	0.2		84	0.8	0.4
				100	failed	

Figure 2: A selection of finite element meshes containing damage parameters.

DAMAGE MODEL

For a composite material that has fibres at off angle inclinations to the loading direction, the mechanisms will involve the matrix as well as the fibres. Since the stronger fibres are no longer in pure tension, but have transverse and shear stresses acting, the interface region and the matrix will also contribute to the fracture mechanism. The damage parameters increase to reflect the damage developed at each stress load level applied.

The initial change in the state of the elements was for the d' damage parameter to increase to 0.1 (damage value = 10). This reflected a small decrease in the transverse modulus. This transverse modulus damage could be analogous to the widespread matrix cracking experience in testing composite materials at low stress levels.

At the higher stress levels the damage zone around the central element spreads out towards the specimen edges. The values for d' and d increase indicating that damage involves not only the pure transverse matrix cracking, but also the fibre debonding damage involving shear and transverse stresses. The matrix cracking has coalesced to form significant cracks that intercept the fibres and debond the matrix from the fibres.

The stress level in the finite element model was increased to 7.0 MPa, at which point the damage calculations would not stabilise even after 11 attempts at this load. The damage continued to grow. This may be the limit for this theoretical model.

CONCLUSION

The finite element damage model demonstrated the progression of damage through the mesh. The central element acted as the stress concentration with damage progressing from this point towards the sample edges.

AE events were clustered using k-means clustering method. The AE event clusters show differing response as composite samples with increasing fibre orientation are subject to stress. Certain of these clusters appear sensitive to sample modulus change. The number of events occurring in certain clusters at specific points in the tests, can be taken as highlighting the differing modes of failure in the material.

The FE damage model and AE waveform analyses do show similarities with regard to the response to stress with few AE events during the initial stage of loading and little response from the damage model. Work is continuing to relate the evolution of AE to the increase in the damage parameter.

REFERENCES

1   Ladeveze, P and LeDantec, E. "Damage modelling of the elementary ply for laminated composites", Composite Science and Technology 43 (1992) 257-267.

DAMAGE PREDICTION USING ASSOCIATED ACOUSTIC EMISSION FROM COMPOSITE MATERIAL.

A-M Priston[1], R Hill[1]* and R Brooks[2]

1. Department of Chemistry and Physics, The Nottingham Trent University, Clifton Campus, Nottingham, NG11 8NS, UK.

2. Department of Mechanical Engineering, The University of Nottingham, Nottingham, NG7 2RD, UK.

*To whom enquiries should be addressed

ABSTRACT

This work compares the acoustic emission (AE) emanating from a composite material and the predictions of a theoretical damage model. The AE events are grouped according to characteristic AE waveform parameters, such as peak amplitude, ringdown count and risetime. Principal component analysis (PCA) produced plots of grouped events with waveform similarities (figure 1). Using a clustering technique, k-means test, events were placed into clusters containing other similar events. These clusters are expected to represent particular damage source mechanisms.

The damage mechanisms occurring in a glass fibre/polyester resin composite material will be due to a complex combination of matrix and fibre dominated fracturing mechanisms. Using the equations by Ladeveze and LeDantec [1], the stresses retrieved from a finite element model of a composite material are used to calculate the development of damage associated with matrix cracking and fibre debonding. These damage parameters relate to the changes in the transverse and shear moduli as a result of fracture mechanisms reducing the strength of the material.

Experimental results from the cluster analysis of AE event data are compared to the results from a theoretical model of the accumulation of damage in a composite material.

REFERENCES

1.   Ladeveze, P and LeDantec, E, "Damage modelling of the elementary ply for laminated composites", Composite Science and Technology 43 (1992) 257-267.
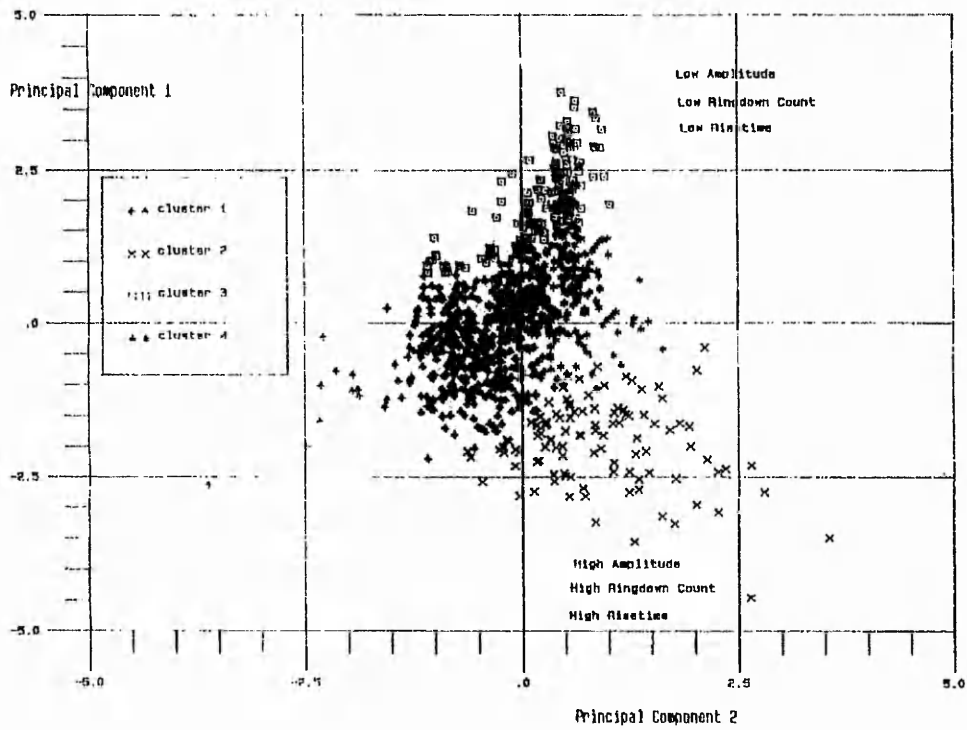
Figure 1: Principal component analysis for AE events from 20" composite.

Damage Mechanisms, Damage Modelling And Associated Acoustic Emission from Composites

A-M Priston[1], R Hill[1] and R Brooks[2]

The damage response of a composite material is complicated by the diverse nature of the constituent materials (fibre, matrix, surface treatment). For structural analysis of components the complexity can be reduced by simplifying the material properties of the anisotropic fibre composite material.

The finite element (FE) based theoretical model investigated in this paper correlates damage with a decreasing material modulus. The changing transverse and shear moduli are combined to reflect the effects of the matrix cracking and fibre debonding during a steady increase in load. The model, a rectangular glass fibre/polyester specimen, has been incorporated into a series of Fortran programs which retrieves the stress output from a finite element model of a composite material, and calculates the degree of damage accumulation on a local element basis. Detail of the programming and the modelling are described here. Results show the gradual development of the two damage mechanisms (d and d') from an initial weak point in the specimen.

Acoustic emission (AE) from a stressed composite material with 20° fibre orientation, was monitored with a piezoelectric transducer and the AE signal digitized for further waveform analysis. Characteristics of the waveform such as peak amplitude, risetime and ringdown count were automatically measured and used as the variables for cluster analysis. Using K-means test to group AE events with similar combinations of waveform characteristics, 4 clusters were chosen to represent the data. An attempt to correlate AE cluster results with the finite element damage analysis did reveal the arrival of one AE cluster at a load that developed significant damage and some failure in the central FE elements.

1. Introduction

The cumulative effect of localised material failure within a composite is reflected by the changing modulus of the stress/strain measurements. The inability of the material to sustain loads expected from previous material history, leads to

[1]The Nottingham Trent University, Chemistry and Physics Department, Clifton Campus, Nottingham, NG8 11NS.

[2]The University of Nottingham, Department of Mechanical Engineering, Nottingham, NG7 2RD

the conclusion that the material has sustained irreversible damage. Predicting (modelling) the likely material deformation processes occurring would aid the design of components made from composite material.

The scale at which the material properties are included in the model determines the effective resolution of the damage mechanism. The micro scale – including individual fibres and the surrounding matrix, does allow direct visualization of the damage mechanism. However this scale is so computationally time consuming that structural analysis of components by this route is not normally possible. Reducing or homogenising the separate fibre or matrix properties to properties for the combined material, allows meso-scale analysis of material deformation and failure.

Defects such as resin cracks and debonding of the fibres from the matrix, can have quite different effects on the stiffness and strength of the material measured in directions relative to the load/fibre orientation. Some damage mechanisms clearly have a more detrimental affect on material performance than others.

A particular model devised by Ledeveze and Le Dantec [1], relates the elastic moduli associated with the transverse and shear stress/strain measurements to damage accumulation. This is made use of in this work. Damage in the form of matrix cracking and fibre debonding is expected to predominate at the lower stress levels. At higher stresses, close to material fracture, fibre failure will have significant effects on the longitudinal material strength, leading to final material fracture. Fibre breakage is not taken into account here.

Acoustic emission is released from the damaged composite material as it deforms. Strain energy in the form of a pressure wave radiates away from the damage location towards the transducer at the surface. Due to the complicated path through the specimen the AE signal is a product of the damage mechanism, the anisotropic material and the characteristics of the transducer/digitizing system. Since the damage mechanism is the only variable thought to change significantly, the differences in the signal characteristics are associated with material fracture mechanisms

The AE waveform variables of peak amplitude, risetime and ringdown count for each event was submitted to the clustering package CLUSTAN, for K-means clustering [ref 2]. From a random sort of the event data, successive comparisons between events and the grouping of similar events reduced the number of clusters to four. Cluster 2 was dominated by events with high amplitude, high ringdown count and high risetime values. Cluster 3 had events with small risetimes and amplitude, and low ringdown count. Clusters 1 and 4 were similar with intermediate values.

2. The Model Composite Material

The 2-D PAFEC finite element model comprises 6 x 48 plane stress orthotropic quadrilateral elements (1 element is approximately 16mm^2). Figure 1 shows the restraints in the load direction for the nodes along one short end, and the pressure loading for the opposite end also in the load direction. The material properties for the orthotropic elements (type 36215) are given in table 1 and correspond to 60% glass fibre/polyester composite.

To initiate the damage and prevent failure occurring at the restraining grips an element near the middle (147) was set to have reduced material property values (-1%).

Stressing the model was achieved by the application of tension in incremental steps. From experimental results on 20° glass/polyester composite material, the failure stress has been found to be about 15MPa. Thus loads up to 7.5MPa were chosen to focus on the first stages of damage initiation.

3. Material Characterisation and Calculation of Damage Parameters

Special glass fibre/polyester laminates were fabricated in a similar way to those of Ladeveze and Le Dantec [1], so as to determine the damage parameters for the material. These include the threshold parameters in the undamaged state and the damage growth rates. Laminates with fibres at $[+/-45]_{2s}$ were tested in order to generate a situation of almost pure shear damage accumulation. A laminate with fibres at $[+/-67]_{2s}$ provided damage accumulation from mechanisms with both transverse and shear components. A parameter, b, controlled the relative proportions of shear and transverse components in the damage parameter d. Mechanical testing acquiring detailed load, longitudinal and transverse strains provided the necessary stress/strain changes resulting from material damage.

The values for the damage parameters d and d' [ref 1], were divided into intervals of 0.1, over a range from 0 to 0.8, with the parameters having a maximum value of 1.0. The value of 0.8 was expected to represent an element so badly damaged that failure was assured. At element failure the mechanical properties were reduced to 50% of the initial values in all directions (since a zero value is not permitted). Each increment of d or d' related to a 0.1 decrease in the shear or transverse initial modulus for the material. For every combination of d and d', the material properties were calculated and presented to the finite element analysis file at each incremental load step.

4. Experimental Procedure

The finite element model was subjected to five load steps from 1.5MPa to

7.5MPa, in steps of 1.5MPa. At each stage the stress output file from the FE analysis was used to evaluate the degree of damage given the magnitude of stress calculated for each element. If the stresses had risen sufficiently to change the value of d or d', then a new value for the material modulus was calculated and changed in the FE input data file. So as to track the changing values of damage another data file recorded the state of the material for each element.

At each load the damage calculations and the same FE load were repeated until the d parameters did not change value.

5. Acoustic Emission Experiments

Rectangular specimens (approximately 25 x 4 x 200mm) were loaded in a R6000 Lloyds testing machine. Tension was applied with a slow crosshead speed of 0.1%/min. The stress and crosshead movements were logged.

The AE transducer (AECL 175KHz) was attached to the sample with a spring clip and gel coupling. The electrical output was preamped (AECL 30dB) and digitized using a DAS50 (Keithley 1MHz). The data was transferred to computer hard disk using a VIEWDAC (Keithley) data handling system. Another program then calculated the waveform parameters for the AE events captured.

6. Results

A pictorial representation of the changing degree of damage within the composite model is shown in Figure 2. In figure 3, the AE event amplitude data and stress curve are plotted for a similar 20° composite.

Damage occurred throughout the whole FE specimen area for the first load step, 1.5MPa, except for a region around the weakened element. The level of damage accumulation was low (< 0.1) and only in the d' parameter. The pattern of elements effected were arranged at an angle across the mesh. There were very few AE events recorded.

Increasing the load to 3.0MPa the FE model required 5 iterations to stabilise the values for d and d'. The value of d' (pure transverse stress component) continued to increase, with only a few elements developing d damage with a shear component. More AE was recorded, with most events from Clusters 1,3,4

At 4.5MPa elements close to the initially weakened element continued to accumulate transverse damage (d'), with shear components also increasing but at a slower rate. The 4 iterations required to stabilise the damage parameters concluded with the first two elements failing. The number of AE events occurring

noticeably increased at this load. Events from Cluster 2 (high amplitude, risetime and ringdown) occurred more often.

No more failures were recorded from the FE analysis at 6.0MPa. But the elements did develop more shear/transverse (d) damage. At 7.5MPa the AE results (fig 3) show that many events occurred in all clusters. The numbers of events in Cluster 2 were also becoming significant. The FE damage analysis continued to predict damage spreading away from the central area. Many elements accumulated high levels of damage and a few failed. After 11 iterations the damage calculations had still not converged.

7. Discussion

The results in fig 2, show how the damage calculations develop a damage pattern extending away from the weakened element. The pattern of the damaged elements sloping across the mesh may reflect the orientation of the material in the model. From reported work examining glass/polyester composite samples, the initial, non critical matrix failure throughout the material may well be represented in the damage model by the change in all elements of the d' transverse parameter. More serious matrix debonding and larger cracks in the 3.0 - 4.5MPa range produced AE events with higher amplitudes, ringdown counts and risetimes. This coincided with the increasing values of the d parameter. Fibre debonding would account for a shear component increase in parameter d. The Cluster 2 AE events coincided with the loading for the first calculated damage failures.

Some mathematical distortion due to the relatively large element size could account, to some extent for the spread of the damage zone.

8. Conclusion

Finite element calculation of damage development in a glass fibre/polyester composite has mirrored damage accumulation observed in experimental work. By altering the finite element model to represent other fibre orientations for the composite material, different damage growth patterns are expected, reflecting the changed stress regimes. With a smaller mesh size it is anticipated that an improvement in the precision of the damage calculations, will occur.

9 Acknowledgments
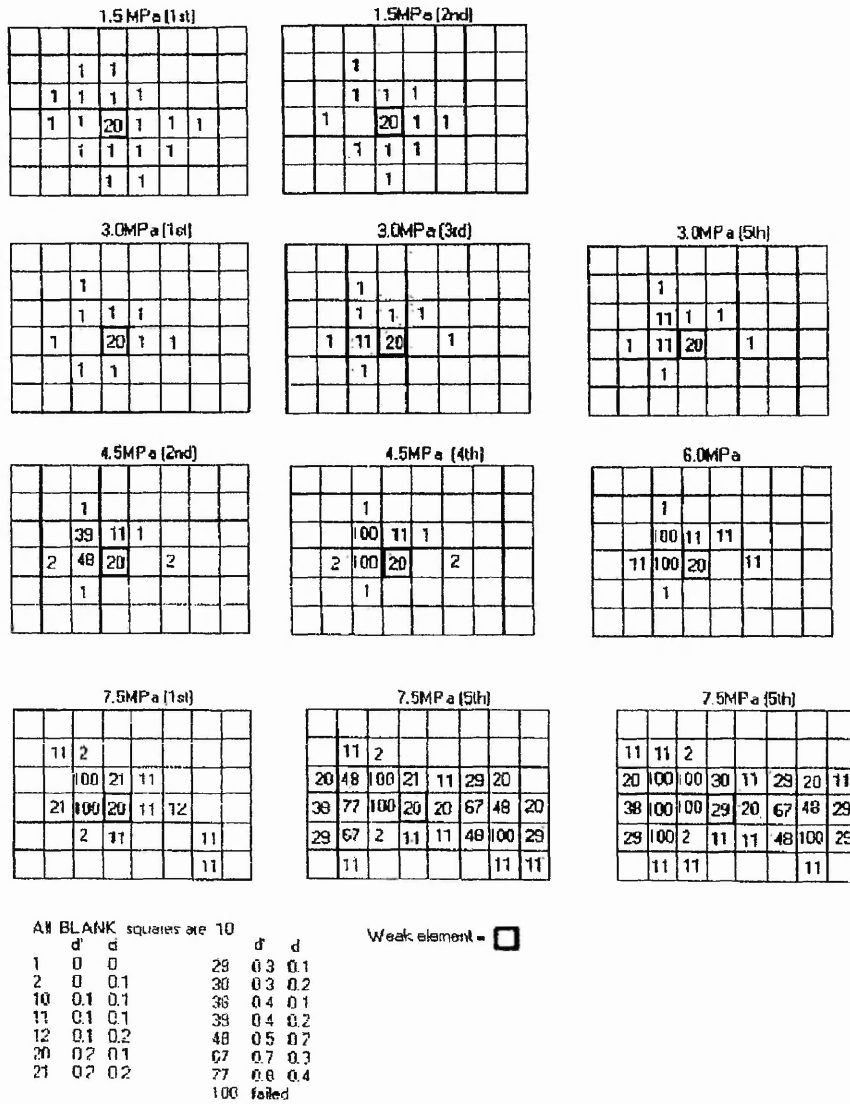
Figure 2. Central portions of finite element model displaying the damage development of parameters d' and d.
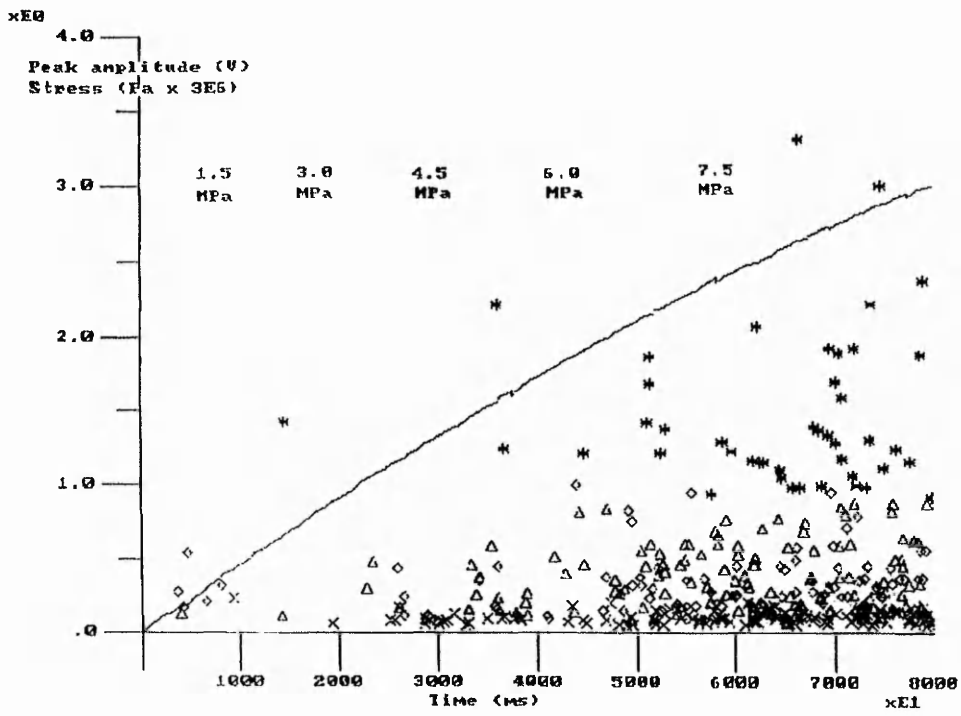
Figure 3. AE event amplitudes and stress data plotted against experiment time. Clusters distinguished by symbols: 1= ◇ ,2= ✳ ,3= ✕ and 4= △ .

Evaluation of the Interfacial Tensile Strength of Composite Materials Using Acoustic Emission.

E.U.OKOROAFOR, A.-M.PRISTON, R.HILL‡.

Department of Chemistry and Physics, The Nottingham Trent University, Clifton Campus, Nottingham NG11 8NS, UK.

‡ To whom inquiries should be addressed.

Abstract:

The nature of fibre–matrix adhesion, the strength of the interface and the type of failure mode have been investigated via the acoustic emission(AE) technique. When unidirectional composites are subjected to transverse tension, the predominant fracture mechanism is interfacial failure events whose stress waves are detected as acoustic emission at ultrasonic frequencies by a piezoelectric transducer placed in intimate contact with the test specimen. The stress and strain range over which these AE events occur determine the strength of the fibre–matrix interface, while the relative total number of recorded AE events give indication as to the interfacial failure mode. The method developed here has been applied to a variety of composite systems and shows potential as a simple and convenient means of monitoring adhesion, interfacial strength and interfacial failure mode in fibre reinforced plastics.

1. Introduction:

The mechanical performance of composite materials depends, among other things, on the characteristics of the interface between the reinforcing fibres and the matrix, since a weak interface will certainly lead to a premature failure when substantial load sharing is expected via the interface. For stresses applied perpendicular to the fibre direction, the knowledge of the characteristic strength of the fibre–matrix interface becomes essential when tailoring performance to applications.

Measurement of the properties of the interface, using real composites, is not a simple task, due to interferences from a variety of failure mechanisms occurring during material testing. The complex state of stress developed during testing of such materials further complicates the situation. In this paper,

2

employing simple composites[1], it becomes possible to reduce the failure mechanisms to that mainly associated with interfacial failure. This also facilitates the description of the state of stress at the interface region.

In a simple bundle of fibres composite(BFC) with the fibre axis perpendicular to the tensile direction, the interfacial tensile strength between the matrix and the fibres has been measured using acoustic emission(AE). The AE indicates the strain and stress level for failure at the interface as well as the failure mode. The method developed here has been applied to monitor the level of fibre—matrix adhesion in composite systems such as: E—glass/polyester; Kevlar—49/polyester; E—glass/epoxy and; Kevlar—49/epoxy. By varying the treatment of the fibre surface(as—received, desized, lubricated), this changes the nature of the interfacial bonding and is reflected in the acoustic emission and mechanical responses.

Test results showed that the method would give an unambiguous idea of the level of fibre—matrix adhesion, the strength of the interface and the failure mode. In addition, the simplicity and convenience of the method shows potential as another means of routine evaluation of adhesion in a variety of composite systems.

2. Experimentation:

2.1 Materials preparation:

Composite reinforcements used in this study include as—received Kevlar—49 (DuPont (UK) Ltd; Den 2160, Dtex 2400, finish—free) and E—glass (Fibre—Glass (UK) Ltd; Equerove, Silane—sized, EC13, 600 Tex). The matrix materials used were Crystic Polyester 272 resin, supplied by SCOTT Bader (UK) Ltd and Epoxy LY 5025 supplied by CIBA—Geigy Polymers (UK). Their preparation followed the recommended procedure for producing composite materials. For polyester: 100 parts of Crystic polyester 272 resin; 2 parts of Crystic catalyst M(methyl ethyl ketone peroxide); and 1 part of cobalt accelerator E in styrene were used. This was cured for 7 days at room temperature. For the epoxy, 100 parts of the resin LY 5025 and 38 parts of the hardener HY 5025 were used and cured for 8 hours at 80°C. These resins, after degassing, were then poured into a dog—bone shaped mould of silicon—rubber, containing the fibre bundle at its' centre but oriented transverse to the longitudinal axis of the mould(TBFC). In the cases where the fibres were subjected to surface—treatment, this was accomplished simply by coating the fibres with a silicon oil. To compare the major failure mechanisms occurring during deformation of composites

with various fibre orientations, some bundle of fibre composites were prepared with a longitudinal orientation(LBFC) of the fibre bundle. All composite gauge dimensions were 40x5x2.5mm.

2.2 Tests conditions:

All tensile tests were performed using a LLOYD–6000R tensile testing machine, at a constant crosshead movement rate of 0.5%/min or equivalently 0.2mm/min.

The AE technique was employed during the tests as a means of monitoring and discriminating the fracture mechanisms occurring during the deformation of the composites. Previously[1], the technique has been employed to monitor fibre failures and their mode(singlets ≡ one fibre failure at a time, doublets, triplets, etc) during tensile testing of fibre bundles in air, yielding the stress–strain response. In another study[2], it has been possible to relate AE signal parameters to fracture stress and hence discriminate fibre systems from each other as well as composite fracture mechanisms. In this study, a commercial AE transducer (Acoustic Emission Technology Corporation, type AC375L, resonant frequency 375kHz) was utilized. This transducer was spring clamped to the middle portion of the composite test specimen mounted in the grips of the tensile machine. Silicon grease was used as an acoustic couplant. The AE signals from the transducer, were preamplified by 60dB, using a preamplifier(AECL 2100/PA, 208–530kHz bandpass) with narrow band filtering around the transducer resonance, and processed using the AECL 2100M acoustic emission system. The processed signals are then extracted and analysed as detailed elsewhere[2]. AE instrument settings were: dead time, 0.2ms and threshold of 0.2Volts. The threshold was chosen to eliminate electronic background noise, noise from the grips and the tensile machine, thus ensuring that received signals were from the fractures occurring in the composite being tested. Figure 1., shows the schematic diagram of the experimental system and specimen types. Some of the possible AE signal parameters(initial peak voltage, event rise time, event duration and the ringdown counts per event or group of events, i.e., number of positive threshold crossings) can be related to the nature of the event. The values obtained for these AE parameters are considered relative since they depend on the threshold voltage applied. As the parameters are interdependent, choice of which one to use is often based on accessibility. In this study the ringdown count was used which is related to the relative acoustic energy[3] released by the fracture events.

4

3. Results/Analysis/Discussion:

The predominant fracture mechanisms occurring during tensile deformation of bundle of fibres composites(BFC), whose fibres are longitudinally(LBFC) or transversely(TBFC) oriented with respect to the tensile direction were monitored using the acoustic emission(AE) technique. The typical mechanical and AE test data are shown in figures 2. Data shown in figure 2a. is typical of LBFCs, while figure 2b., is the case for TBFCs. In the former case, the fracture events occur close to composite failure strain and possess higher ringdown counts per event. These ringdown counts exhibit an increasing trend with applied stress. While in the latter case, the fracture events occur at low strains and with relatively small ringdown counts per event. From known mechanical effects, the events recorded during tensile deformation of the TBFCs were associated with fibre—matrix interfacial failure, while for LBFCs, they were mainly associated with fibre fractures, since in the stress range over which the events occurred, the main load bearing constituent of the composite are the fibres and their fracture led to the failure of the composite as a whole.

Having established that interfacial failure during tensile deformation of BFCs with transverse fibre orientation can be monitored using AE, it becomes obvious that the technique can be employed to measure the true strength of the fibre—matrix interface. In other words, the methodology developed here could be extended to compare unambiguously the level of adhesion between a matrix and different fibre systems and vice versa.

Test data for TBFCs of Kevlar—49/Crystic polyester and E—glass/Crystic polyester are given in figures 3a and 3b respectively. The stress—strain response of the composites did not show any significant difference and this, in either case, is attributed to the low fibre volume fraction. Hence, the role played by the resin—fibre interface is not made manifest in relation to the composite stress—strain response. Nonetheless, examination of the failed composites revealed that failure occurred within the composite region containing the fibre bundle and nowhere else which clearly indicates that fibre—matrix interfacial failure initiated the composite failure.

Using the AE events—strain response as an indicator, since the recorded events are associated with interfacial failure, one notices that the interface characteristics in both composites are completely different: The Kevlar/polyester interface failed at low strains and within the elastic region of the matrix material, while E—glass/polyester interface failed well beyond the yield point of the matrix material. This clearly confirms that the E—glass/polyester interface is much stronger than the Kevlar/polyester interface. Note also, that there are fewer

5

recorded events in the case E–glass/polyester. Optical microscopy of the composites fracture surface revealed, clean fibres in the case of Kevlar/polyester and fibres covered with the matrix material in the case of E–glass/polyester. The latter could be attributed to the silane sizing enhancing E–glass adhesion to polyester[4]. This piece of information from optical microscopy explains why there are fewer recorded events of interfacial failure in the case of E–glass/polyester. When failure occurs predominantly in the interphase region, the number of recorded events is expected to be relatively small, compared to the situation whereby failure occurs at the interface, because the interphase is common to many fibres. This information unambiguously show that E–glass used in this study, unlike Kevlar–49, adheres better to Crystic–polyester due to the interactions between the silane coupling agent and polyester. Test data involving fibres treated with a silicon–oil prior to composite manufacture are presented in figures 4a and 4b for Kevlar and E–glass respectively. Note, now, that event recording started at low strains in both composites. Comparing the AE event–strain data of similar composites in figures 4 and 3, it becomes apparent, particularly in the case of E–glass, that the silicon–oil treatment reduces fibre–matrix adhesion. While the number of recorded interfacial failure events increases with decreasing adhesion, the interfacial failure strain decreases. The small difference of interfacial failure strain in the case of Kevlar further demostrates that Kevlar–49 used in this study, practically, does not adhere to the Crystic–polyester resin used. In these circumstances, adhesion between Kevlar–49 and polyester could only be physical and due to resin shrinkage onto the fibres.

Test data for TBFCs of Kevlar–49/epoxy and E–glass/epoxy are presented in figures 5a and 5b respectively. In figures 6a and 6b, we show the test data when the fibre systems were pretreated with a silicon–oil prior to composite manufacture. While the stress–strain responses, for corresponding composites, in figures 5 and 6 appear identical, the AE events–strain responses show clearly that the silicon–oil treatment reduces adhesion, so interfacial failure events start early in strain and at correspondingly lower stress values. This is expected, indicating that the our experimental approach using AE would give a clearer idea of the level of fibre–matrix adhesion than via a stress–strain method alone.

Since for the TBFCs tested, load sharing is about equal between the fibres and the matrix, the stress range over which the interfacial failure events occurred can be regarded as the range of the fibre–matrix interface strength. However, as there appears to be a closer relationship between the commencement of interfacial failure events and the level of fibre–matrix adhesion, we propose,

6

that the corresponding stress at the occurrence of the first few events be taken as the interfacial failure strength. Interfacial failure strength(IFS) values obtained in this way are presented in table 1.

Table 1. Interfacial failure strength(IFS) for as—received and for silicon—oil treated Kevlar and E—glass fibres embedded in polyester and epoxy resins.

Resin system	Fibre system	Fibre treatment	IFS (MPa)	N*
Polyester	Kevlar—49	Non	11.3	3
	"	Si—Oil	8.7	4
	E—glass	Non	>25.3	5
	"	Si—Oil	12.3	5
Epoxy	Kevlar—49	Non	31.0	3
	"	Si—Oil	10.5	2
	E—glass	Non	25.0	3
	"	Si—Oil	9.5	2

N*: number of specimens tested. Non ≡ As—received and Si—Oil ≡ silicon—oil

It can be seen from table 1. that the interface failure strength of E—glass/polyester is twice that of Kevlar/polyester. E—glass/epoxy and Kevlar/epoxy systems exhibit similar interfacial failure strengths($\sigma_{eglass} \simeq$ 25MPa and $\sigma_{kevlar} \simeq$ 31MPa). Using this parameter as an indicator of level of adhesion, it can be said that there is better adhesion between Kevlar and epoxy than between Kevlar and polyester. This is probably as a result of interactions between Kevlar, the amine hardner and the epoxy resin. For E—glass, both resin systems gave similar levels of adhesion: the silane coupling agent is also known to interact with epoxy[4]. In all cases, silicon—oil treatment of the fibres prior to composite manufacture led to a drastic reduction in the interfacial failure strength. The fact that a zero strength was not observed in these cases, could be due to the resins displacing some of the silicon—oil during wet—out of the fibres.

Conclusion:

From the experimental results obtained during this study, the following conclusions can be drawn.

7

Information relating to composite interface properties can be deduced using simple composites which limits composite fracture mechanisms to those occurring mainly at the interface and also facilitates description of the stress field around the interface region.

Mechanical tests of such simple composites in conjunction with suitably adjusted AE instrumentation would provide a clear idea of the level of fibre—matrix adhesion, the strength of the interface and good indication of the dominant interfacial failure mode(i.e.,at the interface or in the interphase).

In the composite systems studied, the procedure presented in this paper showed clearly that silane—sized E—glass/polyester interface is stronger than the Kevlar—49/polyester interface, which is consistent with silane enhancing E—glass adhesion to polyester. The procedure did provide evidence also that in the Kevlar/polyester composite system, interfacial failure occurred mainly at the interface, while in the E—glass/polyester system, failure occurred largely in the interphase. However, in comparison to polyester, Kevlar exhibited a better level of adhesion with an epoxy matrix. In all cases, when the fibres are pretreated with a silicon—oil prior to composite manufacture, fibre—matrix adhesion is poor.

The simplicity of the method developed here implies that it can be used for routine evaluation of adhesion in a variety of composite systems and monitoring of degradation of the interface. In addition, when the transverse strength of unidirectional composite is dependent on the interface strength, the method would facilitate its estimation.

References:

1. E.U.Okoroafor and R.Hill, " Standardisation in the evaluation of composite fibres and quasi—composites using acoustic emission and mechanical testing.", pp 49—59, in Composites Testing and Standardisation, ECCM—CTS2, Edited by P.J.Hogg, K.Schulte, H.Wittich, Woodhead Publishing Limited, Cambridge, England, 1994.

2. E.U.Okoroafor and R.Hill, " Relating acoustic emission signal parameter to the strength of fibres used in the manufacture of polymeric composites ", (Accepted for publication in the journal, Ultrasonics).

3. A.G.Beattie, "Acoustic emission principles and instrumentation", J.Acoustic Emission, 2, 95, 1983.

4. E.P.Plueddemann, Silane Coupling Agents, Plenum Press, New York and London, 1982.

1

Routine Evaluation of Interfacial adhesion in Fibre Reinforced Plastics

E.U.OKOROAFOR[*], A—M.PRISTON, R.HILL

Department of Chemistry and Physics, The Nottingham Trent University, Clifton—Campus, Nottingham NG11 8NS, UK.

The predominant damage process occurring, when unidirectional composites are subjected to transverse tension, is interfacial failure events which are detected as acoustic emission(AE) by a transducer in contact with the test piece. The stress and strain range over which these AE events occur determine the strength of the fibre—matrix interface, while the relative number of recorded events give indication as to the interfacial failure mode.

Measurement of the properties of the interface, using real composites, is not a simple task, due to interferences from a variety of failure mechanisms occurring during material testing. The complex state of stress developed during testing of such materials further complicates the situation. In this letter we present a method which uses simple composites, making it possible to reduce the composite fracture processes to that mainly associated with interfacial failure. The associated stress waves are detected as acoustic emission(AE) at ultrasonic frequencies by a piezoelectric transducer placed in intimate contact with the test specimen. The AE indicates the strain and stress level for failure at the interface as well as the failure mode. This method differs from previous studies of fibre—matrix adhesion[1] and have not previously, to our knowledge, been reported.

Fig. 1 shows the schematic diagram of the experimental system and specimen types. The AE system was configured to record the fracture events and their relative acoustic energy[2] which is related to the AE signal parameter, ringdown counts per event, which corresponds to the number of positive threshold crossings of the decaying AE signal. The specimen types are bundle of fibres composites with the fibre axis either transverse(TBFC) or longitudinal (LBFC) to the tensile test—direction. The fibres used included as—received Kevlar—49(Dupont UK. Ltd; Den 2160, Dtex 2400, finish—free) and E—glass(Fibre—Glass UK. Ltd; Equerove Silane—sized, EC13, 600 Tex). The matrix materials used were Crystic—polyester 272(SCOTT Bader UK. Ltd) and Epoxy LY 5025(CIBA—Geigy Polymers, UK). Their preparation followed the recommended procedure for producing composite materials.
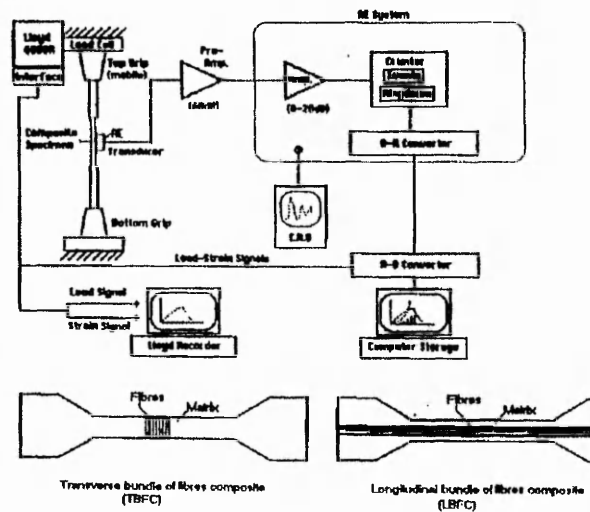

Figure 1. Schematic diagram of the experimental setup, including the acoustic emission system and specimen types.

Results:

To illustrate the validity of our method, we present first in Figs. 2a and 2b typical mechanical and AE test data from TBFCs and LBFCs respectively. TBFC fracture events occur at low strains and with relatively small ringdown counts per event. Fracture events in LBFC occur close to composite failure strain and possess higher ringdown counts per event, which exhibit an increasing trend with applied stress. This trend has previously been reported by us[3,4] in tests involving fibre bundles in air. From known mechanical effects and the AE ringdown patterns in both figures, the TBFC events were associated with fibre–matrix interfacial failure, while the LBFC events were mainly associated with fibre fractures, which led to the failure of the composite as a whole. Having established that it is possible with AE to monitor interfacial failure during tensile deformation of TBFCs, we now extend the method to compare the level of interfacial adhesion between a matrix material and different fibre systems and vice versa, including varying fibre surface treatment
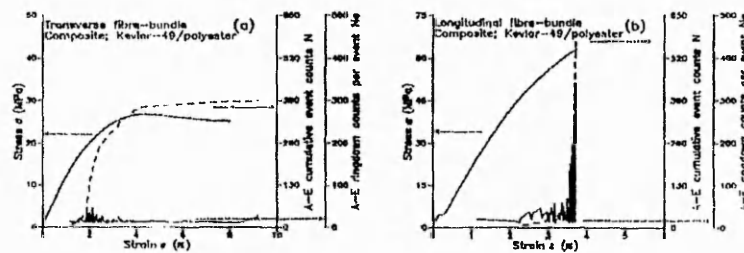
Figures 2. Stress–strain responses of (a) transverse and (b) longitudinal bundle of fibres composites of Kevlar–49/polyester matrix, including the AE events–strain responses(N) and the associated ringdown counts/event(N_e).

Test data for TBFCs of Kevlar/polyester and E–glass/polyester are given in Figs. 3a and 3b respectively. The stress–strain response of the composites did not show any significant difference and is attributed to the low fibre volume fraction. However, the AE data indicates that the interface characteristics in both composites are completely different: The Kevlar/polyester interface failed at low strains, while the E–glass/polyester interface failed well beyond the yield point of the matrix material. One notes also, that there are fewer recorded events in the case E–glass/polyester. In this case, optical microscopy of the composites fracture surface revealed that, interfacial failure occurred predominantly in the interphase region. For the Kevlar/polyester system, the exposed fibres were clean of the matrix material, consistent with failure occurring at the fibre–matrix interface.


Figures 3. Test data of transverse bundle of fibres composites of (a) Kevlar–49/polyester and (b) E–glass/polyester respectively, showing the stress–strain response, the AE events–strain response(N) and the associated ringdown counts/event(N_e).

3
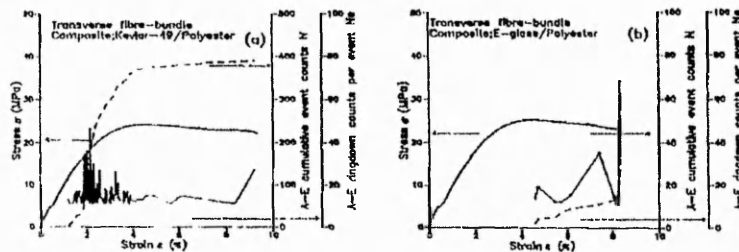
Figs. 4a and 4b show the test data for TBFCs of Kevlar/epoxy and E–glass/epoxy respectively, while Figs. 5a and 5b, correspond to the cases where the fibre systems were pretreated with a silicon–oil prior to composite manufacture. The stress–strain responses for corresponding composites in Figs. 4 and 5 appear identical, but the AE data show clearly that the silicon–oil treatment reduces adhesion, so interfacial failure events start early in strain and at correspondingly lower stress values. One notes also a significant increase in the number of recorded events, which is consistent with failure occurring predominantly at the fibre–matrix interface. This variation of AE response with level of adhesion due to fibre surface treatment is better illustrated in Fig. 6, which is a replot of Figs. 4a and 5a.
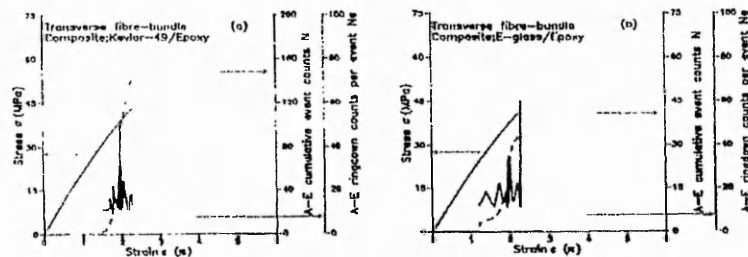
Figures 4. Test data of transverse bundle of fibres composites of (a) Kevlar–49/epoxy and (b) E–glass/epoxy respectively, showing the stress–strain response, the AE events–strain response(N) and the associated ringdown counts/event(N_e).
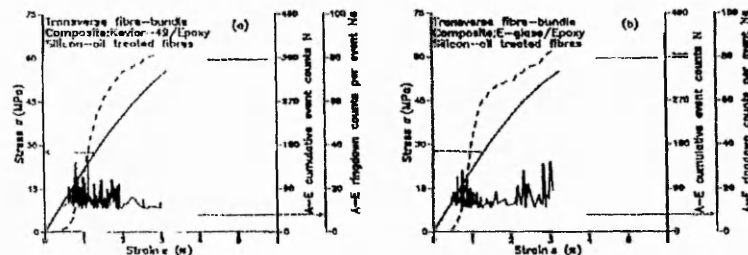
Figures 5. Test data of similar composites as in figures 4a and 4b respectively, but with the fibres pretreated with a silicon–oil prior to composite manufacture.

Since for the TBFCs tested, load sharing is about equal between the fibres and the matrix, the stress range over which the interfacial failure events occurred can be regarded as the range of the fibre–matrix interface strength. However, as there appears to be a closer relationship between the commencement of interfacial failure events and the level of fibre–matrix adhesion, we propose, that the corresponding stress at the occurrence of the first few events be taken as the interfacial failure strength(IFS). IFS values obtained in this way are presented in table 1. It can be seen from table 1. that the interfacial failure strength of E–glass/polyester is twice that of Kevlar/polyester. E–glass/epoxy and Kevlar/epoxy systems exhibit similar interfacial failure strengths($\sigma_{eglass} \simeq 25MPa$ and $\sigma_{kevlar} \simeq 31MPa$). Using this parameter as an indicator of level of adhesion, it can be said that there is better adhesion between Kevlar and epoxy than between Kevlar and polyester. This is probably as a result of interactions between Kevlar, the amine hardner and the epoxy resin. For E–glass, both resin systems gave similar levels of adhesion: the silane coupling agent is known to interact with both polyester and epoxy[5]. In all cases, silicon–oil treatment of the fibres prior to composite manufacture led to a drastic reduction

4

in the interfacial failure strength. The fact that a zero strength was not observed in these cases, could be due to the resins displacing some of the silicon—oil during wet—out of the fibres.

Table 1. Interfacial failure strength(IFS) for as—received and for silicon—oil treated Kevlar and E-glass fibres embedded in polyester and epoxy resins.

Resin system	Fibre system	Fibre treatment	IFS (MPa)	N*
Polyester	Kevlar–49	Non	11.3	3
"	"	Si-Oil	8.7	4
	E–glass	Non	>25.3	5
	"	Si -Oil	12.3	5
Epoxy	Kevlar–49	Non	31.0	3
"	"	Si—Oil	10.5	2
	E–glass	Non	25.0	3
	"	Si Oil	9.5	2

N*: number of specimens tested Non = As-received and Si-Oil = silicon-oil


Figure 6. Replot of stress—strain and events-strain data in figures 4a and 5a, to illustrate the variation of AE response with level of adhesion due to fibre surface treatment.

Conclusion:

From the experimental results obtained during this study, the following conclusions can be drawn.

Information relating to composite interface properties can be deduced using simple composites which limits composite fracture mechanisms to those occurring mainly at the interface and also facilitates description of the stress field around the interface region.

Mechanical tests of such simple composites in conjunction with suitably adjusted AE instrumentation would provide a clear idea of the level of fibre—matrix adhesion, the strength of the interface and good indication of the dominant interfacial failure mode(i.e.,at the interface or in the interphase).

The simplicity of the method developed here implies that it can be used for routine evaluation of adhesion in a variety of composite systems and monitoring of degradation of the interface. In addition, when the transverse strength of unidirectional composite is dependent on the interface strength, the method would facilitate its estimation.

* *Enquiries should be directed to Dr E.U.Okoroafor*

References:

1. P.J. Herrera and L.T. Drzal, " Comparison of methods for the measurement of fibre/matrix adhesion in composites ", Composites, 23, 1, 2—27, 1992.

2. A.G.Beattie, "Acoustic emission principles and instrumentation", J.Acoustic Emission, 2, 95, 1983.

3. E.U.Okoroafor and R.Hill, "Relating acoustic emission signal parameter to the strength of fibres used in the manufacture of polymeric composites", (Accepted for publication in the journal, Ultrasonics).

4. E.U.Okoroafor and R.Hill, "Standardisation in the evaluation of composite fibres and quasi—composites using acoustic emission and mechanical testing.", pp 49—59, in Composites Testing and Standardisation, ECCM—CTS2. Edited by P.J.Hogg, K.Schulte, H.Wittich, Woodhead Publishing Limited, Cambridge, England, 1994.

5. E.P.Plueddemann, Silane Coupling Agents, Plenum Press, New York and London, 1982.

Libraries &
Learning
Resources